Progress Report

UCSF Laboratory for Radiological Informatics Research

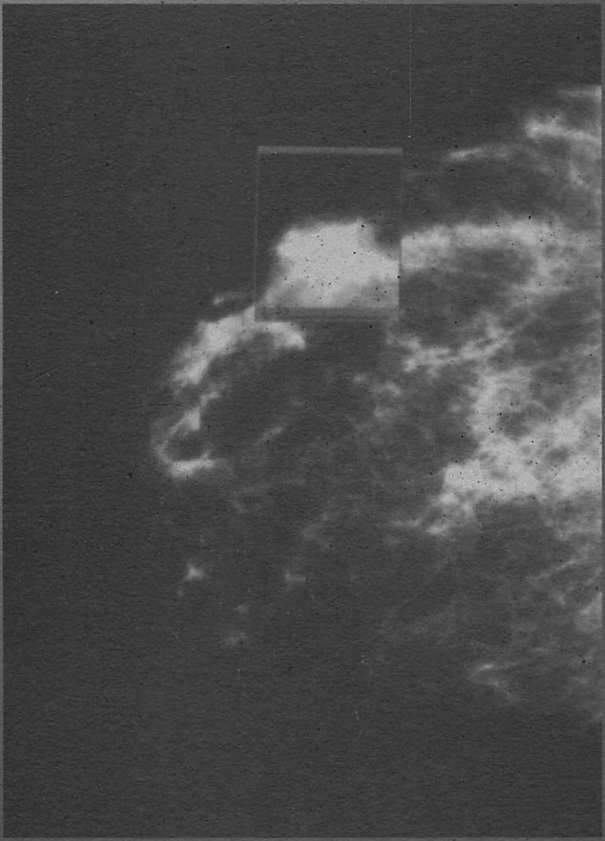

photo courtesy of E. Sickles, MD

February 1998

Laboratory for Radiological Informatics
Department of Radiology
University of California, San Francisco
530 Parnassus Avenue, Rm CL-158
San Francisco, CA 94143-0628

Tel (415) 476-5941
Fax (415) 502-3217

SUMMARY

During the past year, our research efforts have concentrated on three areas: establishing a WAN ATM Token ring for tele-imaging, solving a missing link in PACS, and using PACS as a research tool. A WAN ATM OC-12 token ring has been installed at UCSF connecting six campuses in the San Francisco Bay area. In this ring, the daily clinical PACS and the research imaging network each has its own independent path to avoid interference. A missing link in PACS is digital mammography. Great emphasis in our research has been on the image acquisition, archive, display, and transmission of large digital mammogram files. PACS has matured as a clinical tool, but its applications in basic and clinical research has just begun. Using it as a tool, we have started research projects on image informatics, a digital atlas of hand images, teleconsultation, and tele-microscopic imaging.

This report summarizes the current status of the development of high speed WAN, using PACS as a research tool, and the image informatics research in our laboratory during the past year. It contains preprints of papers to appear in the Proceedings of the *International Society for Optical Engineering, SPIE Medical Imaging* 1997, San Diego, California, February 21-27, 1998. This report also contains selected reprints and preprints from last year; abstracts and presentations from the 83rd RSNA, November - December, 1997.

Our research is supported by:

- NLM contract N01-LM-4-3508
- NLM contract N01-LM-6-3547
- NCHS BPA 50257C-95, National Center for Health Statistics
- US Army Medical R&D DAMD 17-96-C-6111
- Lumisys (equipment)
- Fuji Medical Systems USA, Inc. (equipment)
- Abe Sekkei, Japan (equipment)
- Philips Medical Systems DPA 109
- California Breast Research Program 1RB-0148
- Dept Health & Human Services 282-97-0079
- NIH R01 LM 06270
- Nikon, Japan

TABLE OF CONTENTS

Summary.. i

Table of Contents.. ii

Title Page 1

Laboratory for Radiological Informatics Staff.. 2

Laboratory for Radiological Informatics, UCSF Network Architecture.......................... 3

PREPRINTS FROM SPIE

1. **Johannes Stahl, Jianguo Zhang, Koun Sik Song, H.K. Huang**........................ 4
A new design for medical image display applications in advanced networked environments [3335-36]

2. **Fei Cao, H.K. Huang, E. Piekta**.. 12
Diagnostic workstation for digital hand atlas in bone age assessment [3335-67]

3. **Fei Cao, Edward A. Sickles, H.K. Huang, Xiaoqiang Zhou**............................ 13
Migration of the digital interactive breast imaging teaching file [3335-71]

4. **Stephen T.C. Wong, Kent Soo Hoo, Jr., Robert C. Knowlton, Kenneth D. Laxer, Randall A. Hawkins, Howard Rowley, Michael W. Vannier**.. 23
Presurgical multimodality neuroimaging analysis for complex partial seizures [3337-24]

5. **Guang Pu Lei, Hong Zhang, Albert Wong**.. 32
PC/NT based PACS display workstation with ATM and DICOM connectivity [3339-16]

6. **S.L. Lou, H.K. Huang, Edward Sickles, David Hoogstrate, Fei Cao, Jun Wang**.. 43
Full-field direct digital telemammography: System implementation [3339-17]

7. **Jianguo Zhang, Johannes Stahl, Koun Sik Song, H.K. Huang**........................ 52
Real-time teleconsultation with high resolution and large volume medical imaging [3339-20]

8. **Albert W.K.Wong and H.K. Huang** 58
Integration of multivendor imaging equipment with DICOM into PACS [3339-33]

SELECTED REPRINTS

1. **Pietka, E and Huang HK**. 1997. Image Processing Techniques in Bone Age Assessment. *Chapter in Medical Imaging Techniques and Applications*, Ed. Leondes ,CT., Gordon & Breach Science Publ, Chap 5, 221-272.......... 67

2. **Huang HK, Wong AWK, and Zhu X**. 1997. Performance of Asynchronous Transfer Mode (ATM) Local Area and Wide Area Networks for Medical Image Transmission in Clinical Environment. *J Comp Med Imag & Graphics* 21(3), 165-173.......... 119

3. **Lou SL, Hoogstrate DR, Huang HK**, 1997. An Automated PACS Image Acquisition and Recovery Scheme for Image Integrity based on the DICOM Standard. *J Comp Med Imag & Graphics* Vol 21, No 4, 209-218.......... 128

4. **Huang HK**, 1997. Multimedia Applications in Health Care. Editorial,*IEEE Multimedia,* Special Issue: Multimedia in Medicine Vol 4, No 2, 23.......... 138

5. **Wong STC, Huang, HK**, 1997. Networked Multimedia for Medical Imaging. *IEEE Multimedia* Special Issue: Multimedia in Medicine Vol 4, No 2, 24-35.......... 139

6. **Cho PA, Huang HK**, 1997. Architecture and Ergonomics of Imaging Workstations. In Hendee WR and Wells PNT Eds. *The Perception of Visual Information, 2nd Ed. Sringer, NY,* Chap 11, 343-358.......... 151

7. **Cao F, Sickles EA, Huang HK**, 1997. An Interactive Digital Breast Imaging Teaching File. *RSNA EJ* 1 : 26 pars. Online. Available HTTP: http://ej.rsna.org/EJ_0_96/0037-97.fin/mammo.html. 18 July 1997.......... 169

8. **Zhang J, Huang HK**, 1997. Automatic Background Recognition and Removal (ABRR) of Computed Radiography Images. *IEEE Trans. Medical Imaging. (Preprint)*.......... 185

9. **Huang HK**, 1997. Telemedicine and Teleradiology Technologies and Applications. *Min Invas Therapy*. Vol 6 *(Preprint)*.......... 195

10. **Huang HK, Wong STC, Pietka E**. Medical Image Informatics Infrastructure Design and Applications. *Medical Informatics (Preprint)*.......... 201

11. **Huang HK, Lou SL, Dillon WP**. 1997. Neuroradiology Workstation Reading Room in an Inter-Hospital Environment: A Nineteen Month Study. *Comp. Med Imaging & Graphics*, vol 21, no 5 *(Preprint)*.......... 212

12. **Huang HK, Lou SL, Sickles E, Hoogstrate D, Jahangiri M, Cao F, Wang J**. 1997. Technical Issues in Full-Field Direct Digital Telemammography. *Comp Asst. Rad. and Surgery*, 662-667 *(Proceedings)*.......... 221

RSNA ABSTRACTS AND PRESENTATIONS (RADIOLOGY VOL. 205(P),1997) 227

UCSF Radiological Informatics Research

- A Progress Report -

Laboratory for Radiological Informatics -- LRI
Research Group

Faculty and Post Docs

H.K. Huang, D.Sc.
Professor and Vice Chairman, Dir LRI
Department of Radiology

Stephen Wong, Ph.D.
Assistant Professor

Fei Cao, Ph.D.
Postdoctoral Fellow

Xiaoqiang Zhou, Ph.D.
Postdoctoral Fellow

Shyh-Liang (Andrew) Lou, Ph.D.
Assistant Professor

Mohammed Jahangiri, M.D, MPH
Postdoctoral Fellow

Gretchen Stipec, M.D.
Postdoctoral Fellow

Graduate Student

Kent Soo Hoo
Ph.D. Candidate

Staff

Albert Wong, B.S.
Software System Manager

Laura Snarr, B.S.
Administrative Assistant

David Hoogstrate, B.A.
Programmer/Analyst

Visiting Faculty and Fellows

Stephan Erberich
Visiting Scholar (Germany)

Guang Pu Lei
Fellow (Prof. Shanghai Med U, China)

Ewa Pietka, Ph.D..
Visiting Assistant Professor (Poland)

Koun Sik Song, M.D.
Visiting Scholar (AMC, S. Korea)

Johannes Stahl, M.D.
Visiting Scholar (Germany)

Hong Zhang
Visiting Scholar (China)

Jianguo Zhang, Ph.D.
Fellow (Assoc. Prof. Chang Chun Inst.,
Chinese Acad. Sci)

Hong-Dun Lin
Visiting Scholar (Taiwan, China)

Collaborators

James Sayre, Ph.D.
Statistician, UCLA

Edward Sickles, M.D.
Professor and Chief, Breast Imaging

William Dillon, M.D.
Professor and Chief, Neuroradiology

Vicente Gilsanz, M.D., Ph.D.
Los Angeles Children's Hospital

LRI WAN/LAN ATM Network

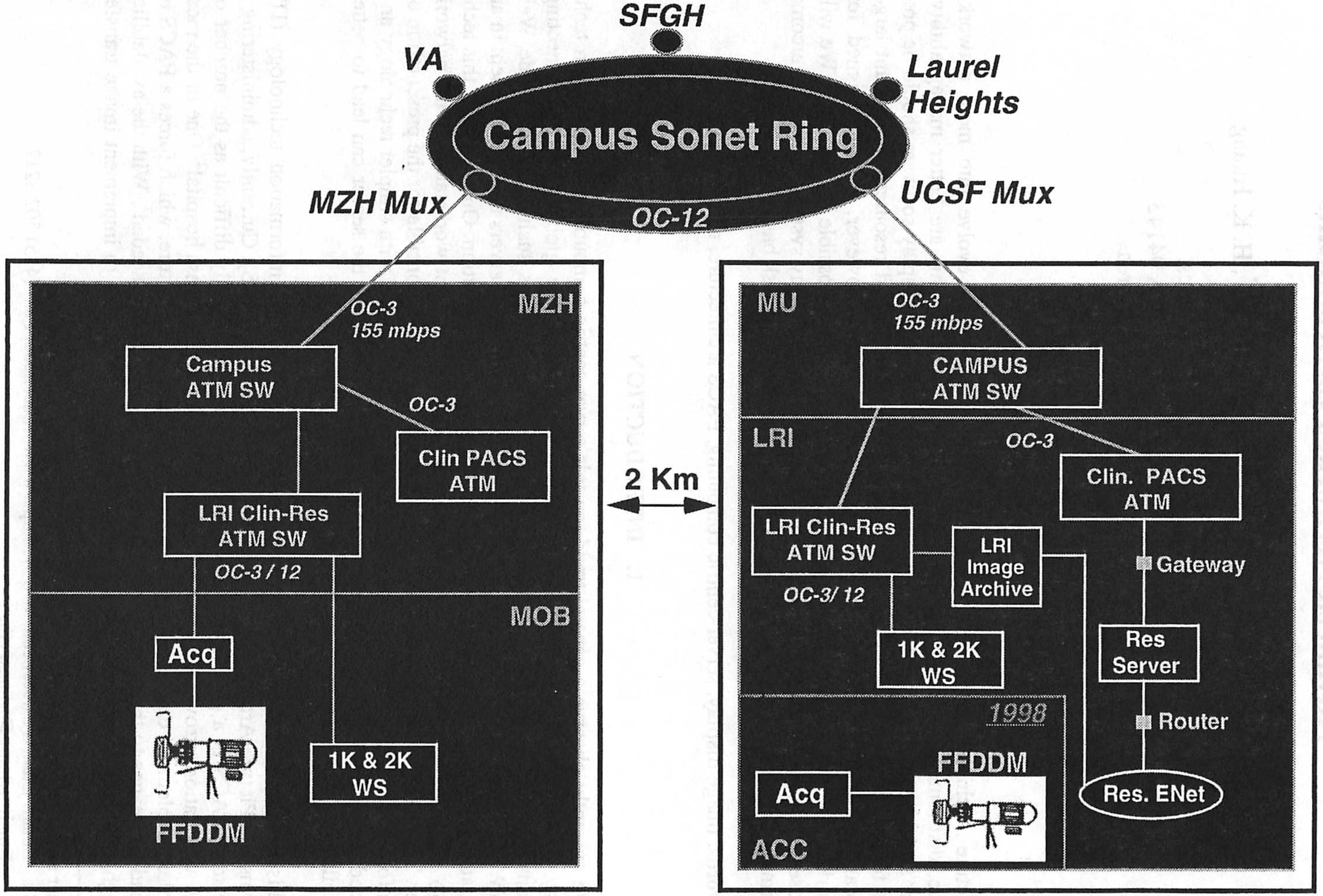

MOB: Medical Offices Building
ACC: Ambulatory Care Center

LRI: Laboratory for Radiological Informatics
MZH: Mount Zion Hospital
MU: Millberry Union

(contributed by David Hoogstrate and Laura Snarr)

A New Design for Medical Image Display Applications in Advanced Networked Environments

Johannes N. Stahl, Jianguo Zhang, Koun Sik Song*, H. K. Huang

Laboratory for Radiological Informatics,
University of California, San Francisco, CA 94143
* ASAN Medical Center, Seoul, S. Korea

ABSTRACT

Picture Archiving and Communication Systems (PACS) will evolve into more network-centric, distributed systems in the near future. The reasons for this are better manageability, higher scalability and reduced cost of ownership. Medical image display software should be prepared for this development by making optimized use of networked resources, for instant large medical image files. Most software products currently used, however, is not designed for networked operation and imposes architectural limitations on the possible performance. We will propose an alternative software architecture for medical image display systems that can overcome this limitations without affecting the performance of conventional disk based I/O.

Keywords: image display, server-centric computing, PACS architecture, network computer

1. INTRODUCTION

We currently observe a general trend towards server-centric computing in information technology. The tremendous growth and success of the Internet, the global network connecting millions of computers, have triggered this evolution. Applications such as World Wide Web (WWW) browsers gather information that is scattered over various servers and present them in an integrated, consistent manner independent of the users physical location. One aspect of this technology is that most of the application logic is moved from the client workstation to the network server. This has several benefits: The client workstation is only responsible for the presentation of the information and can therefore be implemented as a "thin client" with simpler technology and reduced maintenance costs. Implementing the application logic on the server can lead to better scalability and manageability[1].

This development will certainly have an impact on medical information technology (IT) systems and Picture Archiving and Communications Systems (PACS). Currently, administering a large-scale PACS is a challenging task, which becomes increasingly difficult as the number of client workstations grows due to the attempt to implement the filmless hospital[2]. One of the most complex problems is caused by a low-bandwidth network infrastructure, which forces a PACS to preload all images to the workstations where they will probably be needed[3]. With the availability of high-bandwidth networks such as ATM it becomes conceivable to implement image transfer

---

Further author information —
J.N.S.: Email: jstahl@lri.ucsf.edu; WWW: http://www.lri.ucsf.edu; Fax: (415) 502 3217
J.Z.: Email: jzhang@lri.ucsf.edu
H.K.H: Email: bernie.huang@radiology.ucsf.edu

"on demand" where images are transferred to the workstation at precisely the moment when they should be displayed. While this approach would improve the manageability of the system, it imposes new challenges to the display software on the client workstation.

Many medical image display applications operate only with images stored on the local hard disk. When images are located on a network server, they will first make a copy of the images to the local storage, and then display them. While this mode of operation will certainly work under most circumstances, it is not optimized for networked operation regarding speed and overall efficiency.

Another aspect is that the increasing number of clients will cause large-scale PACS to evolve into distributed systems with one ore more archive servers and several departmental application servers. It likely that these systems will maintain connections to distant sites on a wide-area or even global scale. (Figure 1)

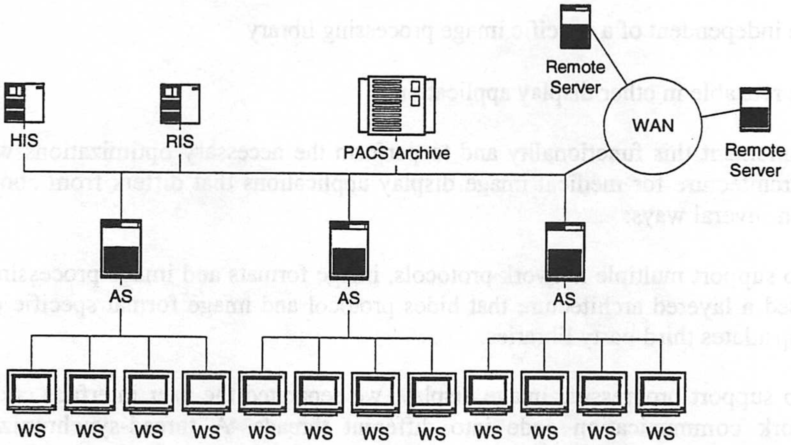

Figure 1: Distributed PACS with three Application Servers (AS) and multiple Workstations (WS). Connections exist to Hospital Information System (HIS), Radiological Information System (RIS), PACS Archive and several remote servers via Wide-Area Network (WAN)

We should therefore expect that images might be located on different network servers spread throughout a local area or wide area network. Each of these servers might use another network protocol to access the images. They may use various image formats to encode the images. A medical imaging application should handle such a situation in an efficient, transparent and consistent manner. We will outline the architectural changes necessary to accomplish this goal.

2. OVERVIEW

At UCSF Laboratory for Radiological Informatics, we have developed a medical image display application optimized for networked operation. According to the described usage scenario, we defined a list of requirements for this application. The software should

- display images transmitted from a network immediately, without storing them to a local disc first

- handle multiple network connections to different servers concurrently
- use a variety of network protocols, including Hypertext Transfer Protocol (HTTP), File Transfer Protocol (FTP) and Digital Imaging and Communications in Medicine (DICOM) Protocol
- decode mages in several image formats, including JPEG, TIFF and DICOM images
- perform the network communications asynchronously, thus not blocking the user interface while receiving images
- display images progressively when detecting a slow network connection. The user should be able to manipulate the part of the image that is already visible.
- maximize throughput when working with a high-speed network
- be independent of a specific image processing library
- be reusable in other display applications

To implement this functionality and to perform the necessary optimizations we developed a new architecture for medical image display applications that differs from conventional software in several ways:

1. To support multiple network protocols, image formats and image processing libraries, we used a layered architecture that hides protocol and image format specific details and encapsulates third-party libraries.
2. To support progressive image display, we separated the user interface code and the network communication code into different threads. A thread-synchronization protocol ensures data integrity.
3. To maximize network throughput and overall efficiency, we used the asynchronous Input/Output (I/O) model for the network communication

We will discuss these items in more detail in the next section.

3. ARCHITECTURE DETAILS

1. Layered Architecture

For an application that communicates with multiple servers in a distributed system, it is essential to be open to all network protocols and file formats. We therefore used a layered architecture to implement the network transport for the display component. This scheme consists of a Protocol Layer, an Image Format Layer and an Image Processing Layer. (Figure 2) The Layers are isolated from each other and communicate through an internal, generic protocol. This architecture allows any combination of network protocol, image format and image processing library to work together. This design also makes it easy to extend the software with additional protocols, image formats or image processing libraries.

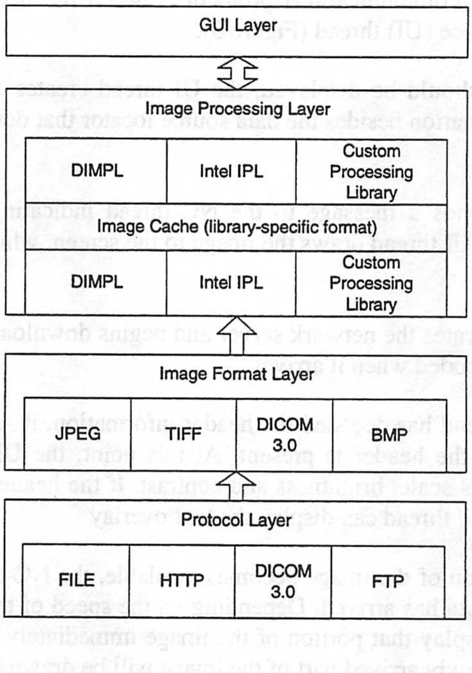

Figure 2: Layered Architecture of the network communication software

We included support for multiple image processing libraries for two reasons: first, each of the libraries used has distinctive advantages and disadvantages. For instance, the DIMPL library is highly optimized to process grayscale radiological images, but lacks support for color images, which can be conveniently processed by the Intel Image Processing Library. Second, it can be useful to replace one image processing library by another for reasons of cross-platform portability.

2. Multithreaded Design

Displaying an image on a computer monitor involves several steps: (1) loading the image data into Random Access Memory (RAM); (2) performing image processing such as Lookup Table (LUT) transformation; and (3) transfer the resulting image into the computers video memory. Step (2) and (3) can then be repeated as the user modifies the display parameters. Conventional image display software performs these steps sequentially, one after the other[4]. During this procedure, no user input is accepted. When images are loaded from a local hard disk and the whole procedure takes only a very short time, this may be acceptable. However, the time required to receive an image from a distant network server can be unpredictable. If user input is ignored during that period, it gives the user the impression that the application has crashed.

One way to avoid this problem is using a multithreaded design. Threads are subroutines within an application process that run independently and quasi-simultaneously. Our software uses two threads: one user interface thread that receives keyboard and mouse input from the user, and a network communication thread. Since both threads run independent from each other, the user can continue to work while an image is downloaded from the network.

Many advanced imaging applications use multiple threads to support image downloading in the background. Enabling progressive image display during the download, however, required us to develop a thread-safe communications protocol between the network communication (NC) thread and the user interface (UI) thread (Figure 3).

1. When an image should be displayed, the UI thread creates a new image object, which contains no information besides the data source locator that describes where to retrieve the image

2. The UI thread sends a message to the NC thread indicating that an image should be downloaded. The UI thread draws the image to the screen, which is a null operation at this time.

3. The NC thread locates the network server and begins downloading the image. Each chunk of data will be decoded when it arrives

4. When the NC thread has decoded the header information, it sends a notification to the UI thread indicating the header is present. At this point, the UI thread adjusts the display parameters such as scale, brightness and contrast. If the header contains patient and study information, the UI thread can display the text overlay

5. Whenever a portion of the image becomes available, the NC thread notifies the UI thread that new image data has arrived. Depending on the speed of the connection, the UI thread may choose to display that portion of the image immediately or to wait unit more data is ready. Only the newly arrived part of the image will be drawn to the screen.

6. After completion of the transfer, the NC thread notifies the UI thread that the image is now ready. The UI thread draws any remaining part of the image to the screen.

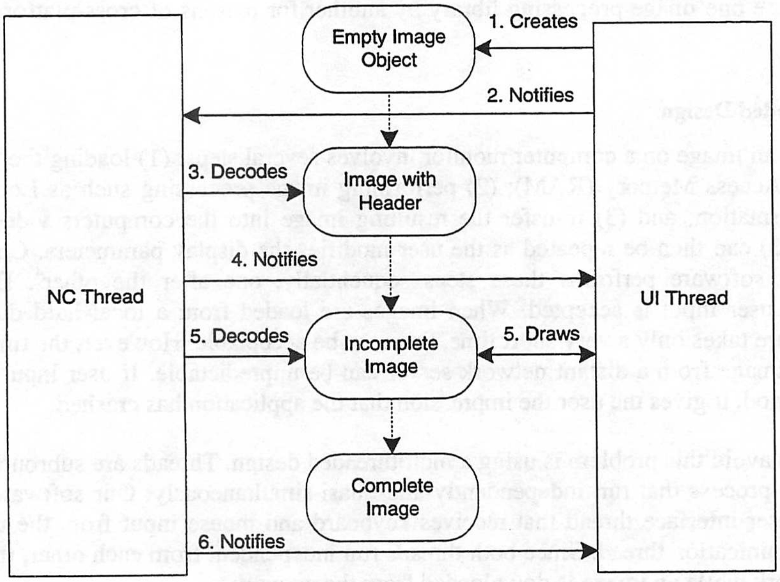

Figure 3: Illustration of the communications protocol between the User Interface (UI) thread, the Network Communications (NC) thread and the image object.

To avoid unnecessary screen redraws when transmitting an image over a high-speed network, we built a mechanism into the NC thread that detects the transfer speed and adjusts the rate of notifications sent to the UI thread automatically. We verified that this mechanism works over a high range of network speeds from modem connections to ATM.

3. Asynchronous I/O

Another important requirement for our software was that it should be capable of downloading images from multiple servers at the same time. The easiest way to implement this in the multi-threaded design would be to create a new thread for each server. The drawback of this solution is that it creates a race condition between these threads. A single-processor computer can only execute a single thread at a time and simulates true multithreading by switching very fast between the threads. Since usually most threads are waiting for a certain input event, this is usually not very serious. However, when several threads are doing processor-intensive tasks such as image processing, switching between threads can become very expensive and a waste of resources.

In our case, this leads to the following effect: When a slow network connection is used, the time used to process the images is small compared to the time each thread waits for the data from the network. When the network speed is high, data is delivered faster than it can be processed, and the threads enter a race condition. This means that using one thread for each server causes a performance degradation that becomes worse when the network speed increases. Such a behavior is of course inefficient and limits the overall throughput of the application.

We used the asynchronous (nonblocking) I/O model to overcome this problem. With asynchronous I/O, a single thread can maintain multiple network connections concurrently. To do so, however, we had to revert the flow of control and data within the application. Instead of "pulling" data out of the network and passing this request down the different software layers (Figure 4), data is "pushed" from the network and passed upwards through the layers (Figure 5).

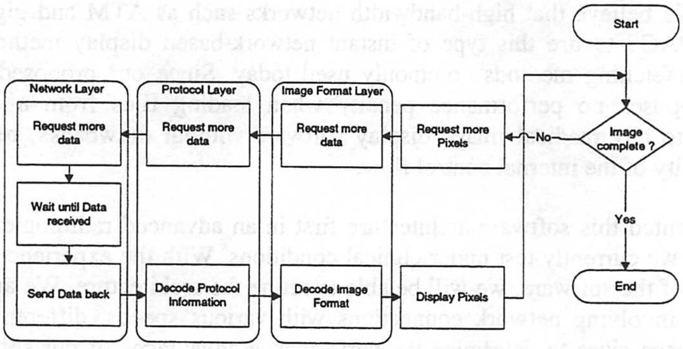

Figure 4: Data and control flow in the conventional, synchronous model using "pulling". Note that this model can handle only a single image/connection per thread.

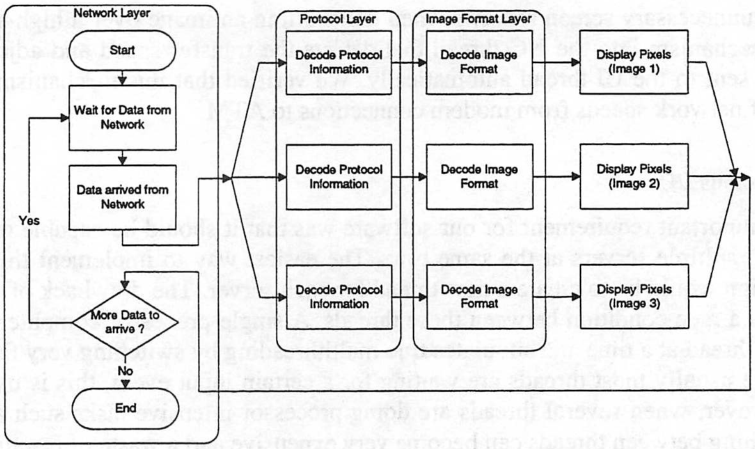

Figure 5: Data and control flow in the asynchronous model as used in the software component described in this paper. Data is "pushed" from the network to the higher levels. This figure shows also how a single thread can effectively handle multiple active server connections simultaneously with a simple dispatch mechanism.

Unfortunately, not all of the software libraries used to implement our software support this mode of operation. For instance, the JPEG and TIFF image format libraries cannot use asynchronous I/O and thus require an additional thread. We are currently evaluating whether the possible performance gains justify the effort to rewrite these libraries.

4. DISCUSSION

The presented image display software implements several new concepts which can enhance the performance and efficiency when images are transferred from a network server and displayed immediately. We believe that high-bandwidth networks such as ATM and gigabit ethernet will enable future PACS to use this type of instant network-based display methods instead of the complicated prefetching methods commonly used today. Since our proposed display software architecture imposes no performance penalty when loading files from a disk, it could be incorporated into any medical image display software without drawbacks, besides the slightly higher complexity of the internal control flow.

We implemented this software architecture first in an advanced radiological teleconsultation system[5], which we currently test under clinical conditions. With the experiences gained from the clinical testing of the software, we will be able to refine the architecture. We are also performing extensive tests involving network connections with various speeds, different server operating systems and image sizes to determine the performance advantages of our software architecture under realistic conditions. Theses measurements will not only enable us to further improve the display architecture details, but will give us valuable hints for optimizing the server software architecture.

5. MATERIALS AND METHODS

We used the following tools and libraries for the described work: Microsoft Visual C++® 5.0, DICOM library of the University of California Davis Medical Center (UCDMC), JPEG library of the Independent JPEG Group (IJG), the TIFF library of Sam Leffler (Silicon Graphics Inc.), and the DOME Image Processing Library (DIMPL) of DOME, Inc.

6. ACKNOWLEDGEMENTS

This work was supported by the National Library of Medicine, contract No. N01-LM-6-3547 and a scholarship from the Deutsche Forschungsgemeinschaft.

7. REFERENCES

1. Kuay, Daniel D., and Kenney, Paul, “Performance monitoring in a client/server environment”, *Enterprise Systems Journal* 11(5), pp. 54-63, 1996.
2. Huang, H.K., Wong, A.W., Lou, A., et al., “Clinical Experience with a second-generation hospital-integrated picture archiving and communication system” *Journal of Digital Imaging*, 9, pp151-166, 1996.
3. Huang, H.K., Lou, S.L., Wong, W.K., “PACS pitfalls and bottlenecks”, in: Horii, S.C., Blain G. J. (edts.) *PACS Design and Evaluation: Engineering and Clinical Issues*, Proc. SPIE, 3053, pp 2-5, 1997
4. Lou, S.L., Huang, H.K., and Arenson, R.L., “Workstation Design”, *Radiologic Clinics of North America*, 34(3), pp. 525-544, 1996.
5. Zhang, J., Song, K., Huang, H.K., Wong, A.W., and Stahl, J., “Tele-Consultation for Thoracic Imaging” *Radiology* 205(P), p 743, 1997.

Diagnostic Workstation for Digital Hand Atlas in Bone Age Assessment

Fei Cao, H.K. Huang, E. Pietka, Vicente Gilsanz, Steven Ominsky

Department of Radiology, University of California, School of Medicine, San Francisco, CA 94143-0628

ABSTRACT

Bone age assessment by a radiological examination of a hand and wrist image is a procedure frequently performed in pediatric patients to evaluate growth disorders, determine growth potential in children and monitor therapy effects. The assessment method currently used in radiological diagnosis is based on atlas matching of the diagnosed hand image with the reference set of atlas patterns, which was developed in 1930s and is not fully applicable for children of today. We intend to implement a diagnostic workstation for creating a new reference set of clinically normal images which will serve as a digital atlas and can be used for a computer-assisted bone age assessment. The diagnostic workstation consists of a 200Mhz Sun Ultra 2 with 14 gigabyte fast-wide SCSI disks, one creator display board and one 1K display monitor. The reference radiographs from CR system and film scanner are stored in the local disks of the diagnostic workstation for rapid image and data retrieval. User interface, image display and feature extraction software have been developed on this diagnostic workstation for creating the digital atlas. We'll then develop a software package for the computer-assisted bone age assessment which will extract radiological findings from a patient image and allow for their comparison with corresponding values extracted from this digital atlas. By the end of this study there will be a medically accepted standard digital atlas. It will remove the disadvantages of the currently out-of-date one and allow the bone age assessment to be computerized and standardized.

In this paper, we describe the initial data-collection and system setup phase of this five-year research program. We presents the system design, user interface and software tools for collection, visualization and management of clinical hand and wrist images for the reference atlas and concurrent comparison study.

Keywords: digital atlas, pediatric radiology, hand image, skeletal age assessment, computers

ACKNOWLEDGMENT

This research is partially supported by a NIH Grant No. R01-LM06270.

Migration of the Digital Interactive Breast Imaging Teaching File

Fei Cao[1], Edward A. Sickles[2], H.K. Huang[3], Xiaoqiang Zhou[4]

Department of Radiology, University of California, School of Medicine, San Francisco, CA 94143-0628

ABSTRACT

The digital breast imaging teaching file developed during the last two years in our laboratory has been used successfully at UCSF (University of California, San Francisco) as a routine teaching tool for training radiology residents and fellows in mammography. Building on this success, we have ported the teaching file from an old Pixar imaging/Sun SPARC 470 display system to our newly designed telemammography display workstation (Ultra SPARC 2 platform with two DOME Md5/SBX display boards). The old Pixar/Sun 470 system, although adequate for fast and high-resolution image display, is 4-year-old technology, expensive to maintain and difficult to upgrade. The new display workstation is more cost-effective and is also compatible with the digital image format from a full-field direct digital mammography system. The digital teaching file is built on a sophisticated computer-aided instruction (CAI) model, which simulates the management sequences used in imaging interpretation and work-up. Each user can be prompted to respond by making his/her own observations, assessments, and work-up decisions as well as the marking of image abnormalities. This effectively replaces the traditional "show-and-tell" teaching file experience with an interactive, response-driven type of instruction.

Keywords: digital imaging; display; breast imaging; computer-aided instruction; education aid

1. INTRODUCTION

Routine screening with periodic mammography has been proved to be effective for early detection of breast cancer and in lowering its death rate[1-2]. Because of limited resources and facilities to provide hands-on instruction in breast imaging interpretation, there is a need to develop an alternate method to supplement or replace the current film-based teaching file method of training. A digital-based system can alleviate this shortage since a digital teaching file can be duplicated easily and disseminated widely, to be used simultaneously by many individuals at different sites for continuing medical education. This promises to improve the quality of breast imaging interpretation, and thereby facilitate mass screening with mammography and the problem-solving imaging evaluation of screening-detected abnormalities.

During the last two years, we have developed a digital breast imaging teaching file on a 2K high-resolution display workstation which is built on the Pixar imaging/Sun SPARC 470 platform [3]. This digital teaching file has been used successfully at UCSF (University of California, San Francisco) as a routine teaching tool. It is available to all radiology residents, fellows, staff radiologists, and visiting radiologists for continuing medical education at UCSF. All radiology residents are now required to complete a set of 25 cases in the digital teaching file during each 4-week breast imaging rotation at UCSF. We also have incorporated use of the digital teaching file into several of the San Francisco-based postgraduate breast imaging courses given at UCSF. The digital teaching file currently contains 50 active cases, with approximately 500 digital mammograms and approximately 800 questions. It takes about 10 hours for an average user to complete a 50 case set. Dr. Sickles and his associates are constantly adding new cases, thereby replenishing the teaching file with new material. Mammograms of 200 carefully selected cases have been scanned in and maintained in digital format, from which active case sets will be updated periodically.

Building on this success, we have ported the teaching file from an old Pixar imaging/Sun SPARC 470 display system to our newly designed telemammography display workstation [4] (Ultra SPARC 2 platform [Mountain View, CA] with two DOME [Waltham, Mass] Md5/SBX display boards). The old Pixar/Sun 470 system, although adequate for fast and high-resolution image display, is 4-year-old technology, expensive to maintain and difficult to upgrade. The new display workstation is more

---

Further author information

[1] F.C.(correspondence): Email: fcao@lri.ucsf.edu; WWW: http://www.lri.ucsf.edu; Tel: 415-502-4288; Fax: 415-502-3217

[2] E.A.S.: Email:edwards@email.his.ucsf.edu; Tel: 415-885-7417; Fax: 415-885-7829

[3] H.K.H.: Email: bernie.huang@radiology.ucsf.edu; WWW: http://www.lri.ucsf.edu; Tel: 415-476-6044; Fax: 415-502-3217

[4] X.Q.Z.: Email: zhou@lri.ucsf.edu; Tel: 415-502-4286; Fax: 415-502-3217

cost-effective and is also compatible with the digital image format from a full-field direct digital mammography system. This system provides mammograms already in digital format, which can be selected and incorporated easily into the digital teaching file.

2. THE PROCESS OF MIGRATION

Migrating of a large clinic application, such as the digital teaching file, to a new display system is not a trivial task. A portability issue arises regarding different hardware, operating system, image format and display software.

old 2K display station

The old 2K mammography display station is sketched in Figure 1. The old 2K station is based on a Sun Sparc 470 workstation, two 21˝ diagonal 2K MegaScan monitors, Pixar image processing hardware and a 7 GByte fast storage disk, packaged by Vicom Inc. (Fremont, CA) .

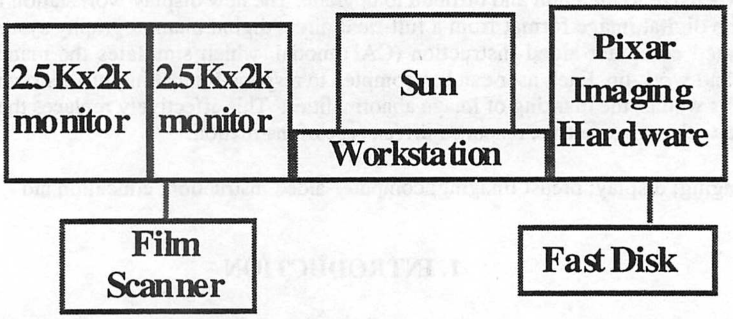

Figure 1. Configuration of old 2K display station.

The Sun 470 workstation (64MB system memory) serves as a platform for the display station. Each of two gray scale monitors has 10 bit resolution and is able to display 2560 scan lines, each with 2048 pixels. The Pixar image processing system can directly access the digital image stored in the fast-disk. A 10MB digital mammogram takes less than 2 seconds to retrieve from the fast-disk and display on the 2K monitors. The Pixar hardware also comes with two 32MB frame buffers and optimized image processing routines. This makes it possible for four mammograms (<10MB each), in a typical display mode, to be easily manipulated on screen in nearly real time. The 7 GB fast-disk is capable of storing 1,000 digital mammograms for fast retrieval by the Pixar system.

new 2k display system

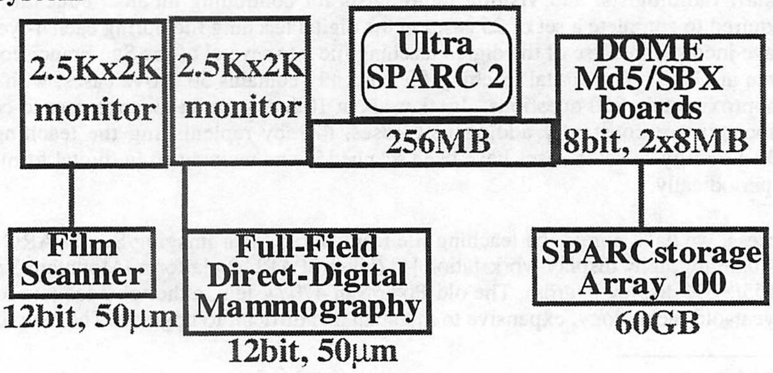

Figure 2. Configuration of new 2K display station.

The new 2K telemammography display station is sketched in Figure 2. This display system was designed in our lab for viewing the 4K x 5.6K breast images from the full-field direct digital mammography system developed by Fischer Imaging Company(Denver, CO) [4]. The display workstation uses the Sun Sparc Ultra-2 platform with one

200 MHz CPU and 256 MByte of memory, two DOME MD5-SBX boards with 8 MByte frame buffer, two 2K x 2.5K Data Ray monitors (Westminster, CO), and Sun Enterprice3000 disk array (Mountain View, CA);

The success of our digital teaching file is due to three factors: (1) high-resolution display which is able to show an entire breast with such fine detail that tiny structures are readily visible; (2) sophisticated computer-aided instruction (CAI) model in simulating an interactive teaching session, especially allowing the user to identify abnormalities by marking displayed images, which is one of key elements in breast imaging interpretation. (3) large set of cases, selected and prepared by expert radiologists, and easy to maintain and replenish. All of those involve with the image display and processing, which is quite different for the old and new display systems.

Following is the portability table summarizing the process of migration we have completed from the old Sun470/Pixar imaging system to the new Ultra 2/DOME MD5-SBX display system.

	Old System Sparc470/Pixar/FD	**New System** SparcUltra2/Dome board	**Compatible**
Operating System	SunOS4.1.3	Solaris 2.5.1	no
User Interface	Xview3.0	Xview3.2	yes
Coding	C	C	yes
Image Display & Processing	Pixar Chap Lib	XIL1.3 (Sun X Image Lib)	None
Digital Image Format	Pixar picio tile ACE-NEMA2.0	Raw & DICOM	no
Teach File Text	plain text	plain text	yes
ROI Data	binary	binary	Conversion

Table 1. Porting guide

Much of our porting efforts are in converting the image display and processing software from the special Pixar image library to XIL (X Image Library). The XIL library is an imaging API (Application Program Interface) that provides a broad set of functions for imaging and video applications. The XIL library is part of a strategy for low-level software interfaces (foundation libraries) and enables imaging library and imaging application developers to port their code to these foundation libraries. The XIL library is hardware-independent image processing library which is MT-hot and fully supported by Sun and is also compatible with DOME MD5-SBX board. The image formats are also converted from the Pixar-specific picio tile and old ACE-NEMA2.0 standard ones to Raw and current DICOM standard formats. The porting from the old to the new display system has made our digital teach file up to date with current standards and technologies, which makes it possible to maintain and future upgrade the digital teaching file.

comparison of image display quality and speed

A mammography display has to be able to portray the entire breast with such fine detail that tiny structures are readily visible. This must be done at near real-time speed. The quality of digital mammograms is highly dependent on the acquired image resolution and display system hardware, while the speed of image display and on-screen image manipulation is determined by system hardware architecture and image processing software.

It is noted that the image display and manipulation on the old Pixar system is faster, and the image quality is also better than the DOME display boards. The faster imaging speed on the old system is due to its special hardware design. Pixar image hardware with two large frame buffers (2 x 32 MByte) and optimized processing software makes the fast on-screen image manipulation possible. The transfer of image data between disk storage and the image computer accounts for a substantial percentage of the total time consumed during an imaging job. The principal difference between the Fast-Disk subsystem used in the old display workstation and a conventional hard disk is the high data throughput rate. The Fast-Disk subsystem achieves its speed by distributing each input/output operation over the four drives within the system. In addition to the high data transfer rate, the Fast-Disk subsystem also operates in conjunction with the Pixar imaging system to deliver data directly to the frame buffers without a layover in the memory of the host . In comparison, the two DOME MD5-SBX boards come only with two 8 MByte frame buffers and use the host computer's memory for image transfer and manipulation. Preliminary results indicate that a 10-MByte digital mammogram takes less than 2 seconds to retrieve from the Fast-Disk and display on the old Pixar system while it takes about 4 seconds for the new Ultra2/DOME system. The 10bit display resolution on the Pixar system is also superior to the Dome's 8bit resolution display.

However, the display speed and the image quality from the new Dome MD5-SBX boards are found to be adequate and acceptable for a clinical application such as our digital teaching file. Furthermore, the new display system costs much less, and is much easier to maintain and upgrade than the old Pixar system.

INTERACTIVE DIGITAL BREAST IMAGING TEACHING FILE: AN EXAMPLE

The implementation method and the CAI model of the digital teaching file have been fully described in our online paper[3]. The CAI model simulates clinically relevant work-up sequences and provides an interactive learning environment.

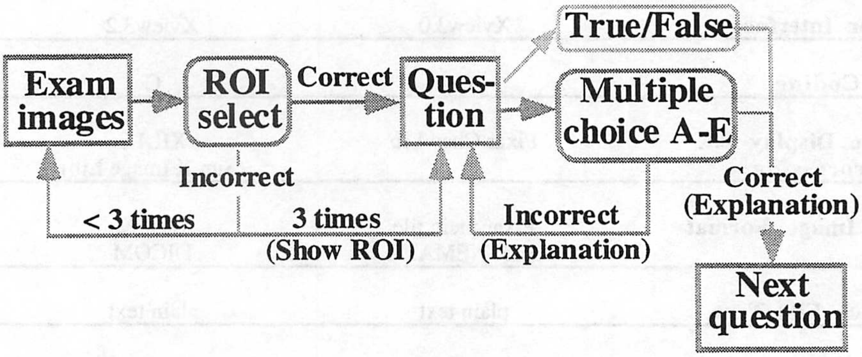

Figure 3. A general algorithm for the CAI model and basic work-up sequences

Figure 3 shows the general control flow of this model and imaging work-up sequences. At the start of each case, the system first gives a brief description of the case history and then presents to the user a set of initial screening mammograms. After examination of those images, the user is asked to use a mouse pointer, identifying on the 2K monitors any mammographic abnormalities. The user's selection is compared with pre-recorded region of interest (ROI) data. If the user succeeds in identifying the ROI, he/she will proceed to a multiple choice or true/false question that is relevant to his/her findings, or the user must try again. If a user has not marked the abnormality after three tries, the system will display the ROI on the 2K monitor, accompanied by an explanation; the user then proceeds to the next question. Based on user response to a question, the computer system presents different work-up sequences, defined in the CAI model as illustrated in Figure 3. The system provides instructions, explanations, and answers to the question, guiding the user toward the next question. During this process, additional images are displayed whenever appropriate. This control flow serves, in a structural way, to aid the user in navigating through the medical knowledge embedded in the teaching file cases.

an example

Following is an example of Case 1 in the digital teaching file. The breast images are shown on the two 2K monitors, while the questions and answers are displayed on the Console monitor

> *CASE 1. 46 year old asymptomatic woman undergoing baseline screening mammography.*
>
> *The next set of questions will ask you whether there is an important mammographic finding on each of the 4 displayed images, and if so, to indicate the location of that finding. Press the Question button once you have fully evaluated the mammographic images.*

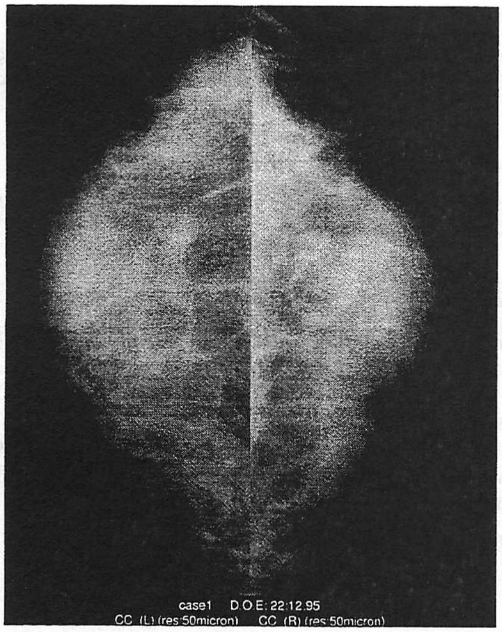
case1 D.O.E: 22.12.95
CC (L) (res:50micron) CC (R) (res:50micron)

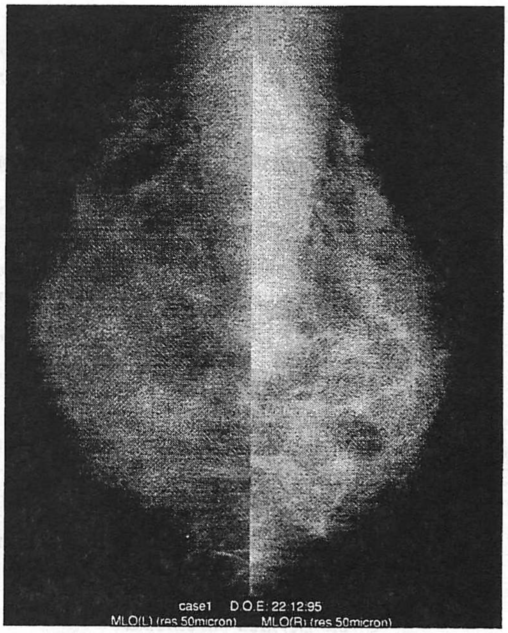
case1 D.O.E: 22.12.95
MLO(L) (res 50micron) MLO(R) (res 50micron)

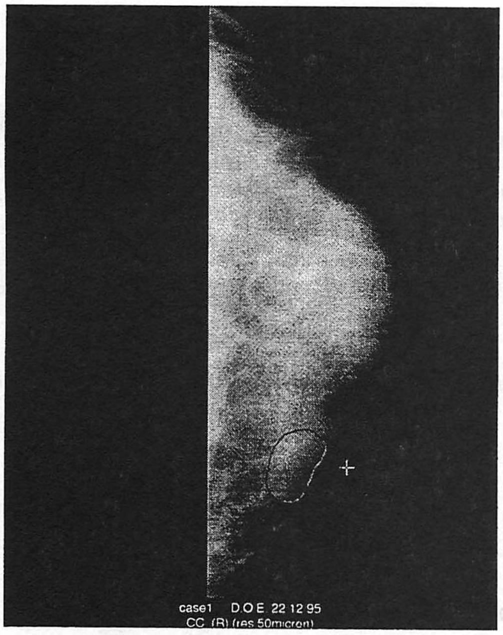
case1 D.O.E 22.12.95
CC (R) (res 50micron)

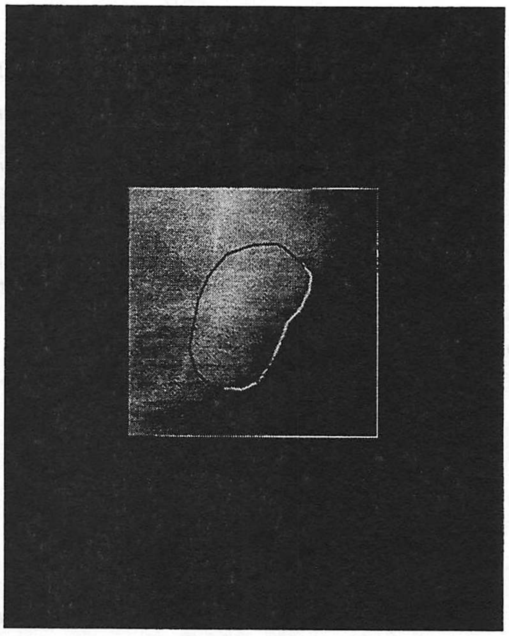

For an example, select the mammographic findings on CC and MLO views of the right breast.

> *Press the ROI-Select button and then use the mouse to point at and select the one mammographic finding that is MOST important on this CC view of the right breast. If there is no important finding, press the middle mouse button.*

The system will display one of the following messages on screen, corresponding to a user's selection

> *INCORRECT. You have not selected the most important mammographic finding on this view, or there is no important finding. CHOOSE AGAIN. Press the question button to repeat this question.*
>
> *CORRECT. There is a noncalcified density in the medial aspect of the right breast on this CC view. Press the Question button to continue to the MLO view of the left breast.*
>
> *You have still not selected the most important mammographic finding. For your assistance, the finding is now highlighted on the monitor. Press the Question button to continue to the next question.*

Then continue to the MLO view of the right breast as shown in the next figure with the finding highlighted on the left monitor and a zoom-in box on the right monitor. After the user has identified the abnormalities on each of the four images, the CC and MLO views of the right breast are shown on the two 2K monitors and the user is then asked to answer the following multiple choice question regarding the mammographic abnormality

> *Which one of the following choices BEST describes the mammographic abnormality in this case?*
>
> A. *Focal asymmetric density*
>
> B. *Circumscribed carcinoma*
>
> C. *Architectural distortion*
>
> D. *Noncalcified mass*
>
> E. *Fibroadenoma*

For the user's choice, such as (A) or (D), the system will response with

> A. *A focal asymmetric density is defined as an asymmetry of fibroglandular-tissue density with similar shape on two views, but lacking the convex-outward borders and conspicuity of a true mass. While such a finding may represent an island of normal fibroglandular tissue, its lack of specific benign characteristics may warrant further evaluation. However, the images provided do not portray a lesion that fits the criteria that define a focal asymmetric density. CHOOSE AGAIN. Press the Question button to repeat this question.*
>
> D. *CORRECT. A mass is a space occupying lesion seen on two projections, with convex-outward borders, usually denser in the center than at the periphery. Press the Question button to continue to the next question.*

Two more follow-up questions

> *Which one of the following choices BEST describes the location of the mammographic abnormality in this case?*
>
> A. *Upper inner quadrant*
>
> B. *Upper outer quadrant*
>
> C. *Lower outer quadrant*
>
> D. *Lower inner quadrant*
>
> *Which one of the following choices indicates the MOST appropriate next step in the imaging work-up?*
>
> A. *Surgical biopsy*
>
> B. *Follow-up mammography in 6 months*
>
> C. *No additional studies are necessary (likely diagnosis, intramammarylymph node).*
>
> D. *Ultrasonography*
>
> E. *Correlation with physical examination*

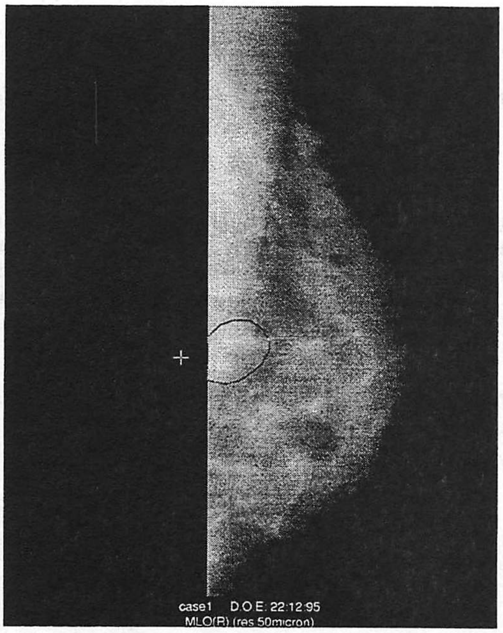
case1 D.O.E: 22:12:95
MLO(R) (res 50micron)

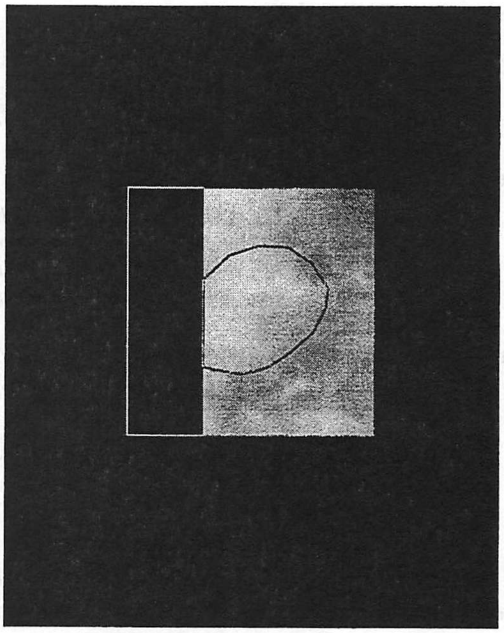

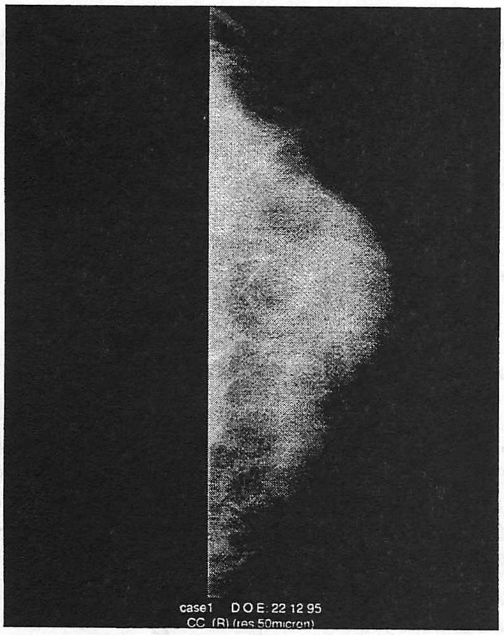
case1 D.O.E: 22:12:95
CC (R) (res 50micron)

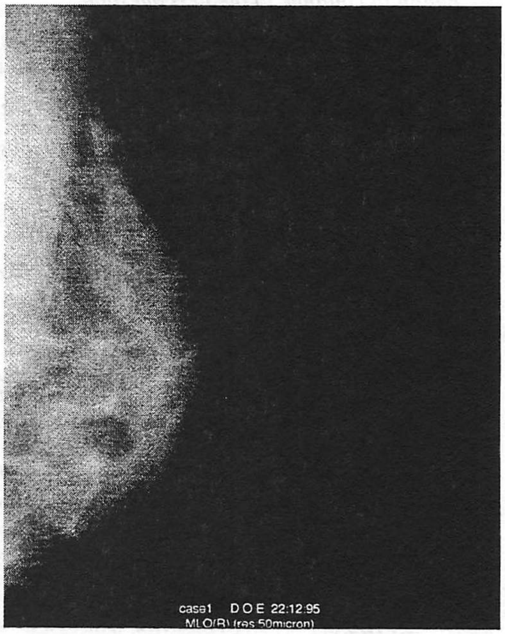
case1 D.O.E: 22:12:95
MLO(R) (res 50micron)

Then standard TRUE/FALSE question

The following four questions are TRUE/FALSE questions concerning the use of breast ultrasonography.

Ultrasonography is important in the work-up of lesions seen on mammography because it reliably distinguishes between cystic and solid masses. (TRUE/FALSE)

If the user's answer is TRUE

You answered TRUE. This is CORRECT. The diagnostic accuracy of ultrasonography in distinguishing simple cysts from solid and complex cystic lesions approaches 100%, if rigid interpretive criteria are utilized. For reliable characterization of a mass as a simple cyst, it should show smooth and well-defined margins, increased through transmission of sound, and be completely anechoic. Press the Question button to continue to the next question.

Next three TRUE/FALSE questions and then followed by

Based on the displayed sonographic images, which one of the following choices indicates the MOST appropriate next step in the work up?

A. Aspiration under sonographic guidance, followed by pneumocystography

B. Surgical biopsy

C. Doppler ultrasound examination

D. Spot-compression magnification mammography

If the user makes a right choice (D), the system will response with

D. CORRECT. The mass is presumed to be solid since it does not display the full complement of sonographic features characteristic of a simple cyst. Spot-compression magnification mammography will provide improved definition of the margins of the mass, and thus may guide management recommendations. Press the Question button to continue to the next question.

Question 9. Based on the displayed additional spot-compression magnification view, which one of the following choices indicates the MOST appropriate management recommendation for this case?

A. Needle localization prior to open surgical biopsy

B. Percutaneous image-guided core biopsy

C. 3 month follow-up mammography

D. 6 month follow-up mammography

E. Routine mammographic screening in one year

For the correct answer, the system will response with

D. CORRECT. The probability of carcinoma for a noncalcified, circumscribed, solid mass is only 1% to 2%. This would result in the need to excise or obtain tissue samples from 50 to 100 lesions in order to identify only one cancer. These procedures are more invasive and more expensive than periodic mammographic surveillance. Furthermore, two independent large-scale prospective studies of long-term mammographic follow-up of such "probably benign" masses have shown that those few lesions which actually are malignant indeed are correctly diagnosed by interval mammographic change while they still remain curable and amenable to treatment with breast conservation surgery. Indeed, the major prognostic factors (tumor size, axillary lymph node status, and tumor stage) of such cancers, although excised months to years after they first were detected, are just as favorable as those for screening-detected cancers.

**** EPILOG *** -> The patient returned in 6 months and the finding was stable in appearance (films not shown). The finding is therefore even more probably benign than had been thought before. Continued mammographic surveillance is needed, at lengthening intervals. Most radiologists would stop requesting mammographic surveillance after two or three years of stability. Following such a protocolreduces both morbidity and cost by substantially decreasing the number of open surgical and percutaneous biopsies performed for benign masses. It does not compromise the identification of early-stage, favorable-prognosis cancers.*

END of Case 1. Press the Question button to begin the next case.

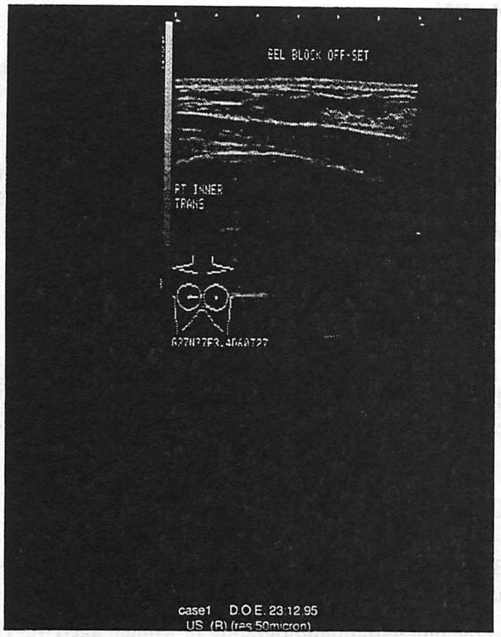
GEL BLOCK OFF-SET
RT INNER
TRANS
622H27F3.4D60T27
case1 D.O.E: 23:12:95
US (B) (res:50micron)

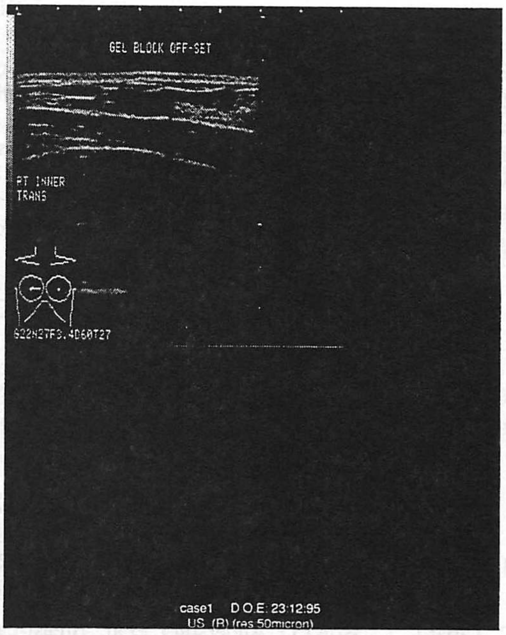
GEL BLOCK OFF-SET
RT INNER
TRANS
622H27F3.4D60T27
case1 D.O.E: 23:12:95
US (B) (res:50micron)

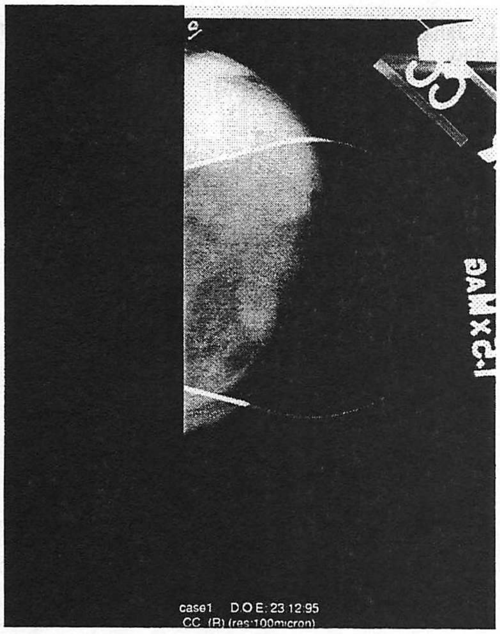
1.5MAG
case1 D.O.E: 23:12:95
CC (B) (res:100micron)

SUMMARY

We have successfully ported the digital teaching file from the old one with the SunOS/Pixar imaging system to the new one with the Solaris/DOME board display system. The new display system is compatible with the current display technology, and also more affordable and easy to maintain. Especially, the large quantity of breast images have been converted to the current standard format, and the image display and processing software have been ported to the fundamental XIL library which is hardware-independent and available for free. This migration from the old system to the new one not only insures maintaining and replenishing of our current digital teaching file, but also makes it possible to distribute the UCSF digital teaching file to other institutions, in an affordable price, for training radiologists in breast imaging.

ACKNOWLEDGMENT

This work is supported by the U.S. Army Medical Research and Material Command under Contracts No. DAMD17-94-J-4338 ("A Digital Breast Imaging Teaching File") and DAMD17-96-C-6111 ("Full-field Direct Digital Telemammography"), and the California Breast Cancer Research Program: "Real-time Telemammography" under Contract No. IRB-0148.

REFERENCES

1. Smart CR, Hendrick RE, Rutledge JH, Smith RA. Benefit of mammography screening in women ages 40 to 49 years: current evidence from randomized controlled trials. *Cancer* 1995; 75:1619-1626.
2. Tabar L, Larsson LG, Anderson I, et al. Breast-cancer screening with mammography in women aged 40-49 years. *Int J Cancer* 1996; 68:693-699.
3. Cao F, Sickles EA, Huang HK. Interactive digital breast imaging teaching file. RSNA, EJ 1 (1997): 26 pars. Online. Available HTTP: http://ej.rsna.org/EJ_0_96/0037-97.fin/mammo.html. 18 July 1997.
4. Lou SL, Sickles EA, Huang HK, Cao F, Hoogstrate D, Jahangiri M. Full-field direct digital telemammography--preliminary. Proc SPIE Med Imaging 1997; 3035:369-379.

Presurgical multimodality neuroimaging analysis for complex partial seizures

Stephen T. C. Wong[a,b], Kent Soo Hoo Jr.[b], Robert C. Knowlton[d], Kenneth D. Laxer[a], Randall A. Hawkins[a], Howard Rowley[a], Michael W. Weiner[a,c]

[a]University of California, School of Medicine, San Francisco CA 94143-0840
[b]Bioengineering Graduate Program, University of California, San Francisco CA 94143-0640
[c]SFVA Medical Center, San Francisco CA 94121
[d]Swedish Medical Center, Seattle WA 98114-0999

ABSTRACT

Surgical treatment of patients suffering from complex partial seizures requires the localization of the epileptogenic zone for surgical resection. Currently, clinicians utilize electroencephalography (EEG), psychological tests, and various neuroimaging modalities together to determine the location of this zone. We investigate the use of positron emission tomography (PET), magnetic resonance imaging (MRI), and magnetic resonance spectroscopy (MRS) in the presurgical workup and analysis of patients with complex partial seizures. The results of imaging studies of 25 patients are compared for lateralization accuracy and relative concordance.

1. INTRODUCTION

Epilepsy refers to a tendency toward recurrent seizures, i.e., paroxysmal derangement of cerebral function due to uncontrolled, excessive discharges from an aggregate of neurons. As a population, patients with epilepsy are undereducated, underemployed, and have a life span approximately 10 years less than their peers[1]. The total cost of epilepsy taking into account unemployment, underemployment, excess mortality, long-term treatment, residential care including institutionalization, costs of drugs, vocational rehabilitation, and special education at the time of the epilepsy commission, is estimated at between 3 and 4 billion dollars per year[2].

Despite the advances made in anti-epileptic drugs, about 25% of epilepsy patients have seizures uncontrolled by medical treatment, i.e., medically refractory. Approximately half of these patients are candidates for surgical treatment. Surgical planning of epilepsy requires the accurate identification of the area of the brain responsible for seizure onset, known as the epileptogenic zone. It has been estimated that approximately 125,000 patients of medically refractory epilepsy in the United States may be suitable candidates for surgical treatment[3], and an estimated 5,000 per year are added to this patient population.

The importance of surgical treatment was recently confirmed by an NIH (National Institutes of Health) consensus conference[3]. The best surgical outcomes are obtained when the various preoperative localizing examinations, e.g., video electroencephalography telemetry (VET) and magnetic resonance imaging (MRI), are concordant, implicating the same brain region as the epileptogenic zone. Unfortunately, a number of patients have either discordant or non-conclusive imaging data.

Currently, intracranial electroencephalography (EEG) recording is the gold standard for evaluating surgical candidates of medically refractory epilepsy. An intracranial EEG study is an invasive surgical procedure which requires placing electrodes directly on the surface of the brain or within the brain itself for recording brain electrical activity during spontaneous seizures to determine where they originate. This array of electrodes remains in the patient from a week to a few weeks for seizure onset monitoring. There are definite risks (6% to 8% morbidity rate) and considerable costs associated with such an invasive procedure ($40,000 to $80,000 per study which includes intracranial EEG monitoring in the hospital).

These invasive and expensive procedures are not performed unless the results of noninvasive studies permit formulation of a reasonable guess about the possible lateralization or location of a resectable epileptogenic region. Usually, the noninvasive presurgical evaluation must identify lateralization choices before invasive testing can be planned.

For further author information -
S.T.C.W.: Email: SWONG@LRI.UCSF.EDU; Web: http://WWW.LRI.UCSF.EDU/~SWONG; Telephone: 415-476-6542; Fax: 415-502-3217

Technological advances in medical imaging bring forth many new noninvasive techniques that not only help to lateralize the epileptogenic region with reasonable certainty before invasive EEG recording is performed, but can also eliminate or reduce the frequency of such invasive testing. The technological revolution began with positron emission tomography (PET) scanning and the ability to display regional metabolic dysfunctions associated with epileptogenic zones. MRI followed, providing unsurpassed anatomic detail to detect structural abnormalities. Research studies utilizing PET and magnetic resonance spectroscopy (MRS) separately have demonstrated noticeable metabolic abnormalities in the epileptogenic zone.

Multiple imaging methods are available to aid in lateralizing complex partial seizures. To reduce the need for intracranial electrodes and to localize the epileptogenic zone with a higher degree of confidence, 2-[18F]fluoro-2-deoxy-D-glucose (FDG) PET and MRI are used to provide confirmatory localizing information. Relative temporal lobe (TL) hypometabolism on FDG-PET and hippocampal atrophy or prolonged T2 on MRI reliably predict lateralization of the epileptogenic zone.[4,5] FDG-PET may demonstrate diminished glucose uptake associated with epileptogenic substrates even when the MRI is unremarkable. MRI-PET findings, however, may be non-localizing when structural and metabolic disturbances are widely distributed or equivocal, or when no abnormality is revealed. ^{1}H-MRS has been used to detect unilateral and bilateral metabolite abnormalities in patients with epilepsy.[6] Unlike EEG, which provides direct evidence of the origin of seizures, MRI, PET, and ^{1}H-MRS provide only indirect evidence of potential epileptogenic zones. Unfortunately, scalp-recorded EEG does not always yield clear localization of the epileptogenic zone either, and the relationship of EEG-detected abnormalities to structural lesions may be ambiguous. The significance of many structural and functional imaging abnormalities cannot be interpreted in isolation.

This study compares FDG-PET, MRI, and ^{1}H-MRS in patients suffering from complex partial seizures. The high resolution FDG-PET is compared with quantitative MRI techniques and ^{1}H-MRS in the lateralization of the epileptogenic zone. The analysis of imaging data is carried out on a computer-assisted diagnostic workstation developed in our laboratory.

2. DIAGNOSTIC WORKUP OF EPILEPSY

Figure 1 outlines the general diagnostic workup for presurgical epilepsy diagnosis[7]. A patient who enters this workup is medically refractory as determined by patient history suggesting partial epilepsy and failure of drug treatment. EEG and MRI are routinely used to classify seizures and localize the epileptogenic zone. MRI provides visualization of brain anatomy with detail greatly surpassing that of any imaging modality, including x-ray computed tomography (CT). The spatial resolution provided by MRI has greatly improved the detection of most mass lesions or tumors. Detection of structural lesions in epilepsy makes surgical evaluation relatively straightforward. Many epilepsy cases, however, do not exhibit structural abnormalities in MR images. Further, paroxysmal abnormalities occur intermittently and may not be easily captured in EEG recordings. Prolonged inpatient recording with video EEG telemetry (VET) is necessary to capture spontaneous seizures.

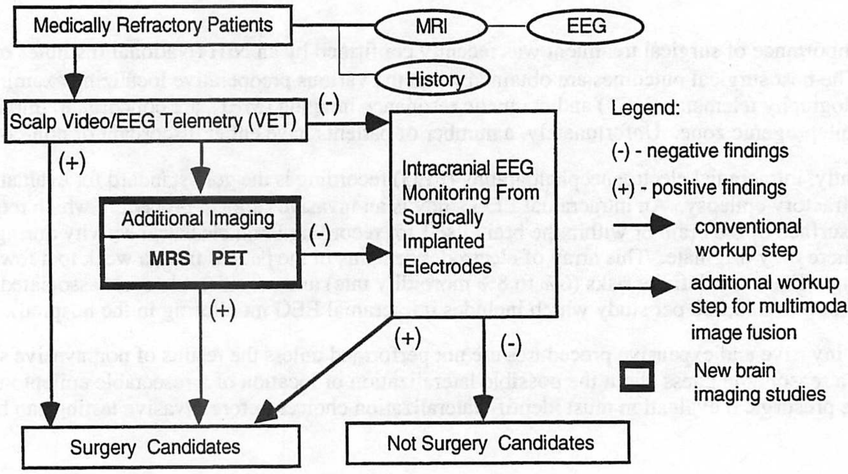
Medically Refractory Patients
MRI
EEG
History
Scalp Video/EEG Telemetry (VET)
(-)
(+)
Legend:
(-) - negative findings
(+) - positive findings
conventional workup step
additional workup step for multimodal image fusion
New brain imaging studies
Intracranial EEG Monitoring From Surgically Implanted Electrodes
Additional Imaging
MRS PET
(-)
(+)
(+)
(-)
Surgery Candidates
Not Surgery Candidates

Figure 1. Diagnostic workup of epilepsy surgical candidates. Neuroimaging modalities are being applied to noninvasive surgical planning of patients with complex partial seizures in hopes to minimize the need for invasive intracranial EEG tests; this contributes major savings in cost, reduced patient risks, and increased center capacity.

Positive results from MRI and VET in localizing the epileptogenic zone typically indicates an outcome of becoming seizure free by surgery. Non-concordance between MRI and VET almost invariably requires invasive EEG recordings with either one or more of the following: subdural strips, arrays, and stereotactically inserted depth electrodes. For example, approximately 35% to 40% of medically refractory epilepsy patients in the Northern California Comprehensive Epilepsy Center operated on at the University of California at San Francisco (UCSF) require invasive intracranial EEG monitoring. The average cost of intracranial EEG is about $60,000 per evaluation and amounts to about $2 million to $3 million per year in the UCSF Epilepsy Center alone for performing this pre-operative procedure.

The UCSF Epilepsy Center is currently performing additional imaging examinations, i.e., ^{1}H-MRS, and PET, on selected epilepsy patients before coming to invasive evaluation. These additional imaging tests cost about $3,000 to $4,000 per patient, a fraction of the cost (< 10%) of an intracranial EEG study. All neuroimaging studies of these patients are collected for computer analysis. The use of combined noninvasive tests to reduce the number and improve the accuracy of intracranial EEG recordings will help to reduce the cost of presurgical evaluation, minimize patient risk, and improve surgical outcome. In addition, a better understanding of decision thresholds from multimodal imaging analysis should improve the selection of candidates for surgery by increasing the identification of patients with previously unlocalized seizure origination.

Nevertheless, an effective means to access, manipulate, and correlate large, heterogeneous multidimensional medical images was lacking. We thus developed a computer-aided diagnostic (CAD) workstation for epilepsy surgical planning to fulfill this need. This medical workstation aims to provide an environment for optimal interpretation of multiple non-invasive image modalities by combining functional information of PET and ^{1}H-MRS with structural MRI anatomy, both qualitatively and quantitatively. Since there is currently little knowledge about the patient populations with positive and negative findings of various imaging and intracranial EEG studies, the data extracted will also be essential for outcome analyses to identify inefficient or duplicative evaluation procedure.

3. INFRASTRUCTURE FOR MULTIMEDIA DATA MANAGEMENT

Our computer-aided neurodiagnostic workstation system is built on top of the existing picture archiving and communication system (PACS) infrastructure at UCSF. PACSs have been the prevalent means for acquisition, storage, communication, and display of digital images related to radiological practice during the last decade[8]. A PACS integrates image acquisition devices, computers, communication networks, image display workstations, and database management systems. Its operations can be summarized as follows: (i) Digital images generated in an examination are captured by an acquisition computer and sent immediately to a central database for long term archive; (ii) these images then will be retrieved later from the central archive and transmitted to display at a remote medical display station automatically or upon the user's request; and (iii) diagnostic findings of viewing these images are appended to the images at the central archive.

4. COMPUTER ASSISTED SURGERY PLANNING

In Figure 2, we show the distributed system architecture of the CAD workstation together with the computer-aided workup steps that the workstation supports. The medical workstation provides a multimedia user interface to: (1) access medical data stored in the PACS file archive and the neuroimaging database and (2) analyze the retrieved data for noninvasive surgical planning of epilepsy[9]. For security reasons, all user queries from non-daily clinical operations pass through a multimedia data file server, which acts as a "firewall" against unauthorized access to the PACS central archive. All computers are SUN SPARC workstations running SUN OS, excepting the neuroimaging database server that resides in a 4-processor SUN SPARC 690 MP running Solaris Operating System. The multimedia user interface of the medical workstation is built on top of the Gain Momentum software package (Gain Technology Division, Sybase, Palo Alto, CA) and X window programming environment. Currently, not all the brain imaging modalities involved in epilepsy surgical planning have been archived into UCSF PACS. Nuclear medicine PET image datasets are manually archived into the neuroimaging database using the File Transfer Protocol (FTP). The neurodiagnostic workstation includes the routing table on which to retrieve these PET image files upon user query.

Image registration and combination. Heterogeneous medical data retrieved from PACS or neuroimaging database are combined and rendered into 2D or 3D images. The visualization work is done in cooperation with the VIDA (volumetric image display and analysis) project at the University of Iowa Medical College. Before any data combination and analysis, however, medical image registration is often required to geometrically align two or more brain image volumes so that voxels representing the same underlying anatomical structure may be superimposed or directly compared. A pair of image volumes might be from the same subject and the same modality (but taken at different positions or different scanning instruments), from the same subject but different modalities, or from the same modality but different subjects.

Our registration strategy in this multimodal image fusion application is to have the high resolution, structural MRI dataset as the reference point for mapping across different imaging modalities. The MRI-MRS registration is straightforward: The MRS scans are performed immediately after the MRI examination of the patient using the same MR scanner (GE Signa or Siemens Vision) such that there is no change of the patient's head position. For the MRI-MRI, PET-PET, and MRI-PET image pairs, we implemented the technique of ratio image uniformity (RIU) described by Woods[10]. For the RIU technique, the translation and rotation parameters were determined such that they minimized the voxel-by-voxel variance of the "ratio" image. The MRI volumes were stripped to remove the skull and scalp (the removal process is done semi-automatically) prior to calculating the ratio image for MRI-PET registration. RIU algorithms then iteratively minimize the ratio image variance using a modified Newton-Raphson method based on explicitly computed derivatives of the variance with respect to each of the registration parameters[10]. Recent study confirms that registration optimization based on measurement of the similarity of spatial distributions of voxel values is superior to techniques that do not use such information[11].

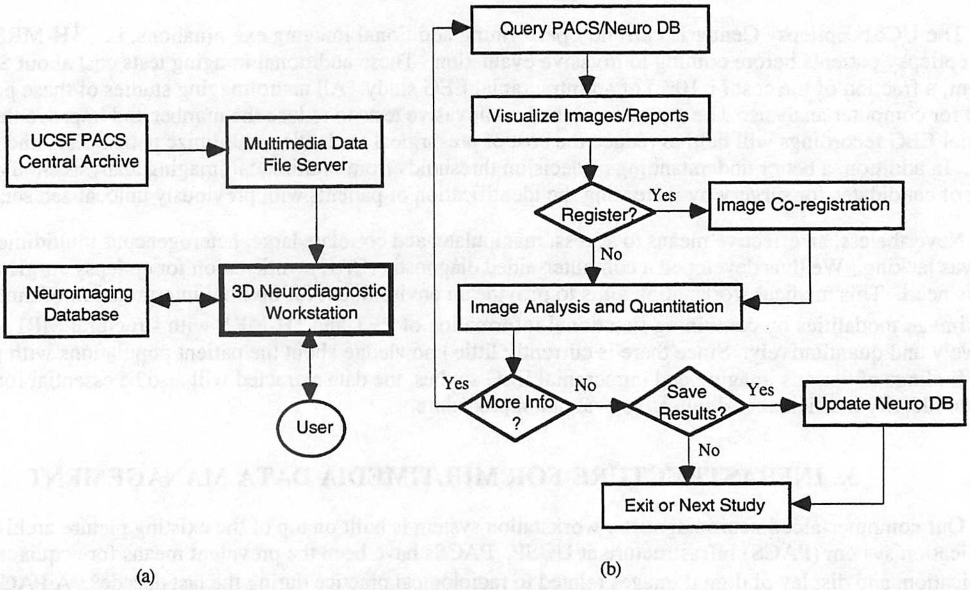

Figure 2. (a) Distributed system architecture of the computer-aided neurodiagnostic workstation, and (b) the computer-aided workup for epilepsy surgical planning that the medical workstation supports.

Extraction of structural and functional information. Once image pairs are registered into common space, their biomedical information can be combined, extracted, and quantitated to obtain important information about the location and nature of the epileptogenic zone. For example, the high resolution MR image provides a basis to anatomically map glucose metabolism. This allows the ability to identify metabolic rates in specific brain regions of interest. The neurodiagnostic workstation incorporates a program developed at Lawrence Berkeley Laboratory (Center of Functional Imaging, LBL) in conjunction with VIDA (VIDA Project, University of Iowa Medical College) to map regions of interest defined on the MRI to the PET sinograms for quantitation of glucose uptake. Figure 3.a illustrates such an example taken from another partial epilepsy case. This figure marked down the values obtained from structural/functional image analysis on volumes and ^{18}FDG glucose uptake per unit volume of hippocampus and amygdala. Note that original MRI and PET images are shown in this figure. Such quantitative data, which are not obtained in conventional workups, can provide sensitive and objective localization information.

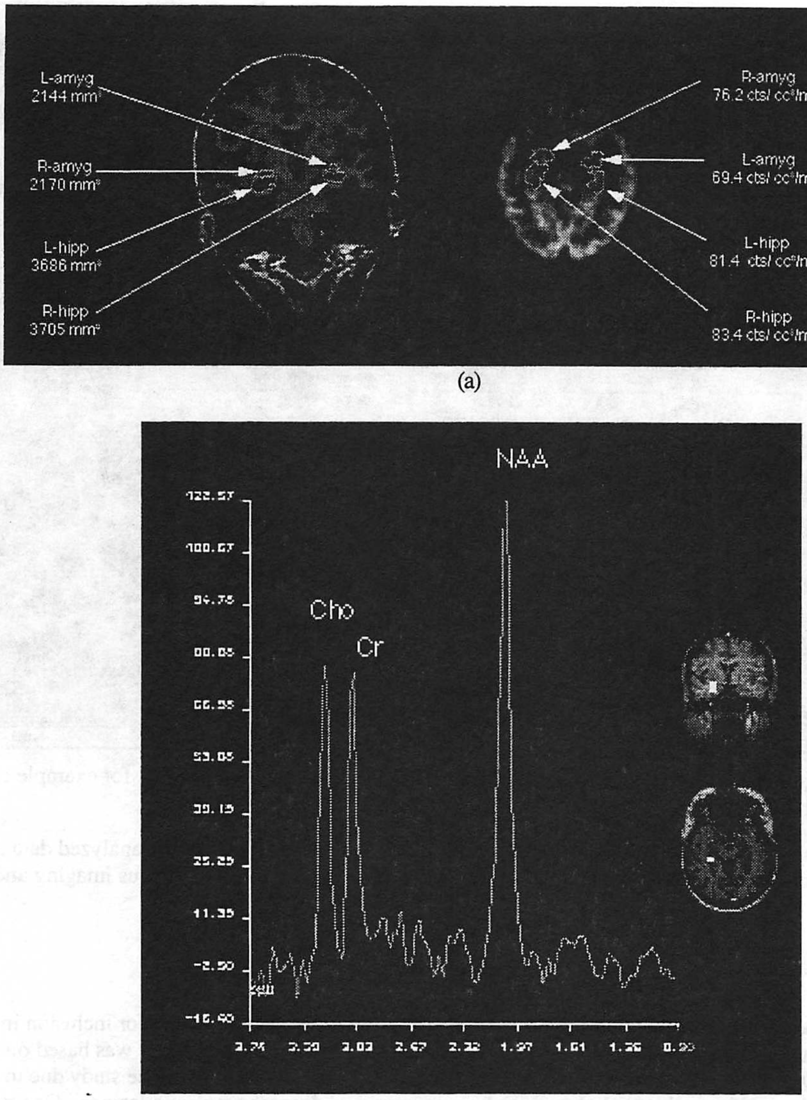

(a)

(b)

Figure 3. (a) Quantitation of hippocampus and amygdala MRI regions and the use of MRI-PET co-registration to obtain FDG concentration per unit volume in FDG-PET (2 dimensional original slices shown here). (b) MRI-MRS coregistration and spectral analysis. ^{1}H-MRS spectra for the defined voxel region (white squares MR images) in the right temporal lobe as seen on the MRI. The peaks measured with ^{1}H MRS in this case represent choline (Cho), creatine (Cr), and N-acetyl-aspartate (NAA).

Image query by contents. The clinician can save the analyzed results of the workup into the neuroimaging database for future reference. For example, structural and functional information extracted as shown in Figure 3.a and 3.b will be stored into the neuroimaging database to enable flexible user query of multimedia medical data. Figure 4 illustrates a graphical user interface for accessing information contained in the neuroimaging database. Query is by image content, i.e., MRI hippocampal volume or PET glucose concentration, or by patient attributes, i.e., age. In this example, three pairs of sliders that specify the range of the three aforementioned patient attributes. The image database returns with a list of patients satisfying the combined attribute ranges. The user can select any patient name to retrieve and display MRI and PET images (only two slices are shown here, and the PET image is registered to MRI image). The multimedia user interface is object-oriented and compositional, such that another interface format, tailored for different applications, can be rapidly implemented

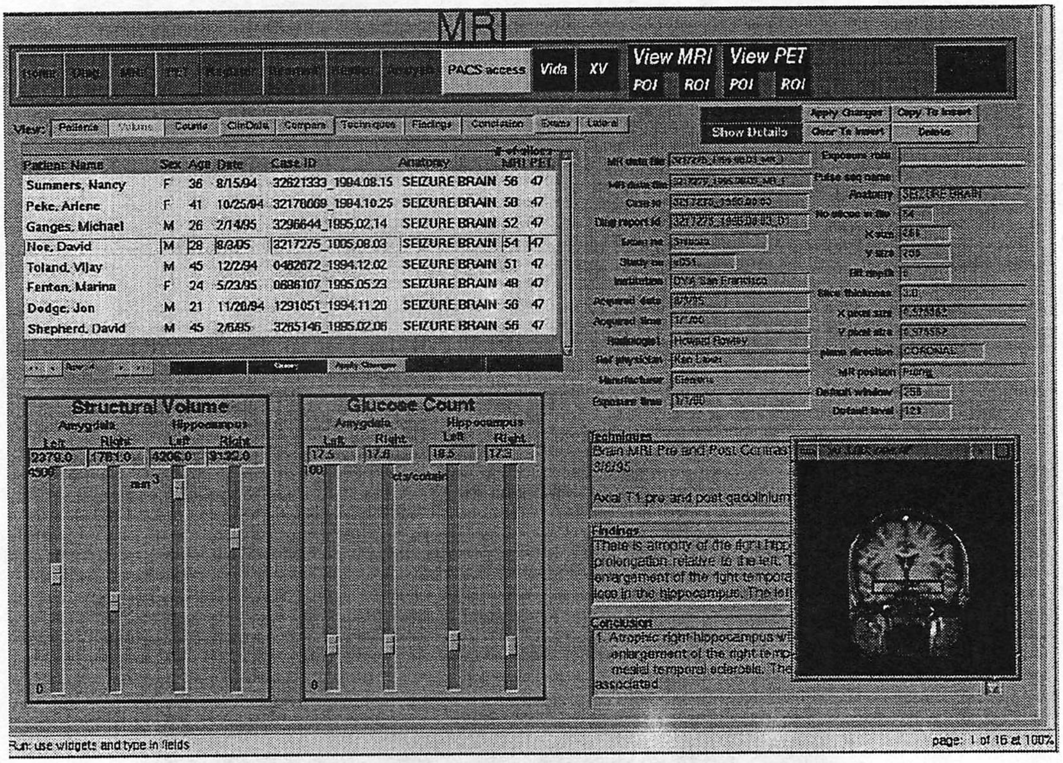

Patient Name	Sex	Age	Date	Case ID	Anatomy	# of slices MRI	PET
Summers, Nancy	F	36	8/15/94	32621333_1994.08.15	SEIZURE BRAIN	56	47
Peke, Arlene	F	41	10/25/94	32178069_1994.10.25	SEIZURE BRAIN	58	47
Ganges, Michael	M	26	2/14/95	3296644_1995.02.14	SEIZURE BRAIN	52	47
Noe, David	M	28	8/3/95	3217275_1995.08.03	SEIZURE BRAIN	54	47
Toland, Vijay	M	45	12/2/94	0482672_1994.12.02	SEIZURE BRAIN	51	47
Fenton, Marina	F	24	5/23/95	0686107_1995.05.23	SEIZURE BRAIN	48	47
Dodge, Jon	M	21	11/20/94	1291051_1994.11.20	SEIZURE BRAIN	56	47
Shepherd, David	M	45	2/6/95	3265146_1995.02.06	SEIZURE BRAIN	56	47

Techniques: Brain MRI Pre and Post Contras 3/6/95 Axial T1 pre and post gadolinium

Findings: There is atrophy of the right hipp prolongation relative to the left. T enlargement of the right tempora ... in the hippocampus. The left

Conclusion: 1. Atrophic right hippocampus wi enlargement of the right temp mesial temporal sclerosis. The associated

Run: use widgets and type in fields

page: 1 of 16 at 100%

Figure 4. Extracted image features can in turn be used for indexing the neuroimaging database, for example comparison and reference during surgical planning and diagnostic workup of a new case.

using the same set of graphical icons and tools. In addition, as the image database grows, the analyzed data accumulated will be important in performing outcome analyses and in evaluating the cost-effectiveness of various imaging and surgical protocols.

5. METHODS

Surgical candidates suspected to have seizures arising from the temporal lobes were screened for inclusion in the prospective study. Informed consent was obtained from all subjects. Diagnosis of temporal lobe epilepsy was based on scalp-sphenoidal EEG/video telemetry. Of the 36 patients diagnosed to have epilepsy, 8 were excluded from the study due to foreign tissue lesions, including vascular malformations, glial tumors, hamartomas, and dysembryoplastic lesions. One patient was excluded because both ^{1}H-MRS and FDG-PET data sets were severely obscured by motion artifact. Two additional patients were excluded because they did not complete protocol examinations for either ^{1}H-MRS or hippocampal volumetry (HV).

Ultimately, 25 patients (12 male, 13 female, age range 14-56, mean 38 years) were included in this study. Because T2 relaxometry did not begin at the start of this project, only 13 patients (6 male, 7 female, age range 14-56, mean 37 years) were studied with all four modalities. Twenty four patients have had surgery in which a tailored subpial temporal lobe resection was performed. All resected tissue demonstrated mild to moderate hippocampal gliosis, a feature of mesial temporal sclerosis, the most common pathology found in complex partial seizures.

FDG-PET. PET scans were performed with a CTI/Siemens 961 HR EXACT scanner. Forty-seven slices were acquired simultaneously over a 15 cm field of view. Axial, coronal, and sagittal planes were reconstructed for visual interpretation.

Diagnostic MRI. All patients underwent diagnostic MRI studies independent of research MR and ^{1}H-MRS exams. UCSF MRI exams are performed at 1.5 T (Signa, General Electric) and the following sequences were acquired: sagittal T1 weighted image (TR 600 ms/TE min) through the hippocampus and temporal lobes; axial T2 weighted (TR > 2000 ms, TE 35/80 ms); 3-D SPGR gradient echo (TR 50 ms, TE min, flip angle 40 deg., slice thickness 1.5 mm); coronal T2* gradient echo (TR 500 ms, TE 15-34 ms, flip angle 20 deg.); and high resolution (512 x 512 matrix) coronal T2 fast spin echo (T2-

FSE) sequence. Interpretation of mesial temporal abnormalities was based on signal, morphological, and volume changes. Abnormalities of hippocampal internal structure were determined from the high-resolution T2-FSE sequence.

Hippocampal volumetry (HV). All 25 patients had an MPRAGE sequence (TR/TE 10/4 ms, flip angle 15 deg, slice thickness 1.5 mm) acquired in the coronal plane orthogonal to the long axis of the hippocampus for HV in the same sitting as T2 and ^{1}H-MRS exams.

T2 relaxometry. Thirteen of the 25 patients had hippocampal T2 measured using a procedure similar to that reported by Jackson et al. and Grunewald et al. [12,13] A multi-spin echo sequence (16 echoes) with TR 2000 ms and TE 22.5, 45...360 ms from an 8mm thick slice of the anterior hippocampus was performed. Two independent operators placed circular regions of interest (ROI) within the margins of the hippocampal body. The average of the two T2 relaxation times was calculated to obtain a final measurement for T2 of the corresponding hippocampus.

^{1}H-MRS. Twenty four of the patients were studied with ^{1}H-MRS. These spectra were acquired on a 1.5 T Magnetom Vision^{TM} (Siemens, Erlangen, Germany) using a standard circularly polarized head coil according to the method previously reported by Ende et al.[14] Quantitation of the metabolites was based on use of the unsuppressed water signal obtained in a second MRS examination with otherwise identical measurement parameters. The concentration of NAA were used to determine metabolite abnormality and lateralization with ^{1}H-MRS.

Image interpretation and analysis. Working on the CAD workstation, the PET images were interpreted for evidence of focal hypometabolism by two investigators. Five temporal lobe ROIs were selected - temporal pole, anterior medial, posterior medial, anterior lateral, and posterior lateral cortex - and scored for relative hypometabolism. the sum of the five regions was used to provide a qualitative measure of the degree of hypometabolism. An asymmetry index (AI) was used to measure the degree of asymmetry for HV, T2 mapping, ^{1}H-MRS:

$$AI = \frac{right - left}{\left(\frac{right + left}{2}\right)} \times 100 \qquad (1)$$

6. RESULTS

Twenty-three of 24 patients studies with PET had one or more regions with relative hypometabolism confined to a single TL. MRI revealed easily discernible relative hippocampal atrophy in fifteen patients. T2 hyperintensity was seen only with concurrent hippocampal atrophy. All cases of MRI identified hippocampal atrophy were concordant with ictal EEG. Seventeen of 25 patients were lateralized with HV. Nine of 13 patients were lateralized with T2 relaxometry. ^{1}H-MRS lateralized 15 of 24 patients with once discordant lateralization in one patient. The results of each modality's ability to lateralize the epileptogenic zone are summarized in Table 1:

modality	**lateralized**	**n**	**%**	**AI**
PET	23	24	96%	NA
MRI - hippocampal atrophy	15	25	60%	NA
MRI - T2 increase	9	25	36%	NA
HV	17	25	68%	≥ 8%
T2 relaxometry	9	13	69%	≥ 4%
^{1}H-MRS	15	24	63%	≥ 12%

Table 1. Lateralization of epileptogenic zone by neuroimaging modalities.

FDG-PET was the most sensitive imaging methodology for lateralizing complex partial seizures in the temporal lobe, lateralizing all but one patient with hippocampal atrophy and 75% of patients without atrophy. HV lateralized 68% of patients, and T2 relaxometry did not provide additional lateralizing information beyond that provided by HV.

Comparisons of lateralization can only be done in those patients who completed all exams included in the evaluation. Table 2 lists the lateralization from the 23 patients who completed FDG-PET, HV, and ^{1}H-MRS studies (from the total of 25 patients, one did not have a PET, and in another the ^{1}H-MRS volume selection owas displaced above the plane of the hippocampi). No discordance was found with FDG-PET or HV. One patient was discordant with ^{1}H-MRS measures.

modality	**concordant**	**discordant**	**non-lateralized**
FDG-PET asymm. score > 3	20	0	3
HV AI $\geq 8\%$	15	0	8
^{1}H-MRS [NAA] AI ≥ 12	15	1	7

Table 2. Comparison of lateralization (n=23)

7. CONCLUSION

The surgical planning of medically refractory epilepsy often requires invasive, intracranial EEG recordings to localize the epileptogenic zone for resection. There are, however, definite risks and considerable costs associated with such invasive procedures. Planning for surgery in epilepsy requires analyzing and combining structural and functional data from numerous sources to localize the seizure foci for resection. This reported work shows the results of studying the lateralizing accuracy of multiple neuroimaging modalities, e.g., MRI, PET, and ^{1}H-MRS, used in noninvasive planning of epilepsy surgery. Image analysis including ROI segmentation, ROI quantitation, and image registration was carried out on a CAD workstation. FDG-PET was the most sensitive imaging modality for lateralization in this study. FDG-PET was even able to lateralize the abnormality even in the absence of HV and other MRI evidence for hippocampal sclerosis, including T2 relaxometry, supporting the continued role for FDG-PET in the evaluation of patients with complex partial seizures in the temporal lobe. ^{1}H-MRS was not as sensitive as other MR methods. Future work will focus on optimizing the use of these multiple imaging modalities in concert to plan surgeries in patients with complex partial seizures.

8. REFERENCES

1. United States commission for the control of epilepsy and its consequences. Plan for national action on epilepsy. U.S. department of health, education, and welfare, I DHEW Pub. No. NIH 78-276, 1978.
2. F. E. Dreifuss, "Establishment of what constitutes medical failure, in J Engel (ed.)", *Surgical Treatment of the Epilepsies*, Raven Press, pp. 133-136, 1993.
3. NIH Consensus Conference -- Surgery for epilepsy. National Institutes of Health Consensus Conference. *J American Medical Association*, **264(6)**, pp. 729-733, 1990.
4. J. J. Engel, T. R. Henry, M. W. Risinger, et al., "Presurgical evaluation for partial epilepsy: relative contributions of chronic depth-electrode recordings versus FDG-PET and scalp-sphenoidal ictal EEG", *Neurology* **40(11)**, pp. 1670-1677, 1990.
5. S. S. Spencer, "The relative contributions of MRI, SPECT, and PET imaging in epilepsy", *Epilepsia*, pp. S72-89, 1994.
6. C. Cendes, F. Andermann, M. Preul, D. Arnold, "Proton magnetic resonance spectroscopic images and MRI volumetric studies for lateralization of temporal lobe epilepsy", *Magnetic Resonance Imaging* **13(8)**, pp. 1187-1191, 1995.
7. J. Engel (ed.), *Surgical Treatment of the Epilepsies*, Appendix II: Presurgical Evaluation Protocols, Raven Press, 1993.
8. H. K. Huang, O. Ratib, et al (ed.), "Picture Archiving and Communication System (PACS)", *J. Digital Imaging* **5(1)**, pp. 22-25, 1992.

9. STC Wong, R Knowlton, M Chew, HK Huang, "Integrating Multidimensional Imaging, Multimodality Registration, and Multimedia Database for Epilepsy Diagnosis", *SPIE Medical Imaging Conference: Image Display*, Feb. 26 - March 2, San Diego, 1995.

10. R. P. Woods, J. C. Mazziotta, S. R. Cherry, "MRI-PET registration with automated algorithm", *J Computer Assisted Tomography* **17(4)**, pp. 536-546, 1993.

11. S. C. Strother, J. R. Anderson, X. L. Xu, J. S. Liow, D. C. Bonar, D. A. Rottenberg, "Quantitative comparisons of image registration techniques based on high-resolution MRI of the brain", *J Computer Assisted Tomography* **18(6)**, pp. 954-962, 1994.

12. G. D. Jackson, A. Connelly, J.S. Duncan, R. A. Grunewald, D. G. Gadian, "Detection of hippocampal pathology in intractable partial epilepsy: increased sensitivity with quantitative magnetic resonance T2 relaxometry", *Neurology* **43**, pp. 1793-1799, 1993.

13. R. A. Grunewald, G. D. Jackson, A. Connely, J.S. Duncan, "MR detection of hippocampal disease in epilepsy: factors influencing T2 releaxation time", *American Journal of Neuroradiology* **15(6)**, pp. 1149-1156, 1994.

14. G. Ende, K. D. Laxer, R. Knowlton, G. B. Matson, M. W. Weiner, "Quantitative ^{1}H SI shows bilateral metabolite changes in unilateral TLE patients with and without hippocampal atrophy", *Proc. SMR Third Meeting*, pp. 144, 1995.

PC/NT based PACS Display Workstation with ATM and DICOM Connectivity

Guang Pu Lei, Hong Zhang, Albert Wong

Laboratory for Radiological Informatics
Department of Radiology, University of California San Francisco
530 Parnassus Ave. Rm. CL158, San Francisco, CA94143-0628

ABSTRACT

We have developed a portable DICOM-compliant low-cost PC NT-based display workstation with Asynchronous Transfer Mode (ATM) and Ethernet connectivity to Picture Archiving and Communication System (PACS).

This paper describes the hardware components and software system of the workstation, and compares the performance of ATM and Ethernet connectivity in the workstation. The display workstation consists of a DOME Md2/PCI board, two 1,600 x 1,280 resolution monitors, and an asynchronous transfer mode (ATM) OC-3 communication board. Implemented software includes: (a) a DICOM server, which automatically receives images from the DICOM-compliant PACS Controller; (b) a patient folder manager, which incorporates the local database to group multiple studies from individual patients; (c) a sophisticated display program with automatic image pre-processing functions, such as pre-set window and level; and (d) a DICOM query and retrieve services to retrieve images from DICOM-compliant archive.

The display workstation demonstrates that: (1) the PC/NT-based display workstation is 100% DICOM-compliant. (2) DICOM query and retrieve services support convenient multi-level retrieval of historical images from PACS archive. (3) Integration of DICOM and ATM into the display workstation facilities and speeds up image communication. (4) Patient folder management provides hierarchical image storage for individual patients, which consequently facilities review of image.

This paper demonstrates that the PC/NT based full-functioned display workstation can be implemented cost-effectively for PACS applications.

Key Words: Picture Archiving and Communication System (PACS), Digital Imaging Communication in Medicine (DICOM), Asynchronous Transfer Mode (ATM), display workstation, query, retrieve, and personal computer (PC).

1. Introduction

The basic and prevalent meaning of PACS is acquisition, storage, manage, display of digital radiological images through communication networks, and the integration of PACS with information systems like the hospital information system (HIS) and radiological information system (RIS) [1, 2, 3]. At present, more and more hospitals are implementing PACS to improve the quality of health care, save doctors' time for reviewing radiological images and reduce the cost of radiology services. Here, inexpensive display workstations play an important role for these purposes. It allows radiologists and referring physicians, Emergency Room (ER), Intensive Care Unit (ICU) and Cardiac Care Unit (CCU) staff to access images quickly, directly, conveniently, and cost effectively.

In recent years, the Pentium Personal Computer (PC) combined with Windows NT operating system becomes an attractive candidate in PACS workstation design for its high power and reasonable price [4, 5].

We developed a PC/NT based PACS display workstation with ATM and DICOM Connectivity. The DCIOM provides a standard communication protocol and the ATM allows quick image delivery. In this paper, we first describe the workstation hardware configuration and software architecture, followed by the performance of ATM versus the Ethernet, and the benefit of using the PC/NT based workstation.

2. Hardware Configuration

We designed the PC/NT based workstation with the goals of high quality display, fast image communication, User friendliness, and cost-effectiveness. The hardware configuration of the workstation is shown in Figure 1.

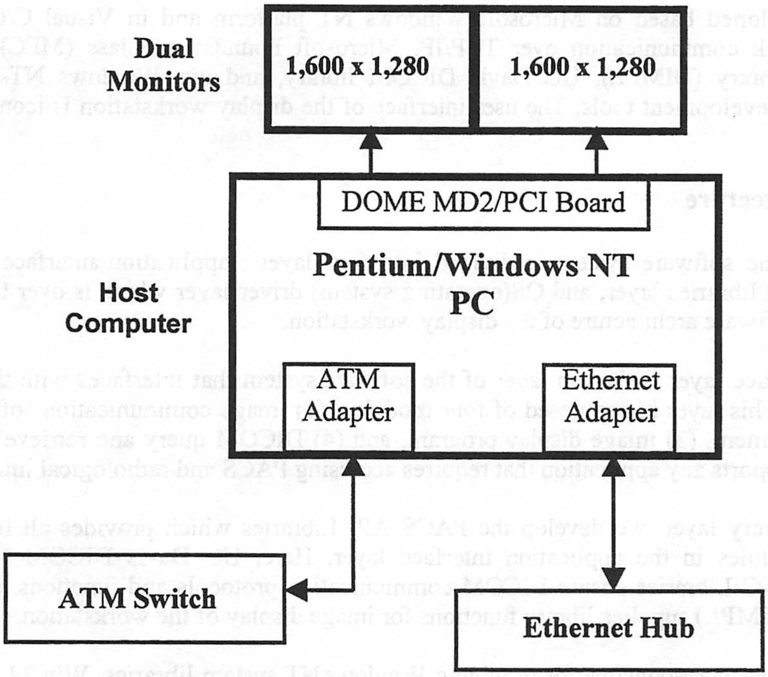

Figure 1 Configuration of the display workstation

2.1 Host Computer

The host computer of the workstation is a PC with Intel Pentium Pro 180 MHz, 128 Mbytes RAM, PCI bus structure and two 40 *Mbps* Ultra SCSI disks as local storage.

2.2 Display Devices

Display devices include single or multiple display monitors and a video board. The display monitor is a 24-inch 1600 x 1280 resolution in portrait mode (*Image Systems Corp., Hopkins, MN*). A DOME Md2/PCI host adapter (*DOME Image Systems, Inc., Waltham, MA*) as the video board.

2.3 Networking Equipment

In the workstation, asynchronous transfer mode (ATM) technology is used as the primary means of communication, and Ethernet as the back-up. In the former, we use the FORE 155-Mbps (OC3) ATM host adapter and FORE ForeRunner ASX-200BX ATM switch (*FORE Systems, Inc. Warrendale, PA*). The 3Com 10Base-T Etherlink adapter is used for the Ethernet.

3. Software System

The software is developed based on Microsoft Windows NT platform and in Visual C/C++ programming environment. WinSock communication over TCP/IP, Microsoft Foundation Class (MFC) libraries, DOME Image Processing Library (DIMPL), UC Davis DICOM library, and our Windows NT-based PACS API libraries are used as development tools. The user interface of the display workstation is icon/menu driven with user-friendly graphic.

3.1 Software Architecture

The architecture of the software system is divided into four layers: application interface layer, application libraries layer, system libraries layer, and OS(operating system) driver layer which is over the hardware layer. Figure 2 shows the software architecture of the display workstation.

The application interface layer is the top layer of the software system that interfaces with the end user of the display workstation. This layer is composed of four modules: (1) image communication software package, (2) patient folder management, (3) image display program, and (4) DICOM query and retrieve software package. This layer directly supports any application that requires accessing PACS and radiological images.

In the application library layer, we develop the PACS API Libraries which provides all library functions to support the four modules in the application interface layer. Here, UC Davis DICOM Network Transport Libraries and DIMSE-C Libraries ensure DICOM communication protocols and functions, and DOME Image Processing Library (DIMPL) supplies library functions for image display of the workstation.

The system library layer is responsible for providing Windows NT system libraries, Win 32 API functions and Microsoft Foundation Class (MFC) to serve as a developmental platform.

The OS driver layer provides Windows NT Operating System and its drivers for connecting with hardware components which includes DOME Md2/PCI driver for DOME Md2/PCI video board, ForeRunner 200E driver for FORE 155 Mbps ATM adapter and 10Based-T Ethernet driver for 10Base-T Ethernet adapter.

All data flow between the layers of the software is shown in Figure 3.

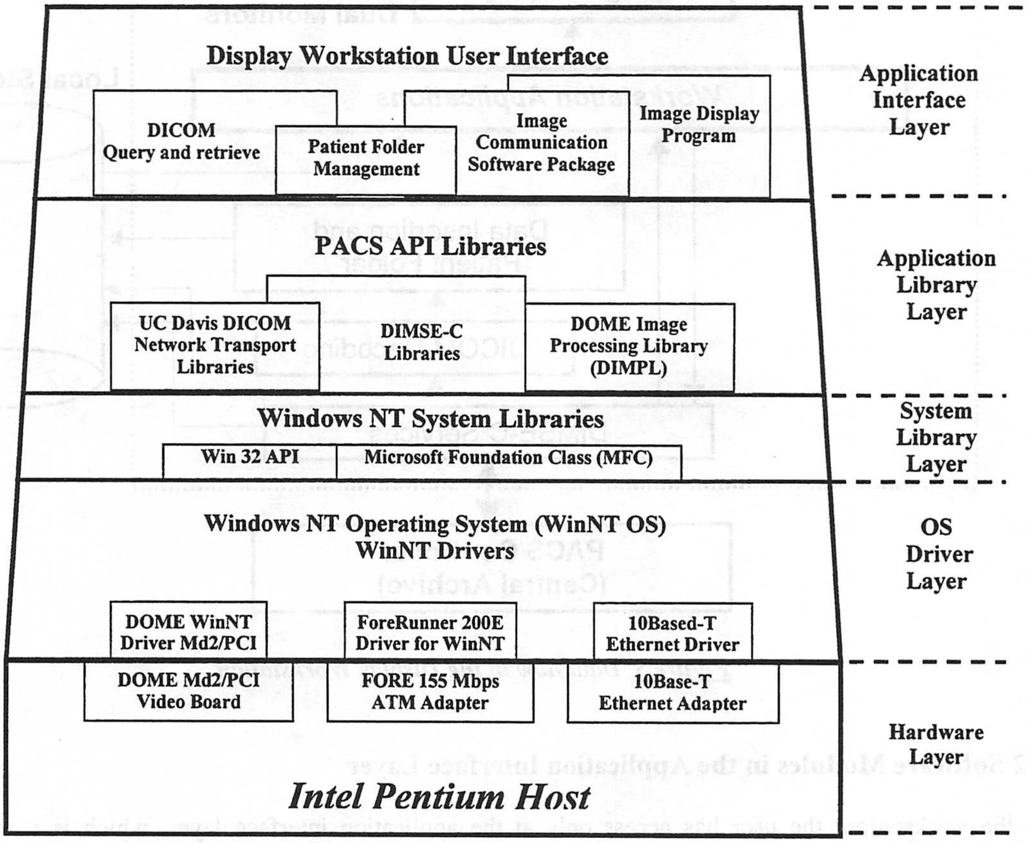
Display Workstation User Interface
DICOM Query and retrieve
Patient Folder Management
Image Communication Software Package
Image Display Program
PACS API Libraries
UC Davis DICOM Network Transport Libraries
DIMSE-C Libraries
DOME Image Processing Library (DIMPL)
Windows NT System Libraries
Win 32 API
Microsoft Foundation Class (MFC)
Windows NT Operating System (WinNT OS) WinNT Drivers
DOME WinNT Driver Md2/PCI
ForeRunner 200E Driver for WinNT
10Based-T Ethernet Driver
DOME Md2/PCI Video Board
FORE 155 Mbps ATM Adapter
10Base-T Ethernet Adapter
Intel Pentium Host
Application Interface Layer
Application Library Layer
System Library Layer
OS Driver Layer
Hardware Layer

Figure 2 Software Architecture of the Display Workstation

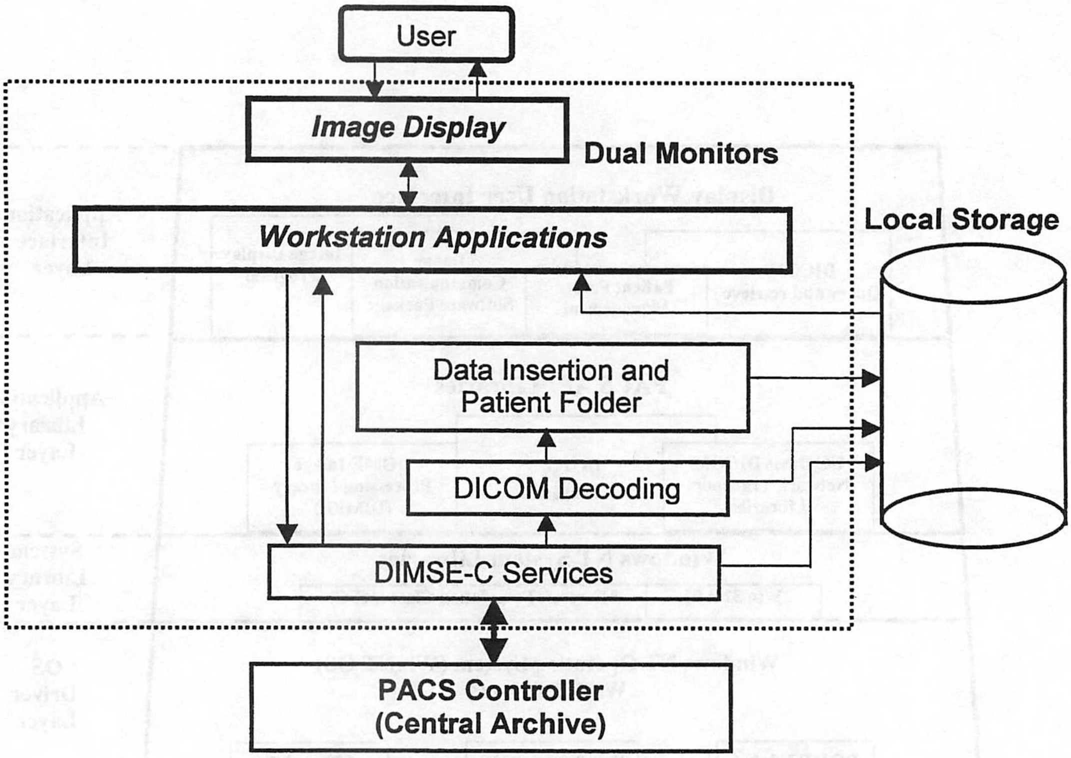

***Figure 3* Data flow in the Display Workstation.**

3.2 Software Modules in the Application Interface Layer

In the workstation, the user has access only at the application interface layer, which is composed of four modules described below.

3.2.1 Image Communication

The module is responsible for supporting DICOM services with DICOM communication protocols over TCP/IP to perform two DICOM services: Storage Service Class Provider *(SCP)* and Storage Service Class User *(SCU)*. The DICOM services include C-Echo for verification, C-Store for storage, C-Find for Querying and C-Move for retrieving [6].

3.2.2 Patient Folder Management

This module manages the local storage with hierarchical, or tree-structure, directories to organize patient folders within the display workstation.

DICOM decoder is used to extract patient demographic data and examination records from the header of a DICOM image. The reformatter of the module changes the image from DICOM format to DOME format for display. The extracted data via the DICOM decoder, and the reformatted image by the reformatter are inserted into an individual patient folder. A patient folder contains three hierarchical levels: patient level, study level, and series level. The hierarchy starts with a root directory in the local storage system, i.e., hard disks of the display workstation. Figure 4 is a diagram of the patient folder structure.

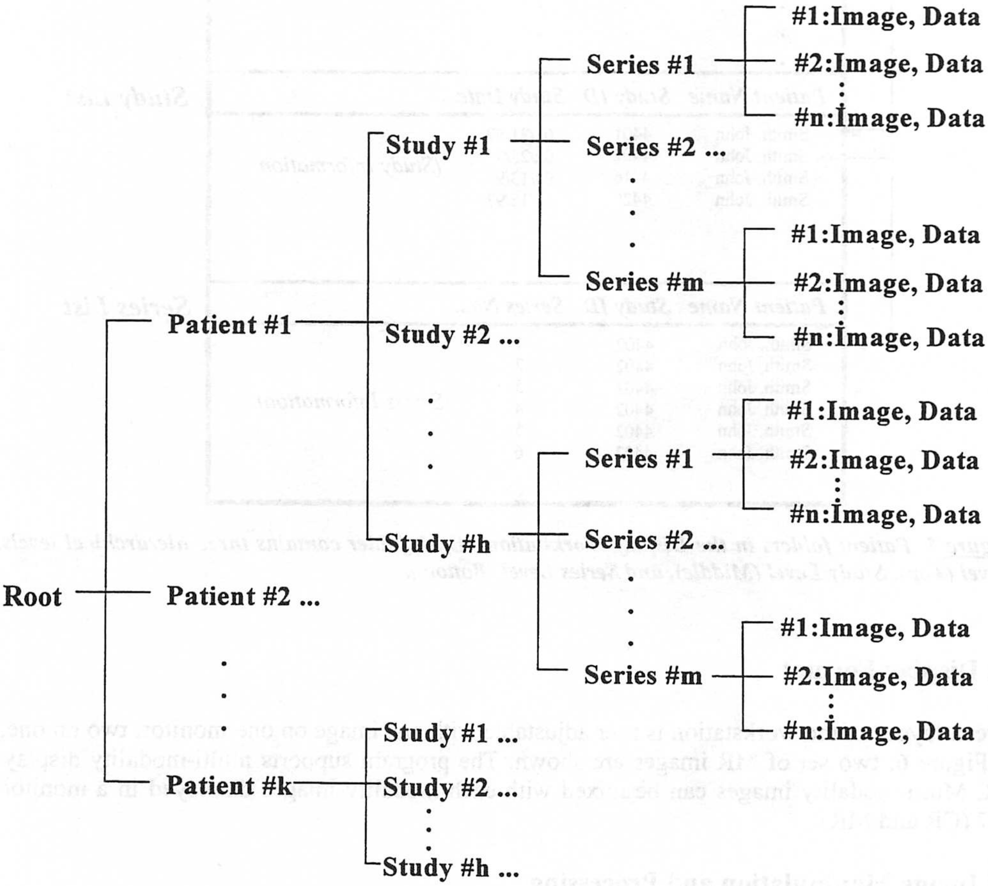

Figure 4 Three-level hierarchy of the patient folders managed by the display software.

A patient folder is automatically created in the workstation upon receipt of the first image of the patient. Subsequent images from individual studies and series are inserted into the patient folder accordingly. The patient folder can be automatically deleted from the workstation based on certain aging criteria such as number of days the folder is created, or discharge or transfer of the patient. Figure 5 presents the interface of three hierarchical levels of patient folders.

3.2.3 Image Display Program

The image display program supports both single and dual 24-inch 1,600 x 1,280-resolution portrait monitors to display patient information and radiological images in the workstation. Images with the DOME image header format in a patient folder can be displayed via the image display program.

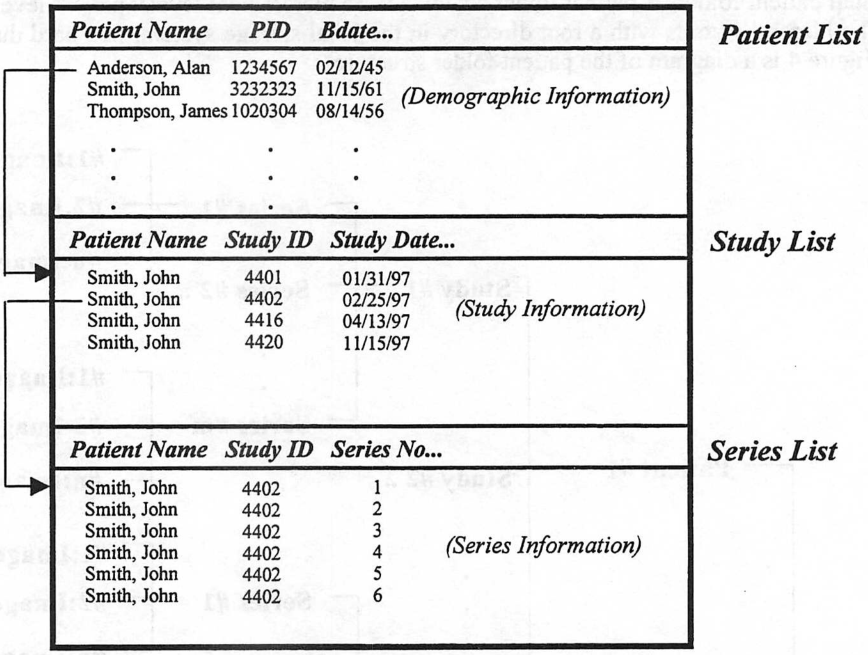

Patient Name	PID	Bdate...
Anderson, Alan	1234567	02/12/45
Smith, John	3232323	11/15/61
Thompson, James	1020304	08/14/56
.	.	.
.	.	.
.	.	.

Patient Name	Study ID	Study Date...
Smith, John	4401	01/31/97
Smith, John	4402	02/25/97
Smith, John	4416	04/13/97
Smith, John	4420	11/15/97

Patient Name	Study ID	Series No...
Smith, John	4402	1
Smith, John	4402	2
Smith, John	4402	3
Smith, John	4402	4
Smith, John	4402	5
Smith, John	4402	6

Figure 5 ***Patient folders in the Display Workstation. Each folder contains three hierarchical levels: Patient Level (Top), Study Level (Middle), and Series Level (Bottom).***

3.2.3.1 Display Format

The screen layout of the workstation is user adjustable with one image on one monitor, two on one, four on one, etc. In Figure 6, two set of MR images are shown. The program supports multi-modality display for CT, MR and CR. Multi-modality images can be mixed with each modality images displayed in a monitor as shown in Figure 7 (CR and MR).

3.2.3.2 Image Manipulation and Processing

Image manipulation functions such as zoom, pan, rotation, flip, window and level adjustment, and invert are available. Automatic defaulted window and level preset function is used during imaging loading to minimize the manipulation time. Real-time zoom and contrast adjustment can be easily done by using the mouse.

3.2.4 Query and Retrieve

This module is a DICOM query/retrieve service class user (Q/R SCU) to query and retrieve patient studies from the PACS long-term archive or directly from radiological imaging systems. The query and retrieve module supports DICOM C-Echo, C-store, C-Find, and C-Move services. With this module, the workstation has access capability to Query/Retrieve Service Class Providers, which use the Q/R information models of patient root and study root. The supported Query/Retrieve levels are shown in Table 1.

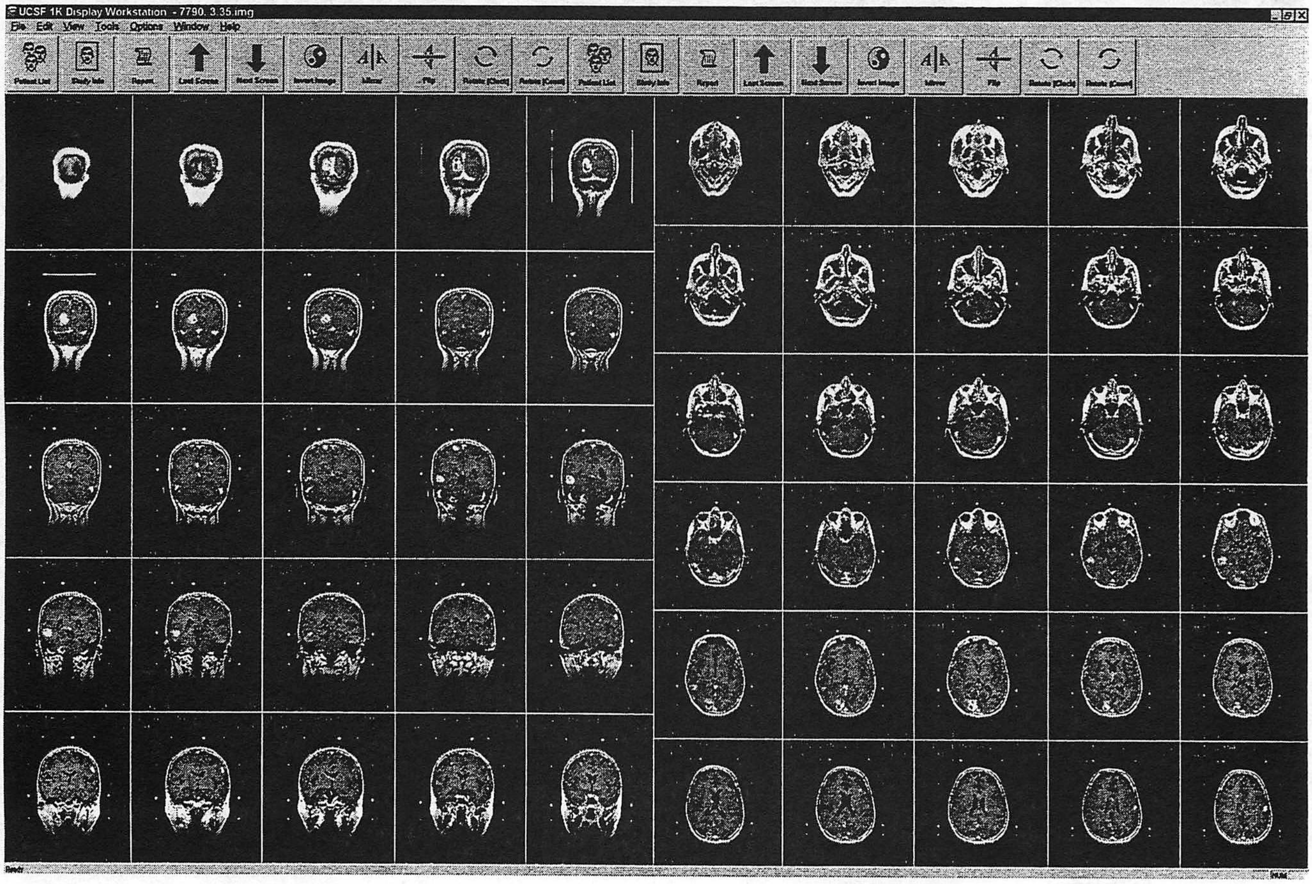

Figure 6
Display coronal (left monitor) and axial (right monitor) MR images in the workstation.

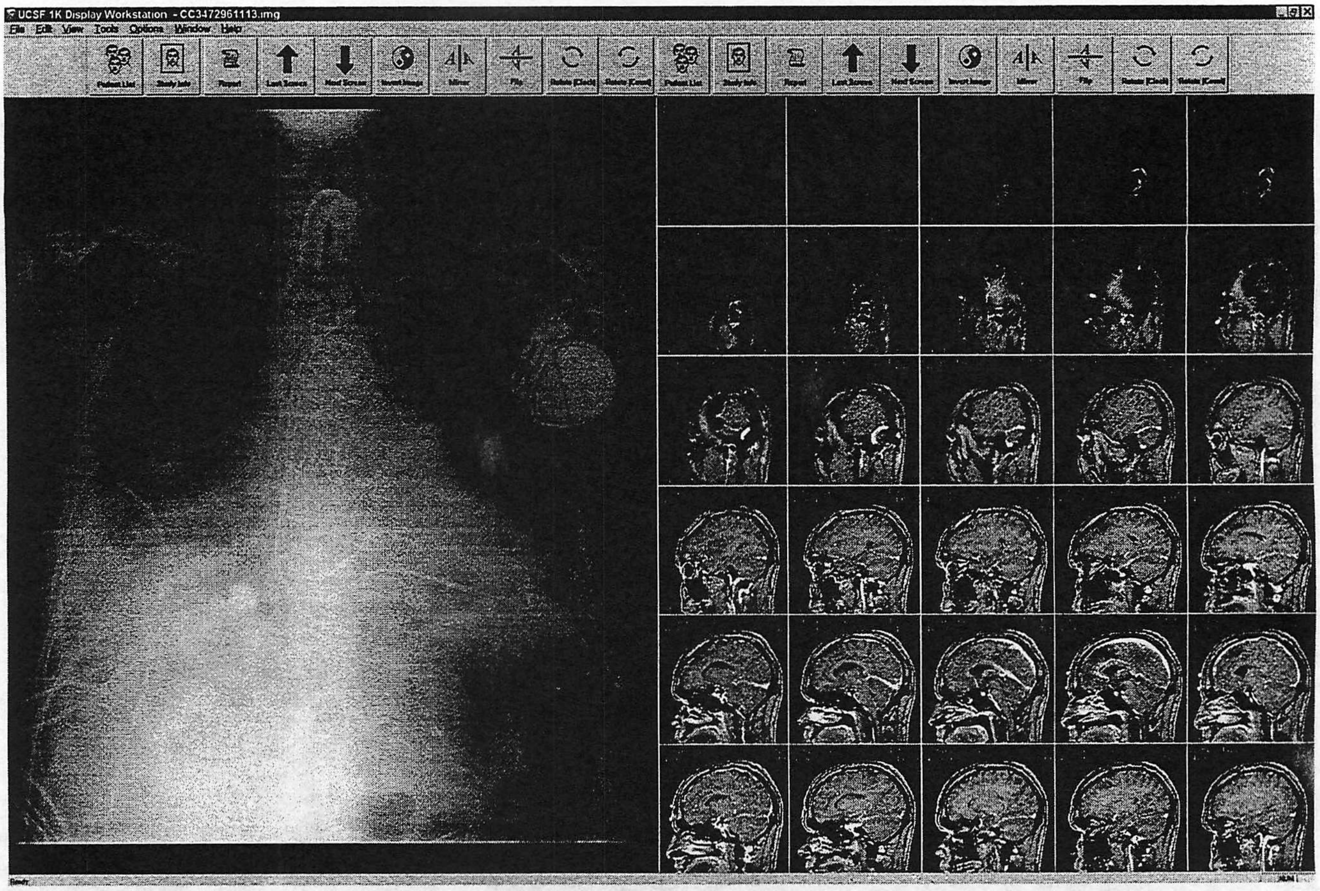

Figure 7
Multi-Modality Display in the workstation: Left monitor, CR image; Right monitor, MR images.

	Q/R SCP Information Model	
	Patient Root	**Study Root**
Workstation Supported Q/R Levels	**Patient Study Series Images**	**Study Series Images**

Table 1
Supported Query/Retrieve Levels in the display workstation

4. ATM and Ethernet Performance

Network communication performance plays an important role in the display workstation for quick access of radiological images and patient information from the PACS Controller. We have evaluated the ATM and the Ethernet performance of the display workstation.

4.1 Testing Equipment

Two nodes are used to test the ATM and the Ethernet performance. Each node is equipped with a host computer with Pentium Pro 180 MHz Processor, 64-Mbyte RAM, Windows NT operating system and ATM and Ethernet adapters. Networking Equipment is the Fore PCA-200EPC ATM PCI Host Adapter, Fore ForeRunner ASX-200BX ATM Switch and 3Com EtherLink Ethernet Host Adapter (see Section 2).

4.2 Types of Data Transmission

We use WinSock communication over TCP/IP to evaluate the ATM and the Ethernet performance of memory-to-memory and disk-to-memory transmission rate. We also measure the disk-to-disk transmission rate using the FTP.

4.3 Testing Results

Figure 8 shows the evaluation result, which demonstrates that ATM can provide much better communication performance in the display workstation than Ethernet. For memory-to-memory, ATM is an order of magnitude faster.

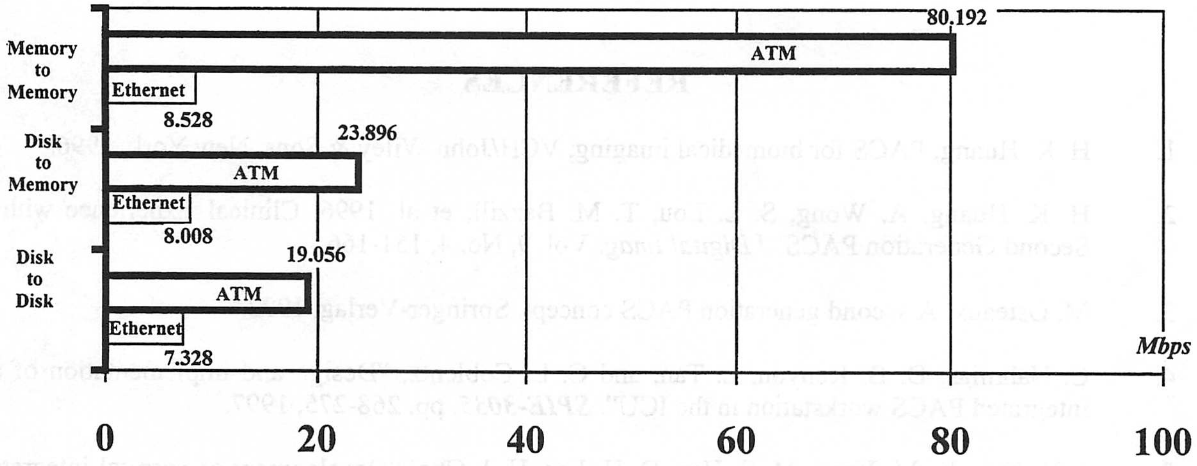

***Figure 8** the test results of the ATM and the Ethernet performances*

5. Conclusion and Discussion

The PC/Windows NT-based full-functioned diagnostic workstation developed in our laboratory demonstrates that it can be implemented cost-effectively for PACS applications. The display workstation provides the following capability:

(1) It is 100% DICOM-compliant.

(2) DICOM Query and Retrieve services support convenient multi-level retrieval of historical images from PACS archive.

(3) The integration of DICOM communication and ATM network into the display workstation facilitates and speeds up the communication of images.

(4) Automatic window and level preset function minimizes requirement for image manipulation thereby improving radiologists' efficiency.

(5) Patient folder management provides hierarchical image storage for individual patients, which facilitates image review at the display workstation.

(6) PC/Windows NT-based display workstation costs less than the Unix-based workstation.

With the fast-developed networking technology for the PCI bus architecture, for examples, 600 Mbps ATM and 100 Mbps fast Ethernet and gigabit Ethernet, will result in a better image transmission performance of the PC/NT-based workstation.

ACKNOWLEDGMENT

This work is partially supported by a contract from **National library of Medicine N01-LM-6-3547.**

REFERENCES

1. H. K. Huang, PACS for biomedical imaging, VCH/John Wiley & Sons, New York, 1996.

2. H. K. Huang, A. Wong, S. L. Lou, T. M. Bazzill, et al. 1996. Clinical Experience with a Second Generation PACS. *J Digital Imag.* Vol. 9, No. 4, 151-166.

3. M. Osteaux. A second generation PACS concept. Springer-Verlag, 1992.

4. C. Nahmias, D. B. Kenyon, L. Tan, and C. L. Coblentz, "Design and implementation of an integrated PACS workstation in the ICU", ***SPIE-3035***, pp. 268-275, 1997.

5. J. H. Kim, K. M. Yeon, M. C. Han, D. H. Lee, H. I. Cho, "Development of hospital-integrated large scale PACS in Seoul National University Hospital", ***SPIE-3035***, pp. 248-255, 1997.

6. NEMA, "Digital Imaging Communication in Medicine (DICOM)", *NEMA Standards Publication PS 3 (1994),* National Electrical Manufacturers Association.

Full-Field Direct Digital Telemammography: System Implementation

S.L. Lou[1], H.K. Huang[1], Edward Sickles[2], David Hoogstrate[1],
Fei Cao[1], and Jun Wang[3]

1. Laboratory for Radiological Informatics,
2. Breast Imaging Section,
Department of Radiology, University of California San Francisco,
530 Parnassus Avenue, Rm. CL-158, San Francisco, CA 94143-0628, USA

3. Now with Philips Research Lab, Palo Alto, CA

ABSTRACT

We are in the process of conducting a research of full-field direct digital telemammography using three protocols: telediagnosis, teleconsultation, and telemanagement. To conduct this research project, an asynchronous transfer mode network based telemammography system was developed across two remote campuses in our facility. The hardware and software components of this system are detailed. The system was embedded in a clinical environment for a four-month test. Some preliminary study results from the current phase of this study are reported.

Key words: digital mammography, high speed networking, high resolution display, teleradiology

I. Introduction

The early detection of breast cancer increases the survival rate in women [1]. Today, film-screen mammography is the most common and effective technique for the detection of breast cancer [2-4]. However, the film-screen image recording system of current mammography has several technical limitations that can reduce the breast cancer diagnostic accuracy. A state-of-the-art technology, full-field direct digital mammography (FFDDM), has the potential to increase the sensitivity of clinical and screening examinations and emerge as a film screen mammography replacement [5]. It is believed that efficiently delivering the superior image quality of FFDDM to expert mammographers will significantly increase the breast cancer diagnostic accuracy. This concept motivates the studies of full-field direct digital (FFDD) telemammography.

In our previous work, we reported on three protocols, telediagnosis, teleconsultation, and telemanagement, to evaluate the FFDD telemammography concept [6,7]. We also presented a plan on how to develop such a test-bed for this evaluation study. Since then we have implemented the FFDD telemammography system between two campuses: UCSF medical center (or main campus) and Mount Zion Hospital (MZH) where our mammography expert center is. These two campuses are two miles apart. In this paper, we first present our newly established asynchronous transfer mode (ATM) network-based telemammography system. Then, a four-month clinical test is described. The test results regarding the time measurements of the system processing and preliminary image quality studies are reported. Bases on these measured results, we estimated the elapsed time required for users to view the FFDDM images either at MZH or at the UCSF main campus. Finally, we discuss the possible approaches to optimize the image delivery performance.

II. Telemammography Test-Bed

We present the telemammography test-bed in two aspects: hardware configuration and software implementation. In the hardware configuration aspect, the major computer and network systems and their associated functions are described. Based upon the hardware setup, software programs that we have developed to integrate all the components into a functional telemammography system are given.

II.1 Hardware configuration

Currently, the major components in our telemammography system include one FFDDM system (the second system will be installed in September 1998), one data management system, two high resolution (2K x 2.5K) digital mammogram display workstations, and one Laser film imager. Figure 1 illustrates the configuration of this telemammography system.

II.1.1 FFDDM system

The FFDDM system serves as the image acquisition component in the telemammography system. It uses a slot-scanning based technology with a novel Charge-Coupled Device (CCD) detector from Fischer Imaging Corporation. (Denver, CO) [8,9]. The system contains an imaging unit and an acquisition computer which is a Sun Ultra-I computer system (Mountain View, CA). The imaging unit and the acquisition computer are linked by an electronic board developed by Fischer.

The image area of the FFDDM system is a rectangular of 240 x 300 mm^2. The spatial resolution of a generated image is 54 x 54 μm^2 per pixel in nominal and 27 x 27 μm^2 in high resolution which is approximately to 9 line-pairs (lp) per mm and 18 lp/mm, respectively. The matrix size of the image is 4,096 x 5,625 (4K x 5.5K) pixels, with 12 bits/pixel which is stored within 2 bytes. As a result, each image is about 46 Mbytes.

II.1.2 Data management system

The data management system functions as the database server for image archival and retrieval. The system is composed of a Sun Enterprise-3000 computer, a 42-Gbyte Sun Network Array Disk, and five fast-wide small computer standard interface (SCSI) disks (4 x 4.2 Gbytes and 1 x 2.1 Gbytes). In this management system, we store the digital mammogram data either in the Array Disk or in the SCSI disks while patient demographic information is managed by an Oracle database software.

II.1.3 Digital mammogram display workstations

The two display workstations provide soft copy display for this telemammography system. Each of the display workstations consist of the following components:

(1) one Sun Ultra-II that contains one 200-MHz CPU, 512-MByte CPU memory, and a 4.2-Gbyte fast-wide SCSI disk,

(2) two DOME MD5-SBX display boards; each is assembled by 5 mega-pixel video RAM, one 10-bit digital to analog converter, and one 16-bit to 8-bit look-up-table, and

(3) two Data Ray monitors (Westminster, CO); each provides 2,048 x 2,560 pixel matrix, 64 Hz frame rate, and 120 foot-lamber (maximum light output).

The image display and manipulation program is developed in-house and based on X-Motif and DOME image processing software libraries.

II.1.4 Laser film imager

The laser film imager prints hard copy (films) which are used to compare image quality between soft copy display and hard copy film. Specifically speaking, the film imager includes two components: a PC computer and the laser imager. The PC computer serves as an interface between other computer systems and the laser imager via an Ethernet. The laser imager is able to photograph 4,096 x 5,120 pixels onto a film with 4096 gray levels.

II.1.5 ATM network

All the components stated above (except for the laser film imager) are linked with an ATM network. In this ATM network configuration, two switches (one at each of the two campus) communicate through a UCSF Sonet ring sharing an OC-3C bandwidth (155 Mbits/second). Locally, the switches serves as a root to exchange information among the computer systems.

II.2 Software implementation

In the present stage of the system development, our aim is to assure the images smoothly flow from the FFDDM system to the display workstations. The fundamental software includes DICOM communication programs, a workstation database program, and an image display and manipulation program.

II.2.1 DICOM communication software

We use the Digital Imaging and Communications in Medicine (DICOM) communication protocols to transfer images such as storage, query, retrieve, and print service classes. The images generated by the FFDDM system contain the file format and information following DICOM information definitions. Digital mammograms transferred between computer systems are based on the DICOM storage service class. Currently, the data management computer system and the two display workstations can provide roles of service class provider (SCP) and service class user (SCU). The FFDDM acquisition computer only acts as an image client. The DICOM query/retrieve service class is established between the data management computer only acts as an image client. The DICOM query/retrieve service class is established between the data management system and the two display workstations. The PC computer associated with the laser film imager provides the DICOM print class service. In the current stage, we only configure this service class between the PC and the digital mammogram display workstation in MZH.

II.2.2 Workstation database software

Before a digital mammogram is ready for users to display in the image display workstation, it is processed by a workstation database software. The process includes (1) dividing the DICOM format file into a DICOM header file and an image pixel file, and (2) extracting information from the header file to form a local database. The database is a three-layer hierarchy which keeps track of information about patients, examinations, and images. The database allows us to present a patient list GUI in the image display software as described in Section II.2.3. In addition, it provides a means to remove old images from the local storage to maintain enough space for new images. Attributes such as patient name, hospital identification number, and birth date are recorded for locating a particular patient. It is possible for patients to have multiple mammography examinations. The patient key is designed to use a combination of the examination date, time, and patient hospital identification number to guarantee that each examination is unique Each examination may contain several images. A description of the patient positioning, such as breast laterality and view, is saved in the database.

II.2.3 Image display and manipulation software

A window-based image display and manipulation software is developed for providing users with a GUI environment for accessing patient information including text and images. A patient list allows users to browse through patients and their associated examinations and images. Images may be displayed in 1:1 (one image per monitor), 2:1, or 4:1 format using the two 2K display monitors. Since the image matrix is 4,096 x 5,625, none of the above display modes can present a full resolution FFDDM image on a single monitor. It is possible the portion of the image displayed on the monitors is background air. To insure the relevant image information is displayed, the breast laterality is used to set the output rectangle of the image. The images in any of the display modes can be instantly expanded to full resolution (4K x 5.6K) in 1:1 format, and vice versa. With these two image display features unnecessary operations of the display workstation are minimized. In addition, functions such as pan-and-scroll, window-and-level, scalable magnifying glass, rotation, and on-screen image exchange are provided to facilitate users' viewing practice.

III. Clinical Test and Preliminary Results

III.1 Patient collection

The telemammography system has been released for clinical testing since September 1997. Based on our clinical protocol, patients who have completed a film-screen mammography may have two additional FFDD mammograms of one breast with informed consent. This is conducted as follows:

(1) Patient examination involves normal and abnormal cases.

(2) Normal patients can be recruited from regular screening examinations.

(3) The abnormal case selection is conducted by the chief of the Breast Imaging Section during conventional mammography readings. From the reading, those patients suspected to have masses or calcifications were called in for FFDDM examinations.

(4) Only one cranio-caudal (CC) view and one medio-lateral oblique (MLO) view would be taken.

In four months, we have examined thirty-one patients with the FFDDM system.

III.2 Telemammography operations

Digital mammograms acquired by the FFDDM system are first sub-sampled to 600 x 800 pixels in the acquisition computer memory and displayed on the console monitor for quality assurance. The technician may adjust the contrast and brightness of the image to assess its quality. If the image quality is poor, it may be rejected and another scan performed. If the image quality is good, the mammogram is automatically transmitted to the display workstation at MZH through the ATM network using the DICOM storage class service. Once the image is received at the workstation, it is first processed by the workstation database program; then it is queued and transmitted to the data management system located at the UCSF campus through the Sonet Ring. The data management system then relays the image to the second image display workstation at the main campus.

We embedded logging software to show the elapsed time spent in the image delivery and display programs. Our preliminary results indicate the image transfer performance of the local area ATM is better than that of wide area ATM. It takes 5-6 seconds to transfer one 46-MByte mammogram from one computer system to another (disk to disk) in ATM network. The image display workstation database program takes about 25 seconds to process one image. For image display, we measured that it requires about 8-9 seconds to display one digital mammogram from the local fast-wide SCSI onto the image display monitor.

III.3 Preliminary image quality study

All images were viewed using the digital mammography display workstation. Preliminary results indicate that the FFDDM images displayed on the display workstation are of good quality. All the lesions shown on conventional mammograms can be clearly identified on the workstation with add-on values of enhancement and manipulation features. Figures 2 shows an example case that soft copy display is particularly useful for viewing dense breast tissues within which mammographers often have difficulty in detecting lesions. Both monitors show the same FFDDM image with different window and level settings. In the left monitor, the window and level values present generally good contrast and brightness for the entire image. However, the region of dense breast tissues enlarged by the magnifying glass is completely washed out. The image can be manipulated by applying a different set of window and level parameters as shown in the right monitor. Here, more detailed structure information can be perceived in the region of dense tissues although the image as a whole seems to be dim. We have also printed two patient cases with the Konica laser imager for comparison of image quality. The printed image quality is comparable to that of the conventional mammogram.

IV. Discussions

The elapsed time from the moment when a digital mammogram is accepted by a technologist in the FFDDM system to the time when the image is displayed on the MZH display workstation includes (1) the transmission time from the FFDDM acquisition computer to the workstation, (2) the queue time and the workstation database processing time, and (3) the image display time. If the image is also required to be displayed on the UCSF campus workstation, the elapsed time also includes: (1) the queue time and the transmission time from the MZH workstation to the data management system, (2) the queue time and transmission time from the data management system to the UCSF campus workstation, (3) the queue time and the workstation database processing time, and (4) the image display time. The queue time for each of the processes is set to 10 seconds. Based on the image transfer and display performances described in Section III.2, it is estimated that the elapsed time for an image to be displayed in the MZH and UCSF campus display workstations is about 50 seconds and 120 seconds, respectively.

The telemammography operations described in Section III.2 were for testing the entire image flow of the system. It is possible to independently transfer images from the FFDDM acquisition computer to the image display workstations in both at MZH and at the main campus. In this way, the time duration spent in the data management system and associated process queue time can be eliminated. As a result, it will be faster for users to view the image at the UCSF campus workstation. On the other hand, the workload of the FFDDM system will be increased which may slow down the following imaging procedures for the technologist.

V. Future Work

We have completed the first phase of a three year comprehensive program in developing the application of telemammography. This phase is to resolve the technical issues of the telemammography system as discussed in this paper. The second phase is to set up a second FFDDM system in the UCSF Ambulatory Care Center where the mission of health care delivery is toward out patient. The goal is to compare the mammography service between the two sites with different operating environment, one being the expert site while the other is an outpatient clinic. The last phase is to collect sufficient patient data to evaluate the effectiveness and efficacy of telemammography with the three clinical protocols.

Acknowledgments

This research is partially supported by the California Breast Cancer Research Program:"Real-Time Telemammography" (IRB-0148), the US Army Medical Research Materiel Command: "Full-field Direct Digital Telemammography" (DAMD-96-C-6111), the National HPCC Program, National Library of Medicine: "A High-Performance Testbed Network for Collaborative Health Care" (N01-LM-4-3508), and the Department of Health and Human Services: "Optimization of Soft Copy Display Parameters for Digital Mammograms" (282-97-0079).

References

[.1] O. Noriaki, Y. Koichi, "Improved Detection Rate of Early Breast Cancer in mass screening combined with mammography," *Hap. J. Cancer Res.* vol. 84, no. 7, pp. 807-812, 1993.

[.2] S. Feig, "Decreased breast cancer mortality through mammographic screening: Results of clinical trials," *Radiology*, vol. 167, pp. 659-665, 1988.

[3] S. Shaprio, W. Venet, P. Strax, et. al., "Selection, follow-up, and analysis of the health insurance plan study: a randomized trial with breast cancer screening," *J. Natl Cancer Inst Monogr.* vol. 67, pp. 65-74, 1985.

[.4] L. Tabar, G. Faberberg G, W. Duffy, N. Day, A. Gad, and O. Grontoft, "Update of the Swedish tw_-county program of mammographic screening for breast cancer," *Radiol Clin North Am.* vol. 30, pp. 187-210, 1992.

[5] National Cancer Institute (NCI) / National Aeronautics and Space Adminastration. (NASA) Workshop "Digital Mammograph", May 19-20, Washington, D.C.

[6] S.L. Lou, E.A. Sickles, H.K. Huang, et. al. Full-Field Direct Digital Telemammography - Preliminary *SPIE Proceedings*, Medical Imaging, PACS Design and Evaluation, vol 3035, pp. 369-379, 1997.

[7] H. Huang, "Teleradiology Technologies and Some Service Models," *Comp. Med. Imaging & Graphics* vol. 20, pp. 59-68, 1996

[8] E. Toker and M. Piccaro, 1993. Design and Development of a Fiber Optic TDI CCD-Based Slot-Scan Digital Mammography System. *SPIE Proceedings*, Medical Imaging, 2009.

[9] M. Tesic and M. Piccaro, "Digital Mammography Scanner: Performance Characteristics and Preliminary Clinical Results," *IEEE*, Savoy Place, London WC2R OBL, UK, pp. 3/1-3/7, 1996.

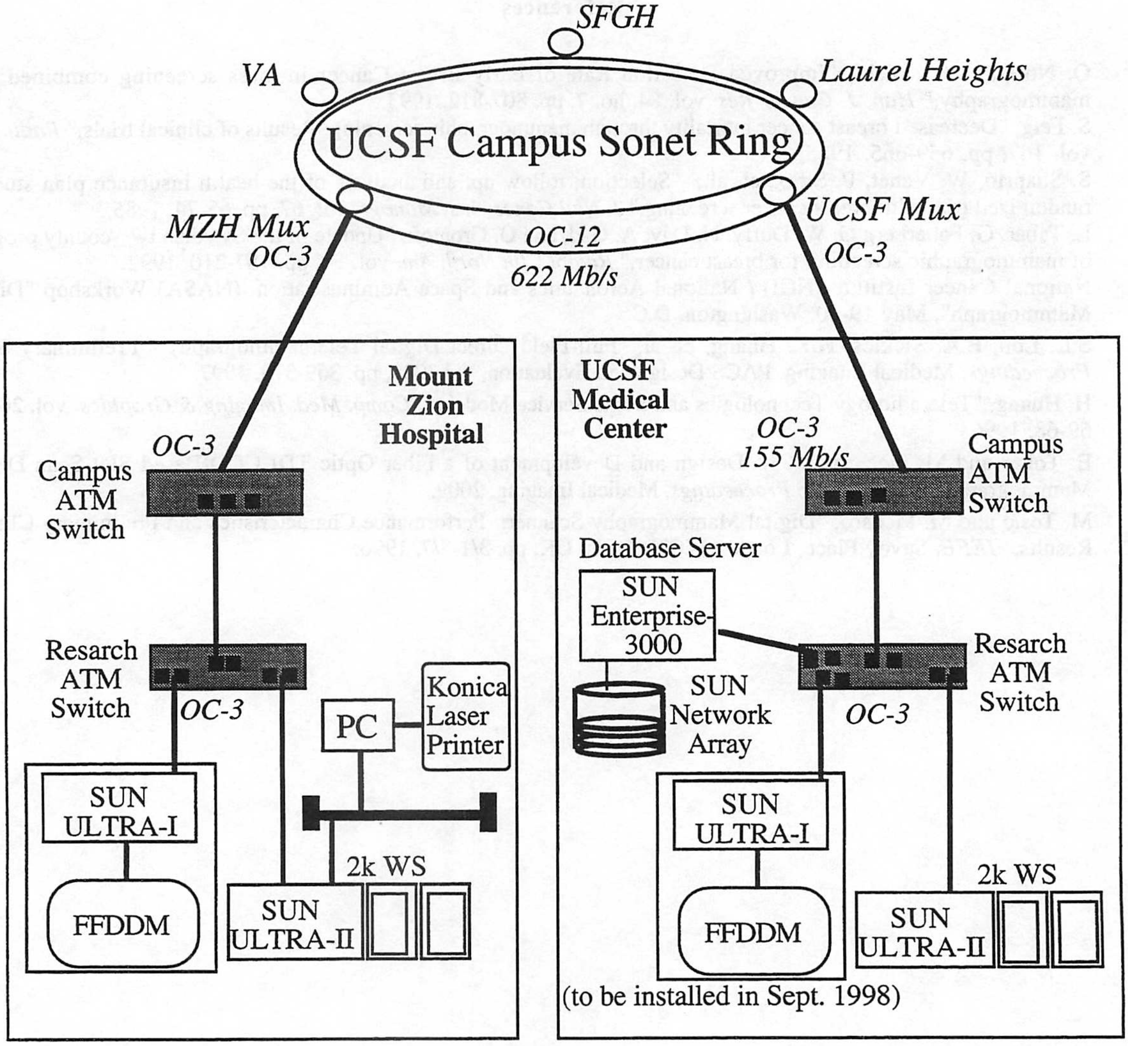
SFGH
VA
Laurel Heights
UCSF Campus Sonet Ring
MZH Mux
OC-3
OC-12
622 Mb/s
UCSF Mux
OC-3
Mount Zion Hospital
OC-3
Campus ATM Switch
Resarch ATM Switch
OC-3
Konica Laser Printer
PC
SUN ULTRA-I
FFDDM
2k WS
SUN ULTRA-II
UCSF Medical Center
OC-3
155 Mb/s
Campus ATM Switch
Database Server
SUN Enterprise-3000
SUN Network Array
Resarch ATM Switch
OC-3
SUN ULTRA-I
FFDDM
2k WS
SUN ULTRA-II
(to be installed in Sept. 1998)

Figure 1

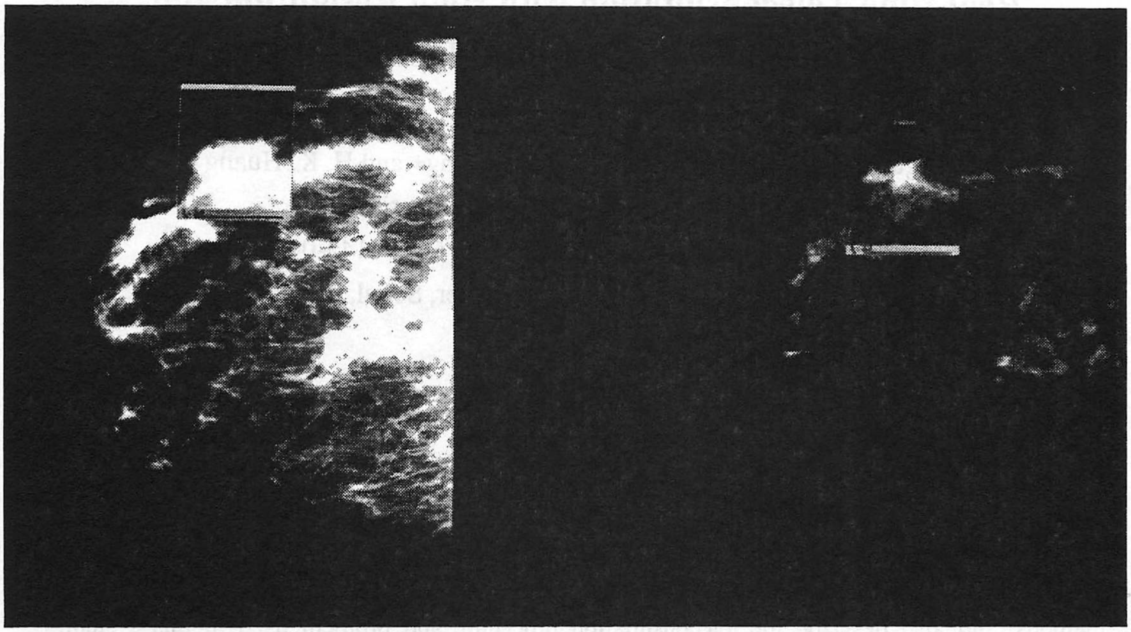

Figure 2

Real-time Teleconsultation with High Resolution and Large Volume Medical Imaging

Jianguo Zhang, Johannes Stahl, Koun S. Song+ and H. K. Huang
Laboratory for Radiological Informatics,
University of California, San Francisco, CA 94143-0628
+ Now with ASAN Medical Center, Seoul, South Korea

ABSTRACT

Real-time consultation between referring physicians or radiologists with an expert is critical for timely and adequate management of problem cases. During consultation, both sides need to (1) synchronously manipulate high resolution digital radiographic images or large volume MR/CT images, (2) perform interpretation interactively, and (3) converse with audio. We present a specific designed teleconsultation system with bi-directional remote control technology to meet critical teleconsultation application with high resolution and large volume medical images in a limited bandwidth network environment. We give the system design and implementation methods, and also describe the teleconsultation procedure and protocol used in this system. Finally, preliminary results are discussed.

Keywords: Teleconsultation, medical imaging, bi-directional remote control, networked multi-media, teleconsultation protocol, collaborative health care.

1. INTRODUCTION

The managed care trend in health care delivery system expedites the formation of teleradiology expert centers. In the expert center model of teleradiology [1], the medical images are sent from the examination sites to a remote site where an expert radiologist will make the diagnosis. The report is sent to the examination site where a primary physician can then prescribe the patient's treatment immediately. During teleradiology, real-time consultation between general physicians or radiologists with an expert to study the same images interactively are sometimes required. In real-time consultation, both sides need to synchronously manipulate and interpret high-resolution digital radiographic images (16 MB/exam.) and/or large volume MR/CT sequential images (8-20 MB/exam.). Here, we present a specific designed teleconsultation system with bi-directional remote control technology to meet critical teleconsultation application with high-resolution and large-volume medical images in a limited bandwidth network environment.

2. BACKGROUND AND REQUIREMENTS

The University of California at San Francisco (UCSF) comprises of two medical centers. The distance between the main campus (UCSF Medical Center) and Mt. Zion hospital (MZH) is 2 km. There are almost 1.0 gigabytes/day of MR/CT images transmitted through an asynchronous transfer mode (ATM) network (T1 line as backup) from MZH to UCSF Medical Center. These images are first sent to the clinical PACS server and then routed to display workstations [2] for expert to make diagnosis. Usually, referring physicians or radiologists view films at MZH, and when necessary, would request the expert to view softcopy images in display workstations at UCSF. They would discuss the cases through the telephone. With this type of consultation, both parties can not synchronize their operation on the images and can not manipulation them (e.g., to use cine mode, zoom and window/level operations) collaboratively.

In order to provide real-time consultation services for serious or difficult cases, a real-time teleconsultation system has been developed in our laboratory which is based on a distributed data storage in a shared window environment. This teleconsultation system meets the following requirements:

1) Provide real-time teleconsultation services with high-resolution and large volume medical images (MR/CT, CR, US, Mammography);
2) Synchronously manipulate images on both local and remote sites including remote cursor, window/level, zoom, cine mode, overlay, and measurement;
3) Support multimedia including audio and video (option) communications;
4) Interface to PACS through the DICOM standard;
5) Can be used in intranet (LAN) and internet (WAN) environment with TCP/IP protocol;
6) Scalable network connections including ATM, Ethernet, and modem;
7) Use low cost NT/PC based system.

3. SYSTEM DESIGN AND IMPLEMENTATION

In teleconsultation, it involves a referring site and an expert site. Between these sites three kinds of data communication are necessary: images transferred from the referring physician or general radiologist site to the expert site; remote control messages between the two sites; and voice communication between the referring physician and the expert. Among these three types of data, transmitting images requires very high bandwidth network but they normally can be preloaded before the consultation session unless it is an emergency case. Images preloading can be done with various kinds of network, e. g., ATM, T1 line, Ethernet, or telephone line through non-peak hour, evenings or weekends dependent on the turn around time requirement. Remote control message routing and voice communication are real-time on-line procedures but with low bandwidth requirement.

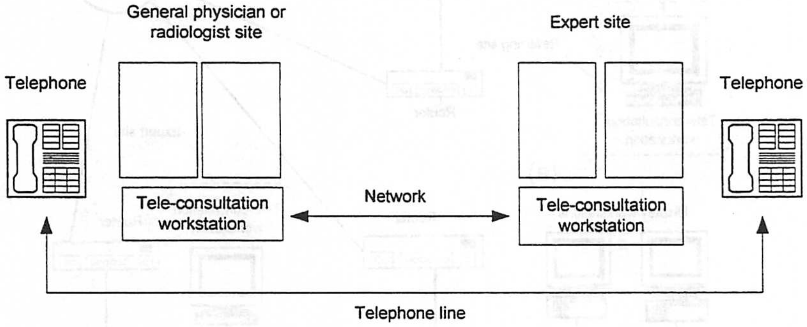
General physician or radiologist site
Expert site
Telephone
Telephone
Tele-consultation workstation
Network
Tele-consultation workstation
Telephone line

Figure 1. Diagram of teleconsultation system

Based on the above analysis and our PACS network infrastructure [3], we have designed a real-time teleconsultation system and implemented it at UCSF. Figure 1. shows the diagram of the teleconsultation system.

According to the expert model of teleradiology, the teleconsultation system is composed of two sites: the expert and the general physician or radiologist site. The hardware configuration of the teleconsultation system at each site includes:

1) One Pentium II NT workstations, each with 128 MB SDRAM, and 4 GB hard disk, as well as Ethernet, ATM and modem connections. One workstation located at the expert site and the other at the general physician site ;
2) One DOME Md2/PCI high resolution display boards which can be configured to support single or dual monitors;
3) Two high resolution gray scale monitors (Image System Inc.);
4) One telephones for audio communication.

The software modules (TeleConApp) in the teleconsultation system consists of:

1) Image display graphic user interface for teleconsultation;
2) Event Interpreter for local and remote message dispatching;
3) Remote Control Manager for routing messages between local and remote sites;
4) View and Memory Manager for view controlling and image data memory management;
5) Graphic Manager for image rendering and display;
6) DICOM communication services for DICOM image receiving and sending between the teleconsultation system, scanners and PACS server;
7) Image database for medical image display and teleconsultation authoring.

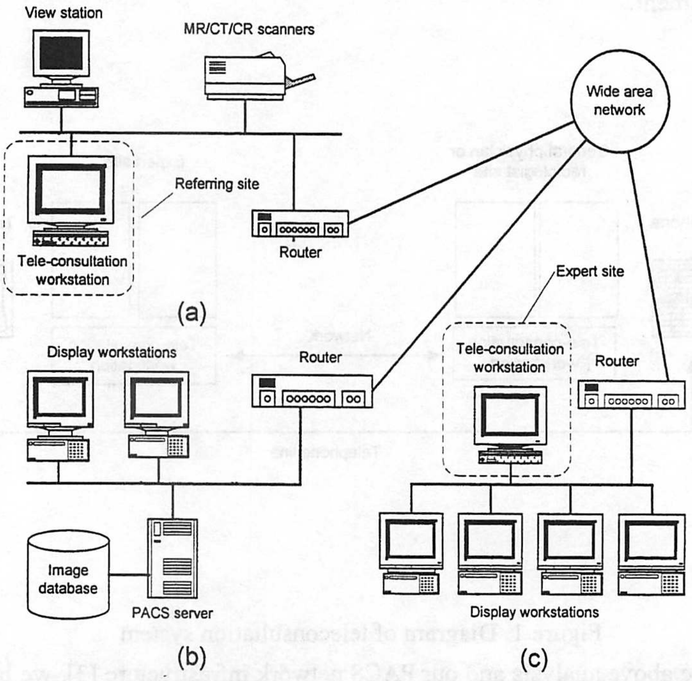

Figure 2. Network connection of teleconsultation system in clinical environment. (a) general physician or radiologist site; (b) PACS central archiving; (c) expert site.

The data flow and network connection of teleconsultation system in clinic network environment is shown in Figure 2. There are three parts in Figure 2: (a) The General physician or radiologist site; (b) PACS central archiving; and (c) The expert site.

4. TELECONSULTATION PROCEDURE AND PROTOCOL

A teleconsultation session proceeds as follows. When cases are needed to be consulted, a general physician or radiologist first collects the images from the scanners, display workstations or PACS image database, and pushes them to the teleconsultation workstation located at the local reading room. At the teleconsultation workstation, the referring physician then performs data authoring supplied by the teleconsultation system and sends them to the teleconsultation workstation located at the expert site through either the local area network if it is within the same building or campus, or through the wide area network if it is distant away. Later, either the general physician or an expert can call the other site to start the consultation session.

We develop a teleconsultation protocol with three steps: data formatting; data authoring and data presentation as follows:

Data formatting: The first step is to convert all input images for teleconsultation to the DICOM standard. This is done at the acquisition gateway or the PACS server.

Data authoring: The authoring procedure is to authorize data for teleconsultation. The authoring function module is an integrated component in the software package "TeleConApp". Figure 3 shows the data authoring procedure. There are three steps in data authoring:

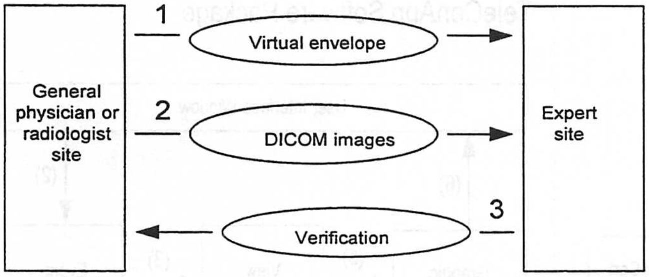

Figure 3. Data authoring steps

1) The general physician or radiologist uses the TeleConApp program to create an object called the virtual envelope which includes information of the selected patients, studies, and series; as well as the host name of the expert site, the name of the consultant from the teleconsultation local database. Note that the virtue envelope does not contain images. The virtual envelope is sent to the expert site through a network with DICOM communication services;
2) After the expert site receives the envelope, either site can create a consultation session and the general physician site sends the DICOM image objects related to the patient as dictated by the virtual envelope to the expert site;
3) After sending images, the general physician site automatically performs a DICOM query to the expert site, and the expert site verifies the receipt of the virtual envelope and image object to the general physician site. The consultation session can start once the data is verified.

Data presentation: Before the data presentation, both the expert and the general physician site have the virtual envelope and image data. Either site can operate the TeleConApp program to display and manipulate images and related information. TeleConApp synchronizes the operation of image display and manipulation at both sites. Figure 4 shows the teleconsultation operation procedure in either site:

1) Either the expert or general physician site can start the consultation procedure by selecting a session and load image objects from the site's local database to the memory and display them at both sites (5, 6).

2) Either site can manipulate the displayed images at the User Interface Window to create events, which are received by Event Interpreter. The site starts an event is called the local, whereas the other is the remote.

3) Event Interpreter sends the events to the local View Manager and Remote Control Manager.

4) Remote Control Manager encodes events and sends them to the remote site (Note: If the general physician site starts the event, it is the local; whereas the expert is the remote. On the other hand, if the expert site starts the event, it is the local and the physician site is the remote.). At the remote site, events are received and decoded by Remote Control Manager and send to View Manager (shaded (4) and dotted line).

5) View Manager handles both local and remote events and processes images according to the event types and sends processed image data to Graphic Manager;

6) After receiving processed image data, Graphic Manager renders them to display windows, which are managed by User Interface Window.

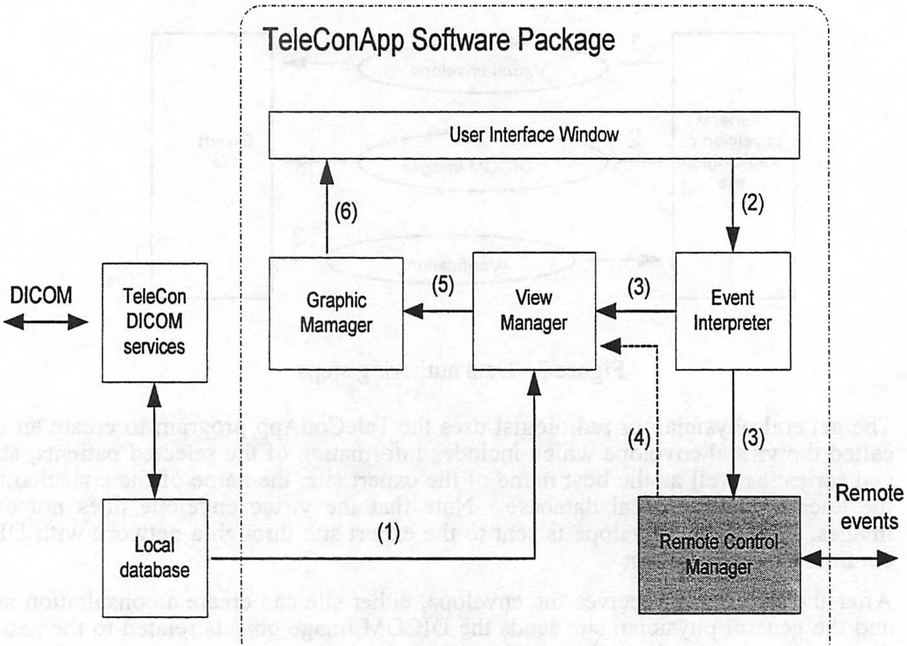

Figure 4. Operation procedure of data presentation in the local site during a teleconsultation session. Shaded area and dotted line represent events happened at the remote site. Numerals represent the data flow.

5. PRELIMINARY RESULTS

We selected 20 patients with more than 2,000 different modality images including GE MR/CT, Siemens CT, Fuji and Agfa CR, and pushed them from PACS server to one teleconsultation workstation through PACS network with the DICOM communication standard. Then we authored the data in the workstation and created teleconsultation sessions in both sites.

We performed the teleconsultation operations through intranet and internet with Ethernet and modem connections, respectively. During consultation, both sites manipulated images, did ROI and talked with telephones. There were no crash, no data lost, no delay feeling on both sites in a two month testing in the laboratory setting. The system was exhibited at InfoRAD, RSNA 97, Chicago, IL [4].

Currently, we are in the process of deploying the teleconsultation system to Neuro-imaging Section at UCSF and MZH for clinical evaluation.

6. CONCLUSIONS

We have developed a cost-effective teleconsultation system for collaborative health care application. This system provides data authoring, and synchronizes image display and manipulation on both the general physician/radiologist and the expert site during consultation through remote cursors. This system allows real-time collaborative consultation of serious or difficult cases with high resolution and large volume medical images in a limited bandwidth network environment.

7. ACKNOWLEDGMENT

This work is partially supported by the National Library of Medicine Contract No. N01-LM-6-3547

8. REFERENCES

[1]. H. K. Huang, “Teleradiology technologies and some service models”, *Computerized Medical Imaging and Graphics,* Vol. 20, pp 59-68, 1996.

[2]. H. K. Huang, Albert Wong, Andrew Lou, et al., “Clinical experience with a second-generation hospital-integrated picture archiving and communication system”, *Journal of Digital Imaging,* Vol. 9, pp 151-166, 1996.

[3]. H. K. Huang, K. Andriole, T. Bazzill, et al., “Design and implementation of a picture archiving and communication system: the second time”, *Journal of Digital Imaging,* Vol. 9, pp 47-59, 1996.

[4]. J. Zhang, K. Song, H. K. Huang, A. W. Wong, and J. Stahl, “Tele-consultation for thoracic imaging”, *Radiology,* Vol. 120(P), p734, 1997.

Integration of multi-vendor imaging equipment with DICOM into PACS

Albert W.K. Wong and H.K. Huang

Laboratory for Radiological Informatics
Department of Radiology
University of California, San Francisco
San Francisco, CA 94143-0628
E-mail: Albert.Wong@radiology.ucsf.edu

ABSTRACT

DICOM provides integration solutions for PACS to interconnect multi-vendor imaging equipment, regardless of computer hardware and operating system platforms, for communication of images. This paper describes our three-year experience integrating heterogeneous imaging systems into a large-scale PACS based on DICOM.

Vendor imaging equipment connected to the PACS include (a) six CT and MR imaging devices; (b) two CR systems; (c) two laser film digitizers; (d) one commercial ultrasound PACS module; and (e) eight DICOM-based display workstations. The image communication software implemented in the PACS was modified from Mallinckrodt's Central Test Node software and University of California at Davis' DICOM software to support the Unix-based and Windows NT-based computer systems, respectively. Images acquired from the individual CT/MR devices, CR systems, film digitizers, and the commercial PACS module were transmitted from the acquisition computers to the PACS Controller, where these images were routed to the display workstations and the archive server. Problems during integration included: (a) missing slice image(s) from an image sequence during the acquisition process; (b) incorrect data encoding in image header; (c) DICOM Service Object Pair Class not supported by the Service Class Provider vendor; and (d) DICOM conformance mismatching and shadow group conflict between the individual vendors. These problems were resolved by the mechanisms we implemented in our Image Acquisition Gateways and PACS Controller.

The DICOM communications standard provides a simple means of interconnecting multi-vendor equipment for communication of images. However, operating a large-scale PACS configured with heterogeneous imaging systems requires significant effort in software integration to ensure data integrity and operation efficiency.

Keywords: Digital imaging and communications in medicine (DICOM), image communication, service object pair (SOP) service class, service class provider (SCP), service class user (SCU).

1. INTRODUCTION

The four major components of a Picture Archiving and Communication System (PACS) are: acquisition, archive, display, and communication. Images generated from the radiologic imaging devices such as the computed tomographic (CT) systems, magnetic resonance (MR) imagers, and computed radiographic (CR) systems are acquired by the acquisition computers. These images are then transmitted to the archive server, where they are routed to the display workstations for manipulation and review, and to the storage subsystem for long-term and short-term archiving.

The Digital Imaging and Communications in Medicine (DICOM) standard is intended to promote a generic communication method for heterogeneous imaging systems, allowing the transfer of images and associated information. By adapting the DICOM standard, a PACS is capable of interconnecting its individual components and the radiologic imaging devices to support image acquisition, archiving, and display. However, imaging equipment vendors often take different DICOM compliant implementations for their systems, which consequently lead to certain difficulties for these systems to interoperate.

We have implemented in our PACS two mechanisms that incorporate our DICOM-based applications to ensure data integrity and to guarantee interoperability. One mechanism was installed in the acquisition computers to provide a reliable and efficient process in acquiring images from the radiologic imaging devices; and the other was employed in the archive server to provide interoperability for multi-vendor imaging systems in the transfer of images.

This paper describes our three-year experience integrating multi-vendor imaging equipment into a large-scale PACS, and the data integrity and interoperability problems we encountered during the DICOM/PACS integration.

2. MATERIALS AND METHODS

2.1 DICOM Communication

Two major DICOM Service Object Pair (SOP) Classes used in our PACS for communication of images are the Storage Service Class and the Query/Retrieve (Q/R) Service Class:

- Storage Service Class allows a PACS application running on vendor A's system (i.e. a CT scanner) to play the role of a Storage Service Class User (SCU) that initiates storage requests and transmits images to vendor B's system (i.e. an image acquisition computer), which serves as a Storage Service Class Provider (SCP) accepting images into its local storage device.
- Q/R Service Class allows PACS applications running on vendor A's system (i.e. a display station) to play the role of a Q/R SCU that queries and retrieves images from vendor B' system (i.e. an archive server), which serves as a Q/R SCP processing query and retrieval requests.

Figure 1 illustrates the communication of images utilizing the Storage Service Class and Q/R Service Class in a PACS environment.

The communication software used in our PACS are based on Mallinckrodt's Central Test Node (CTN) software and University of California at Davis' (UCD) DICOM software, which support our Sun/Unix-based and PC/Windows NT-based computer systems, respectively. These two software packages were modified to include several enhanced features that provide reliable and efficient communication for images. For more detailed information regarding our DICOM communication software, please refer to the '97 SPIE Proceedings paper entitled "Adaptation of DICOM to an operational PACS."[1]

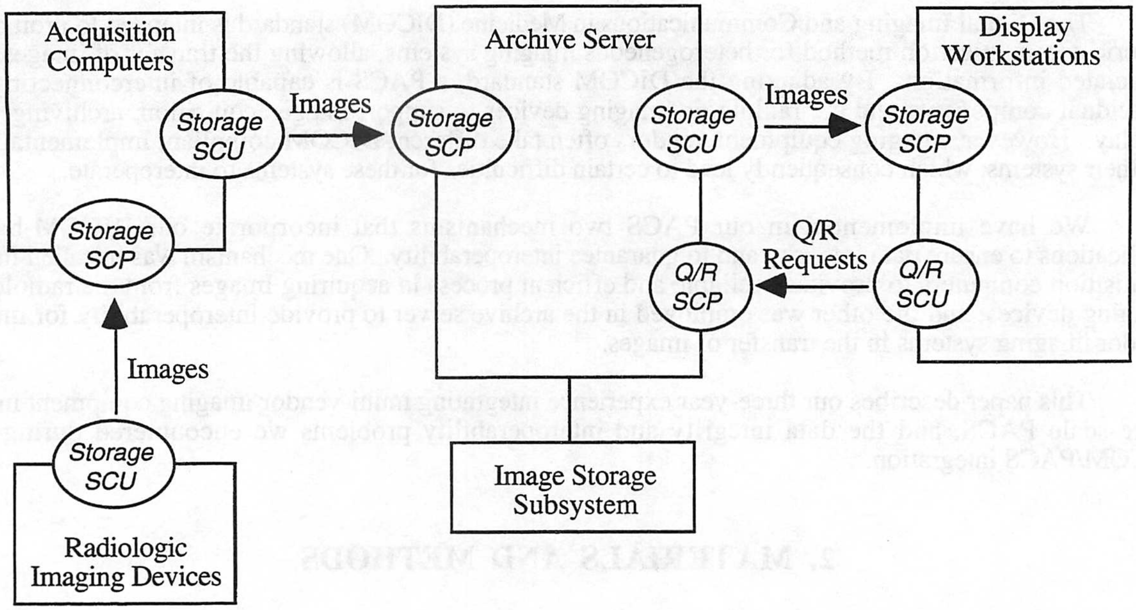

Figure 1. Image communication utilizing DICOM SOP services in PACS. Images generated from the radiologic imaging devices are acquired by the image acquisition computers via the Storage SOP service. These images are then transmitted to the archive server, where they are routed to the storage subsystem and the display workstations. The archive server supports Query/Retrieve (Q/R) SOP service, handling all Q/R requests from the display workstations. *Abbreviations: SOP - Service Object Pair; SCU - Service Class User; SCP - Service Class Provider.*

2.2 Networking with Multi-Vendor Imaging Equipment

The communication network implemented for the UCSF PACS is based on a two-tiered architecture composed of the OC-3 (155 mbps) Asynchronous Transfer Mode (ATM) and the 10BaseT (100 mbps) Ethernet networks^{2,3,4}. This two-tiered network interconnects four major campus buildings (Moffitt and Long Hospitals, UC Imaging Center, and the Campus Library) and a remote affiliated hospital (Mt. Zion Hospital; 2 kilometers from UCSF), allowing the communication of images and associated information.

In the past three years, we have successfully integrated the following vendor-specific imaging systems with DICOM and connected them to the infrastructure of our PACS :

(1) six computed tomography (CT) and magnetic resonance (MR) imaging devices;

(2) two computed radiographic (CR) systems;

(3) two laser film digitizers;

(4) one commercial ultrasound (US) PACS module; and

(5) eight DICOM-based display workstations.

By utilizing the DICOM communications standard, images generated from the imaging devices are acquired by the image acquisition gateways (IAGs). These images are then transmitted to the PACS Controller (Archive Server), where they are routed to the storage subsystem and display workstations. Figure 2 illustrates the connections and data flow between the imaging devices, the IAGs, the PACS Controller, and the display workstations.

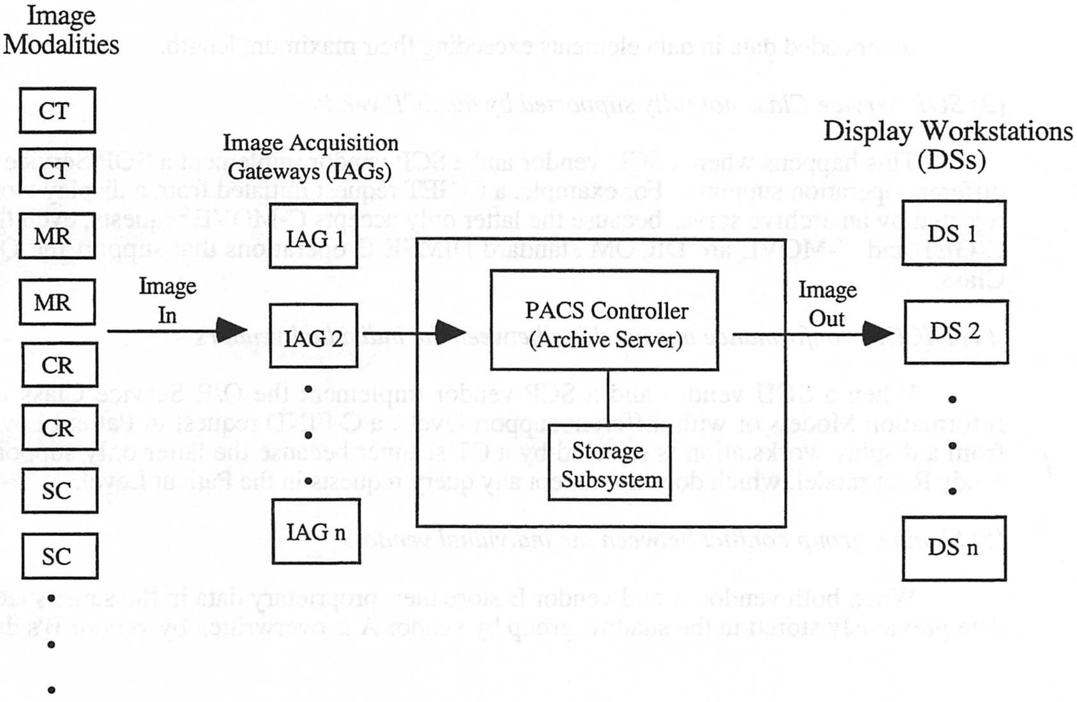

Figure 2. Image communication in PACS. Images from the imaging devices are acquired by the *Image Acquisition Gateways (IAGs)* and transmitted to the *PACS Controller (Archive Server)*, where they are routed to the display workstations (DSs) for manipulation and reviw, and to the storage subsystem for long-term and short-term archiving.

3. RESULTS

The problems during the integration of the aforementioned imaging systems with DICOM included the following:

(1) Missing slice image(s) from an image sequence during an acquisition process

When a CT or MR scanner (Storage SCU) transmits individual slice images from an image sequence to an IAG (Storage SCP), the scanner initiates the transfer with a a push operation. The reliability of transmission is dependent on the transfer mechanism implemented by the scanner.

(2) Incorrect data encoding in image header

Some of these examples are:

(a) missing Type 1 data elements, which are mandatory attributes in the DICOM standard;

(b) incorrect value representation (VR) of data elements; and

(c) encoded data in data elements exceeding their maximum length.

(3) SOP Service Class not fully supported by the SCP vendor

This happens when a SCU vendor and a SCP vendor implement a SOP Service Class with different operation supports. For example, a C-GET request initiated from a display workstation is rejected by an archive server because the latter only accepts C-MOVE requests, even though both C-GET and C-MOVE are DICOM standard DIMSE-C operations that support the Q/R Service Class.

(4) DICOM conformance mismatching between the individual vendors

When a SCU vendor and a SCP vendor implement the Q/R Service Class in different Information Models or with different support levels, a C-FIND request in Patient Level initiated from a display workstation is rejected by a CT scanner because the latter only supports the Q/R Study Root model, which does not accept any query requests in the Patient Level.

(5) Shadow group conflict between the individual vendors

When both vendor A and vendor B store their proprietary data in the same shadow group, data previously stored in the shadow group by vendor A is overwritten by vendor B's data.

4. IMAGE ACQUISITION GATEWAYS AND PACS CONTROLLER

Based on our experience with the PACS/DICOM integration, we have implemented two mechanisms incorporating the DICOM-based applications to provide better connectivity solutions for multi-vendor imaging equipment in a large-scale PACS environment.

One of these mechanism is operated in the IAGs to provide a reliable and efficient process for acquiring images from the radiologic imaging devices; the other is operated in the PACS Controller to provide integration solutions for multi-vendor imaging equipment, allowing their interoperability for the transfer of images. The configurations of the IAGs and PACS Controller, and the implemented mechanisms are described in the following sections.

4.1 Image Acquisition Gateways

(A) System Configuration

The IAGs are based on two computer system platforms: the Sun Microsystems computers and the Personal Computers (PCs). Each IAG serves as an acquisition node and can be connected to one or more radiologic imaging devices for the acquisition of images.

Sun-Based IAG

- Solaris operating system
- C programming language
- ATM and Ethernet network interfaces
- Unix socket communication over TCP/IP
- Mallinckrodt CTN-based DICOM communication software
- Informix local database

PC-Based IAG

- Windows NT operating system
- C and C++ programming languages
- ATM and Ethernet network interfaces
- WinSock communication over TCP/IP
- UCD DICOM-based communication software
- Microsoft Access local database

(B) Software Modules

The software running on an IAG supports two types of image acquisition, the push-mode and the pull-mode operations.

(a) Push Mode

Push-mode operation utilizes DICOM's Storage SOP service. An imaging device such as a CT scanner takes the role of a storage SCU initiating storage requests. The requesting IAG (storage SCP) accepts these requests and receives the images.

(b) Pull Mode

Pull-mode operation, on the other hand, utilizes DICOM's Q/R SOP service. An IAG plays the role of a Q/R SCU initiating query requests, selecting desired images, and retrieving images from an imaging device (Q/R SCP). Pull-mode operation requires the image acquisition process running on an IAG to incorporate IAG's local database to perform data integrity checking. This checking mechanism ensures that no images are lost during the acquisition process.

Figure 3 summarizes the characteristics of these two operations.

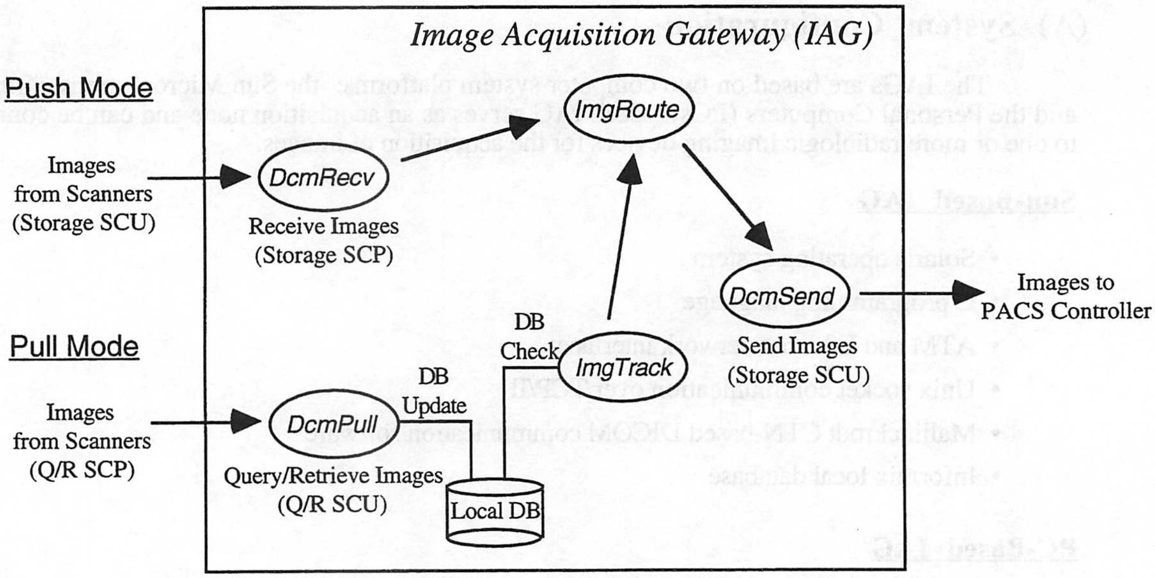
Image Acquisition Gateway (IAG)
Push Mode
Images from Scanners (Storage SCU)
DcmRecv
Receive Images (Storage SCP)
ImgRoute
DcmSend
Images to PACS Controller
Send Images (Storage SCU)
DB Check
ImgTrack
Pull Mode
Images from Scanners (Q/R SCP)
DcmPull
DB Update
Query/Retrieve Images (Q/R SCU)
Local DB

Figure 3. Interprocess communication among the major processes running on an image acquisition gateway (IAG). IAG supports both push and pull operations for acquiring images from the scanners. The *DcmPull* process incorporates IAG's local database to perform data integrity checking, ensuring no missing slice images from any image sequences during the acquisition process.

The *ImgTrack* process performs data integrity checking using the following procedures:

(1) Query study information from the scanners

(2) Generate acquisition status table

(3) Periodically check acquisition status of individual image sequences

(4) Invoke *DcmPull* process to retrieve images from the scanners

The *DcmPull* process, when invoked by the *ImgTrack* process, will retrieve desired images from the scanners and update the acquisition status table accordingly.

4.2 PACS Controller

(A) System Configuration

The PACS Controller, a Sun Microsystems Ultra Enterprise 3000 Multi-CPU server running Solaris operating system, is configured with the following components:

- Redundant array of inexpensive disks (RAID) cache storage
- Digital video disc (DVD) long-term storage†
- ATM and Ethernet network interfaces

- Mallinckrodt CTN-based DICOM communication software
- Oracle database

†The DVD storage subsystem will be implemented when it becomes available.

(B) Software Modules

The PACS Controller supports communication for images with the following DICOM implementations:

(1) a Storage SCP that accepts images from the IAGs;

(2) a Storage SCU that routes images to the display workstations; and

(3) a Q/R SCP that handles query and retrieval requests from the display workstations

Figure 4 illustrates the management of images in the PACS Controller. The *DcmBroker* process serves as an arbitrator ensuring images acquired from the radiologic imaging devices can be adequately distributed to the display workstations. This process checks the individual images in the PACS Controller's cache storage to determine if any changes in their headers are necessary. The major tasks of the *DcmBroker* process include:

(1) Correct any mis-coded data in the existing elements;

(2) modify existing elements;

(3) add new elements or shadow groups; and

(4) remove existing elements or shadow groups.

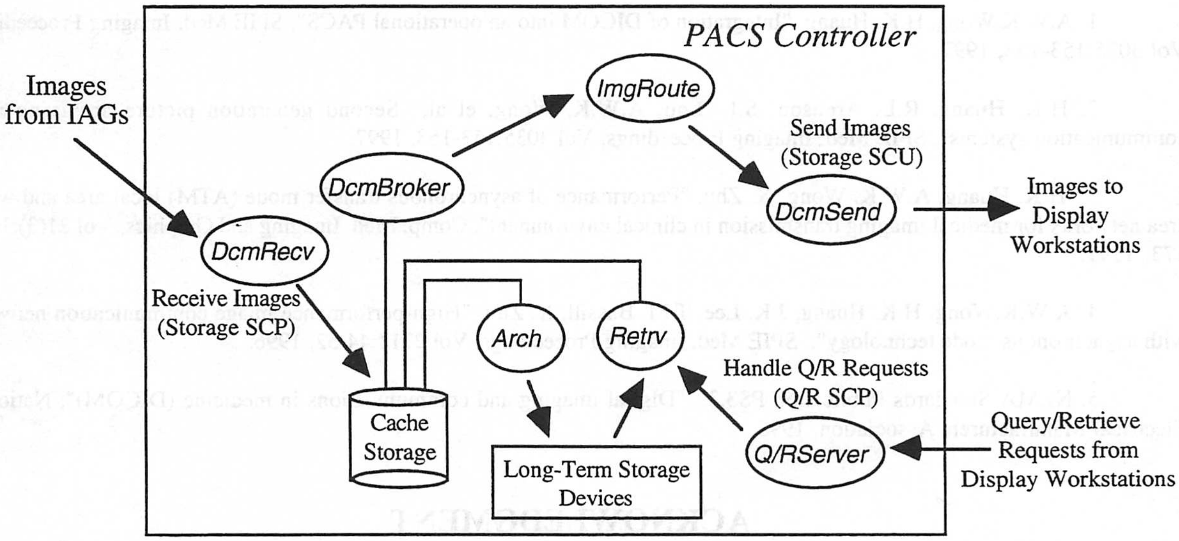
PACS Controller
Images from IAGs
ImgRoute
Send Images (Storage SCU)
DcmBroker
DcmSend
Images to Display Workstations
DcmRecv
Receive Images (Storage SCP)
Arch
Retrv
Handle Q/R Requests (Q/R SCP)
Cache Storage
Long-Term Storage Devices
Q/RServer
Query/Retrieve Requests from Display Workstations

Figure 4. Interprocess communication among the major processes running on the PACS Controller. The *DcmBroker* serves as an arbitrator ensuring images acquired from the radiologic imaging devices can be adequately distributed to the display workstations.

5. CONCLUSION

DICOM provides a simple means of interconnecting multi-vendor imaging equipment for communication of images, regardless of computer hardware and operating system platforms. However, while DICOM is intended to promote a communications standard towards connectivity, it does not necessarily guarantee interoperability. Because of vendors' different approaches in their DICOM implementations, one major challenge in PACS integration using DICOM has been the interconnections of vendor-specific imaging systems, allowing their mutual communications for images and associated information.

Two major aspects, data integrity and interoperability, are worth considering when integrating multi-vendor imaging equipment with DICOM into PACS. Unfortunately, the limitations of access to vendor-specific applications have often led to certain difficulties for PACS to interoperate the imaging equipment in a multi-vendor environment. As a consequence, interoperation failure of these equipment means loss of images and relevant information, which is definitely unacceptable in a clinical setting.

Our implemented mechanisms to ensure data integrity and cross-platform interoperability have significantly improved system reliability and operation efficiency of our PACS. The key issue of these improvements is to allow our in-house PACS components such as the IAGs and the PACS Controller to take most of the control in the communications with vendor-specific imaging systems. However, operating a large-scale PACS configured with multi-vendor imaging equipment requires significant effort in software integration in order to achieve a fully operational system.

6. REFERENCES

1. A.W.K.Wong, H.K. Huang, "Integration of DICOM into an operational PACS", SPIE Med. Imaging Proceeding, Vol 3035:153-158, 1997.

2. H.K. Huang, R.L. Arenson, S.L. Lou, A.W.K. Wong, et al, "Second generation picture archiving and communication systems", SPIE Med. Imaging Proceedings, Vol 3035:153-158, 1997.

3. H.K. Huang, A.W.K. Wong, X. Zhu, "Performance of asynchronous transfer mode (ATM) local area and wide area networks for medical imaging transmission in clinical environment", Comp. Med. Imaging and Graphics, Vol 21(3):165-173, 1997.

4. A.W.K.Wong, H.K. Huang, J.K. Lee, T.M. Bassill, X. Zhu, "High-performance image communication network with asynchronous mode technology", SPIE Med. Imaging Proceedings, Vol 2711:44-52, 1996.

5. NEMA Standards Publication PS3.3, "Digital imaging and communications in medicine (DICOM)", National Electrical Manufacturers Association, 1993.

ACKNOWLEDGMENT

This work is partially supported by a contract from National Library of Medicine N01-LM-6-3547.

Medical Imaging Techniques and Applications,
Ed. Leondes, CT., Gordon & Breach Science
Publ, Chap 5, 221-272. 1997.

5 IMAGE PROCESSING TECHNIQUES IN BONE AGE ASSESSMENT

EWA PIETKA and H.K. HUANG

The University of California, San Francisco,
Department of Radiology, Laboratory for Radiological Informatics,
530 Parnassus Avenue, Rm Cl-158,
San Francisco, CA 94143-0628, USA
e-mail: bernie_huang@radmac1.ucsf.edu

ABBREVIATIONS

ROI	region of interest
PROI	phalangeal region of interest
CROI	carpal bones region of interest
EROI	epiphyseal region of interest
LHFC	horizontal Low and vertical High Frequency Component
HLFC	horizontal High and vertical Low Frequency Component
LLFC	horizontal Low and vertical Low Frequency Component
HHDC	horizontal High and vertical High Frequency Component
PBA	phalangeal bone age
CBA	carpal bone age
RBA	radiological bone age
SEF	stage of epiphyseal fusion
EM	energy measure

5.1. INTRODUCTION

Part of the motivation for a computer-assisted diagnosis stems from our desire to understand the way in which human intelligence perceives the objects and, based on the visual perception, solves the pattern recognition tasks. Visual perception, being part of the pattern recognition leads to an extraction of certain elements from the object content. These elements, including certain parts of the object as well as their color, brightness, density, shape, size, etc. and often being very imprecisely defined even by the observer himself, serve as a basis for the object recognition. The larger the similarity between objects to be compared the many more details are necessary to make a distinction. Moreover, the details become more and more sophisticated and may be searched by the observer interactively while the recognition process proceeds. The interactive perception-recognition process may also proceed unconsciously.

Zadeh[1] has defined a human pattern recognition as a mapping of a pattern from pattern space into class-membership space. This kind of mapping carried out by nature can be thought of in terms of an opaque mapping. Unfortunately, very often neither the recognition process as such is understandable nor many details are accessible. In order to be implemented as a computer-aided recognition approach, the opaque mapping has to be replaced with a transparent mapping described in terms of an algorithm, understandable and able to perform on a computer.

Curiosity, whether we are able to make computers "intelligent" is not the only motivation. In clinical application we deal with problems which have to be solved in a fast and objective way. However, human observation is influenced by internal (coming form the observer) as well as external (often independent from the observer) impacts. The objectivity of classification is restricted by the receptivity of human senses which are influenced by the experiences or level of training, psychological conditions (tiredness, hurry, etc.), as well as external conditions (lighting, destructive noise, etc.). A failure in perception questions the entire recognition process. The recognition process itself, influenced also by the above mentioned conditions, may cause a slow down and/or lead to a false diagnosis. Therefore, the diagnostic results are evaluated by the inter-observer (multi-observer performing one observation) and intra-observer (one observer performing multiple observations) discrepancy. The first evaluation reflects more the level of training and experiences, whereas, the other one — the replicability of the recognition method. Both can assess the influence of the changing conditions.

The implementation of computers in the medical diagnosis improves the analysis in three different areas. Firstly, it increases the objectivity by using quantitative features instead of a visual interpolation. These features are extracted automatically rather than manually in order to accelerate the analysis and make the measurements independent from the external conditions (light), measurement inexactness, or errors (calibration errors, etc.). Secondly, a transparent algorithm is defined to standardize the decision-making process in the feature analysis. This again increases the objectivity and solves the problem of replicability. Finally, it permits a set of images and features describing them to be collected and recognized as a medical standard.

In this approach we refer to the human observation performed in the clinical routine. Therefore, before going into the technical details, let us look at diagnostic methods employed by radiologists.

5.1.1. Medical Background

Bone age assessment is a procedure frequently performed in the pediatric radiology. Based on a radiological examination of skeletal development of a left hand wrist, the bone age is assessed and then compared with the chronological age. A discrepancy between these two values indicates abnormalities in skeletal development. This examination is universally used due to the advantage of simplicity, a minimum of radiation exposure, and the availability of multiple ossification centers for evaluation of maturity. It is an important procedure in the diagnosis and management of endocrine disorders serving subsequently as one index of therapeutic effect.[2] Being a useful procedure in the diagnostic evaluation of metabolic and growth abnormalities[3] it indicates as well the acceleration or decrease of maturation in a variety of syndromes, malformations, and bone dysplasias.[4] Bone age assessment procedure is referred to for patients with gonadal dysgenesis[5] or while metacarpal sign occurs.[6] It is also consulted in planning an orthopedic procedure which will be used for the correction of angular deformities or abnormalities of length involving the vertebral column or long bones.

Bone age assessment is based on an analysis of ossification centers in the carpal bones and epiphyses of tubular bones including distals, middles, proximals, radius, and ulna (Figure 1). Epiphyses ossify usually after the birth. With increasing of age the bony penetration advances from the initial focus (Figure 2a) in all directions (Figure 2b). Penetration continues until the edges of metaphyses are reached (Figure 2c). The strip between the shaft and the ossification center diminishes progressively (Figure 2d) in thickness until it disappears completely at the completion of growth (Figure 2e), when the epiphysis and metaphysis fuse into one adult bone.

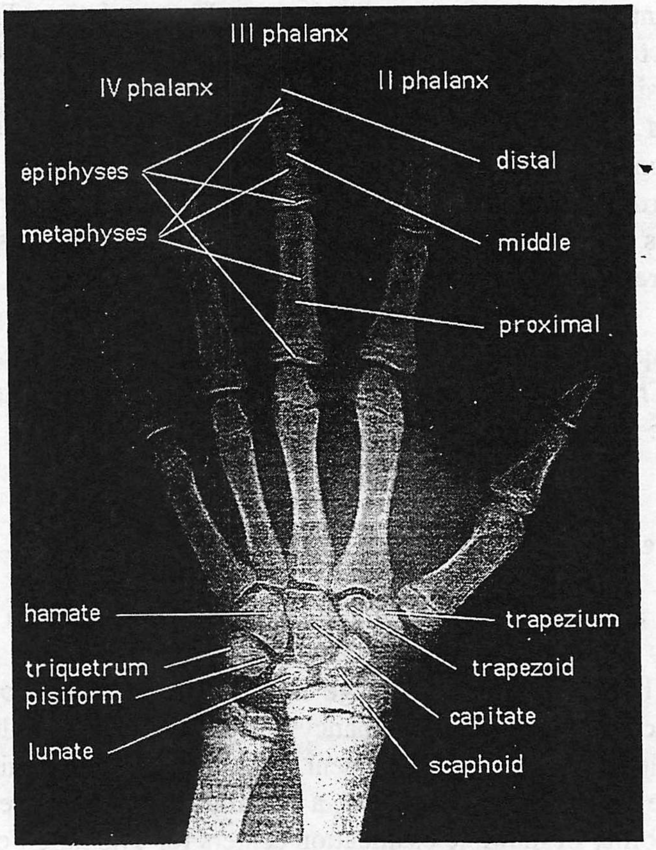

Figure 1. Hand wrist radiograph.

Carpal bones are another part of the information source. In the early stage they appear as a dense pin point on a radiograph. While developing, they increase in size until finally they reach their optimal size and characteristic shape. In the developmental order of appearance[7] capitate (Figure 1) and hamate is followed by triquetrum and lunate. Then scaphoid, trapezoid, and trapezium occur. Finally, pisiform overlaps the already existing triquetrum and hamate. The girl's development is noticeably more advanced and may differ from boy's development as many as 3 years.

Medical studies[8] indicate that, due to the carpal bones nature of maturity, their analysis does not provide accurate and significant information for patients older than 9–12 years of age. In this stage of development the phalangeal analysis yield more reliable results. Besides, more reliable results can be obtained while analyzing the most distal hand area.[4]

Numerous roentgen methods have been proposed for assessing the bone age according to the time of appearance, size, and differentiation of the

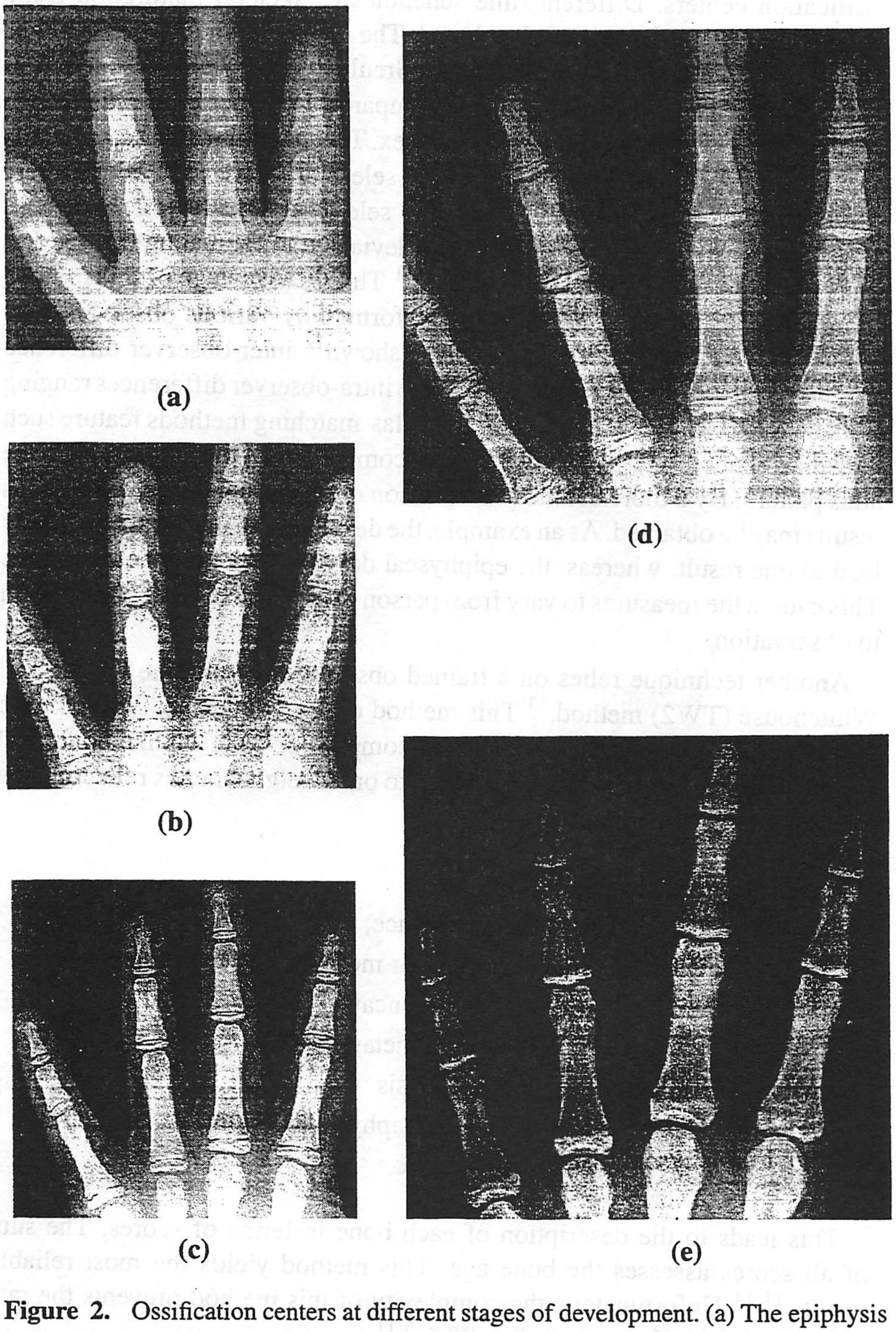

Figure 2. Ossification centers at different stages of development. (a) The epiphysis is distinct in appearance and disc-shaped with a smooth continuous border, (b) the epiphysis is half or more the width of the metaphysis, (c) the epiphysis is as wide as the metaphysis and follows closely its shape, (d) fusion of epiphysis and metaphysis has begun, (e) fusion of epiphysis and metaphysis is completed.

ossification centers. Different time schedules of skeletal maturation from fetal until adult life have been developed. The most commonly used method (76%)[9] is the atlas matching method by Greulich and Pyle.[10] Based on this method, a left hand wrist radiograph is compared to the series of radiographs grouped in the atlas according to age and sex. The pattern which superficially appears to resemble the clinical image is selected. Since each atlas pattern is assigned to a certain year of age, the selection assesses the bone age. However, there is still concern about the deviation in estimating the age that leads to a high rate of mis-classification.[11] The disadvantage of this method is a subjective nature of the analysis performed by various observers with different levels of training. Studies have shown[12] inter-observer difference ranging from 0.37 to 0.6 years, whereas the intra-observer differences ranging from 0.25 to 0.47 years. The reason that atlas-matching methods feature such high discrepancies, results from a general comparison of the radiograph to the atlas pattern. By a more detailed comparison of individual bones, ambiguous results may be obtained. As an example, the development of carpal bones may lead to one result, whereas, the epiphyseal development may yield another. This causes the measures to vary from person to person and from observation to observation.

Another technique relies on a trained observer applying the Tanner and Whitehouse (TW2) method.[13] This method uses a detailed analysis of each individual bone (epiphysis-metaphysis complex of each tubular bone and carpal bones). Each complex is assigned to one of eight classes reflecting the following developmental stage:[13]

stage B: single deposit of calcium,
stage C: center is distinct in appearance,
stage D: maximum diameter is half or more the width of metaphysis
stage E: border of the epiphysis is concave
stage F: epiphysis is as wide as the metaphysis
stage G: epiphysis caps the metaphysis
stage H: fusion of epiphysis and metaphysis has begun
stage I: epiphyseal fusion completed.

This leads to the description of each bone in terms of scores. The sum of all scores assesses the bone age. This method yields the most reliable results.[11,14] Unfortunately, the complexity of this method prevents the rate of its application from exceeding 20%.[5,11]

The above presented remarks show that it is worthwhile to develop a computerized system to assist the radiologists in performing a more objective and accurate analysis yielding the bone age assessment.

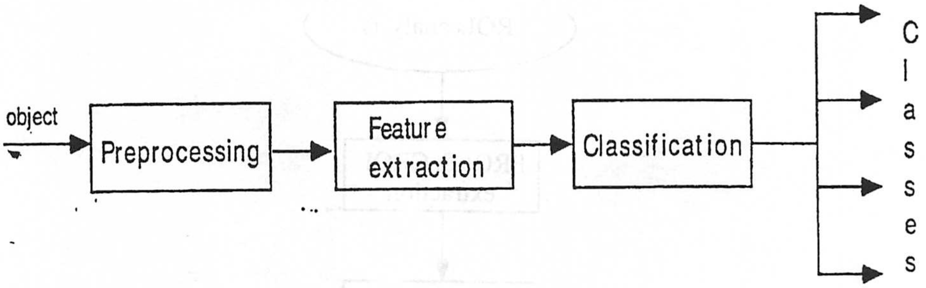

Figure 3. Pattern recognition phases.

5.1.2. General Computerized Approach

Referring to human observations, in a classical pattern recognition approach three phases can be distinguished (Figure 3). Firstly, a preprocessing step standardizes the image in terms of the background and orientation. The background standardization removes parts of the image background caused by blocking of the collimator during the X-ray exposure, which do not deliver any pertinent information, adversely affecting observer performance and/or computerized image analysis.[15] The orientation procedure rotates images (if necessary) to a standard position viewed by radiologists and clinicians. The preprocessing part[16] refers to the very first action, done by radiologists or technicians, namely, to place the hard copy onto the illuminated panel (light box) at a standard position. Additionally, the computerized approach offers a reduction of background light.

Secondly, the feature extraction step (Figure 4) develops measurement procedures which extract a set of parameters describing the object. This turns a natural object into a mathematical model which describes the object in terms of quantitative measures. In this approach three regions of interest (ROI) are selected: phalangeal region of interest (PROI), carpal bones region of interest (CROI), and epiphyseal regions of interest (EROIs). The analysis of certain regions depends on a rough estimation of the developmental stage of the patient performed on the basis of the length of tubular bones. This estimation (not being used directly in the final bone age assessment) indicates which ROIs are to be considered. The phalangeal length is extracted from the PROI whose analysis is performed for all patients. It delivers also the epiphyseal and metaphyseal diameters whose ratio is employed as a feature in the final phalangeal bone age assessment. The diameters themselves serve as edges of the EROI. For young patients, up to 9-years-old, the CROI analysis is initialized. For older patients carpal bones do not deliver pertinent

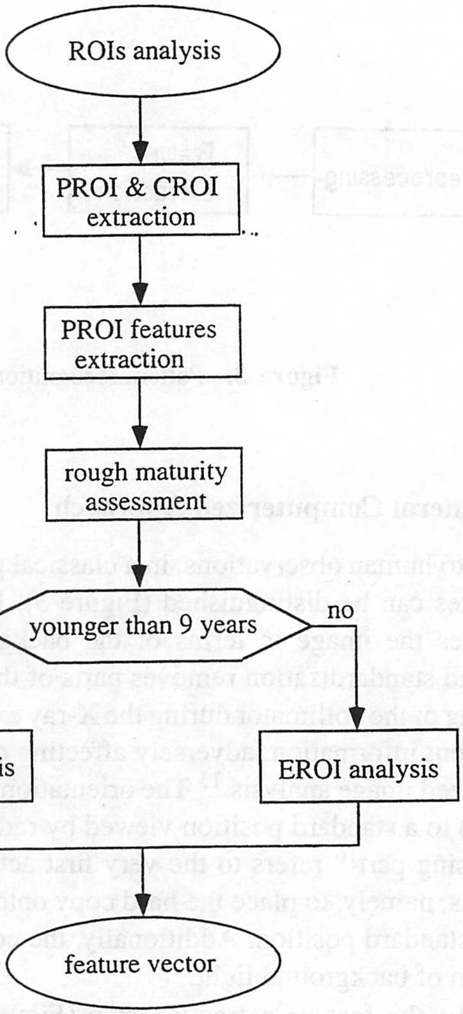

Figure 4. Flow diagram of feature extraction phase.

information. The EROIs, although can be employed for all patients, are advised to be used for patients older than 9 years of age. For younger patients epiphyses are not fused and the extracted feature remains unchangeable. From each of the selected ROIs, certain features are extracted and passed to the next phase.

Finally, in the classification phase (Figure 3), a transparent algorithm, developed on the basis of an opaque clinical method of radiological analysis, is employed. The algorithm is again split into three independent classifiers (one for each ROI). The initialization of each classifier depends on whether in the feature extraction phase a corresponding ROI has been analyzed.

This method, analyzing a hand wrist Computed Radiography (CR) image (Figure 1), turns it into a mathematical model (feature extraction phase) and compares with a mathematically developed standard to be able to assess the developmental stage. Since all regions are evaluated independently, the assessments reflect the maturity featured by each region individually.

The computerized analysis still remains a computer-assisted or computer-aided diagnosis. Due to the variety of human nature none of the computer system designer is able to foresee all possible cases and, thus, none of the computerized system is able to provide a 100% classification rate. This is true not only for the computerized systems. Additional medical consultation is often required when an unusual case is diagnosed. Therefore, each automatically performed analysis can serve as an assistant in order to improve the examination terms discussed above. Yet, the clinician is still responsible for each final diagnosis.

5.2. FEATURE SELECTION

There is no general approach to the problem of feature selection. Features should provide an adequate description of the pattern and be sensitive to the structural changes on the basis of which an image is classified. Thus, features applied to assess the bone age should reflect the morphological changes which are able to distinguish one developmental stage from the other, for example, the increase in size of epiphyses, tubular bones, or carpal bones. They may also point out an object or a change of an object which appears at a certain stage of development. The more accurate a feature is able to describe the changes between certain stages, as a more reliable classification result can be obtained. If features do not reflect the structural changes, no classifier of whatever sophistication can yield a reasonable result.

On the other hand, the features have to be extracted reliably (i.e. with a high rate of correct extraction) and cannot require too sophisticated and time consuming algorithms. It happens often that some features of a high discriminant power do not meet the above condition and cannot be extracted automatically. Looking at some features taken into consideration by the TW2 method,[13] these remarks become clear. As an example, let us compare features which distinguish stage F (Figure 2c) from stage G (Figure 2d) in the analysis of proximal phalanges. It is hard to think of a fully automated method which determines whether the epiphysis caps the metaphysis. The feature selection step is then a compromise between the features discriminant power and the ability and reliability of their extraction. Therefore, the computerized approach often uses features which reflect the changes, yet, which have not been implemented in the clinical diagnosis.

5.2.1. Phalangeal Analysis

In the phalangeal analysis three types of features have been extracted. The first type includes the length of distals, middles, and proximals. While applying the standard phalangeal length table[17] each measure can be assigned to a year of age. However, they do not appear to be reliable bone age indicators and are only used for a rough maturity assessment.[18] The second type measures the diameters of epiphyses and metaphyses. Since diameters themselves are sensitive to the size of the hand and its rotation along the forearm axis during the examination procedure, their ratios have been calculated. This reflects to a certain extent the classification done by Tanner and Whitehouse[13] which distinguishes stages B through F. This is also a finding compared by some radiologists while applying the Greulich and Pyle method.[10] In the clinical approach it is not a quantitative finding, yet, it is considered during the visual comparison of the radiographs with the atlas patterns. The third type of features, again used only visually in the diagnostic procedure, describes the stage of epiphyseal fusion (stages H and I). In our approach this feature is quantified and assigned to one of four classes (no fused, early fusion, advanced fusion, fusion completed).

5.2.2. Carpal Bones Analysis

Carpal bones (capitate, hamate, triquetrum, lunate, scaphoid, trapezoid, and trapezium in Figure 1) are another part of information source in different methods of bone age assessment.[8,10,13,19] Their development differs from the long tubular bones. As explained in section 5.1.1, they do not appear all at the same time. Capitate and hamate appear in the first year of age, whereas, pisiform appears at the age of 8 for girls and at the age of 11 for boys.[20]

At the early stage of development, the carpal bones appear on the radiograph individually. Their separation and description in terms of features is relatively simple. However, at the age of 9–10 they start overlapping. At this point, further analysis becomes very difficult. As mentioned in section 5.1.1, due to their nature, they do not deliver pertinent information for patients older than 9–12 years of age. At this stage of development the phalangeal features lead to more reliable results. Kirks says:[4] "*The more distal, the better*". Thus, the carpal bones analysis is performed only for patients younger than 9 years of age.

5.2.3. Evaluation of Extraction of Features

The feature selection problem returns after the feature extraction algorithms have been developed. Two reasons may cause a selected feature to be rejected from being used in the clinical application: firstly, the accuracy of its extraction, secondly, its discriminant power.

In the accuracy of extraction two problems have to be taken into consideration. The first one includes mis-extraction of objects. This means, that instead of finding, for example, a particular carpal bone, a noisy object reflecting soft tissue has been extracted and considered by the algorithm as a carpal bone, or, due to an unusual position of the hand, a length that has been found is not the desired diameter but a measure of a different object (or bone). In this case the answer of the evaluation procedure is binary: correct/incorrect extraction, meaning, a correct or incorrect extraction of the measured object. The second problem in the accuracy evaluation refers to the accuracy of the measures themselves and is performed for all bones correctly identified. In this measurement evaluation, computer measures are compared with the manual measures. The conventional evaluation for measuring the significance of a difference of means is referred to as a t-test.[21] Assuming, that both distributions are thought to have the same variance, the following steps are required:

- calculation of the mean difference m_1 and m_2 and the mean standard error s_D,
- computation of $t = (m_1 + m_2)/s_D$
- evaluation of the significance of the t value for Student's distribution probability function

The second aspect includes the evaluation of the discriminant power of each feature. It may eliminate some features as well as restrict the implementation of others. This evaluation can be performed by plotting clustered measures (or their normalized values) versus the classes which are taken into consideration in the classification stage. Then, certain statistical parameters (mean value, standard diviation, distances from the cluster centers, common cluster area, etc.) are calculated to evaluate the overlapping of clusters. Finally, certain rules (discussed in the next sections) are applied to evaluate the discriminant power.

Another statistical approach,[22] uses the F statistic which is a ratio of the between class variation to the within class variation. A feature of a large between class variation and yet low within class variation giving a large F is a good discriminator.

5.3. REGIONS OF INTEREST

As a region, we term an area within an image that contains a certain type of information of equal importance for further analysis. The meaning "importance" can be evaluated as negative as well as positive. While talking about importance in a negative sense, we consider information that is of no pertinent context for further analysis. These areas are called regions of no interest (RONI). On the other hand, importance in a positive sense is referred to regions which include information to be considered in further processing. These areas are termed regions of interest (ROI).

In our approach one RONI has to be excluded, namely, the unexposed image background, caused by blocking of the X-ray collimator and resulting in white borders surrounding the image field and adding a significant amount of unwanted transparent area. The removal of this area is done by turning to black all pixels from this area. Since the area is not of a rectangular shape, it cannot be removed by "cutting off" the border, which leads to the restriction of the image size. The algorithm[23] first searches for the row edges of the radiation field. The row edges points are those with standard deviation in the desired direction exceeding an empirically determined threshold. Then, the edges are reconciled to find the corner points. From these corner points, straight lines boundaries are interpolated. Points outside the contour are set to black.

After removing the undesirable information (Figure 5a), two ROIs are defined: phalangeal region of interest (PROI) and carpal bones region of interest (CROI). They are extracted from a thresholded image. Since at this point the entire image has to be scanned, a fast average thresholding technique is applied. It turns to 0 all pixel values below the average image gray-scale threshold and to 1 all the values above. This method can be successfully applied only after removing the unexposed background. Otherwise, the threshold is too high. The thresholding procedure yields a "glove" image (Figure 5b) which is then scanned in the horizontal and vertical direction.

The upper edge of the PROI (Figure 6) is found by scanning a horizontal profile from the top of the image down to the tip of the third phalanx. The lower edge cuts the image at the soft tissue junction between the thumb and the index. Then, two vertical profiles are scanned from the left and right radiograph edges towards its central part. The first intersection with the "glove" defines the left and right PROI, respectively. The lower PROI edge serves also as upper CROI edge. The lower CROI edge is determined by scanning the forearm upward from the bottom of the image. The line intersecting the forearm with the minimum width fixes the lower edge. Two vertical profiles are scanned similarly to the PROI profiles, yet, independently from them. Again, the first intersection between the profiles and the pixels within the hand contour marks the CROI boundaries. Though, the PROI includes distals, middles, proximals, and parts of metacarpals, whereas, the CROI includes all carpal bones, parts of metacarpals, parts of radius and ulna.

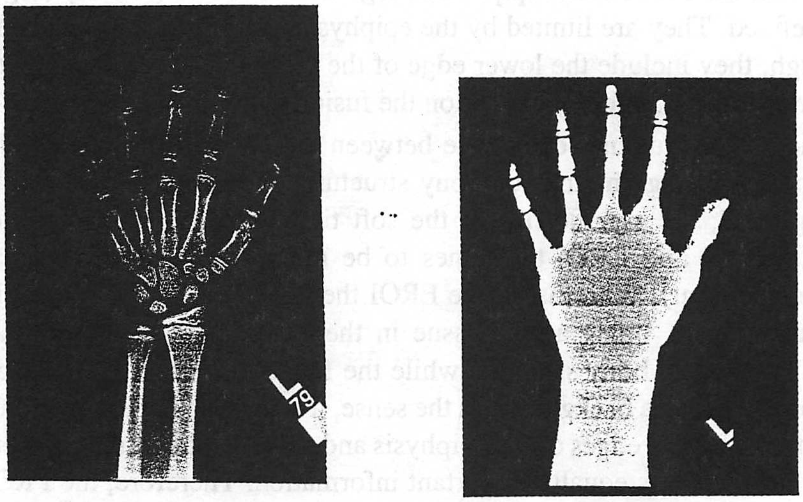

Figure 5. Hand wrist radiograph (left) and its "glove" version (right).

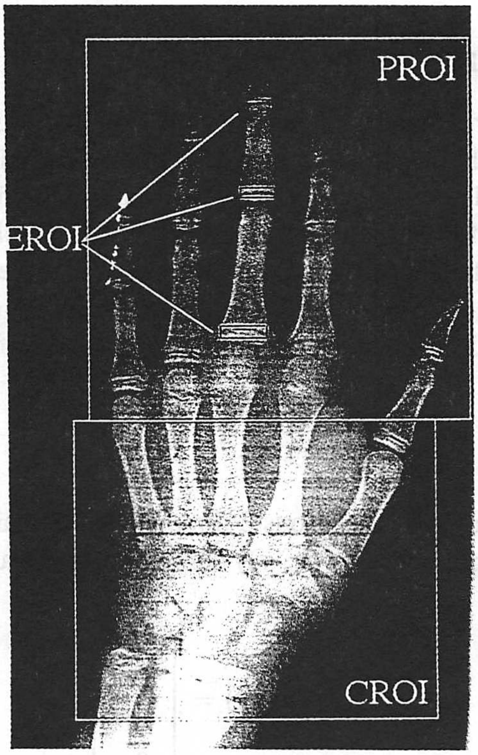

Figure 6. Hand wrist radiograph with marked edges of the phalangeal region of interest (PROI), carpal bones region of interest (CROI), and epiphyseal regions of interest (EROI) of the III phalanx. Corresponding EROIs are extracted for the II and IV phalanx.

Within the PROI small epiphyseal regions of interest (EROIs) (Figure 6) are defined. They are limited by the epiphyseal and metaphyseal diameters. Though, they include the lower edge of the metaphyses and the upper edge of the epiphyses. Within this region the fusion analysis is performed.

There is a structural difference between the PROI/CROI and the EROI. Although, all regions include bony structures displayed on the soft tissue background, the significance of the soft tissue is different in both cases. In the PROI and CROI the bones to be measured have to be separated (segmented out). Whereas, in the EROI the gap between the epiphysis and the metaphysis, being a soft tissue in the early stage of development is filled out by the bony structure while the fusion proceeds. Thus, it cannot be considered as a background in the sense, it is done in the PROI and CROI. Together with the edges of the epiphysis and the metaphysis the gap between the bones delivers equally important information. Therefore, the PROI and EROI, although, describing the developmental stage of the same region, are discussed separately.

5.4. EXTRACTION OF PROI FEATURES

The phalangeal region of interest (PROI) includes distals, middles, and proximals of all phalanges, as well as parts of metacarpals which are ignored in the approach. The first group of features reflects the developmental stage of phalanges, as far as their size is concerned. Each phalanx is described in terms of the phalangeal length and the ratio of the epiphyseal diameter divided by the metaphyseal diameter. All distance measures are extracted from a gradient PROI in which the bone edges are significantly enhanced.

5.4.1. Gradient PROI

Since the edges are in a continuous 2-dimensional domain $f(x, y)$, they can be detected by a gradient $\mathbf{G}(f(x, y))$ defined for the x and y coordinates as

$$\mathbf{G}(f(x, y)) = \begin{bmatrix} \dfrac{\partial f}{\partial x} \\ \dfrac{\partial f}{\partial y} \end{bmatrix}$$

This means, that the gradient along the line normal to the edge slope is defined as derivatives along orthogonal axes. The vector $\mathbf{G}(f(x, y))$, describing separately the row edge gradient $\partial f/\partial x$ and the column edge gradient $\partial f/\partial y$

can be presented in terms of a spatial gradient amplitude also called its magnitude

$$\mathrm{G}(f(x, y)) = \left[\left(\frac{\partial f}{\partial x} \right)^2 + \left(\frac{\partial f}{\partial x} \right)^2 \right]^{1/2}$$

which is the maximum rate of change of $f(x, y)$ per a unit distance in the G direction. For computation efficiency, the gradient may be approximated by the absolute value

$$\mathrm{G}(f(x, y)) = \left| \frac{\partial f}{\partial x} \right| + \left| \frac{\partial f}{\partial y} \right|$$

Computation of the gradient is based on partial derivatives $\partial f / \partial x$ and $\partial f / \partial y$ computed at every pixel. For a 2 × 2 region

$$\begin{array}{cc} x_1 & x_2 \\ x_3 & x_4 \end{array}$$

$\partial f / \partial x$ is computed by using a mask

$$\begin{array}{cc} 1 & -1 \\ 0 & 0 \end{array}$$

and the computation of $\partial f / \partial y$ uses a mask

$$\begin{array}{cc} 1 & 0 \\ -1 & 0 \end{array}$$

For a 3 × 3 region

$$\begin{array}{ccc} x_1 & x_2 & x_3 \\ x_4 & x_5 & x_6 \\ x_7 & x_8 & x_9 \end{array}$$

$\partial f / \partial x$ is computed by using a mask

$$\begin{array}{ccc} -1 & -2 & -1 \\ 0 & 0 & 0 \\ 1 & 2 & 1 \end{array}$$

and the computation of $\partial f / \partial y$ uses a mask

$$\begin{array}{ccc} -1 & 0 & 1 \\ -2 & 0 & 2 \\ -1 & 0 & 1 \end{array}$$

These two masks are often referred to as Sobel operators. Combination of both masks at any point results in obtaining the gradient at that point. A convolution of these masks with a region (image) yields a gradient at each point and is often referred to as a gradient region (image). The gradient computation can be based on a larger neighborhood. Then, it decreases the sensitivity to noise, yet, it decreases also the computational speed. Therefore, 3 × 3 neighborhood is by far the most popular.[24]

The entire PROI is subjected to the gradient analysis. In the gradient PROI (Figure 7a) two anatomical regions are significantly enhanced. One covers the phalangeal edges, resulting in a clear separation between phalanges and the soft tissue surrounding the phalanges. The second dense region reflects the bone non-uniformity of epiphyses and metaphyses. As a result, these two regions concentrate the largest number of pixels of a high gradient.

5.4.2. Extraction of Phalangeal Length Measures

While analyzing the gradient PROI (Figure 7a) one can easily notice an increased concentration of pixels in the epiphyseal and metaphyseal area. It reflects the edges between epiphyses and metaphyses as well as the bony structure itself. An extraction of this region is necessary to separate the distals, middles, and proximals (in order to find their length) and to locate their extremities (in order to find the epiphyseal and metaphyseal diameters and extract the epiphyseal regions of interest for the analysis of fusion). For each phalanx, the separation is performed in three steps:

- extraction of the phalangeal tip
- rough extraction of the entire phalanx
- extraction of epiphyses.

These steps are performed interchangeably for all phalanges under consideration.

Location of the phalangeal tip starts with the location of its candidate. The search is based on an analysis of profiles scanned from the top of the gradient PROI towards the bottom. Due to the length of fingers, the first tip to be found is the tip of the III phalanx. Then, based on mathematical morphology,[25] a dilation/intersection reconstruction sequence measures the object size. A contiguous set of non-zero pixels is dilated (described in Appendix A) and then logically intersected with the thresholded image to form an object. This procedure is repeated up to a certain number of iterations. It is interrupted in order to accelerate the performance. If it is smaller than empirically defined, it is considered as noise generated by processing the soft tissue with the Sobel gradient operator and is removed from the PROI. The search is then continued. If the examined object is large enough, it is considered as the tip of the III phalanx.

In order to roughly locate the entire III phalanx, a predefined window covering the width of the phalanx (Figure 7b), is shifted from the tip over the entire phalanx (to the bottom of the PROI). Bone edges marked on the gradient PROI, serve as a basis to locate the phalangeal central axis. This permits each window to be centered, meaning, that the window central axis is intended to cover the bone central axis by shifting the window to the right or to the left depending on the rotation angle of the finger.

The extraction of epiphyses (Figure 7c) is based on an analysis of the concentration of pixels in each window. The concentration is considered as a function versus the distance from the phalangeal tip. Since the concentration of the high gradient pixels increases significantly in the epiphyseal area, this function is searched for three local maxima. The distances between them cannot be smaller than a predefined value. Its assessment depends on the range of age considered in a certain application. It has to be smaller than the length of distals, middles, and proximals of patients belonging to the youngest group. This measure can be derived directly from the radiographs or assessed on the basis of the standard phalangeal length table.[17] If the distance measures do not meet the predefined conditions, certain correction steps[26] can be applied.

Once the epiphyses are found the separation lines between the distals, middles, and proximals are extracted (Figure 7d). These lines are defined as short profiles (of a length of the predefined window) perpendicular to the phalangeal central axis and having the smallest intersection with the bone. Two cases are possible. For older patients whose epiphyses are already developed, one profile of minimum intersection with the bone is found. For younger patients a gap between epiphyses and metaphyses causes several profiles not intersecting the bone to be found. In this case, a profile tangential to the epiphysis marks the bottom of the epiphysis, whereas, a profile tangential to the metaphysis located below marks its top. The Euclidean distances between the already found intersection points serve as the length measures.

Above the separation lines the left and right extremities of epiphyses and metaphyses are located. Based on the analysis of distances between the phalangeal central axis and the bone edge, three following points on the bone edge are detected one each side of the central axis:

- maximum distance which reflects the metaphyseal extremity,
- minimum distance which locates the narrowest area between the epiphysis and metaphysis (can be equal to 0 for very young patients),
- maximum distance which reflects the epiphyseal extremity.

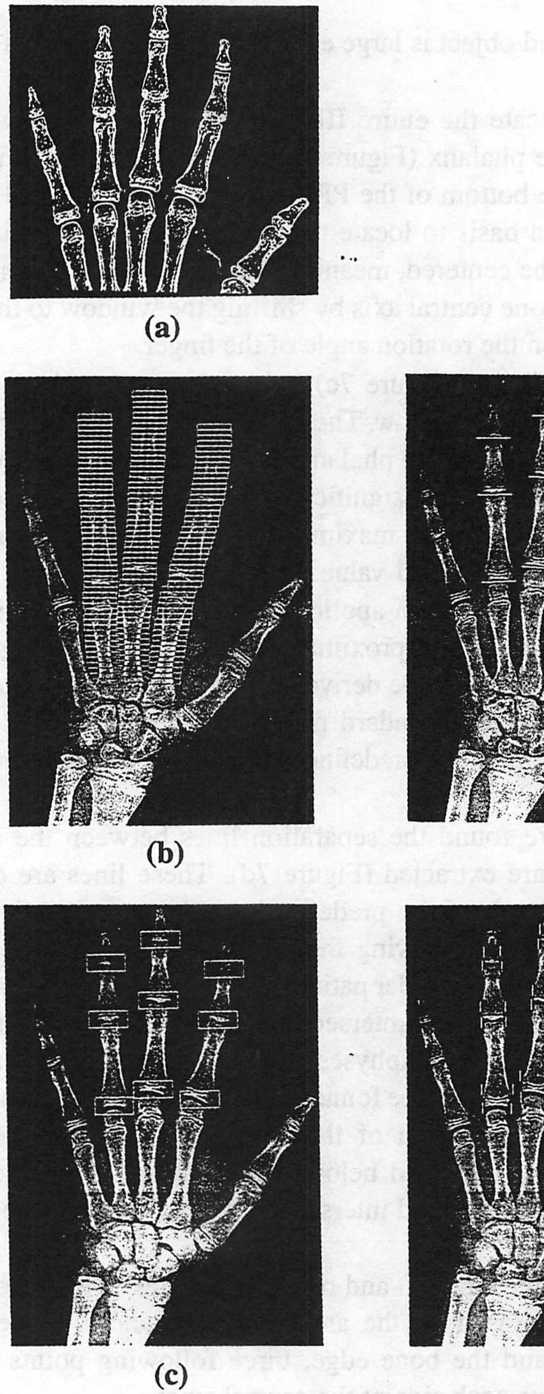

Figure 7. Phalangeal region of interest (a) processed with the Sobel gradient operator. (b) The II, III, and IV phalanx overlapped with scanned windows (in each iteration the window is centered), (c) extraction of epiphyses, (d) separation lines for the II, III, IV phalanx, (e) extremities of epiphyses and metaphyses marked for the II, III, and IV phalanx.

In the analysis, first, the bone edge is searched for the minimum. Then, both maxima are found, one above and the other below the minimum. These points are located on the left and right bone edge (Figure 7e). The diameters of epiphyses and metaphyses are defined as Euclidean distances between the left and right extremities of epiphyses and metaphyses, respectively.

Since distance measures are sensitive to the hand size, the length of fingers, and the rotation of the hand during the examination procedure, extracted values of phalangeal diameters for a certain year of bone age vary from one patient to another. While clustering the measures with respect to years of bone age, the neighbor clusters overlap significantly. To lower the sensitivity, ratios of epiphyseal diameters divided by metaphyseal diameters are calculated.

These three steps (extraction of the phalangeal tip, rough extraction of the entire phalanx, extraction of epiphyses) performed on the III phalanx (as described above) are repeated for the II and IV phalanx. As a result, the following measures have been received:

- length of phalanges (9 features),
- ratios of epiphyseal diameter to metaphyseal diameter (9 features).

Using the phalangeal lengths a rough assessment of the skeletal maturity is performed on the basis of the standard phalangeal length table.[17] The estimation associated with a single phalangeal length is obtained by a linear interpolation of the table values. This single estimators are then averaged to assess the global developmental stage. Unfortunately, it does not appear to be a sufficient indicator of skeletal maturity and can only be used as a rough estimate. Thus, it is used internally in the algorithm to limit the CROI analysis and initialized the epiphyseal fusion assessment.

The ratios of the epiphyseal diameter to the metaphyseal diameter serve as a reliable indicator up to about 14 years of age. Due to the anatomical development of epiphyses, for older patients their discriminant power decreases. At this point the epiphyseal fusion becomes a crucial parameter. However, the PROI analysis is performed for all patients and the extremities of epiphyses and metaphyses indicate the EROIs.

5.5. EXTRACTION OF EROI FEATURES

Image analysis based on distance measures does not provide adequate information in the later stage of development, when the diameters of phalanges and epiphyses does not change. Epiphyseal fusion effects neither their length nor their width significantly enough to yield a reliable assessment. At this step the stage of fusion itself has to be assessed.

The analysis starts with an extraction of an epiphyseal region of interest (EROI) (as described in section 5.3). It contains the upper part of the epiphysis and the lower part of the metaphysis (Figure 6). The gap between both bones reflects either the soft tissue (before the fusion starts) or the bony structure (while the fusion proceeds). In this step a texture analysis is performed on the entire EROI, meaning, that all pixels included in the region are considered in the direct analysis.

The EROI boundaries are defined by the diameters of epiphyses and metaphyses. The longest diameter determines the width of the region. Then, the EROI is rotated to align the metaphyseal diameter with the horizontal direction. This region is subjected to the wavelets decomposition algorithm.

5.5.1. Wavelets Decomposition

In this section, we introduce a 2-dimensional notation of the orthogonal wavelets representation. No proofs will be given. For more details we refer to [27–30].

A multiresolution approximation is a sequence of subspaces $\underline{V}_m$ of $\underline{L}^2(\underline{R}^2)$

$$\underline{V}_m \subset \underline{V}_{m+1} \quad \text{for } m \in \underline{Z}$$

$$\bigcap_{m\in\underline{Z}} \underline{V}_m = \{0\}$$

and

$$\bigcup_{m\in\underline{Z}} \underline{V}_m \text{ is dense in } \underline{L}^2(\underline{R}^2)$$

The $\underline{V}_{m+1}$ subspace is derived from $\underline{V}_m$ by scaling the approximated image (region or function) $f(x, y)$ by the ratio of its resolution value

$$f(x, y) \in \underline{V}_m \Rightarrow f(2x, 2y) \in \underline{V}_{m+1} \qquad \text{for } m \in \underline{Z}$$

In this application we approximate an image at a 2^j resolution ($j \in Z$). The approximation of an image $f(x, y)$ at a resolution 2^j is equal to its orthogonal projection on the vector space $\underline{V}_{2^j}$. Let $\phi(x, y) \in \underline{L}^2(\underline{R}^2)$ be a scaling function such that if $\phi_{2^j}(x, y) = 2^{2j}\phi(2^j x, 2^j y)$, then for $m, n \in \underline{Z}^2$, $2^{-j}\phi_{2^j}(x - 2^{-j}n, y - 2^{-j}m)$ forms an orthonormal basis of $\underline{V}_{2^j}$.[29] For a particular case of separable multiresolution approximation, the scaling function $\phi(x, y)$ can be written as $\phi(x, y) = \phi(x)\phi(y)$ where $\phi(x)$ and

$\phi(y)$ are one-dimensional scaling functions of the decomposed subspace. Let $\psi(x)$ be the one-dimensional wavelets associated with the scaling function $\phi(x)$. Then, we can build an orthogonal basis by scaling and translating three wavelets functions

$$\underline{\Psi}^1(x, y) = \phi(x)\psi(y)$$

$$\underline{\Psi}^2(x, y) = \psi(x)\phi(y)$$

$$\underline{\Psi}^3(x, y) = \psi(x)\psi(y)$$

The family of functions

$$\begin{aligned} m, n \in \underline{Z}^2(2^{-j}\phi_{2^j}(x - 2^{-j}n)&\psi_{2^j}(y - 2^{-j}m) \\ \psi_{2^j}(x - 2^{-j}n)&\phi_{2^j}(y - 2^{-j}m) \\ \psi_{2^j}(x - 2^{-j}n)&\psi_{2^j}(y - 2^{-j}m)) \end{aligned}$$

is an orthonormal basis of complement of $\underline{V}_{2^j}$ in $\underline{V}_{2^{j+1}}$.[27] The difference of information between the projection of $f(x, y)$ at 2^{j+1} and 2^j resolution is equal to the orthonormal projection of $f(x, y)$ on this complement. Therefore, an image at a 2^{j+1} resolution can be replaced by four images at a 2^j resolution. They are described in terms of a set of inner products which are equal to 2-dimensional convolution products evaluated at $2^{-j}n$

$$\begin{aligned} R^0_{2^j} &= \langle f(x, y), \Psi^0(x, y)\rangle = \langle f(x, y), \Psi^0_{2^j}(x - 2^{-j}n, y - 2^{-j}m)\rangle \\ &= (f(x, y)^*\phi_{2^j}(-x)\phi_{2^j}(-y))(2^{-j}n, 2^{-j}m) \\ R^1_{2^j} &= \langle f(x, y), \Psi^1(x, y)\rangle = \langle f(x, y), \Psi^1_{2^j}(x - 2^{-j}n, y - 2^{-j}m)\rangle \\ &= (f(x, y)^*\phi_{2^j}(-x)\psi_{2^j}(-y))(2^{-j}n, 2^{-j}m) \\ R^2_{2^j} &= \langle f(x, y), \Psi^2(x, y)\rangle = \langle f(x, y), \Psi^2_{2^j}(x - 2^{-j}n, y - 2^{-j}m)\rangle \\ &= (f(x, y)^*\psi_{2^j}(-x)\phi_{2^j}(-y))(2^{-j}n, 2^{-j}m) \\ R^3_{2^j} &= \langle f(x, y), \Psi^3(x, y)\rangle = \langle f(x, y), \Psi^3_{2^j}(x - 2^{-j}n, y - 2^{-j}m)\rangle \\ &= (f(x, y)^*\psi_{2^j}(-x)\psi_{2^j}(-y))(2^{-j}n, 2^{-j}m) \end{aligned}$$

There are different approaches to the scaling function ϕ and construction function ψ. One, used by Lemarie[30] starts from a multiresolution analysis framework. Two other approaches[27,28] start from a sequence $h(n)$. The summary of both approaches can be found in Appendix B. In this application the family of wavelets with compact support (derived in Appendix B) has been tested for $N = 11$, 13, and 15.

5.5.2. Assessment of Epiphyseal Fusion

The 2-dimensional wavelets decomposition algorithm, performed on a $2^j \times 2^j$ resolution region results in obtaining four images each at a $2^{j-1} \times 2^{j-1}$ resolution. The $R^0_{2^{j-1}}$ is the low frequency in both direction component, $R^1_{2^{j-1}}$ — the vertical high frequency component (horizontal edges), $R^2_{2^{j-1}}$ — the horizontal high frequency component (vertical edges), and $R^3_{2^{j-1}}$ — the high frequency in both direction component. Each of these components is obtained by two one-dimensional convolutions of rows and columns separately with ϕ and ψ filters described in Appendix B. After the convolution only every other row and column is retained. This reduces the resolution from 2^j to 2^{j-1}.

In a standard application of a wavelets decomposition algorithm, this process is a repeated predefined number of iterations. In following iterations only $R^0_{2^{j-1}}$ components are convolved. However, in this study only the $R^1_{2^{j-1}}$ and $R^3_{2^{j-1}}$ components are analyzed. The $R^3_{2^{j-1}}$ component is tested in the preliminary step, whereas, the $R^1_{2^{j-1}}$ is a basis for the fusion assessment. It preserves the horizontal edges of epiphyses and metaphyses and, therefore, reflects the degree of fusion.

Thus, subjecting the image region (Figure 8a) to the wavelets decomposition procedure, four components are received. They correspond to the combination of low and high pass filter applied to the original image interchangeably in the horizontal and vertical direction. The top left component is a result of the low pass filter convolved in both directions. This component preserves 99% of the energy. The top right component shows the results of the vertical high frequency and horizontal low frequency analysis. It enhances mostly the horizontal lines. The bottom left component is the horizontal high frequency and vertical low frequency component in which the vertical lines are enhanced. Finally, in the bottom right component the high pass filter has been applied in both directions. It shows high gradient in both direction points.

While comparing the wavelets decomposition components of the EROI for patients at different developmental stages (Figure 8), one can notice that their density decreases while the epiphyseal fusion proceeds. Epiphyses (a) through (c) in Figure 8 are not fused. Fusion starts in (d) and (e), proceeds

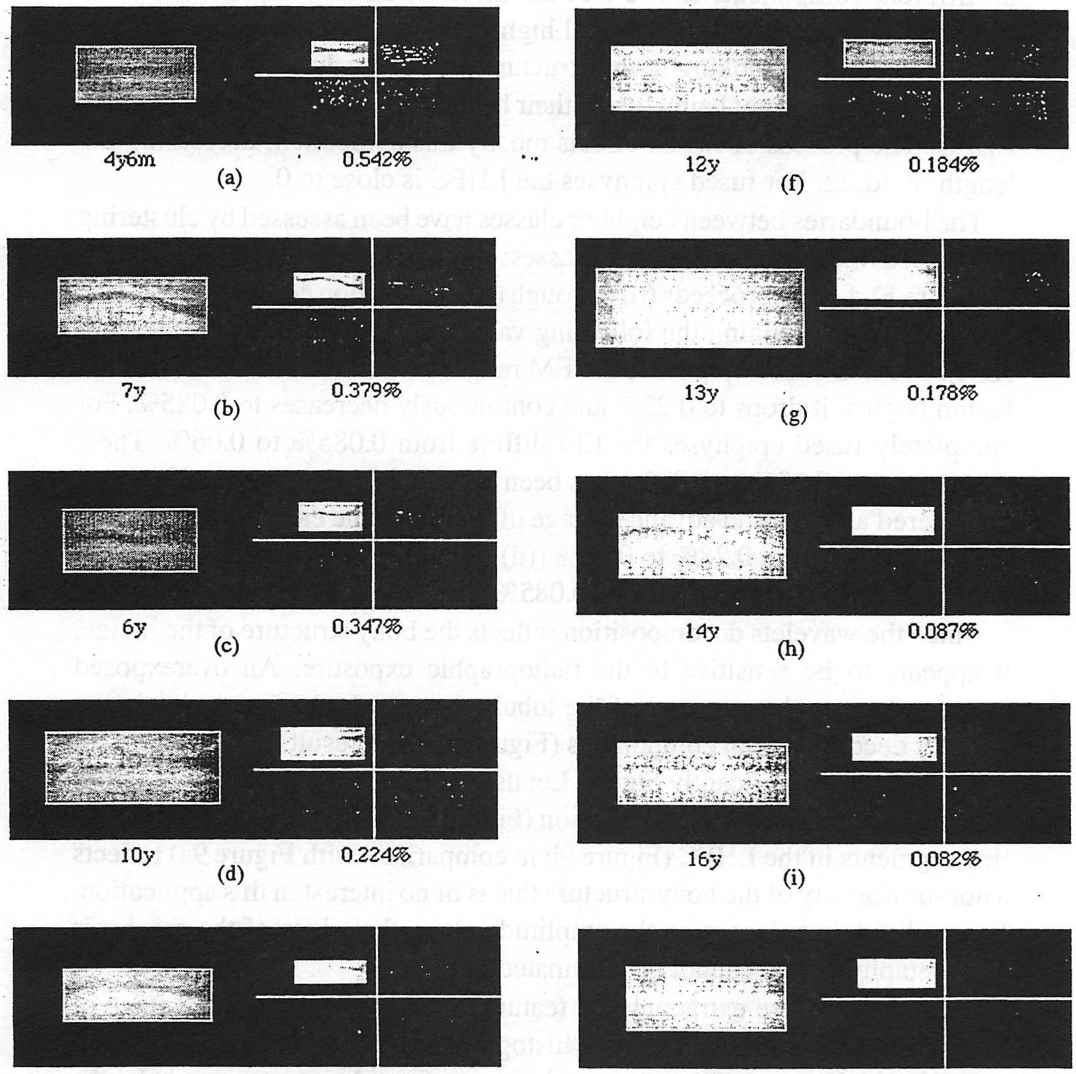

4y6m (a) 0.542%

12y (f) 0.184%

7y (b) 0.379%

13y (g) 0.178%

6y (c) 0.347%

14y (h) 0.087%

10y (d) 0.224%

16y (i) 0.082%

11y (e) 0.198%

17y (j) 0.065%

Figure 8. Epiphyseal region of interest (EROI) arranged in the order of decreasing values of the horizontal low and vertical high frequency component (LHFC) energy. The left region presents the original EROI, the right region — the wavelets representation. The top left shows the low frequency in both directions component (LLFC), the top right — the horizontal low and vertical high frequency component (LHFC), the bottom left — the horizontal high and vertical low frequency component (HLFC), and the bottom right — the high frequency in both directions component (HHFC). The numbers describe the bone age assessment (in years) and the energy of the LHFC with respect to the energy of the original region.

in (f) through (h), and is completed in (i) and (j). A comparison of the percentage of energy calculated versus the energy of the original region of different components shows that the most sensitive component appears to be the horizontal low and vertical high frequency component (LHFC). It can be justified by looking at the structure of the developed epiphyses and metaphyses. While not being fused, their horizontal edges are included in the LHFC. The process of fusion effects mostly this component decreasing the length of edges. For fused epiphyses the LHFC is close to 0.

The boundaries between neighbor classes have been assessed by clustering the features individually into three classes: epiphysis not fused ((a) through (c) in Figure 8), fusion proceeds ((d) through (h)), and fusion completed ((i), (j)). This results in obtaining the following values of the LHFC energy measure (EM). For non-fused epiphyses the EM ranges from 0.54% to 0.34%. While fusion begins, it drops to 0.22% and continuously decreases to 0.085%. For completely fused epiphyses the EM differs from 0.085% to 0.06%. Then, the interval of 0.23% to 0.085% has been divided into two classes which are considered as early and advanced stage of fusion. In the early stage of fusion the EM ranges from 0.28% to 0.18% ((d) through (f) in Figure 3) and in the advanced stage — from 0.18% to 0.085% ((g), (h)).

Since the wavelets decomposition reflects the bony structure of the image, it appears to be sensitive to the radiographic exposure. An overexposed image enhances the structure of the tubular bones which appear also in the wavelet decomposition components (Figure 9). As a result, the energy of all components is significantly higher. Let us compare two LHFC derived from two images of a similar stage of fusion (Figure 9). The presence of additional line segments in the LHFC (Figure 9b in comparison with Figure 9a) reflects a non-uniformity of the bony structure that is of no interest in this application. Its amplitude overlaps with the amplitude along the edges of the epiphysis and metaphysis and cannot be eliminated.

Therefore, before extracting the feature, employed to assess the stage of fusion, the LHFC is subjected to a histogram analysis. It serves as a quality control which prevents overexposed images from being analyzed. In the LHFC histograms of normally exposed images, a minimum value is followed by an increase of values reflecting the edges. While analyzing an overexposed image, the LHFC and its histogram is influenced rather by the structure of bones than by the edges. This results in a decrease of the histogram values. The amplitude reflecting the bony structure and epiphyseal and metaphyseal edges overlap and cannot be separated. The differences in the histogram shape defines the condition each image has to meet to be subjected to a further analysis. If the derivative of the histogram is negative in each point, the image is rejected. The second test applied to reject the overexposed image compares the high frequency in both direction components (HHFC in Figure 9).

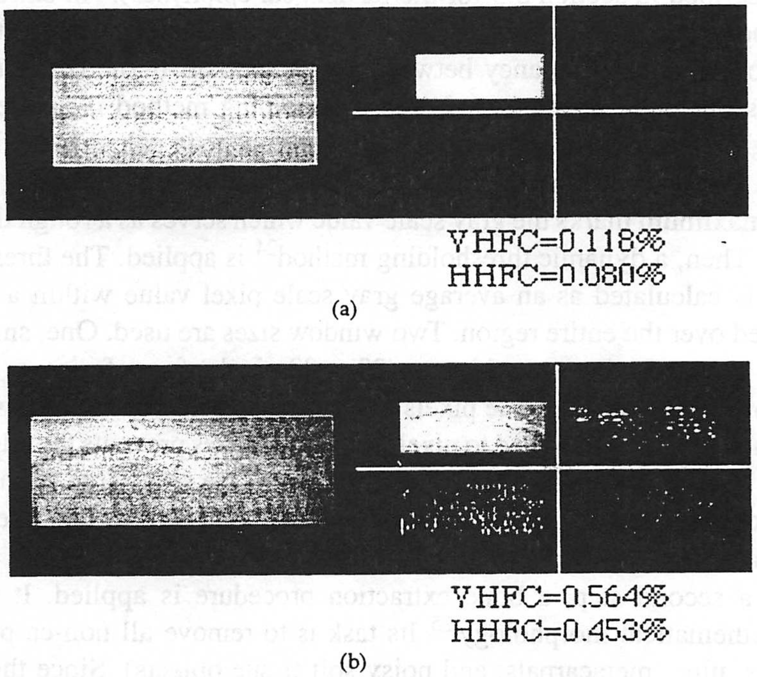

Figure 9. Wavelets decomposition performed on (a) normal and (b) overexposed image. For the explanation of both regions see description of Figure 8.

In a correctly exposed image it is much lower than in an overexposed image. Experimentally, limits are defined for each class of images.

If none of these two tests reject the image its analysis is continued. The minimum of the histogram value serves as a threshold. Then, the energy of the LHFC computed over amplitudes exceeding the threshold value is calculated and divided by the energy of the original region (in %). This value is considered as the measure which indicates the stage of fusion. For non-fused bones, it is higher and is decreasing while the fusion proceeds (Figure 8).

5.6. EXTRACTION OF CROI FEATURES

5.6.1. Extraction of Bones and their Description in Terms of Features

Carpal bones region of interest (CROI) includes (Figure 6) carpal bones, parts of the radius, ulna, and metacarpals. From this region two types of bones are extracted. Firstly, the carpal bones whose size is being described in terms of features, secondly, the radius, which is subjected to the wavelets decomposition analysis leading to the assessment of the epiphyseal fusion (as described in section 5.5 for the phalangeal epiphyses). An extraction of each bone is related to its separation from the background (the soft tissue). Due to a small discrepancy between bones and soft tissue (particularly in images of young patients), a 2-step thresholding method is applied. First, a rough separation is based on a histogram analysis calculated within the CROI. After smoothing the histogram, a local minimum following the first local maximum marks the gray scale value which serves as a rough threshold value. Then, a dynamic thresholding method[24] is applied. The thresholding value is calculated as an average gray scale pixel value within a window scanned over the entire region. Two window sizes are used. One, smaller (of 9 × 9 pixels) for bones and larger (33 × 33 pixels) for soft tissue. A larger window, used for soft tissue pixels reduces the sensitivity to noise, whereas, the smaller window applied to pixels reflecting bones prevents the edges from being blurred. This procedure removes most of the soft tissue (Figure 10a). Yet, some objects (called later in this section noisy soft tissue objects) still remain.

As a second step, a bone extraction procedure is applied. It is based on mathematical morphology.[25] Its task is to remove all non-carpal bones (radius, ulna, metacarpals, and noisy soft tissue objects). Since the radius, ulna, and metacarpals are attached to the CROI borders, they can be distinguished from carpal bones. This property is used for their extraction. The routine is based on a dilation/intersection reconstruction sequence. A non-zero pixel is dilated (described in Appendix A) and then logically intersected with the thresholded image to form an object. This procedure is repeated until the total area of the object does not increase in two subsequent iterations. This means, that the entire object is covered. This object is then removed by subtracting it from the CROI. This procedure is repeated for all non-zero pixels attached to the CROI borders. An opening operation (erosion/dilation reconstruction sequence) reduces some noisy objects. The current CROI (Figure 10b) contains carpal bones, epiphyses which are not attached to the radius, ulna, or metacarpals, and some noisy soft tissue objects. Their identification is based on features extracted from each of these objects.

Therefore, the dilation/intersection reconstruction sequence, already performed for border pixels for now repeated in the entire CROI. After an object has been separated, a filling-holes routine is used to reconstruct the missing information. The routine consists of an iterating dilation/intersection reconstruction sequence performed on the inverse of the region which includes the object to be corrected. The routine stops after reconstructing the entire object.

For each object the following parameters have been calculated: area, perimeter, compactness ratio, convexity coefficient, lengthening rate, gray-scale pixel value average, and gray scale pixel value discrepancy.

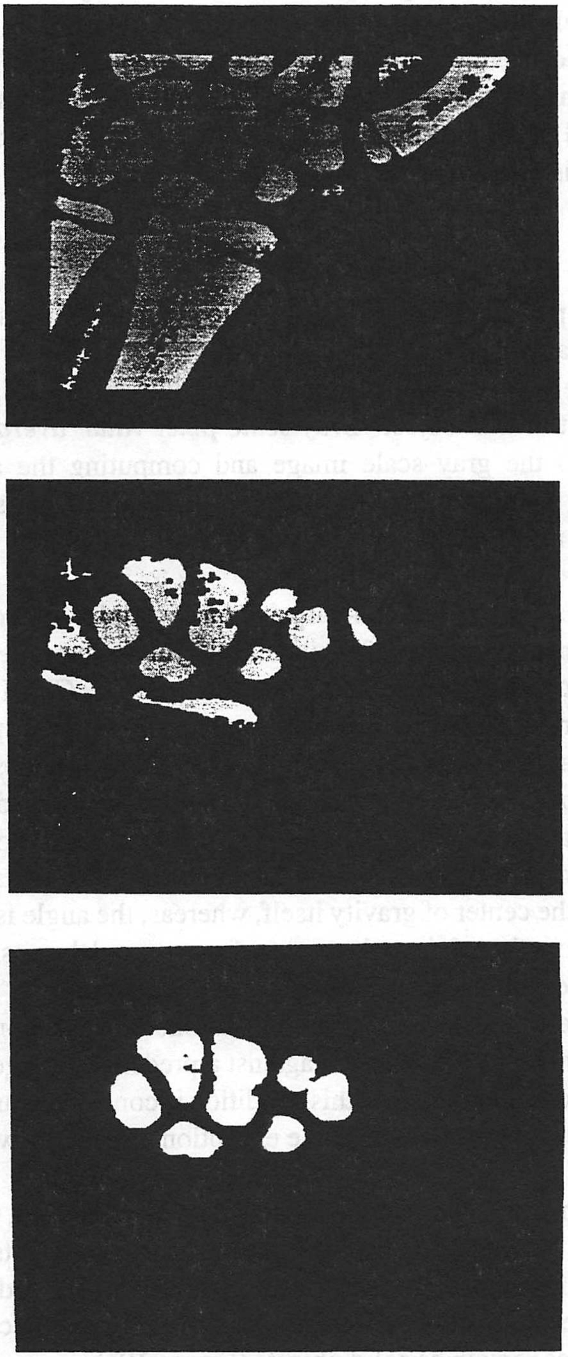

Figure 10. Carpal bone region of interest (CROI) (top) after the thresholding procedure, (centre) after removing bones attached to the CROI borders, (bottom) after removing all non-carpal bones objects and smoothing the carpal bones using mathematical morphology.

Area is the number of pixels included in the object. *Perimeter* is the number of pixels forming the contour. It has been obtained by subtracting the object from its dilated version. *Compactness ratio* is obtained by dividing the perimeter by the area and multiplying the result by a constant value. *Center of gravity* (CG) is found by eroding the object until the minimum number (>0) of pixels is left. *Convexity coefficient* is given by:

$$I_{CC} = P_{\text{conv.hull}}/P$$

where P is the perimeter and $P_{\text{conv.hull}}$ is the perimeter of the smallest convex set which contains the entire object.

Lengthening rate is obtained by dividing the smallest diameter by the largest one within the object. *Gray-scale pixel value average* is obtained by referring to the gray scale image and computing the average of the corresponding pixel values. *Discrepancy* is obtained by subtracting the maximum and minimum pixel values of an object computed within the gray scale images.

In order to separate the non-carpal bones, a polar coordinate plane is defined. The center of gravity of capitate, being the largest object of the largest average gray-scale pixel value serves as the origin. The CROI is then divided into five empirical sectors. Each may contain only one carpal bone or no carpal bone at all (for young patients). The multiangular bones section which contains two bones is the only exception. This division in based on the average anatomical location of the carpal bones. The center of gravity of each object is described in terms of the polar coordinates. The radius is a distance between the origin and the center of gravity itself, whereas, the angle is measured as a ray radiating from the origin to the center of gravity and the positive horizontal axis. Thus, determining the radius and angle of each object, all of them are assigned to one of the sectors. If more than one object belongs to a sector, described above features are tested against a predefined range of variability. The object, whose features meet this condition is considered as a carpal bone. All other objects are discarded. In the exceptional section, two carpal bones are accepted.

Due to the anatomical order of appearance of carpal bones, the assignment can be doubly proved. If a carpal bone is missing, objects belonging to the corresponding sector are tested again within an enlarged range of each interval. As a result, from the CROI all non-carpal bones objects are excluded and carpal bones remain as solid objects (Figure 10c).

As soon as the carpal bones are identified two additional parameters are computed to be used in the bone age assessment. They are:

$$\text{ratio1}_b = \frac{\text{area}_b}{\text{area}_c}$$

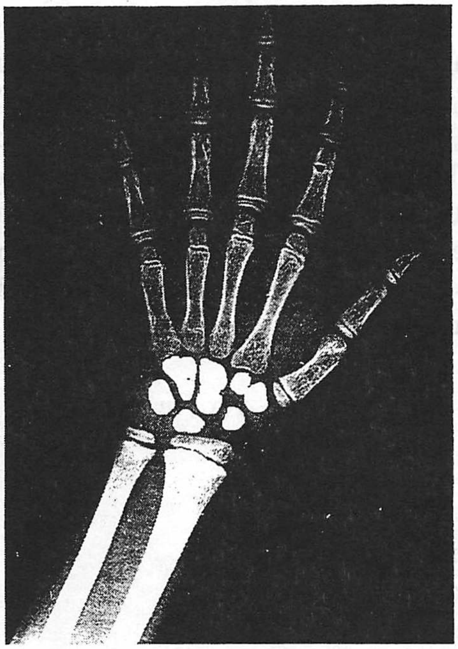

Figure 11. Original image with superimposed carpal bones extracted by the algorithm.

where

$$\text{ratio2}_b = \frac{\text{area}_b}{\sum_{i=1}^{n} \text{area}_i}$$

where ratio1$_b$ and ratio2$_b$ are parameters computed for the considered carpal bone, area$_c$ is the capitate area, area$_b$ is the area of the considered carpal bone and n is the number of carpal bones.

Features extracted from selected normal and pathological hand radiographs have been published in [31]. Adding the extracted objects back to the original image highlights the detected carpal bones (Figure 11).

5.6.2. Feature Selection

After all carpal bones are defined, a 2-dimensional feature selection analysis is performed to compare their discriminant power in the bone age assessment. The following eight features are subjected to this analysis: area, perimeter, compactness ratio, convexity coefficient, lengthening rate, ratio1, ratio2, and number of carpal bones. Features describing the location of carpal bones are not considered in further analysis. The number of features in each bone age group depends on the number of carpal bones developed in a certain year of bone age.

As reference images, a set of radiographs assessed clinically as normal, has been subjected to the feature extraction procedure. Then, each feature describing a carpal bone has been plotted versus the bone age (assessed by a radiologist). This gives a set of clusters. In order to exclude the most external measures, the set of observations for each year of bone age is fitted to a Gaussian curve. The mean value m is assumed to be the center of the corresponding cluster, whereas, the variance δ is adjusted by minimizing over δ the following expression:

$$\sum_i [y_i - y(x_i; m, \delta)]^2$$

where

$y()$ is the Gaussian distribution
m is the mean value
δ is the variance
y_i are measures
x_i are arguments.

All values within the interval $\pm 2\delta_{\min}$ remain in the cluster, others are excluded. In order to assess, whether a feature is suitable for further analysis, two discriminators are used:

$$\begin{aligned} \text{dist} &= \text{mean}_i - \text{mean}_{i+1} \\ \text{dist}_{\max} &= \text{dist\_max}_i + \text{dist\_max}_{i+1} \end{aligned}$$

where dist_max_i and dist_max_{i+1} are maxima of feature distances form the corresponding cluster centers.

A feature is selected, if dist $\geq$ dist_max.

Only four features (area, perimeter, ratio2, number of carpal bones) satisfy the above condition. Compactness ratio, convexity coefficient, lengthening rate, and ratio1 have been discarded.

5.7. CLASSIFICATION BASED ON A FUZZY CLASSIFIER

Already described image processing techniques lead to a description of each image in terms of quantitative parameters. This turns the image into a mathematical model in which the developmental stage of phalanges and carpal bones is described individually. In the phalangeal region, first, the length of tubular bones assesses roughly the developmental stage. This value is exclusively used by the feature extraction algorithm in order to initialize a certain option of further analysis. Then, the phalangeal diameters analysis is employed. This procedure delivers nine features (for distals, middles, and proximals of the II, III, and IV phalanx). Next, the epiphyseal fusion is described in terms of a percentage of energy of a selected wavelets decomposition component in comparison with the energy of the original region. Finally, the carpal bones extraction is included, when the roughly assessed maturity does not indicate their overlap. In this stage the area, perimeter, and ratios of a single carpal bone area divided by the global area of all carpal bones are extracted for existing carpal bones. Due to the order of appearance the number of features change from one image to another. Once a mathematical model is derived, an algorithm which assigns the model to one of the predefined classes needs to be defined. The classification method depends on the discrepancy of the size and shape of objects (a single carpal bone, epiphysis, etc.) belonging to one class (intra-class variety) and to different classes (inter-class variety), discriminant power of features, and precision with which the clinical decision-making method can be described.

The first two criteria may refer to two different levels of object definitions, firstly, to the object itself, secondly to its mathematical model. However, in order to estimate the inter- and intra-class variety by means of quantitative methods, objects have to be turned to mathematical models. Otherwise, we are only able to estimate the variety in terms of such intuitively understood abstracts like 'large', 'small', etc. Therefore, the assessment of the object variety is in fact the assessment of the discrepancy between features in the inter- and intra-class context. This is, how the discriminant power of features can be estimated. The variety of objects is assessed while clustering the features. In the most desirable case, we expect the features to be concentrated around the center of the cluster and the clusters not to overlap between each others. Unfortunately, it would be very unrealistic to expect such clusters while dealing with natural objects. Moreover, a certain feature may have a high discriminant power with an acceptable overlap between classes for a limited number of classes showing no discriminant power for others. This is particularly true while analyzing the development of a certain type of objects from earliest to the most advanced stage. We may be able to find features that describe a certain state existing from the earliest to the most advanced stages of development (e.g. epiphyseal fusion). Yet, there may also be features of a limited usage. Firstly, the difficulty of extraction may occur (as it can be seen in the carpal bones analysis), secondly, a feature may reflect developmental changes up to a certain stage (ratios of phalangeal diameters) or may occur at a certain stage of development (appearance of carpal bones).

Nature of features and the way they are extracted impose the first condition which the developed classifier has to meet. Due to the variety of human nature, the developmental process, as well as pathological changes, features may exceed the limits defined for each year of age or may not be available at all. This causes an overlap of clusters referring to neighbor classes. Besides, all features are extracted automatically with an accuracy of about 90%. This means, that on an average, one feature per image fails. This implies the first condition. The classifier cannot be sensitive to an abnormal or mis-extracted feature.

Another criteria which influences the choice of the classifier refers to the clinical assessment which is performed by radiologists on the basis of the original radiograph. This defines, to a certain extent, the nature of the classification problem. The inter- and intra-observer discrepancies (described in section 5.1.1) indicate the bone age assessment problem as very imprecisely defined. Furthermore, the lack of an updated, medically approved set of hand wrist images (the medically used set has been collected in the 1950s from a highly selected population) contributes to the low rate of accuracy.

The above described imprecision related to the feature extraction and classification is included in three types of inexactness, defined by Kandel.[32] *Generality* features a concept applied to a variety of situation. This refers to the variety in human nature as well as the variety related to different developmental stage combined often with other pathological conditions. *Ambiguity* describes more than one distinguishable subconcept. Each year of patient age is considered as a separate class which causes the classification function to have more than one maximum. *Vagueness* occurs when precise boundaries cannot be defined and functions take values other than just 0 and 1. As mentioned above, the clusters overlap leading to an ambiguous assignment of certain features to two classes. Since the above described recognition problem does not lend itself to a precise formulation, it requires imprecise techniques able to handle its inexactness.

Before converting the clinical bone age assessment method into a computerized technique, describable in terms of an algorithm, the clinical method itself (considered as a source) needs to be understood. The most commonly used is the Greulich and Pyle method[10] which refers each image to an atlas pattern. This means that in the classification procedure each image is compared with patterns recognized medically as a standard. Since entire images are compared, the reference patterns have to be images of a corresponding structure. The process of comparison itself can be regarded as a personal (subjective) way of treating objects with individual judgments. These judgments are based on individual criteria for evaluation. In the bone age assessment this criteria can be defined as "image resembles an atlas pattern". However, while comparing two images, certain anatomical regions are compared separately. The Tanner and Whitehouse method[13] indicates certain anatomical changes very precisely and scores these changes, whereas, the Greulich and Pyle method is based on an overall comparison. A problem arises, when two regions of the diagnosed image (e.g. phalanges and carpal bones), while being analyzed individually, are associated with two different years of age. Certain medical indicators can be found. Due to the "the more distal, the better" rule, the greatest accuracy is obtained[4] by comparing epiphyseal ossification of the distal phalanges with the standards. The relationship between epiphyses and metaphyses of distal phalanges may be evaluated by looking at the shape of epiphysis, modeling of epiphysis by adjacent metaphysis and bony structures, size of epiphysis, and diameter of epiphysis compared with adjacent metaphysis.[10] However, an individual criteria, very subjective and difficult to be defined is also possible.

Following the medical evaluation scheme, in our classification approach, we refer to both steps, the comparison and the judgment. Thus, for the comparison, the mathematical model describing the image is referred to as a mathematical pattern which maps all features to comparable measures. In other words, features of different nature (area, perimeter, ratio, etc.) extracted from the image are mapped into a space of homogeneous measures. Then, for the judgment, a classification rule is defined to assess the bone age. Due to the inexactness described above, fuzzy techniques have been applied rather than "hard" classification algorithms.[33]

5.7.1. Membership Function

The classification step is based on the fuzzy set theory introduced by Zadeh[34] in 1965 which admits the possibility of partial membership of an object in a set called a fuzzy set. Let $X = \{x\}$ denotes a space of objects (or features). Then, a fuzzy set A in X is a set of ordered pairs $X = \{(x, \mu_A(x))\}, x \in X$ where $\mu_A(x)$ is a membership function. Intuitively, it defines the grade of membership of x in A. More precisely, it means that a membership function is a mapping from the set of features to a value from a predefined interval. We assume, that $\mu_A(x)$ is a number in the interval [0, 1]. The grade 1 denotes a full membership, whereas, 0 refers to a non-membership.

As an example, let us consider a class of real numbers that concentrate around a real value R. We may define a membership function

$$\mu(x) = 1/(1 + (x - R)^2).$$

Its assignment is subjective in nature and reflects the context in which the problem is viewed. The membership value is in the interval [0, 1]. It increases while x comes close to R. Mathematical foundations of the fuzzy set theory can be found in [32,34,35].

The classification process leading to the bone age assessment is performed separately for the PROI, EROI, and CROI. Since the classification is performed individually, we received three assessments reflecting individually the phalangeal development, epiphyseal fusion, and carpal bones development. Thus, for all regions a membership function has been developed. It assigns the developmental stage of the region to a class. For the PROI and CROI each class is associated with a year of bone age, whereas, for the EROI four classes are predefined (no fusion, early fusion, advanced fusion, fusion completed). Since a fuzzy set theory is applied, the mapping does not deliver a binary value, meaning, that only one class is pointed out. Therefore, the mapping results in a set of membership values, each reflecting the grade-membership of the developmental stage in a certain class.

Definition of membership functions is based on a membership operator

$$\chi(a, b, x) = 1/(1 + a(x - b)^2). \tag{1}$$

This operator can be considered as a membership function for a single class and a single feature. Parameters a and b depends on the range of variability of the feature within each class and their inter-class discrepancy. Each input feature x is mapped into a membership value in the interval [0, 1]. The larger the membership value is the more the feature reflects the corresponding class. Using the membership operator defined in Equation (1), the membership function defined for all classes becomes a vector

$$\alpha(\mathbf{a}, \mathbf{b}, x) = \begin{bmatrix} \chi(a_1, b_1, x) \\ \vdots \\ \chi(a_n, b_n, x) \end{bmatrix} \tag{2}$$

where n is the range of the year of bone age.

The calculation of a_i and b_i $(i = 1, \dots, n)$ is described later.

Since the mathematical model describes each image by the means of multiple features including three ratio of phalangeal diameters, epiphyseal fusion for each phalanx in the PROI and area, perimeter, and ratios for each carpal bone in the CROI, Equation (2) is extended to reflect a multiple feature environment giving a matrix

$$\beta(\mathbf{a}, \mathbf{b}, \mathbf{x}) = [\alpha(\mathbf{a}, \mathbf{b}, x_1] \cdots \alpha(\mathbf{a}, \mathbf{b}, x_m)] \tag{3}$$

where m is the number of features.

Both PROI and CROI are multi-object regions. In the PROI the analysis is performed on the II, III, and IV phalanx, whereas, in the CROI up to 7 carpal bones are taken into account. Thus, each region is described in terms of a feature vector $\mathbf{y} = [\mathbf{x}_1, \ldots \mathbf{x}_k]$ and k is a number of objects. For a multi-object region, the membership function in Equation (3) is extended to

$$\mu(\mathbf{a}, \mathbf{b}, \mathbf{y}) = [\beta(\mathbf{a}, \mathbf{b}, \mathbf{x}_1) \cdots \beta(\mathbf{a}, \mathbf{b}, \mathbf{x_k})] \qquad (4)$$

This format of the membership function is used unchangeably only for the PROI. Due to specific changes featured by the mathematical model of carpal bones and epiphyseal fusion, this function has to be adjusted. For the CROI, the adjustment is caused by the developmental order of appearance of carpal bones. Their development differs from the development of long tubular bones. In the early stages they appear as a dense pin point on a radiograph. While developing, they increase in size until finally they reach their optimal size and characteristic shape. In the developmental order of appearance (Figure 1) capitate and hamate is followed by triquetrum and lunate (at the age of 3–4). Then, scaphoid, trapezoid, and trapezium occur (at the age of 5–6). Thus, in the CROI analysis not all carpal bones exist in the early stage. As a result, not all features have to be present at each year of age. This means, that the number of membership function components in Equation (2) differs. Thus, α is defined as

$$\alpha(\mathbf{a}, \mathbf{b}, x) = \begin{bmatrix} 0 \\ \vdots \\ \chi_c(a_{j-1}, x) \\ \chi(a_j, b_j, x) \\ \vdots \\ \chi(a_n, b_n, x) \end{bmatrix} \qquad (5)$$

The membership function component χ_c related to the year of the carpal bone appearance is defined as

$$\chi_c(a_j, x) = 1/(1 + a_j x^2) \qquad (6)$$

and is included in Equation (5). For the following components, the dependency of j from the object is related to the developmental order of appearance of carpal bones. Thus, for capitate and hamate j is equal to 1 and 2, respectively, for triquetrum and lunate j is, respectively, 3 and 4, and for scaphoid, trapezoid, and trapezium – 5, 6, and 7, respectively. Vector (5) is substituted in Equations (3) and (4).

The third membership function classifies the epiphyseal region of interest (EROI). Due to the lack of unambiguous medical assessment based on epiphyseal fusion, the extracted features (percentage of energy) is mapped to four predefined classes: no fusion, early fusion, advanced fusion, and fusion completed. Thus, the membership function consists of four components. Following the increasing order of the features, the membership function component for the 'fusion completed' class is defined as

$$\chi_1(a_1, x) = 1/(1 + a_1 x^2) \qquad x > 0 \tag{7}$$

for the advanced and early fusion

$$\chi_i(a_i, b_i, x) = 1/(1 + a_1(x - b_i)^2) \tag{8}$$

where $i = 2, 3$ for advanced and early fusion, respectively, whereas, for 'no fusion'

$$\chi_4(a_4, b_4, x) = \begin{cases} 1/(1 + a_4(x - b_4)^2) & x \leq b_4 \\ 1 & x > b_4 \end{cases} \tag{9}$$

Then, α is defined as

$$\alpha(\mathbf{a}, \mathbf{b}, x) = \begin{bmatrix} \chi_1(a_1, x) \\ \chi_2(a_2, b_2, x) \\ \chi_3(a_3, b_3, x) \\ \chi_4(a_4, b_4, x) \end{bmatrix} \tag{10}$$

Substituting Equation (10) in Equations (3) and (4), the membership function for a multi-feature and multi-object environment is received.

All parameters a_i and b_i are found on the basis of a training set. Since the membership function serves as a reference for the diagnosed images, it has to be defined on the basis of hand radiographs diagnosed as normal. Thus, the standard set being referred to as a pattern has been carefully selected. Then, each image has been subjected to the feature extraction procedure. The extracted features have been clustered according to the year of bone age. Due to imprecise nature of problems, (as discussed earlier) the neighbor clusters overlap, particularly for older patients, when the growth of epiphyses and carpal bones slows down. Since the assessment of a_i and b_i depends on the overlap of two neighbor clusters, these parameters are determined separately for each membership component. Therefore, corresponding features of each object (bone) within each region are selected over all images of a certain class. Obviously, clusters corresponding to the j-th class overlap with cluster corresponding to the $j-1$ and $j+1$ class. The overlap width w_j is measured as

$$w_j = d\max_j + d\max_{j+1} - w_c \tag{11}$$

where w_c is the distance between the centers of clusters and $d\max_j$, $d\max_{j+1}$ are maximum distances between the features and the corresponding center of the cluster for clusters j and $j+1$, respectively.

If two neighbor clusters overlap, the center of the common area is found. If the overlap does not occur, a point equally distant from their boundaries is found. Two types of membership function components can be distinguished. One type reflects clusters, located in a neighborhood of two other clusters, the other one reflects external clusters with one neighbor cluster only (membership function components defined by Equations (6), (7), and (9)). As far as the first type is concerned, for each cluster two such boundary points are located (one on each side). They serve as crossover points d_j and d_{j-1} (membership function value is equal to 0.5). These yields to a set of equations

$$\begin{aligned} \chi(a, b, d_j) &= 0.5 \\ \chi(a, b, d_{j-1}) &= 0.5 \end{aligned} \tag{12}$$

whose solution fixes the values of parameters a_i and b_i for each membership function component. As an example, membership function components defined on the basis of distal ratios of patients between 8 and 13 years of age are shown in Figure 12a.

The external cluster, having one neighbor cluster only, have also one boundary point. In membership function components defined in Equation (6) the carpal bone under consideration appears at a certain year of age. Thus, it is assumed, that b_j is equal to 0 and the common area center serves as a crossover point d_j in order to calculate a_j

$$\chi_c(a_j, d_j) = 0.5 \tag{13}$$

As an example, the membership function components defined for the area of the trapezoid are shown in Figure 12b. Since the trapezoid appears at the age of 6, four components are defined. Three of them are assigned to the age of 7 to 9, respectively, whereas, the additional component is assigned to the age of 6. Due to a large overlap between clusters in the group age 8 and 9, the last membership function component has been shifted (Figure 12b).

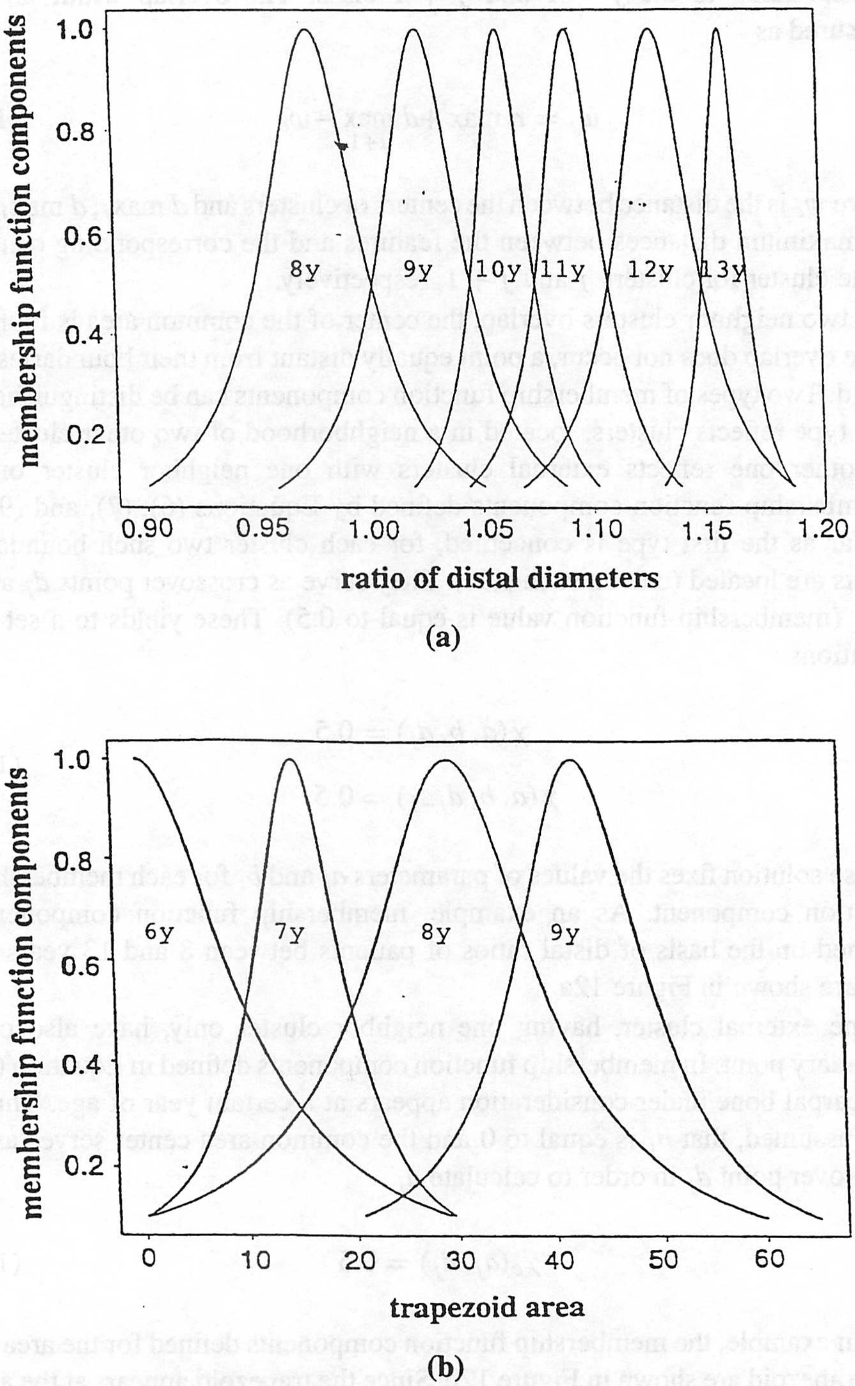

(a)

(b)

Figure 12. Membership function components defined on the basis of (a) distal diameters for 8- to 13-year-old patients, (b) areas of the trapezoids (in CROI). Each curve represents an age group.

Finally, for both external membership function components describing the epiphyseal fusion (Equations (7) and (9)) both b_j parameters are assumed to be equal to the corresponding centers of clusters, whereas, the a_j parameters are calculated based on the common area center as shown in Equations (9).

The classification step refers to the comparison stage of the clinical bone age assessment. It results in a fuzzy mapping from a set of features $X = \{x\}$ to the set $Y = \{y\}$ of years of bone age (for the PROI and CROI) or epiphyseal fusion assessment (for the EROI). This fuzzy mapping is a subset of characterized by a membership function that associates with each pair (x, y) its grade-membership function, being a value in [0, 1].

5.7.2. Classification Rule

The second step in the medical evaluation of a hand radiograph is a judgment. Based on a comparison between the radiograph and atlas patterns, the radiologist has to decide which pattern appears to resemble the clinical radiograph. This judgment leads to the bone age assessment.

In comparison with the clinical diagnosis, the computerized decision making process being based on a fuzzy binary relation $Q, Q \subseteq X \times Y$ between features X and the predefined classes Y points out the bone age reflecting the developmental stage of the region under consideration (PROI, CROI, or EROI). Due to the shape of the membership function components for each feature, the maximum of grade-membership values calculated over all classes indicates the corresponding bone age. Therefore, a global maximum operation calculated over all classes should also indicate the global bone age corresponding to the developmental stage of the ROI. Yet, the fuzzy relation maps more than just one feature to each year of bone age (or the state of fusion for the EROI). Therefore, we cannot apply a single maximum rule to assess the bone age. The maximum operation has to be preceded by another one which compresses all grade-membership values mapped to one class. Then, the composition of both operations may lead to the extraction of the desired bone age. Two such operators (giving two compositions) have been tested. The first one, called later a max-min rule performed on Equation 4 is defined as

$$\max_y \left[\min_x \mu(x, y) \right]$$

where x denotes the features and y denotes the years of bone age for the PROI and CROI or the state of epiphyseal fusion for the EROI.

This means, that for each class a minimum grade-membership value is found. This gives one grade-membership value for each class. Then, the maximum grade-membership value over all classes yields the desired bone age (or fusion state) assessment.

The second rule, called later a max-sum rule is defined as

$$\max_y \left[\sum_x \mu(x, y) \right]$$

which means, that the minimum operator of the max-min rule is replaced by the summation over all grade-membership values belonging to one class. The maximum value calculated over all classes yields the bone age (or fusion state) assessment.

As an example, grade-membership values of a selected image have been placed in a matrix (Table 1). They show the fuzzy relation between ratios of epiphyseal diameters divided by metaphyseal diameters and predefined years of bone age. Columns marked as $d1$ through $p3$ stand for distal ratios ($d1$ through $d3$), middle ratios ($m1$ through $m3$), proximal ratios ($p1$ through $p3$), respectively. These columns are followed by the result of the sum and min operation. The "age" column shows the years of bone age related to each membership value. Due to the shape of membership function components, the membership values should be close to 1 for the year of age which corresponds to the bone age and close to 0 for other classes. If the bone age is assessed as a non-integer value (i.e. 4 years and 7 months) the values close to 1 are distributed between both neighbor integer age values. If features are mis-extracted or are out of a predefined range caused by pathological conditions this regularity can be destroyed (i.e. membership values of $d2$, $d3$, and $m1$ in Table 1). One can easily notice (Table 1) that the max-min rule is much more sensitive to these failures than the max-sum rule. Although in the presence of the out-of-range features the overall sum decreases, yet, it is still significantly higher than the neighbor values. Thus, in the final classification procedure, the max-sum rule is applied.

Finally, the max-sum value is compared with its largest neighbor sum value. If the neighbor value is smaller than 8% (refers to one month on the age axis) this value is ignored. Otherwise, an interpolation (with the accuracy of one month) yields the bone age. This permits the bone age to be assessed with the accuracy of one month.

5.8. RESULTS AND CONCLUSION

The evaluation of final results obtained in the classification phase by assessing the phalangeal bone age (PBA), carpal bone age (CBA), and the stage of epiphyseal fusion (SEF) is preceded by the evaluation of the extraction

Table 1. An example of membership function values calculated for a hand image. Columns marked as $d1$ through $p3$ stand, correspondingly, for features extracted from distals (d), middles (m), and proximals (p) of the II, III, and IV phalanx. The third and second last columns show the results of the $\min_x \mu(x, y)$ and $\sum_x \mu(x, y)$ operators, respectively. The last column marks the bone age assigned to each membership function. The patients chronological age is 10 years, the radiologically assessed bone age is 8 years and 5 months, whereas the phalangeal analysis results in 9 years (max-sum result 4.21).

$d1$	$d2$	$d3$	$m1$	$m2$	$m3$	$p1$	$p2$	$p3$	sum	min	age
0.08	0.01	0.02	0.00	0.04	0.06	0.03	0.07	0.22	0.54	0.00	7
0.23	0.02	0.03	0.01	0.15	0.30	0.09	0.35	0.94	2.11	0.01	8
0.94	0.01	0.02	0.03	1.00	0.73	0.61	0.67	0.20	4.21	0.01	9
0.26	0.03	0.06	0.03	0.15	0.09	0.41	0.12	0.06	1.21	0.03	10
0.09	0.11	0.34	0.27	0.11	0.08	0.12	0.06	0.04	1.23	0.04	11
0.01	0.11	0.96	0.88	0.04	0.03	0.02	0.01	0.01	2.07	0.01	12
0.05	0.88	0.34	0.05	0.00	0.00	0.01	0.01	0.01	1.35	0.00	13

of features. The feature extraction phase, first, locates the objects (epiphysis, metaphysis, capitate, hamate, triquetrum, etc.) subjected to the extraction of features, then extracts the features. Thus, in the evaluation analysis both steps are considered independently. Due to different types of extractions (objects or bones extraction and feature extraction), the evaluation methods differ as well. For the location of objects the accuracy measurement is binary. An object may be correctly or incorrectly located. It is assumed to be correctly defined if its identification permits a correct feature extraction. Each partial identification (e.g. part of an object has been erased by the segmentation procedure) leads to a mis-extraction of a feature. Therefore, the identification of such an object is considered as incorrect. In other words, an object is evaluated as correctly located if the entire measurement field of the object, meaning, all parts of the object used in the feature extraction procedure are found. Then, in the feature extraction evaluation, the accuracy of measures is evaluated. It is based on a comparison with another measurement technique. In our evaluation it is compared with measures extracted by fixing manually corresponding points on the soft copy display and measuring the distances between these points automatically.

In the evaluation of the classification phase, first, the discriminant power of each feature with respect to the bone age are estimated. Then, the PBA and CBA are compared with the bone age evaluated by a radiologist and called later a radiological bone age (RBA) assessment. Both PBA and CBA are considered individually. Finally, the epiphyseal fusion is referred to the RBA assessment.

Based on this scheme, the accuracy evaluation is performed for:

- detection of epiphyses and metaphyses
- accuracy of phalangeal length
- accuracy of epiphyseal and metaphyseal diameters
- detection of carpal bones
- accuracy of the carpal bone measures
- discriminant power of features
- evaluation of classifications for PROI, CROI, and EROI.

The evaluation has been carried out on 120 clinical radiographs giving 1080 epiphyses and metaphyses and 727 carpal bones to be located and analyzed.

For the PROI analysis, each epiphysis with the corresponding metaphysis is considered as one object. Thus, a failure in detecting one of these two elements, resulting in an incorrect extraction of the corresponding ratio of diameters, is considered as an incorrect detection of the entire object. A correct detection of 973 objects (out of 1080) has been obtained giving a rate of 90%.

While comparing the phalangeal length with a manual measurement, the mean difference of 0.02 mm with a mean standard error of 0.08 mm have been obtained. A paired *t* test has indicated a significance level of 0.05. The correlation coefficient has been 0.995.

A comparison of the computerized and manual measurements of the ratios performed separately for distals, middles, and proximals shows, that the mean difference between these two methods is 0.02 mm, 0.006 mm, and 0.003 mm, respectively, with a mean standard error of 0.038, 0.017, and 0.022, respectively. A paired *t* test has indicated that a difference of 0.02 given a standard deviation of 0.02 has been detected with a power of 0.85 and significance level of 0.05. The correlation coefficient is about 0.95 for all cases.

For the CROI, a correct detection of 689 carpal bones has been obtained, giving the rate of 94%. The size of the missing carpal bones has not exceeded 3 mm in diameter. The overall comparison of the accuracy of measures has been based on a visual comparison of the detected carpal bones overlapped with the original image. A significant enlargement of the carpal bones area has been observed in 45 (6%) cases. It has been caused by soft tissue attached to the bones during thresholding the CROI. A mis-extraction of the area influences also the perimeter of the corresponding carpal bone. Unfortunately, causing an increase of the total carpal bone area, all ratios are influenced.

The evaluation of the discriminant power is based on the analysis of clusters of features grouped for each year of bone age. The most external measures have been excluded by fitting the data to a Gaussian curve (as described in section 5.6.2). If the limited clusters still overlap, the feature is rejected. The results are shown in Figure 13. Ratios of distals, middles, and proximals have been plotted in Figures 13a, 13b, 13c. For the CROI analysis, area (Figure 13d), perimeter (Figure 13e), and ratio of each individual carpal bone area divided by the total carpal bone area (Figure 13f) have met the evaluation condition (section 5.6.2). Other features have been rejected.

Evaluation of the computerized phalangeal and carpal bone age assessment is based on an individual comparison of PBA and CPA with RBA (Table 2). Due to the inter-observer difference of the Greulich and Pyle method applied by radiologists, the computerized bone age assessment is accepted as being correct if it does not differ from the RBA more than 6 months. Results indicate that the phalangeal parameters seem to be more reliable than the carpal bone features. This shows, that phalanges are more sensitive to the developmental changes than carpal bones, particularly in pathological cases. Moreover, a discrepancy of more than 6 months between the PBA and CBA has been noticed[36] reflecting a difference in the development between phalanges and carpal bones in abnormal conditions.

The results of the stage of epiphyseal fusion (SEF) (Table 3) show, that a non-fused region is unambiguously separated from the regions in which the fusion has begun. The interval of the energy measure (EM) of this class (section 5.5.2., Figure 8), although needed to be extended to 0.32%, is still separated from the EM of epiphyses in which the fusion has already begun (its upper limit has also been extended to 0.27%). This means, that a non-fused epiphysis is not classified into a stage of 'fusion proceeds' or 'fusion completed'. A similar situation can be noticed while epiphyses are completely fused. However, due to different conditions during the X-ray exposure, in early stage of fusion, an epiphysis can be classified as not fused. An overexposed image exhibits a structural non-uniformity

Table 2. Accuracy of computerized bone age assessment based on an individual comparison of CBA and PBA with RBA.

	differs from RBA less than 6 mth	differs from RBA less than 1 yr	differs from RBA more than 1 yr
PBA	75%	19%	6%
CBA	63%	20%	47%

Table 3. Classification results for four stages of fusion.

truth / results	no fusion	early fusion	advanced fusion	fusion completed
no fusion	100%	0%	0%	0%
early fusion	8%	92%	0%	0%
advanced fusion	0%	14%	86%	0%
fusion completed	0%	0%	0%	100%

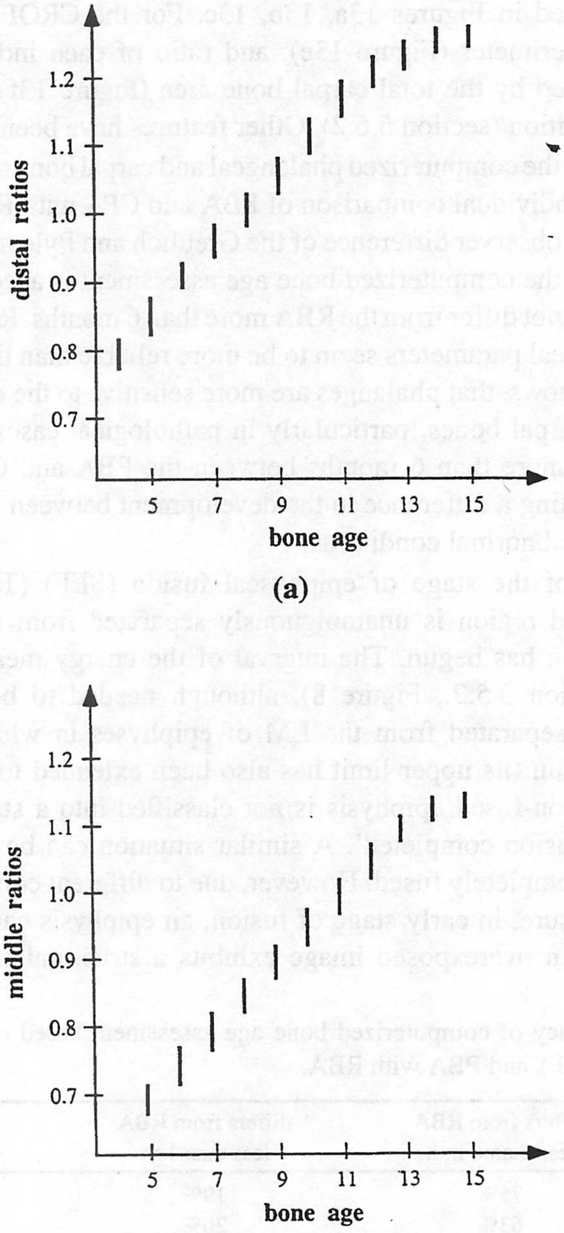

(a)

(b)

Figure 13. Features plotted versus the bone age assessed clinically (a) ratios of distal epiphyseal diameters to metaphyseal diameters, (b) ratios of middle epiphyseal diameters to metaphyseal diameters, (c) ratios of proximal epiphyseal diameters to metaphyseal diameters, (d) normalized area of carpal bones, (e) normalized perimeter of carpal bones, (f) normalized ratio of individual carpal bones area divided by the total carpal bone area.

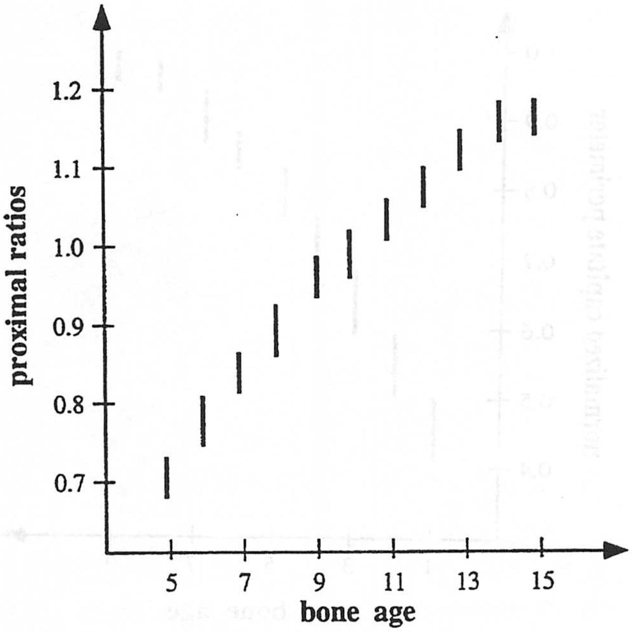
proximal ratios
1.2
1.1
1.0
0.9
0.8
0.7
5
7
9
11
13
15
bone age

(c)

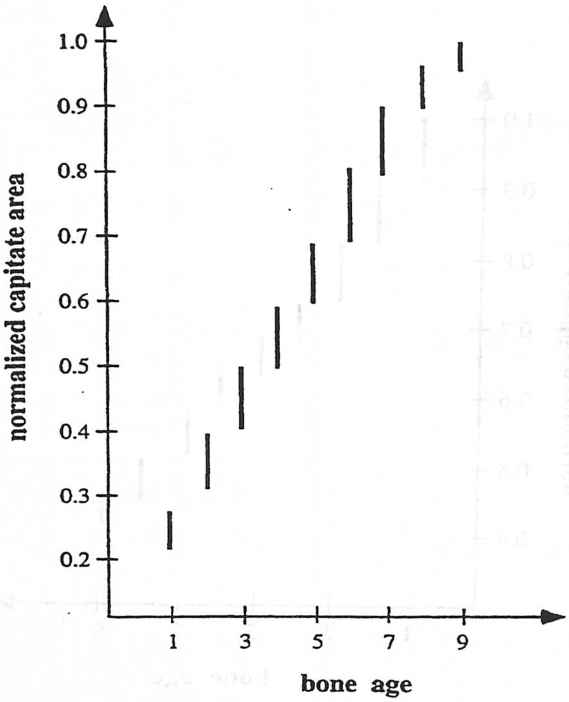
normalized capitate area
1.0
0.9
0.8
0.7
0.6
0.5
0.4
0.3
0.2
1
3
5
7
9
bone age

(d)

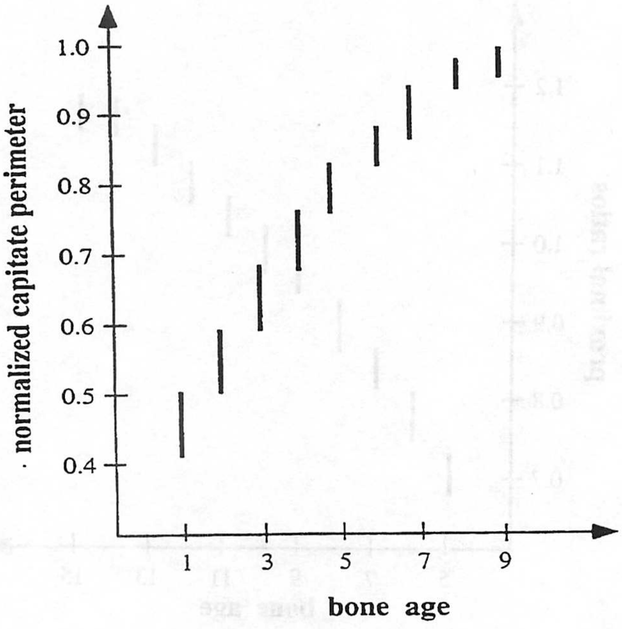
normalized capitate perimeter
1.0
0.9
0.8
0.7
0.6
0.5
0.4
1
3
5
7
9
bone age

(e)

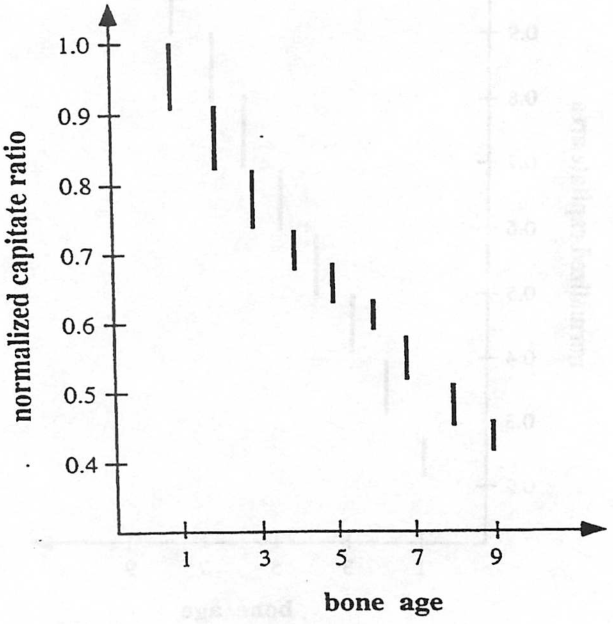
normalized capitate ratio
1.0
0.9
0.8
0.7
0.6
0.5
0.4
1
3
5
7
9
bone age

(f)

of bones (particularly the metaphysis). While being subjected to the wavelets decomposition procedure, the resulting wavelet coefficients of both types (fusion and bone non uniformity) overlap and its separation is impossible. A significant overexposure effects the histogram and the energy of the HHFC, permitting the image to be rejected automatically. However, a moderate overexposure may not change the shape of the histogram, yet, increases the LHFC energy and leads to a mis-classification.

The general evaluation shows that 10% of images have been considered as overexposed and rejected. If not imposing the quality condition, all of them would be classified as non-fused (due to a high energy of the LHFC). The next 6.7% are mis-classified. This gives a result of 83.3% of correct classification. While improving the quality of radiographs, the accuracy may reach 90%.

In conclusion, the phalangeal length[17] applied to the standard phalangeal length table does not appear to be a sufficient indicator of the skeletal maturity and can only be used as a rough estimator in an early stage of the hand image analysis. The measure is influenced by the length of the fingers and the overall length of tubular bones. Therefore, the phalangeal length table is appropriate for American-born subjects of European derivation. It cannot be applied for African ancestry who are generally longer in measure bone size.

The comparison of the atlas matching method with the PBA and CBA shows a better agreement and accuracy of the PBA. This indicates, that phalanges are more sensitive to the skeletal development reflecting the changes more accurately. This confirms certain medical approaches[4,8,10,13] to the problem of the bone age assessment.

The EROI analysis shows that some components of the wavelets representation can efficiently be used for the classification of epiphyseal fusion, supporting the bone age assessment, particularly, for older patients when the size of bones does not serve as a reliable indicator. At this step, the internal structure of the bones has to be analyzed.

While being applied as a clinical routine, this software package requires standardized images to be used as an input. The standardization has to include the background, orientation, and exposure. The first two elements are corrected by the pre-processing routines,[16] whereas, the exposure is only tested during the EROI analysis. Due to the lack of correction, it effects the results of the overall analysis.

The entire computer package, integrated as an application package in a clinical PACS (Picture Archiving and Communication System) permits the hand radiographs to be archived automatically. The growing database creates opportunities to collect and approve medically a set of radiographs which may confirm or improve the already existing set of radiographs, collected in 1950s. This improved set of images may serve as a reference for the clinical bone age assessment.

5.9. APPENDIX A: MATHEMATICAL MORPHOLOGY – BASIC OPERATIONS

Mathematical morphology is to provide a quantitative description of geometrical structures of an image. The general approach is to probe and transform an image object with different patterns of predefined shape called structuring elements.

The basic operations are the erosion and dilation. The erosion can be viewed geometrically as a transformation set which shrinks the considered object. For a binary image (in this study only binary mathematical morphology has been used), an erosion of X by a structuring element B is the intersection of the translates of X by all elements of B and is defined as

$$E(X, B) = \bigcap_{b \in B} X_b$$

where X_b is the translate of X by b and b is an element of B.

Dilation is the union of the translates of X by all elements of B and can be expressed by:

$$D(X, B) = \bigcup_{b \in B} X_b$$

Dilation is a dual operation with respect to the complement of erosion:

$$D(X^C, B) = E(X, B)^C$$

When an object is eroded and then dilated, this operation is called an opening and is denoted by:

$$O(X, B) = D(E(X, B), X).$$

Similar, the closing

$$C(X, B) = E(D(X, B), X)$$

is found by first dilating and then eroding the image.

5.10. APPENDIX B: WAVELET DECOMPOSITION – DERIVATIVES OF SCALING FUNCTIONS

Mallat[27] reconstruction and decomposition algorithm uses the multiresolution analysis while computing the filter operators. Following Lemarie's definition of the scaling function

$$\phi(\omega) = \frac{1}{\omega^n \sqrt{\sum_{2n}(\omega)}}$$

and

$$\sum_n(\omega) = \sum_{k=-\infty}^{\infty} \frac{1}{(\omega + 2\pi)^n}$$

the multiresolution approximation is based on cubic splines obtained by computing the 6-th derivative of

$$\sum_2(\omega) = \frac{1}{4\sin^2(\omega/2)}$$

Since

$$\phi(2\omega) = H(\omega)\phi(\omega)$$

$H(\omega)$ can be obtained as

$$H(\omega) = \sqrt{\frac{\sum_{2n}(\omega)}{2^{2n}\sum_{2n}(\omega)}}$$

The Fourier transform of the corresponding orthonormal wavelet can be derived from

$$\psi(2\omega) = G(\omega)\phi(\omega)$$

and is given by

$$\psi(\omega) = \frac{e^{-i\omega/2}}{\omega^n}\sqrt{\frac{\sum_{2n}(\omega/2+\pi)}{\sum_{2n}(\omega)\sum_{2n}(\omega/2)}}$$

The coefficients of the impulse response $h(n)$ are computed from the transfer function. The impulse response $g(n)$ is given by

$$g(n) = (-1)^{1-n}h(1-n).$$

Daubechies[28] has extracted the properties of the filter operator without reference to the multiresolution analysis. This permits the following set of conditions to be defined.

(1) Since

$$\sum_n |h(n)| < \infty$$

$$\sum_n |g(n)| < \infty$$

the operators

$$(Ha)_k = \sum_n h(n-2k)a_n$$

$$(Ga)_k = \sum_n g(n-2k)a_n$$

are bounded.

(2) The reconstruction and decomposition scheme will work if $H^*H + G^*G = 1$.

(3) The orthogonality of subspaces requires that $HG^* = 0$.

(4) The final condition identifies G as a difference operator which corresponds to a band pass filter and H as an averaging operator which corresponds to a low pass filter. Thus, we require

$$\sum_n h(n) = C$$

$$\sum_n g(n) = 0$$

It can be proven that $C = \sqrt{2}$.

If a sequence has finite length, then the corresponding basic wavelet has compact support. This means that there are values N_- and N_+ for which $h(n) = 0$ if $n < N_-$ or $n > N_+$.

Conditions (1)–(4) imply the following equation[28]

$$|m_N(\nu)|^2 + |m_N(\nu+\pi)|^2 = 1$$

with the following structure on m

$$m_N(\nu) = [0.5(1+e^{i\nu})]^N Q_N(e^{i\nu})$$

where Q is a polynomial such that

$$|Q_N(e^{i\nu})|^2 = \sum_{k=0}^{N-1} \binom{N+k-1}{k} \sin^{2k}\frac{\nu}{2} + \left[\sin^{2k}\frac{\nu}{2}\right] R\left(\frac{1}{2}\cos\nu\right)$$

and R is an add polynomial.

The above equation is solved by a polynomial P_N of order $N-1$

$$P_N(z) = \sum_{j=0}^{N-1} \binom{N-1+j}{j} z^j$$

where $z = \cos^2\nu/2$.

In our application Q of minimal order has been chosen. This means that

$$R \equiv 0 \text{ and } |Q_n(e^{i\nu})|^2 = P_N \sin^{2k}\frac{\nu}{2}$$

In order to find $Q_N(e^{i\nu})$ the following Riesz lemma is used.

Let A be a positive trigonometric polynomial containing only cosines, $A(\nu) = \sum_{n=0}^{N} a_n \cos(n\nu)$.

Then, there exists a trigonometric polynomial $B(\nu) = \sum_{n=0}^{N} b_n e^{in\nu}$ such that $|B(\nu)|^2 = A(\nu)$.

The proof can be found in [28].

This defines

$$Q_N(e^{i\nu}) = \sum_{n=0}^{N-1} q_n e^{in\nu}$$

and

$$m_n = \left[\frac{1}{2}(1+e^{i\nu})\right]^N \sum_{n=0}^{N-1} q_n(n)e^{in\nu} = 2^{-1/2}\sum_{n=0}^{N-1} h_N(n)e^{in\nu}$$

5.11. REFERENCES

1. Zadeh, L.A., 1977, Fuzzy sets and their application to classification and clustering. In J. Van Ryzin (Ed.), *Classification and Clustering* (Academic Press, New York) pp. 251–299.
2. Darling, D.B., 1979, *Radiography of Infants and Children* (Charles C Thomas Publisher), 1-st ed., Chap. 6, pp. 370–372.
3. Poznanski, A., S.M. Garn, J.M. Nagy, J.C. Gall, 1972, *Radiology*, **104**, 1–11.
4. Kirks, D.R., 1984, *Practical Pediatric Imaging. Diagnostic Radiology of Infants and Children* (Little, Brown & Company, Boston/Toronto), 1st ed., Chap. 6, 198–201.

5. Kosowicz, J., 1965, *Radiology*, **93**, 354–361.
6. Archibald, R.M., N. Finby and F. de Vito, 1959, *J. Clin. Endocr.*, **19**, 1312–1322.
7. Pryor, J.W., 1975, *Am. J. Phys. Anthrop.*, 401–410.
8. Johnston, F.E. and S.B. Jahina, 1965, *Am. J. Phys. Anthrop.*, **23**, 349–354.
9. Miler, G.R., R.K. Levick and R. Kay, 1986, *Clin. Radiol.*, **37**, 119–121.
10. Greulich, W.W. and S.I. Pyle, 1971, *Radiographic Atlas of Skeletal Development of Hand Wrist* (Stanford CA, Standford University Press) 2nd ed.
11. Buckler, J.M.H., 1983, *Archives Disease Childhood*, **58**, 761–763.
12. Roch, A.F., C.G. Rohmann and G.H. Davila, 1970, *Amer. J. Roentgenol.*, **108**, 511–515.
13. Tanner, J.M. and R.H. Whitehouse, 1975, *Assessment of Skeletal Maturity and Prediction of Adult Height (TW2 Method).* (Academic Press, London).
14. Cole, A.L.J., L. Webb and T.J. Cole, 1988, *Brit. J. Radiol.*, **108**, 683–686.
15. Razavi, M., T. Hall, D. Aberle, A. Hayreptian, M. Loloyan and S. Eldredge, 1993, *Proc. SPIE*, **1234**, 776–782.
16. McNitt-Gray, M.F., E. Pietka and H.K. Huang, 1992, *Investigative Radiology*, **7**, 529–535.
17. Garn, S.M., K.P. Hertzog, A.K. Poznanski and J.M. Nagy, 1972, *Radiology*, **105**, 375–381.
18. Pietka, E., M. McNitt-Gray, M.K. Kuo and H.K. Huang, 1991, *IEEE Trans. Medical Imaging*, **10**, 616–629.
19. Poznanski, A.K., R.J. Hernandez and K.E. Guire, 1978, *Radiology*, **129**, 661–668.
20. Keats, T.E. and L.B. Lusted, 1985, *Atlas of Roentgenographic Measurement*, Year Book Medical Publishers, Inc., Chicago.
21. von Mises, 1964, *Mathematical Theory of Probability and Statictics*, (Academic Press: New York).
22. McNitt-Gray, M., 1993, Segmentation of Chest Radiographs as a Pattern Classification Problem, *Ph.D. Thesis*, UCLA.
23. McNitt-Gray, M., S.L. Eldredge, J. Tagawa and H.K. Huang, 1992, *Proc. SPIE*, **1653**, 451–457.
24. Gonzalez, R.C. and P. Wintz, 1987, *Digital Image Processing*, (Addison-Wesley Publishing Company), 2nd ed.
25. Serra, J. (ed.), 1988, *Image Analysis and Mathematical Morphology*, **2**)Academic Press, London).
26. Pietka, E., M. McNitt-Gray, T. Hall and H.K. Huang, 1992, *Proc. SPIE*, **1652**, 522–528.
27. Mallat, S.G., 1989, *IEEE Trans. Pattern Anal. Machin Intell.*, **11**, 674–693.
28. Daubechies, I., 1988, *Comm. Pure & Applied Math.*, **41**, 909–996.
29. Mallat, S.G., 1989, *Trans. Am. Math. Society*, **315**, 69–87.
30. Battle, G., 1987, *Commun. Math. Phys.*, **110**, 601–615.
31. Pietka, E., L. Kaabi, M.L. Kuo and H.K. Huang, 1993, *IEEE Trans. Medical Imaging*, **12**, 44–49.
32. Kandel, A., 1982, *Fuzzy Techniques in Pattern Recognition.* A Wiley-Interscience Publication, John Wiley & Sons.
33. Duda, R.O. and P.E. Hart, 1973, *Pattern Classification and Scene Analysis* (Wiley: New York).
34. Zadeh, L.A., 1965, *Inf. Control*, **8**, 338–353.
35. Dubois, D. and H. Prade, 1980, *Fuzzy Sets and Systems: Theory and Application* (Academic Press: New York).
36. Pietka, E., *Comp. Med. Img. & Graph*, (to be published).

Pergamon

Computerized Medical Imaging and Graphics, Vol. 21, No. 3, pp. 165–173, 1997
© 1997 Elsevier Science Ltd. All rights reserved
Printed in Great Britain
0895-6111/97 $17.00 + .00

PII: S0895-6111(97)000014-1

PERFORMANCE OF ASYNCHRONOUS TRANSFER MODE (ATM) LOCAL AREA AND WIDE AREA NETWORKS FOR MEDICAL IMAGING TRANSMISSION IN CLINICAL ENVIRONMENT

H.K. Huang,* Albert W.K. Wong and Xiaoming Zhu[1]
Laboratory for Radiological Informatics, Department of Radiology, University of California, San Francisco,
530 Parnassus Ave., San Francisco, CA 91413-0628, USA

(*Received* 23 *May* 1996; *revised* 31 *March* 1997)

Abstract—Asynchronous transfer mode (ATM) technology emerges as a leading candidate for medical image transmission in both local area network (LAN) and wide area network (WAN) applications. This paper describes the performance of an ATM LAN and WAN network at the University of California, San Francisco. The measurements were obtained using an intensive care unit (ICU) server connecting to four image workstations (WS) at four different locations of a hospital-integrated picture archiving and communication system (HI-PACS) in a daily regular clinical environment. Four types of performance were evaluated: magnetic disk-to-disk, disk-to-redundant array of inexpensive disks (RAID), RAID-to-memory, and memory-to-memory. Results demonstrate that the transmission rate between two workstations can reach 5–6 Mbytes/s from RAID-to-memory, and 8–10 Mbytes/s from memory-to-memory. When the server has to send images to all four workstations simultaneously, the transmission rate to each WS is about 4 Mbytes/s. Both situations are adequate for radiologic image communications for picture archiving and communication systems (PACS) and teleradiology applications. © 1997 Elsevier Science Ltd.

Key Words: Image communication, Asynchronous transfer mode (ATM), Local area network (LAN), Wide area network (WAN), Picture archiving and communication systems (PACS)

INTRODUCTION

A picture archiving and communication system (PACS) uses local area networks (LAN) to transmit images within a medical center, whereas teleradiology relies on wide area network (WAN) technology. In radiology applications, proprietary LAN can achieve up to 1 Gbit/s, whereas WAN is limited to 1.5 Mbits/s (1, 2). Since LAN and WAN use different technologies (3, 4) this creates potential integration problems when both PACS and teleradiology services are required. The slower transmission rate in WAN is not because of inadequate technology but is due to the cost imposed by long distance carriers for high speed communication lines. The current concept in medical image communication is that no physical or logical boundaries should exist between LANs and WANs (5). Asynchronous transfer mode (ATM) technology satisfies this requirement.

ATM transports data by dividing them into 53 byte fixed-length cells. Each cell consists of 5 bytes of header information and 48 bytes of data. The basic signaling rate of ATM is 51.84 Mbits/s called OC-1 (Optical Carrier Level 1). Others are multiples of OC-1, e.g. OC-3 (155 Mbits/s) and OC-12 (622 Mbits/s) (6–8). In imaging applications, the user can use the standard TCP/IP (Transmission Control Protocol/Internet Protocol) protocols for both LAN and WAN or application software containing TCP/IP like the DICOM (Digital Imaging and Communication in Medicine) (9).

An early large scale ATM project for high speed data transmission was the BERKOM (Berlin Communication) testbed in 1986 (10). The project was terminated in 1991 because the ATM technology was not mature enough for such large scale implementation. Another experimental project using ATM for high speed image communication was the B-ISDN (Integrated Services Digital Network) field trial at North Carolina. In this testbed, an OC-12 was used to connect several remote sites for radiation therapy planning application and an OC-3 for remote medical consultation (11).

We set up an ATM OC-3 (155 Mbits/s) WAN and LAN testbed network, shown in Fig. 1, connecting the University of California at San Francisco (UCSF), Mount Zion Hospital (MZH), and the San Francisco VA Medical Center (SFVAMC) in the San Francisco Bay area for image transmission in 1994. Results demonstrated

---

*Author to whom correspondence should be addressed. Tel.: 415-476-6044; Fax: 415-502-3217.

[1] Now with IBM Almaden Research Center, 650 Harry Road, San Jose, CA 95120-6099, USA.

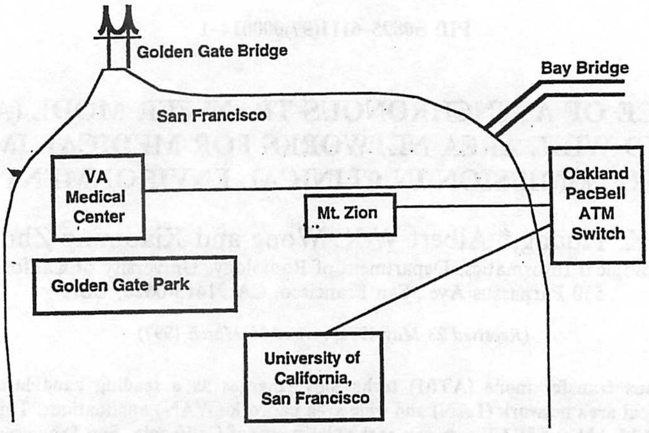

Fig. 1. Wide Area Network (WAN) with ATM OC-3 (155 Mbits/s) Technology connecting UCSF, MZH, and SFVAMC in a star architecture.

that both LAN and WAN can achieve up to 60 Mbits/s between a SUN SPARC 10 and a SPARC 20 workstation (SUN Microsystems, Mountain View, CA) with FORE ATM switches and adapter boards (FORE, Warrendale, PA) with TCP/IP protocols (5).

Since then we have designed and implemented a large scale ATM OC-3 LAN and WAN connecting UCSF, MZH, and SFVAMC (12). Figure 2 shows the network architecture. This paper describes several experiments to measure the performance of this ATM LAN and WAN in a clinical environment.

PERFORMANCE OF ATM LAN

The purpose of this experiment was to investigate the ATM performance in LAN connected with workstations using different types of computers and operating systems. Referring to Fig. 2, while the hospital-integrated PACS was running in a daily routine clinical mode, we inserted additional TCP/IP communication processes in six workstations using different SUN computers connected to the LAN at UCSF. Each workstation had its own specific functions in the PACS and was running different operating systems. Data were transmitted memory-to-memory continuously between two workstations. Transmission rates for both sending and receiving were measured separately at each workstation. The transmission rate in the experiments described in this paper is defined as the time required from when the data were sent to when the data were received. Table 1 shows the results. The workstations shown in each row represent the sending sites while workstations in the columns represent the receiving sites. Thus, for example, matrix (1,2) = 1.35 Mbytes/s means that the performance was measured by sending images from SPARC 5 running Solaris 2.3 operating system and received by SPARC 20 running Solaris 2.4.

Based on this table, we observe that, for memory-to-memory transmission:

1. The ATM LAN can achieve over 9.0 Mbytes/s between two SPARC 20s.
2. For a given pair of workstations, the performance is different if the order of sending and receiving is reversed. This can be explained as follows. In TCP/IP protocols, the receiving site is responsible for managing the incoming flow of data. Therefore, a lower performance computer used in the receiving workstation will result in a poorer transmission rate compared with when it is used for sending.
3. The performance depends on the type of workstation and the operating system used.

The poor performance of SPARC 5 for receiving prompted us to replace all SPARC 5 workstations in our network. The inferior performance of the newer operating system Solaris 2.4 compared with the earlier version Solaris 2.3 was puzzling. The ATM manufacturer has since identified that the problem was in the ATM driver and it has been resolved. The measurements reported in the next section were obtained exclusively with the Solaris 2.4 operating system.

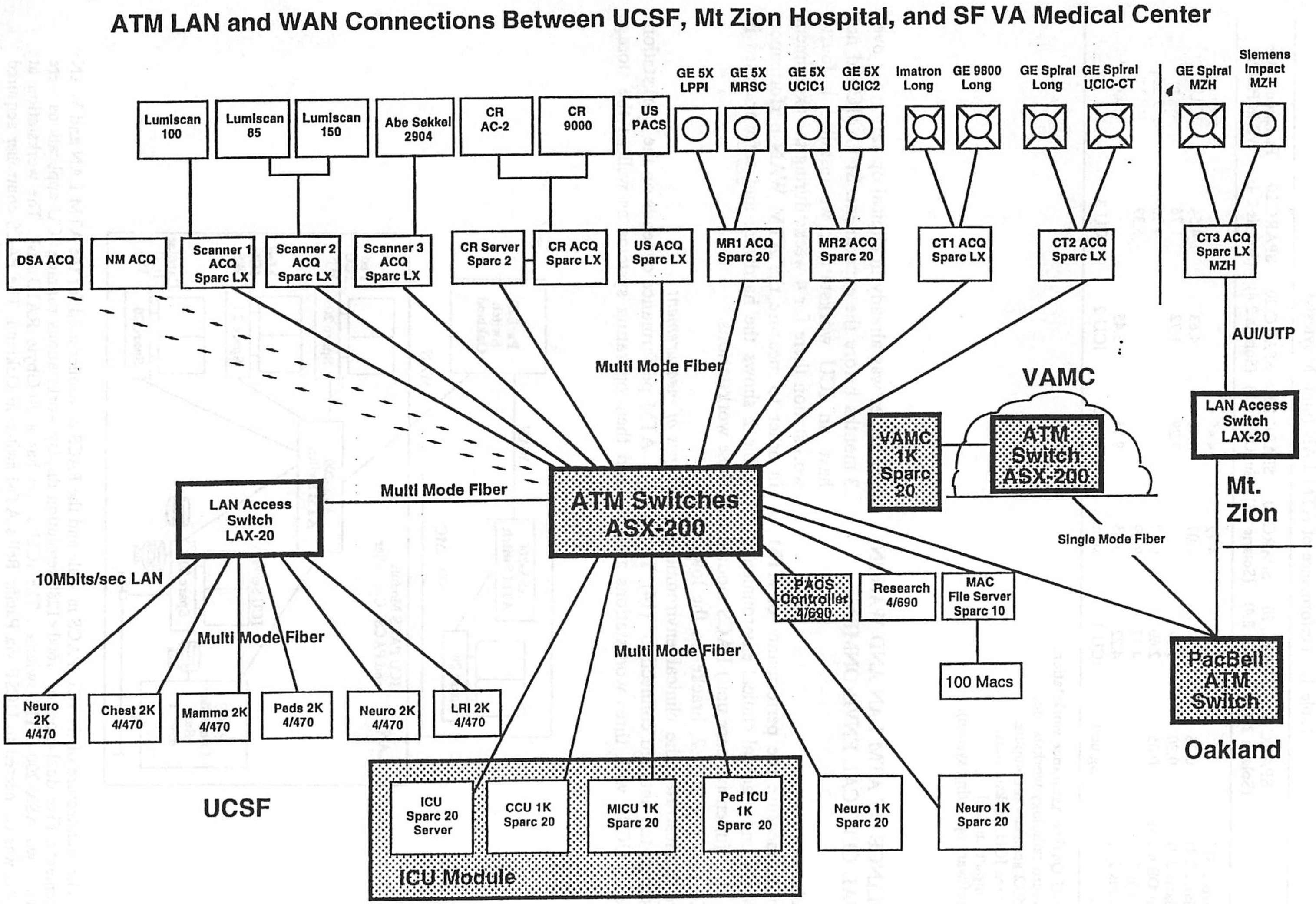

Fig. 2. ATM LAN and WAN connections between UCSF, MZH, and SFVAMC. AUI/UTP: attachment unit interface/unshielded twisted pair. The components in the top row are all image acquisition devices, dotted lines are components not yet connected; the second row components are image acquisition computers; the ICU module is in the bottom row with a bracket.The dotted components are used for the measurements of ATM LAN and WAN. See also Fig. 3. (Modified from Fig. 3, Ref. (12).)

Table 1. Performance of ATM LAN (unit: Mbytes/s)

REC SEND	SPARC 5 (Solaris 2.3)	SPARC 20 (Solaris 2.4)	SPARC 20 (Solaris 2.3)	SPARC 20 (SunOS 4.1.3)	SPARC 20 (Solaris 2.4)	SPARC 20 (Solaris 2.4)	Function of the WS in PACS*
SPARC 5 (Solaris 2.3)		1.35	4.72	4.45			isg.ucsf
SPARC 20 (Solaris 2.4)	0.25		9.07	5.50	4.63	4.54	ICU 1
SPARC 20 (Solaris 2.3)	0.30	1.57		7.29	1.72	1.76	isg.nr
SPARC 20 (Sun OS 4.1.3)	0.05	2.60	9.47			4.76	mr2.acq
SPARC 20 (Solaris 2.4)		4.17	9.59			5.39	ICU 2
SPARC 20 (Solaris 2.4)		4.22	9.65	9.75	5.45		ICU 3
	isg.ucsf	ICU 1	isg.nr	mr2.acq	ICU 2	ICU 3	

*isg.ucsf:	ICU Quality Assurance workstation.
isg.nr:	Neuro radiology workstation.
mr2.acq:	MR2 acquisition computer.
ICU 1,2,3:	Three ICU workstations.
SPARC:	computer model.
(Solaris 2.3):	(software operating system).

PERFORMANCE OF ATM LAN AND WAN IN ACTUAL CLINICAL ENVIRONMENT

Experimental set-up

In order to measure the performance of ATM LAN and WAN under actual clinical environments, we used the ICU (intensive care unit) PACS module in our PACS (13) (see Fig. 2, bracket in the lower row). Figure 2 illustrates the clinical environment and Fig. 3 shows the detailed connections (14). The ICU module at UCSF with three workstations and one server was already in clinical operation for over 3 months before the experiment. SFVAMC did not have an ICU workstation, we installed a fourth workstation there for 4 weeks during the experiment in order to measure the ATM WAN performance. Table 2 shows the hardware and software used in these workstations.

Types of measurement

ATM performance depends on the workstations and their operating systems as well as the storage

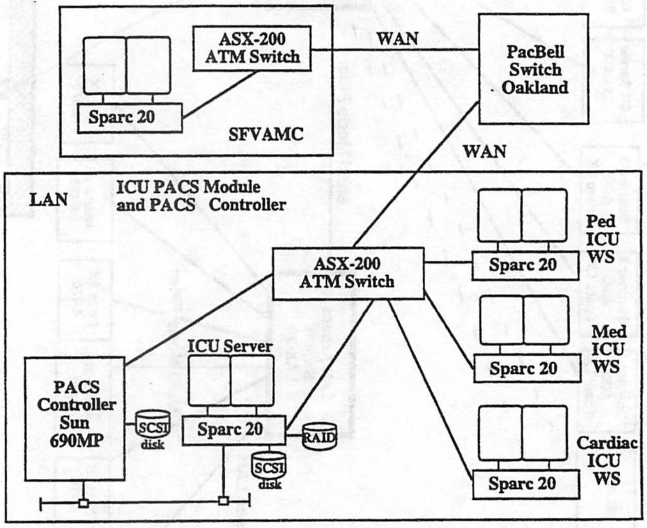

Fig. 3. The architecture of the ICU PACS module and the PACS controller used for the ATM LAN and WAN measurements. Five dual-monitor, 1600×1280-resolution display workstations running ICU applications were used with two ASX-200 ATM switches. The ICU server has a 30 Gbyte RAID disk. The workstation at SFVAMC was connected to UCSF via Pacific Bell's ATM switch in Oakland. The PACS controller acquired images from all acquisition devices and transmitted to the ICU server through the ASX-200 ATM switch and the Ethernet during the experiment.

Table 2. Hardware and software used in the ATM WAN and LAN measurements

Hardware:

- ICU server
    - SUN SPARC 20
    - Dual-monitor with 1600×1280 resolution
    - FORE S-Bus ATM host adapter card (OC-3: 155 Mbits/s)
    - Sun S-Bus Ethernet host adapter card (10 Mbits/s)
    - 30 Gbytes redundant array of inexpensive disks (RAID)
- ICU workstation
    - Same as the ICU server except no RAID
- PACS controller
    - Sun 690MP with four central processing units (CPUs)
    - Small computer systems interface (SCSI) disks
- FORE ASX-200 ATM Switch (non-blocking, 24 ports, 2.5 Gbits/s)
- Newbridge ATM Switch (Pacific Bell, Oakland)

Software:

- Solaris 2.4 operating system in the ICU server and workstations
- SUN OS 4.1.3 operating system in the SUN 690 MP
- C programming language
- TCP/IP communication protocols
- Unix socket communication
- Client/server applications

Transmission speed between local disks and memory:

- SCSI→Memory: 4.0 Mbytes/sec
- RAID (level 5)→Memory: 9.0–20.0 Mbytes/sec

devices used. Four common storage devices are local SCSI magnetic disk, remote SCSI magnetic disk, redundant array of inexpensive disks (RAID), and computer memory. For this reason, four types of measurements were obtained: local disk to remote disk; local disk to remote RAID; local RAID-to-remote memory; and local memory-to-remote memory. The measured total transmission time, **TOTAL**, is in general, a combination of five different times required during the transmission:

$$TOTAL = T_1 + T_2 + T_3 + T_4 + T_5$$

where

T_1: sender disk (or RAID) to local memory,
T_2: sender local memory buffering,
T_3: ATM transmission time,
T_4: receiver local memory buffering, and
T_5: receiver local memory to disk (or RAID).

Since the local disk input/output (I/O) speed (about 4 Mbytes/s) is slower than that of the ATM OC-3 155 Mbits/s (about 19.3 Mbytes/s), the transmission rate between two workstations, either both with magnetic disks, or one with a magnetic disk and the other with RAID, was dominated by T_1 and/or T_5. Therefore the measurement did not truly reflect the ATM performance. The I/O speeds of RAID-to-memory (about 20 Mbytes/s) and memory-to-memory (higher than 20 Mbytes/s) are in the same range or faster than the ATM signaling rate, therefore the measurements between workstations from RAID-to-memory, or memory-to-memory, would be a better measure of the ATM performance.

Experiment 1: magnetic disk-to-magnetic disk with ATM and Ethernet. The first experiment was to measure the ATM performance from disk-to-disk and compare the result with that of the conventional Ethernet network (10 Mbits/s). Figure 4a shows the configuration. During regular clinical hours, we measured the disk-to-disk transmission rates of CR (computed radiography) images from the PACS controller's disks via: (1) the Ethernet; and (2) the ATM to the ICU image server's disks. For each individual image, the ICU server received two copies of the image, one over the Ethernet and the other over the ATM, from the PACS controller.

The transmission rate for the PACS controller to send CR images to the ICU server were measured on a 24 h/day, 7 days/week basis. Approximately 1 month of transaction data was analyzed. The performance measurements were 1247 and 452 Kbytes/s for ATM and for Ethernet, respectively. This result indicates that even with the constraint of slow disk input/output speed, the ATM is almost three times faster than the Ethernet.

Experiment 2: magnetic disk-to-RAID with ATM. The second experiment was performed using the configuration shown in Fig. 4b. The set-up is almost identical to experiment 1 except that the receiving site at the ICU server uses the RAID. The average transmission rate is 1500 Kbytes/s. Results from

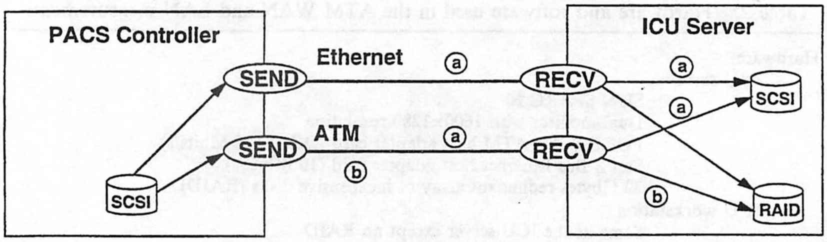

Fig. 4. Configuration used for ATM performance measurements. (a) magnetic disk-disk, ATM and Ethernet; (b) magnetic disk-RAID, ATM only.

experiments 1 and 2 demonstrate that the ATM performance from disk-to-RAID is only about 20% better than from disk-to-disk. This is due to the limitation of the regular disk I/O speed which dictates the transmission rate despite higher I/O performance of the RAID.

Experiment 3: RAID-to-memory transmission. We used the ICU PACS module to measure RAID-to-memory and memory-to-memory transmission rates of the ATM. In these two experiments, five dual-monitor, 1600×1280-resolution ICU workstations using Sun. SPARC 20 computers were interconnected via two ASX-200 ATM switches (Fig. 3). The ICU server distributed CR images over ATM to three ICU display workstations (Pediatrics, Medical Surgical, and Cardiac Care) within UCSF, and a workstation at SFVAMC. This image server uses a 30 Gbyte RAID for all ICU images. In this environment, the three ICU WS connections are in the LAN whereas the SFVAMC WS is in the WAN.

RAID-to-memory transmission rates were measured for transferring 80 CR images, each 8 Mbytes in size, from the image server's RAID over ATM to individual SUN SPARC 20 system memory of the workstations. The communication processes allocated 64 Kbyte TCP window size and 128 Kbyte image buffer size for the data transfers.

Table 3 shows the results from point-to-point and concurrent transmissions of data over the LAN and the WAN. The average point-to-point transmission rate between the ICU server within UCSF was 5.8 Mbytes/s and to SFVAMC was 5.2 Mbytes/s. These transmission rates correspond to transferring an 8 Mbyte CR image in less than 2 s. When the server had to send images to all workstations simultaneously, the rates deteriorated to about 1.8 Mbytes/s. In all these measurements, the standard deviations computed were less than 2%, insignificant to affect the accuracy of the average values.

Table 3. RAID-to-memory transmission rates (unit: Mbytes/s)

Number of concurrent processes	From the server to VA	PED	MS	CARD
1 WAN WS	5.2			
1 LAN WS		5.8		
1 WAN & 1 LAN WSs	3.31	3.68		
1 WAN & 3 LAN WSs	1.8	1.8	1.9	1.9

Experiment 4: memory-to-memory transmission. Memory-to-memory transmission rates were measured for transferring 2000 data packets, each 128 Kbytes in size, from the image server's SUN SPARC 20 memory over ATM to the individual SUN SPARC 20 memory of the workstations. This amount of data is equivalent to 256 Mbytes or 32 CR images. Again, 64 Kbytes of TCP window size were used for the communication processes.

Results from point-to-point and concurrent transmissions of data over the LAN and the WAN are shown in Table 4. The average point-to-point transmission rate between UCSF and SFVAMC was 8.1 Mbytes/s and within UCSF was 9.8 Mbytes/s. These transmission rates correspond to sending a 40-slice (about 20 Mbytes) CT examination over LAN or WAN in less than 3 s. When the server had to send images to all four workstations, the performance deteriorated to about 4 Mbytes/s.

Table 4. Memory-to-memory transmission rates (unit: Mbytes/s)

Number of concurrent processes	From the server to VA	PED	MS	CARD
1 WAN WS	8.1			
1 LAN WS		9.8		
1 WAN & 1 LAN WSs	6.3	7.2		
1 WAN & 3 LAN WSs	3.7	4.0	4.1	4.3

DISCUSSION

We have successfully implemented an ATM LAN and WAN network at UCSF and two affiliated hospitals, Mount Zion Hospital and San Francisco VA Medical Center in the San Francisco Bay area. The ATM, back-up by the Ethernet network, provides a comprehensive high-speed and reliable communication for radiologic images and related data over both LAN and WAN. Our experiments demonstrate that ATM can be used for both LAN and WAN with standard TCP/IP protocols without changing the physical network set up. As for the performance, with the RAID, the transmission rate can reach 5–6 Mbytes/s, and memory-to-memory, 8–10 Mbytes/s, about 25–50% of the ATM OC-3 theoretical limits.

From the results of our measurements, we believe that the transmission rates of ATM can satisfy most radiologic image communication requirements in PACS and teleradiology applications (15–17). Hence, a digital communication network with ATM technology would be a suitable choice for large-scale PACS involving both LAN and WAN. Ethernet, on the other hand, is inadequate for image communication, particularly in a hospital-integrated PACS environment, because of the shared bandwidth characteristics in standard Ethernet.

It is important to note that ATM technology treats both textual and image data identically if TCP/IP protocols are used. The only difference is that the size of the image data file is normally much larger and therefore the data buffer used during communication is also set to be larger. However, when the TCP/IP protocols are embedded in an application software, for example, in the DICOM communication software (9), commonly used in radiology applications, the application software treats the textual data and image data differently. The application software has to validate the image data according to the DICOM format after the receiving. This process will increase the transmission overhead and reduce the transmission rate as compared to textual data which is a stream of bits of information. Therefore, for a hospital already using Ethernet with TCP/IP protocols for image transmission, it is not difficult to convert it to ATM for two reasons. First, the communication software for both technologies are almost identical, and second, no application level software needs to be changed. On the other hand, if the hospital is using DICOM for image communication then the application level software in DICOM has to be modified.

Factors affecting the throughputs of an ATM network include: (1) the computer and the operating system used in the workstation; (2) the number of simultaneous transmissions; (3) processing overhead of the network protocols (e.g. TCP/IP); (4) storage device used in the workstation; and (5) data buffering in the computer system and the ATM switch. Among these factors, improvement of network transmission protocols and storage speed are two major determining parameters for optimization of ATM throughput performance.

The use of ATM for LAN has no other costs except purchasing the ATM switches and adapter boards assuming that the fiber cables are already in place. On the other hand, using ATM for WAN requires a long distance connection that the user must pay to a carrier. The price depends on the distance between the sites as well as the availability of optical fibers from carriers. Currently the charge from long distance carriers for ATM is still prohibitively high, a major detrimental factor for using ATM in WAN applications. An alternative is to lease dark fibers from companies other than long distance carriers. In this case, WAN becomes very much like LAN except that the cable distance is longer. The cost of ATM technology is decreasing very rapidly except for the use of long distance cables. It is important that ATM users form a forum to convince the long distance carriers that lowering the long distance cost so that more users can take advantage of ATM WAN technology for medical image transmission would be to their benefit.

SUMMARY

We introduced the ATM LAN and WAN technology for medical image applications and described some earlier experiments and testbed ATM networks by other investigators. The ATM LAN and WAN architecture at UCSF connecting to Mount Zion Hospital and the San Francisco VA Medical Center in the San Francisco Bay area are given. We described a preliminary experiment on measuring the performance of the ATM LAN. Results demonstrate that ATM LAN can achieve over 9.0 Mbytes/s memory-to-memory between two SUN SPARC 20 workstations. Four other experiments using a clinical ICU PACS module operating 24 h/day, 7 days/week which consists of one server and four workstations all with SPARC 20 computers are detailed. The four experiments measure the ATM LAN and WAN performance of: disk-to-disk; disk-to-RAID; RAID-to-memory; and memory-to-memory. The result from the case of one pair of connections confirms the performance obtained in the earlier ATM LAN experiment which is about 8–10 Mbytes/s. The transmission rates start to deteriorate gradually when the server has to send images to different workstations simultaneously. In the case of memory-to-memory, each can still achieve 4.0 Mbytes/s or about 2 s for a CR image.

Acknowledgement—This work was partially supported by a CalREN grant ATMN-007 from Pacific Bell, and NLM Contracts N01-LM-4-3508 and N01-LM-6-3547.

REFERENCES

1. Huang, H.K.; Wong, A.W.K.; Lou, S.L. Architecture of a comprehensive radiologic imaging network. IEEE J. Sel. Areas Commun. 10:1188–1196; 1992.
2. Huang, H.K. Picture archiving and communication systems in biomedical imaging, Chap. 8. New York: VCH/Wiley; 1996.
3. Tanenbaum, A.S. Computer networks, 2nd ed. Englewood Cliffs, New Jersey: Prentice-Hall; 1989: 373–375.
4. Halsall, F. Data communications, computer networks and open systems, Chaps 7 and 8. Addison-Wesley, New York, 1992.
5. Huang, H.K.; Arenson, R.L.; Dillon, W.P. *et al.* Asynchronous transfer mode technology for radiologic image communication. Am. J. Roentgen. 164:1533–1536; 1995.
6. ATM Forum, ATM user-network interface specification version 3.0. Englewood Cliffs, New Jersey: Prentice-Hall; 1993.
7. de Prycker, M. Asynchronous transfer mode—solution for broadband ISDN. New York: Ellis Horwood; 1993.
8. McDysan, D.E.; Spohn, D.L. ATM—theory and application, Chaps. 7 and 10. New York: McGraw-Hill; 1994.
9. Hindel, R., ed. Implementation of the DICOM 3.0 standard. Oak Brook, IL: Radiological Society of North America; 1994.
10. Lemke, H.U. The Berlin Communication System (BERKOM). In Huang, H.K. *et al.*, eds, Picture Archiving and Communication Systems (PACS) in Medicine, Vol. 74, NATO ASI Series F, Berlin: Springer-Verlag; 1989: 275–281.
11. Chipman, K.; Holzworth, P.; Loop, J. *et al.* Medical applications in a B-ISDN Field Trial. IEEE J.Selec. Areas Commun. 10:1173–1182; 1992.
12. Huang, H.K.; Andriole, K.; Bazzill, T., Lou, S.L.; Wong, A.W.K.; Arenson, R.L. Design and implementation of a picture archiving and communication system: the second time. J. Med. Imaging 92:1–14; 1996.
13. Wong, A.W.K.; Huang, H.K.; Bazzill, T.M.; Lee, J.K.; Bobkov, I.; Moskowitz, M.J. Performance characteristics of a digital imaging network with asynchronous transfer mode technology. Radiol. 197P:259; 1995.
14. Lee, J.K.; Wong, A.W.K.; Huang, H.K.; Bazziel, T.; Zhang, J.; Andriole, K. ATM distributed PACS server for ICU application. Proc. SPIE Med. Imag. 2711:14–21; 1996.
15. Thiel, A.; Bernarding, J. Distributed medical services within the ATM-based Berlin regional test bed. Proc. SPIE Med. Imag. 2711:32–43; 1996.
16. Duerinckx, A.J.; Hayrapetian, A.S.; Valentino, D.J. *et al.* Assessment of asynchronous transfer mode (ATM) networks for regional teleradiology. Proc. SPIE Med. Imag. 2711:61–70; 1996.
17. Chimiak, W.J.; Wolfman, N.T.; Boehme, J.M. Results of a clinical test of an ATM tele-ultrasound system. Proc. SPIE Med. Imaging 2711:180–184; 1996.

About the Author—H.K. HUANG, DSc, FRCR (Hon.), Professor and Vice Chairman, Director of Radiological Informatics Laboratory, Department of Radiology, UCSF with a joint appointment in the UCSF/UC Berkeley Bioengineering Graduate Program. Dr Huang has been working on PACS research and development since 1982. He implemented a PACS at UCLA in 1991, and a second generation PACS at UCSF in 1994. His current research interests are in medical multimedia, high speed medical image transmission and medical imaging informatics infrastructure design.

About the Author—ALBERT W.K. WONG is a systems manager for the Laboratory for Radiological Informatics (LRI) in the Radiology Department at the University of California, San Francisco (UCSF). He is presently involved in the design and implementation of databases, display stations, PACS/RIS/HIS interface, DICOM communications, image archiving, and networking for the UCSF PACS project. His current research interests include systems integration, image database, optical and RAID storage, DICOM interface, and high-speed communication networks.

About the Author—XIAOMING ZHU was a postdoctoral fellow in the Department of Radiology, University of California, San Francisco. His research interests include distributed computing, medical image database management, image processing and display. Dr Zhu received his PhD from the University of California, Los Angeles.

APPENDIX 1
LIST OF ACRONYMS AND DEFINITIONS

ATM:	Asynchronous transfer mode
ATM board:	A computer circuit board inserted to the workstation for ATM transmission
ATM switch (SW):	A relay box to direct ATM transmission
BERKOM:	Berlin Communication
CR:	Computed radiography
DICOM:	Digital Imaging and Communication in Medicine, a standard image format and communication protocol for radiologic images
Ethernet network:	A most popular computer network with 10 Mbits/s signaling rate
Gbit:	gigabit
HI-PACS:	Hospital-integrated picture archiving and communication system
I/O (input/output) speed:	Time required to read or write data from a storage device to a computer memory
ICU server:	An image server supplies images to ICU workstations
ICU:	Intensive care unit
ISDN:	Integrated Services Digital Network, a most inexpensive way of transmitting digital data through WAN
Kbyte:	kilobyte
LAN:	Local area network
Mbit:	megabit

Mbyte:	megabyte
MZH:	Mount Zion Hospital
OC-1:	Optical Carrier Level 1
OC-3:	Optical Carrier Level 3 which provides a maximum signaling rate of 155 Mbits/s
PACS controller:	The control device of the PACS
RAID:	Redundant array of inexpensive disks
SCSI magnetic disk:	A common storage device connected to a computer with the small computer systems interface (SCSI)
SFVAMC:	San Francisco VA Medical Center
Solaris 2.4:	A computer operating system used in a SUN SPARC workstation
SPARC 20:	A workstation made by SUN Microsystems
SUN OP:	SUN computer operating system
TCP/IP:	Transmission Control Protocol/Internet Protocol, two most common protocols of transmitting data between computers through a network
UCSF:	University of California at San Francisco
WAN:	Wide area network
WS:	Workstation

Pergamon

Computerized Medical Imaging and Graphics, Vol. 21, No. 4, pp. 209–218, 1997
© 1997 Elsevier Science Ltd. All rights reserved
Printed in Great Britain
0895–6111/97 $17.00 + .00

PII: S0895–6111(97)00011–6

AN AUTOMATED PACS IMAGE ACQUISITION AND RECOVERY SCHEME FOR IMAGE INTEGRITY BASED ON THE DICOM STANDARD

S.L. Lou*, David R. Hoogstrate and H.K. Huang
Laboratory for Radiological Informatics, Department of Radiology, University of California, San Francisco,
Box 0628, 505 Parnassus Avenue, San Francisco, CA 94143-0628, USA

(*Received* 4 *September* 1996)

Abstract—The data quality and completeness of acquired images, which we refer to as integrity, is considered as the most important requirement in the image acquisition design of the Picture Archiving and Communication System (PACS). The Digital Imaging and Communications in Medicine (DICOM) standard significantly simplifies the task of acquiring radiological images from a DICOM compliant imaging system into the PACS. However, human interaction with the imaging system by changing the DICOM communication settings can result in missing images during the PACS image acquisition. A scheme based on the DICOM Query and Retrieve (Q/R) service class was developed to automatically identify and recover missing images. In addition, grouping sequential scanned images such as a CT and MR image series is another potential process that can miss images because of no indication of the end of series. Two methods are presented for determining the end of series and the pros and cons of each method are discussed in detail. Two experiments in a real clinical environment were conducted; one with and one without the Q/R implementation. The statistical results indicate two highlights from this work. First, the Q/R scheme faithfully recovered all missing images caused by human interaction with the DICOM compliant imaging system. Second, there was no single image slice missed when grouping slices into a series using the presented grouping algorithm in the two experimental periods. © 1997 Elsevier Science Ltd.

Key Words: Picture archiving and communication system, Digital imaging and communications in medicine, Image acquisition, Image integrity, Fault tolerance, Magnetic resonance imaging

INTRODUCTION

DICOM compliance among manufacturers is a major factor contributing to the interoperability of different medical imaging systems in a hospital environment (1, 2). The DICOM standard developed by the American College of Radiology and the National Electrical Manufacturers Association (ACR-NEMA) defines the basis of the interface mechanism allowing different manufacturers' digital imaging systems to communicate images (3–5). With the standardized interface mechanism, the task of acquiring images from the DICOM complaint imaging systems to PACS and/or multimedia integration systems is much easier than from those with a "closed" architectural design (6, 7). Figure 1 shows the schematic diagram of the PACS image acquisition. The design of the PACS image acquisition task must consider the automatic recovery from failures. Failures may be a hardware malfunction, a software error, or a manual interruption during the PACS acquisition process. Methods for automatically detecting and recovering hardware and software malfunctions have been discussed in our previous work (6). In the case of acquiring images from the DICOM compliant imaging system, interruptions are generally caused by human interaction with the imaging system. Regardless of failure type, the consequence is always the same: some images will be lost.

From our experience, one characteristic of the DICOM compliant imaging system is that it allows image communication settings to be manually changed whenever required. All DICOM service classes require registration (or configuration) for communications. In an imaging system, this configuration is usually implemented as a communication setting by maintaining a list of communicating peer and method (either image sending or receiving). Typically, one communication peer and method at a time can be selected for image communication. With this implementation, the operator of the imaging system can easily change the communication setting. This flexibility, in fact, is one of the main factors causing PACS image acquisition failures. For example, if the manual change occurs while images are being transferred to the PACS acquisition system, the image transferring process will be interrupted.

---

*Author to whom all correspondence should be addressed.

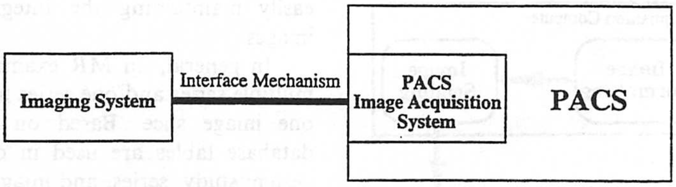

Fig. 1. A schematic diagram shows that the PACS image acquisition involves an interface mechanism to connect the imaging system.

Furthermore, if the operator waits too long or does not resume the PACS communication setting, the images will have to be manually re-transmitted or they will be lost. Suffice it to say, neither manual transmission nor the loss of images is acceptable under the automated PACS image acquisition design.

For cross-sectional images such as CT and MR, acquiring a complete series of image slices covering the body region of interest is important. In order to group multiple images into a series entity, the end of series, which indicates the completeness of sequential image scans, must be known. Unfortunately, there is no indication for the end of series in most imaging systems today including those that are compliant with the DICOM standard. This has been a problem for the PACS acquisition task. To circumvent this problem, the algorithmic determination of the end of series has to be integrated into the PACS acquisition process. Note that this task is far from trivial. An ill chosen algorithm can result in missing images and/or slow acquisition performance.

We first present the concepts of an automatic PACS image acquisition process based on the DICOM standard. In section 2, the configuration of the image client and image server along with the acquisition database dedicated to the PACS image acquisition are described. Two possible methods for the algorithmic detection of the end of series, which are combined and implemented in our image acquisition process, are presented. In section 3, the performance and results of the preliminary experiment using the DICOM compliant PACS system are reported. We also discuss the situation when the image acquisition operation is interrupted during transmission and its consequences. In section 4, a comprehensive scheme based on the DICOM Q/R service class for automatically recovering lost images is described. Results from the second experiment using this DICOM compliant PACS acquisition system with the integrated Q/R recovery scheme are also given. We summarize this research by reviewing the performance of the implemented acquisition system and present suggestions to PACS developers and manufacturers of the imaging systems.

CONCEPT OF DICOM-BASED PACS IMAGE ACQUISITION

Hardware configuration and software packages

Figures 2 and 3 show the hardware configuration and software program modules used in this study, respectively. The configuration includes one General Electric Medical Systems (GEMS) (Milwaukee, Wisconsin) Signa 5.4 MR scanner and one Sun SPARC LX (Sun Microsystems, Mountain View, California) for the PACS acquisition computer.

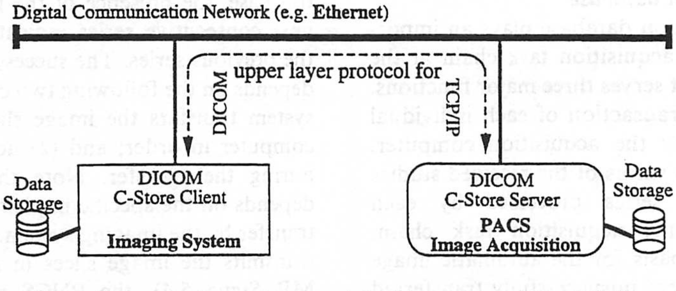

Fig. 2. The diagram shows the computer systems used in this study and the interface mechanism includes Ethernet and the DICOM C-Store server and client programs developed according to the DICOM upper layer protocol for TCP/IP.

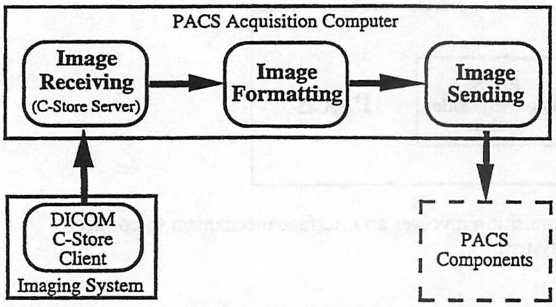

Fig. 3. The diagram shows the major software modules running in the imaging system and the PACS acquisition computer which form the PACS acquisition task chain.

These two computer systems are networked via Ethernet. The program modules consist of the Central Test Node (CTN) software package developed by the Mallinckrodt Institute of Radiology (St Louis, Missouri), and our own PACS image acquisition software package. The image transfer from the MR scanner to the acquisition computer is based on a client–server communication paradigm of the ICOM Composite-Store (C-Store) service. The C-Store client process runs on the MR scanner to send images to the PACS acquisition computer. The task of receiving images is performed by the C-Store server process (one of the CTN example programs) running on the PACS acquisition computer. The formatting process groups the received image slices into a series file and standardizes every pixel of the images according to a predetermined byte ordering (e.g. big-endian or little-endian). The sending process transfers the formatted image series file to one component of the PACS which can be either an image display workstation or an image archiving system. These processes form the task chain of the PACS image acquisition (6).

PACS image acquisition database

The PACS acquisition database plays an important role in the entire acquisition task chain at the acquisition computer. It serves three major functions. First, it supports the transaction of each individual image slice received by the acquisition computer. Second, it monitors the status of the received studies and their associated series processed by each program module of the acquisition task chain. Third, it provides the basis for the automatic image recovery scheme to detect unsuccessfully transferred images which will be described in section 4. In summary, the database provides a foundation for easily maintaining the integrity of the acquired images.

In general, an MR examination study includes multiple series and one series may contain more than one image slice. Based on this hierarchy, three database tables are used in our PACS acquisition design: study, series, and image. Each table contains a group of records and each record contains a set of useful data elements. For the study and series database tables, a unique data element as the primary key is preferred for accessing a particular record in a timely fashion. We use the study name and the series name as the primary keys for the two database tables, respectively. In addition to the primary keys, the following major data elements are recorded: (1) patient name and hospital identification number; (2) dates and times when the study and series were created in the imaging system and when they were acquired in the acquisition computer; (3) the number of acquired slices per series; (4) the acquisition status; and (5) the DICOM unique identification (UID) value for the study and series. The detailed description of the image transaction database table will be presented in section 2.3.3.

Determination of the end of image series

The images of the series can only be grouped together by the formatting process when the end of series is determined by the image receiving process. To algorithmically determine the end of series in a manner both accurate and timely efficient is not trivial. We present two methods used for determining the end of series and discuss the advantages and drawbacks of each as follows.

Presence of the next consecutive series. The first method for detecting the end of series is based on the presence of the next consecutive series (PNCS). This method assumes that the total number of image slices for the current series will be transferred to the acquisition computer before the next series begins. In this case, the presence of the first image slice of the next consecutive series indicates the termination of the previous series. The success of the PNCS method depends on the following two criteria: (1) the imaging system transfers the image slices to the acquisition computer in order; and (2) no image slices are lost during the transfer. Note that the first criterion depends on the specific implementation of the image transfer by the imaging system. If the imaging system transmits the image slices in sequence (e.g. GEMS MR Signa 5.4), the PNCS method can faithfully group the images of a series intact. On the other hand, if the imaging system transfers the image slices in a random fashion (e.g. SIEMENS MR Vision), the PNCS method may conclude the end of series incorrectly. Even though one could verify the second criterion by checking the image slice order, whether or not the last image slice has been transferred remains unknown to the acquisition computer. Another drawback of the PNCS method relates to the determination of the last series of a particular study which is based on the presence of the first image slice of the next study. The time delay for this determination could be lengthy because the next study may not begin for hours.

Number of consistent acquired images for a time-interval. The second method for determining the end of series is based on a time-interval criterion. The hypothesis of this method assumes that an image series should be completed within a certain period of time. With this method, the end of series is determined when the acquisition time of the first image slice plus a designated time interval has elapsed. This method is obviously straight forward and simple, but with a static time interval criterion chosen *a priori*, it is not dynamic enough to be practical in a clinical environment. Thus, an alternative recourse is preferred in terms of the number of consistent acquired images for a time-interval (NCAITI).

The NCAITI method requires one to store the number of acquired images for a given series at two different times, say time $t1$ and time $t2 = t1 + \Delta t$, for some predetermined constant Δt. By comparing the number of slices acquired at time $t1$ vs the number of slices acquired at time $t2$, a premise is constructed for determining whether or not the series is completed. If the number of slices is constant, we conclude the series is completed, otherwise, we conclude the series is not yet completed. This process (time-interval with image slice verification) is iterated until a consistent number of slices has been reached. General issues of this method in regards to the length of Δt and whether Δt should be constant or variable are core parts of the NCAITI method.

One argument in favor of the NCAITI method in terms of the variable Δt is that for a given series, the number of slices transferred from the imaging system to the PACS acquisition computer tend to decrease while the iterations of the NCAITI method increase. Therefore it seems reasonable to believe that Δt may be reduced proportional to the number of increasing iterations of the algorithm. A counter argument of this observation is that the number of slices transferred to the PACS acquisition computer may vary with time depending on the imaging system design. For example, an imaging system may be designed to transfer image slices according to the imaging system workload and priority schedule. If the image transfer process has a low priority, then the number of slices transferred during a period when the system workload is heavy will be less compared with when it is light. In this case, using a constant Δt is more appropriate. Despite whether Δt should be constant or variable, the first assigned Δt is crucial because a short Δt may result in missing images whereas a long Δt may result in a lengthy and inefficient image acquisition.

Usually, the first Δt chosen for the NCAITI method is empirical dependent upon the imaging protocols used by the imaging system. For example, if the imaging protocols frequently used to scan patients generate a lot of images per series, then the Δt should be long, otherwise, a shorter Δt is preferred. However, it is possible for the NCAITI method to conclude a series is completed before it really is. This is because in some rare cases the operator or clinician is required to interrupt the scanning process in the middle of a series to conduct a patient position alignment or to inject contrast agent. If the time it takes to conduct such procedures is longer than the Δt, then the images scanned after the procedure will not be grouped into the current series. For a careless PACS design, this could result in a severe problem—missing images.

For our PACS image acquisition design, the NCAITI method and the PNCS method were combined to determine the end of series for the GEMS MR scanner. We set the Δt equal to a constant value of 10 min. In addition, we implemented this task in the following stages: (1) identify and count the acquired slices for a particular series; (2) record the time stamp whenever the number of acquired slices has changed; and (3) update the acquisition status of the series. In order to do all of these, we need to track the acquired image slices using a transaction table designed in association with the series database table.

Image transaction table. Whenever a DICOM image slice is acquired from the imaging system, a record with a designed PACS slice name is created in the transaction table. The PACS slice name is composed of the modality type, the imaging system identification, the study number, the series number, and the slice number. The task of identifying and counting slices can be accomplished by using the image slice records in the transaction table. Three major events are recorded in the transaction table: (1) the number of acquired slices; (2) the comparison time when the number of acquired slices are compared with the previous iteration; and (3) the acquisition status declaring the series as stand-by, ongoing, completed, or image missing. Here, the information regarding the number of acquired slices and acquisition status is useful for the maintenance of the image receiving process. If the series is still ongoing, the comparison time is updated for the verification of the number of slices during the next iteration of the NCAITI algorithm. After the NCAITI algorithm detects the end of series, it can be further verified by the PNCS method. If the next series exists in the series database table or the next study exists in the study table, the image series is determined complete. Otherwise, one more NCAITI iteration is given and the series remains in stand-by status. In this case, the end of series will be concluded in the next NCAITI iteration regardless of the existence of the next series or study. In this way, the completeness of an image series is verified by both methods and the potential lengthy time delay problem of the PNCS method is minimized.

PRELIMINARY EXPERIMENT

The PACS acquisition system was tested in a clinical environment for the acquisition of GEMS MR images via the Ethernet and DICOM C-Store service. In the testing environment, there were six other CT and MR imaging systems along with one volumetric image display workstation connected to the same network (8). Figure 4 shows the imaging system configuration of the test environment. Although these systems were not included in the data gathering, the operators might change the DICOM setting to communicate images with the experimental MR system as needed. The test was conducted on a daily basis between 16 October 1995 and 16 January 1996. The acquired data were inspected in two ways. First, the completeness of each image study hierarchy (i.e. study, series, and slice) was verified using the PACS acquisition database. The acquisition database contains the number of events per study hierarchy which was compared to the same information in the scanner database. The scanner database information was obtained through queries issued by a manufacturers' proprietary software. This information was considered to be the actual number of events which should be reflected in the PACS acquisition database if no images were lost. Second, the acquired images were sent to a high resolution (2048×2560) image display workstation for inspecting the data integrity of the acquired images and text (image header) information (see Fig. 4) (9).

On the console of the GEMS MR system, the DICOM C-Store client transfers images using one of the following three modes: auto-transfer, auto-queue, or manual-transfer. Only one transfer mode can be in operation at a time. The auto-transfer mode transmits a reconstructed MR image slice whenever it is made available. The auto-queue mode transfers images only when the entire study has been completed. The manual-transfer mode allows a user

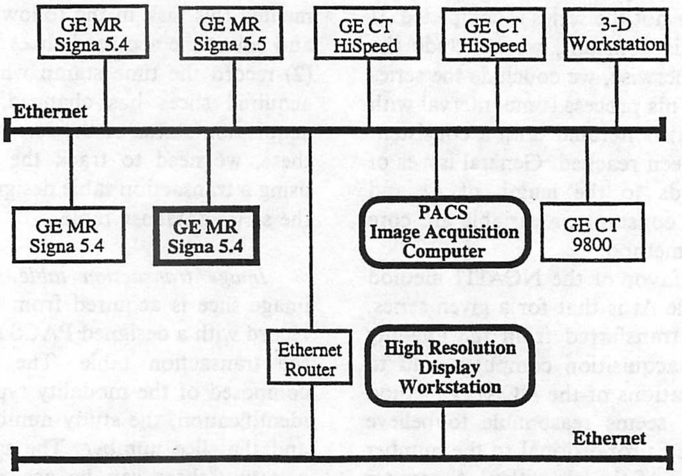

Fig. 4. The diagram shows the network connections of the imaging systems and image display workstations in our clinical environment. The systems used in this study involve the PACS acquisition computer, the high resolution display workstation and one of the GE MR Signa 5.4 systems.

to select and transfer multiple image slices, series, or studies. As mentioned earlier, an image series covering the body region of interest is clinically meaningful. This implies that a complete image series must be made available to the clinician as soon as possible. For this reason, on the MR console the auto-transfer mode was set to transfer images to the PACS acquisition computer rather than the auto-queue mode. Since the auto-transfer mode transfers images whenever they are made available, it is much faster than the auto-queue mode. The manual-transfer mode was used only when a re-transmission was required.

Statistical results from the preliminary trial were compiled using the PACS acquisition database tables. Table 1 shows a tabulation of these results. There were a total of 475 studies comprising 1886 series acquired during the preliminary test period. The image data and the image header information of these studies were intact and could be viewed in the high resolution image display workstation. Of the 475 total studies, 133 (28%) were completely lost and 29 (6.1%) were partially acquired, meaning one or more series or image slices were missing. Upon further investigation it was determined that all of the completely or partially lost studies, which we refer to as the missing studies in this context, were caused by an abrupt change in the image transfer mode; while images were being transferred to the PACS acquisition computer, or sometime just before, the console operator changed the transfer mode and/or destination computer. We had to inform the console operator to manually re-transmit the missing studies and resume the auto-transfer mode. We found this procedure to be unacceptable in our automated DICOM compliant image acquisition design.

AUTOMATIC IMAGE RECOVERY SCHEME

Resulting from the preliminary experiment was the need to improve the integrity of the acquired image data by addressing the problems of the missing studies. A method for automatic detection and recovery of the missing studies was crucial to the success of a DICOM compliant PACS acquisition system. In the following sections, we present how we designed an automatic image recovery scheme for this purpose.

Basis for the image recovery scheme

The automatic image recovery scheme includes two tasks: identifying the missing image studies and recovering them. These two tasks can be accomplished by using the DICOM Q/R service class in conjunction with the PACS acquisition database. The operation mechanism of the Q/R service class involves three other DICOM services: the Composite-Find (C-Find), the Composite-Move (C-Move), and C-Store. The task of identifying missing studies is performed through the C-Find service class by matching one of the image grouping hierarchies, such as study level or series level, between the PACS acquisition database and the scanner database. The recovering task follows the missing study detection and is carried out by the C-Move and C-Store services. In this study, the Q/R operation is performed via a server process and a client process which run in the MR system and the PACS acquisition computer, respectively.

Design and implementation of the image recovery scheme

Figure 5 shows the flow diagram of the automatic image recovery scheme. In the beginning, the Q/R client encodes a C-Find query object which contains the major information elements such as image study level and a zero-length UID value (unique identification value) defined by the DICOM standard. The zero-length UID prompts the Q/R server to return every single UID for the queried level. Then, the Q/R server responds with all the matching objects in the scanner database according to the requested image study level. The content of each responded object mainly includes information such as a study number and the corresponding study UID. The information of each responded object is then compared with the records in the PACS acquisition database. Those study numbers which are in the responded objects but not recorded in the

Table 1

Items	Total no. of studies conducted	No. of missing studies due to human intervention errors		No. of missing studies manually recovered	No. of missing studies automatically recovered	No. of series missing images due to grouping process
Experiments		Completely	Partially			
Preliminary	475	133 (28%)	29 (6.1%)	162	0	0
Pre-clinical	259	49 (19%)	9 (3.5%)	0	58	0

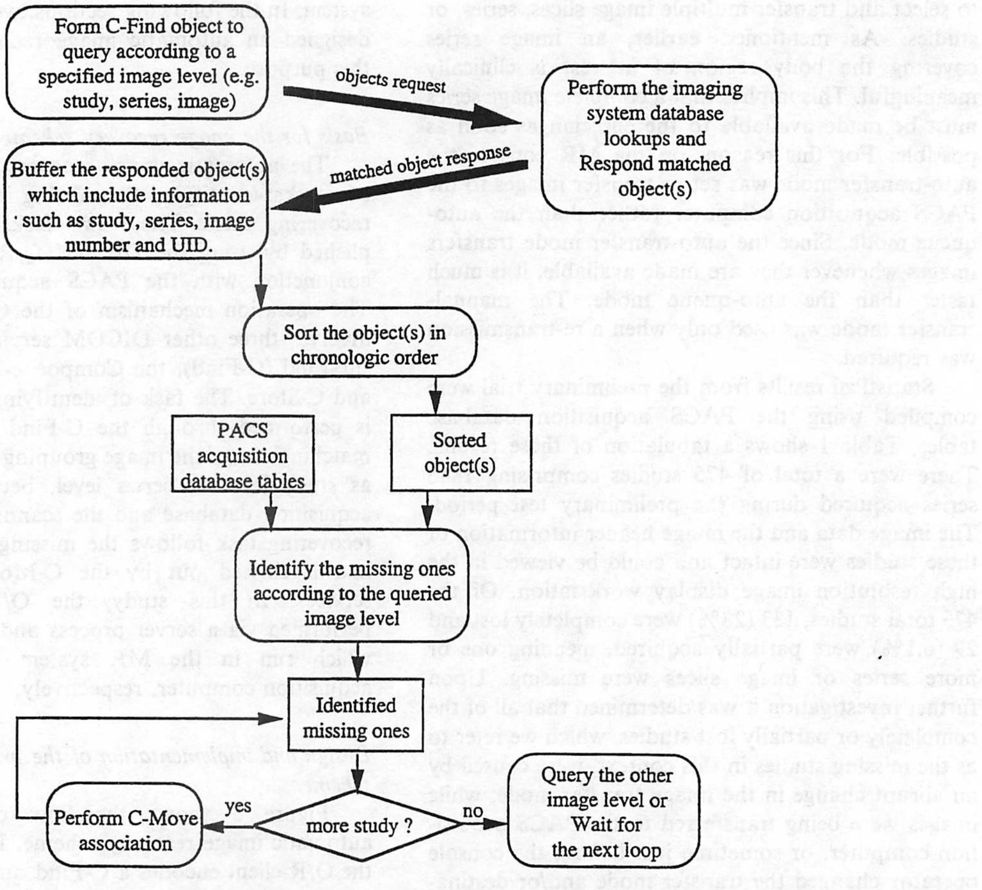
Form C-Find object to query according to a specified image level (e.g. study, series, image)
objects request
Perform the imaging system database lookups and Respond matched object(s)
matched object response
Buffer the responded object(s) which include information such as study, series, image number and UID.
Sort the object(s) in chronologic order
PACS acquisition database tables
Sorted object(s)
Identify the missing ones according to the queried image level
Identified missing ones
Perform C-Move association
yes
more study ?
no
Query the other image level or Wait for the next loop

Fig. 5. A general processing flow diagram of the automatic query/retrieve image recovery scheme.

PACS acquisition database are considered as missing studies. Each of them can be retrieved by issuing a C-Move object which is equivalent to an image retrieval request. Since the retrieval is study specific, the study UID has to be included in the C-Move object explicitly. In the scanner, after the C-Move object was received by the Q/R server, it relays the retrieval request to the C-Store client. As a result, the image transfer is actually conducted by the C-Store client and server processes. The tasks of identifying and recovering missing series are performed with the same recovery operation mechanism following the study level. The difference between the study level and the series level in this recovery scheme is that a specific study UID must be encoded in the C-Find query object for the series level as opposed to a zero-length UID for the study level.

The records of available images in the scanner database and the PACS acquisition database may not synchronize. This scenario can happen in the current study when its associated series and image slices are being generated in the scanner but not yet transferred to the PACS acquisition computer. This asynchronization can result in incorrect identification that the image recovery process mistakes the current study as a missing one. A method of avoiding this is described as follows: The responded objects from the Q/R server are first sorted in chronological order by the study creation date and time. If the creation date and time of the most recent study is less than a predefined time-interval compared with the current time, it is considered as the study being generated by the scanner. Thus, the image recovery process will not identify the most recent study as a missing study.

Concurrent image receiving server

A very important factor relating to the success of the automatic image recovery process is the ability of the C-Store server to handle multiple image transfer requests concurrently (10). Not only will the C-Store server handle its regular work load of acquiring images into the PACS acquisition system, it now must be able to handle a C-Store request associated with the C-Move service sent by the Q/R server. From our experience, with the image recovery process running, the probability that the C-Store server will receive multiple image transfer requests at the same time is high. This indicates that the C-Store server running in the PACS acquisition computer must consider the design of managing multiple C-Store requests in parallel. In order to achieve this goal, any factor that may hamper the concurrent image transfer must be excluded. For example, the locking mechanism of accessing the image transaction database used in the early version of the CTN C-Store server program is not preferred. This is because this transaction database can be only accessed by one C-Store server process at a time and others may be timed-out while waiting. In our implementation, we removed the database from the C-Store server program because the PACS image acquisition database is comprehensive enough to cover the image transaction functionality as mentioned in section 2.2.

Pre-clinical experiment

The integration of the Q/R-based image recovery process with the entire acquisition task chain was evaluated from 18 March 1996 to 22 April 1996. The environment and system set-up were identical to the preliminary experiment. In this evaluation period, 259 studies consisting of 1128 series were acquired into the PACS acquisition computer. Among the acquired data, there were 49 studies completely lost and nine studies partially acquired during the image receiving process. They were all identified and recovered automatically through the image recovery process. Overall, no single series was missed and no manual re-transmission was ever required.

DISCUSSIONS

Through our research we have found that the DICOM standard both helps and hinders the PACS acquisition system. On one hand, it significantly simplifies the implementation of PACS image acquisition. On the other hand, due to its open architectural design, it hinders the integrity of acquired data by rendering image studies incomplete. It is our belief that this problematic issue can be a major concern for DICOM compliant PACS acquisition systems in numerous health care institutions around the country. We proposed a solution for this problem by integrating the DICOM Q/R service class into the PACS image recovery process.

With the Q/R-based image recovery process fully functional and running, the problem of the missing studies effectively vanished. During the preliminary experiment, when the image recovery process was not running, all of the missing studies had to be manually re-transmitted, a procedure unacceptable in an automated PACS acquisition system. After the image recovery process had been implemented, every single missing study was automatically detected and recovered during the pre-clinical experiment. This algorithm guarantees the data integrity of the DICOM compliant PACS acquisition system that each study will be acquired in its entirety.

Although the image recovery scheme is effective in the PACS acquisition, minimizing the human intervention that causes the missing studies is important. Two approaches are suggested: The first approach is for the manufacturers of the imaging systems to incorporate an automatic reset feature. When an operator changes the DICOM communication setting for an application, the imaging system can automatically resume a pre-defined communication setting (e.g. PACS transmission) when the application is detected inactive. In this way, there would be no need for the operator to have to manually reset the communication setting. The second approach involves an automatic dial-up paging scheme similar to the one described in our previous work (6). Whenever a missing study is detected by the image recovery scheme, a designated pager residing on the operator console will be activated to remind the operator to reset the PACS transmission setting.

So far, our discussion has focused on solving the missing studies caused by human intervention during the PACS acquisition. The proposed Q/R-based image recovery scheme can also solve the missing studies due to hardware and software malfunctions during the DICOM image transmission as well. The reason is that these missing studies have no characteristic difference from those caused by the human intervention. Thus, they can be automatically recovered provided that the factors causing malfunction are removed.

Although the results from our experiments indicate that the NCAITI method in conjunction with the PNCS method detects the end of series perfectly, the algorithm may miss unusual cases as discussed in section 2.3.2. In fact, there is no method that can accurately and efficiently determine the end of series. However, the indication of the end of series may be implemented by the manufacturers of the imaging systems. With such an implementation, not only can all the effort spent in detecting the completeness of an image series be saved but also the overall image acquisition performance will be greatly improved.

One final thought, the proposed Q/R image recovery scheme can be used to initiate image transfer. In this way, the PACS acquisition computer acquires images from the imaging system in a pulling fashion. On the other hand, using the DICOM C-Store server and client paradigm to perform the PACS image acquisition task is considered a pushing scheme. For a DICOM compliant PACS image acquisition system, the advantage of the pulling scheme versus the pushing scheme is that the PACS image receiving task will not depend on the DICOM communication setting; thus, human intervention errors are eliminated. However, the downside of the pulling scheme is that the operation workload of the imaging system will be increased.

SUMMARY

We have integrated an interface mechanism based on the DICOM standard which automatically acquires images from a GEMS MR scanner into a PACS acquisition computer. Since both systems follow the DICOM communications protocol, we were able to acquire the images quite easily. One remaining obstacle is that no end of series can be obtained from either the MR scanner or the DICOM protocol. Grouping the images into customary sets based on their clinical characteristics is an essential task of the PACS acquisition process. Two methods were introduced for the determination of the end of series and their advantages and disadvantages were discussed. The design and major functions of the PACS image acquisition database were also presented. With the DICOM-based PACS acquisition setup, we performed a preliminary experiment for a 3 month period. The results of this experiment indicate that over 34% of the studies were not automatically acquired into the PACS acquisition computer. This result was disappointing and not acceptable. An investigation of the missing studies discovered that all of them occurred when the transfer mode and/or the transfer destination were changed and not reset again. A DICOM Q/R service class was implemented with the PACS acquisition database to detect the missing studies and automatically recover them. The PACS image acquisition system with the image recovery scheme was evaluated through a two-month pre-clinical experiment. The statistical results of this experiment show that 259 studies were automatically acquired and not a single one was missing. This indicates that the Q/R-based image recovery process effectively eliminated the missing studies from the PACS image receiving process.

Acknowledgement—This work was supported in part by the National Library of Medicine HPCC program N01-LM-4-3508 and the California Research and Education Network (CalREN) grant number ATMN-007

REFERENCES

1. Hindel, R. Ed. Implementation of the DICOM 3.0 standard: a pragmatic handbook. Oak Brook, Illinois: RSNA: 1994.
2. Van Syckle D.E.; Sipple-Schmidt T.; Parisot C.R. Buying imaging products with DICOM interface—made easy, In: Boehme J.M., Rowberg A.H., Wolfman N.T., eds. SCAR '94. Carlsbad, California: Symposia Foundation; 1994: 529–536.
3. Moore, S.M. Observation on DICOM demonstration at the RSNA annual meetings. Proc. SPIE, Med. Imag. 2711:89–97; 1996.
4. American College of Radiology, National Electrical Manufacturers Association. Digital Imaging and Communications in Medicine (DICOM): network communication support for message exchange. Washington DC: NEMA publication PS 3.8—1992, 1992.
5. American College of Radiology, National Electrical Manufacturers Association. Digital Imaging and Communications in Medicine (DICOM): point-to-point communication support for message exchange. Washington DC: NEMA publication PS 3.9—1993, 1993.
6. Lou, S.L.; Wang, J.; Moskowitz, M.; Bazzill, T.; Huang, H.K. Methods of automatically acquiring images from digital medical systems. Comput. Med. Imag. Graph. 19:369–376; 1995.
7. Prior, F.W. Specifying DICOM compliance for modality interface. Radiographics 13:1381–1388; 1993.
8. Huang, H.K.; Andriole, K.; Bazzill, T.; Lou, S.L.; Wong, A.W.K.; Arenson, R.L. Design and implementation of a picture archiving and communication system: the second time. J. Dig. Imag. 92:47–59; 1994.
9. Lou, S.L.; Huang, H.K.; Taira, R.; Breant, C. A 2K radiological image display station. Proc. SPIE, Med. Imag. 1899:95–102; 1993.
10. Maekawa, M.; Oldehoeft, A.E.; Oldehoeft, R.R. Operating systems—advanced concepts. Menlo Park, California: Benjamin/Cummings; 1987.

About the Author—S.L. Lou received a BS degree in Biomedical Engineering from Chung-Yuan Christian University at Taiwan, R.O.C. in 1982 and the PhD degree in Biomedical Physics from University of California at Los Angeles (UCLA) in 1991. He was a Visiting Assistant Professor in the Division of Medical Imaging, Department of Radiological Sciences at UCLA from 1991 to 1992. He is currently an Assistant Professor in the Laboratory for Radiological Informatics, Department of Radiology, University of California at San Francisco (UCSF). He also holds a joint faculty appointment in the UCSF/UC Berkeley Bio-Engineering Graduate Program. His major research activities over the past 8 years have been in design and implementation of Picture Archiving and Communication Systems (PACS), digital communication methodology applied in PACS, image data compression, and image mapping techniques.

About the Author—David Hoogstrate received a BA degree in Mathematics and Geography from the University of Colorado in 1994. He was employed as a research assistant at the Cooperative Institute for Research in Environmental Science (CIRES) from

1994 to 1995. Mr Hoogstrate is currently the system manager of the Laboratory for Radiological Informatics, Department of Radiology, University of California at San Francisco. For the past 3 years his research activity has focused on cryospheric research, PACS image acquisition, multimedia interface, digital mammography imaging, and Asynchronous Transfer Mode (ATM) network.

About the Author—H.K. Huang is Professor and Vice Chairman, Director of the Laboratory of Radiological Informatics, UCSF. He also holds a joint faculty appointment in the UCSF/UC Berkeley Bio-Engineering Graduate Program. Dr Huang designed an implemented the UCLA PACS from 1982 to 1992 which is now in daily clinical operation. At UCSF he is establishing the Radiological Informatics Laboratory (LRI). Two primary functions in the LRI are hospital-integrated PACS and multimedia radiological database. His other research interests are in ATM wide and local area networks, and image processing.

IEEE Multimedia in Medicine, April-June 1997

Multimedia Applications in Health Care

H.K. Huang
University of California, San Francisco

Two major events have transformed the high technology and health care industries during the past several years: the rapid development of multimedia technology and health care reform. Multimedia software and hardware developers have largely targeted the consumer market, shaping the development of computing, communication, and visualization technologies to emphasize entertainment and education. The health care industry, on the other hand, is going through structural, institution-level changes that will alter how health care is delivered in the coming years. Such reform highlights the need for high technology like multimedia to facilitate the shift to such cost-effective methods as wide-area networks, databases, and telemedicine.

Health care is a triad emphasizing patient care, education, and research. Patient care focuses on quality care with minimum cost; education focuses on training future health care professionals and creating patient and community health awareness; research focuses on new discoveries in diagnostic and therapeutic methods and procedures. Multimedia technology can facilitate a synergism among these components. In the health care industry, major advances in the past ten years include the development of hospital information systems (HIS) and picture archiving and communication systems (PACS). HIS manages patient data flow including demographics, billing, scheduling, reports, and statistics. PACS, on the other hand, was developed to help clinicians and researchers manage medical images. The integration of HIS and PACS opens the door for the health care industry to use multimedia technology widely.

This special issue singles out developments and applications of multimedia technology for the health care industry. The article "Networked Multimedia for Medical Imaging" by Wong and Huang describes the state of the art of HIS and PACS and their use for patient care. It also introduces a novel methodology that integrates HIS and PACS in the networked multimedia environment for better health care delivery, education, and research.

Thoma and Long's article, "Visible Human Images," describes a type of medical image developed by the National Library of Medicine, a US government agency. The images are now ready for dissemination to the public for education and research purposes. The authors describe the technology behind the project and note that speed and ease of access and low cost are the keys to public awareness and acceptance.

The article "Opportunities for Visual Computing and Communications in Healthcare" by Kitson, Malzbender, and Bhaskaran discusses technology industry efforts to develop multimedia components for health care applications. Interest in bringing multimedia applications to health care will continue to grow rapidly and will surely benefit patient care, reduce costs, and advance research and education. These three articles unveil general multimedia requirements in health care and forecast trends in multimedia technology development. Read on, and explore the future of multimedia in medicine. **MM**

H.K. Huang is a professor and vice chairman of the Department of Radiology and director of the Radiological Informatics Laboratory at the University of California, San Francisco; he also holds a joint appointment in the UCSF/UC-Berkeley Bioengineering Graduate Program. Huang implemented a PACS at UCLA in 1991 and a second-generation PACS at UCSF in 1994. His current research interests include medical multimedia, high-speed medical image transmission, and image content indexing and retrieval.

Contact Huang at the Department of Radiology, University of California, San Francisco, 505 Parnassus Ave., San Francisco, CA 94143-0628, e-mail bernie_huang@radmac1.ucsf.edu.

1070-986X/97/$10.00 © 1997 IEEE

IEEE Multimedia in Medicine
April-June 1997

Networked Multimedia for Medical Imaging

Stephen T.C. Wong and H.K. Huang
University of California, San Francisco

The development of biomedical imaging has revolutionized medical practice and health care delivery. The next wave of change, however, will come from merging medical imaging with multimedia technology. This article discusses the necessary information infrastructure and supporting technology for this evolving field. We describe four types of clinical applications to illustrate the use and versatility of networked multimedia systems for image-assisted medical care.

Today's medical images come from a broad spectrum of imaging sources and contribute important information in a wide range of medical contexts. In the United States, about 30 percent of diagnostic imaging examinations are taken directly in digital media. These include X-ray computed tomography (CT), magnetic resonance imaging (MRI), ultrasound (US), positron emission tomography (PET), single photon emission computed tomography (SPECT), digital subtraction angiography (DSA), and computed radiography (CR). The other 70 percent of examinations—skull, chest, breast, abdomen, and bone—employ conventional X-rays and microscopy. Digitizers such as laser scanners, solid-state cameras, drum scanners, and video cameras can be used to convert X-ray films and microscopic image pictures into digital format for processing.[1] The amount of digital medical image data captured per year in the United States alone is estimated on the order of petabytes—10^{15} bytes—and increases rapidly every year.

These modalities have revolutionized how we acquire patient images and even permit evaluation of various biologic processes and events as they occur *in vivo*. For example, the emergence of MRI methods and improvements in CT acquisition techniques have led to safe and convenient ways to visualize fine anatomical structures such as blood vessels. Nuclear medicine scans such as PET and SPECT generate functional images of blood flow and metabolism essential to diagnosis and to research on various organs such as the brain, heart, liver, bones, and kidneys.

Medical images thus form the cornerstone of the patient record and lie at the heart of diagnosis, therapy, and follow up. While physics and mathematical research have contributed greatly to medical imaging and will continue to do so, new development efforts are shifting from generation and acquisition to postprocessing and management of medical images and associated data. Medical imaging information types include

- still images, whether 2D such as mammograms or 3D such as CT scans;
- pictures, such as image slices from a biopsy;
- moving images, whether motion video such as ultrasound or cine images such as cardiac MRIs;
- structured text such as image headers;
- plain text (unformatted) such as diagnostic reports;
- sound such as a physician's dictation; and
- graphics such as a geometrical model of the brain or annotation overlaid on an image.

Several factors drive this shift toward multimedia applications in medical imaging:

- increasing market demands for cost-effective health care delivery,
- high capital investment in imaging device development,
- the need to organize and store large amounts of multimodal image data and complement them with relevant clinical data,
- improved performance and falling costs of computers and communication systems, and
- the ability to extract rich information embedded in images.

This last factor exceeds the sum of individual imaging technologies and generates computer-based multimedia applications for a wide range of diagnosis and therapeutic procedures. Such applications use the computer to integrate, control, and correlate several types of clinical information that can be represented, stored, transmitted, processed, and manipulated digitally.

Fluckiger divided computer-based multimedia

1070-986X/97/$10.00 © 1997 IEEE

applications into two categories: local and networked multimedia.[2] This classification also applies to medical imaging.

Local multimedia applications run on standalone systems and use no remote resources. An example is a series of self-guided teaching files distributed by the American College of Radiology (ACR). Such computer-based education programs run on CD-ROM-equipped PCs and interactively take residents and practitioners through the steps of diagnosing selected imaging cases.

Networked multimedia applications provide services via remote systems communicating across networks. Picture archiving and communication systems (PACS) used in many digital radiology departments acquire images directly from hospital scanners, consolidate image files in a central on-line archive, and transmit the files to remote high-resolution display stations for review.[3]

We focus here on networked digital multimedia in medical imaging. Networked multimedia can support genuinely networked applications or a client-server set-up. Genuinely networked applications such as telemedicine and teleradiology offer healthcare services across distances. Even when supporting applications for which stand-alone systems might suffice, a client-server model provides a cost-effective means to pool resources such as large-scale multimedia storage capacity into servers remotely accessed by client medical workstations.

A networked multimedia framework

To develop new networked multimedia applications, we first need to build a new infrastructure that can support them. Figure 1 shows a logical framework to support multimedia medical imaging. Its components include data sources (PACS archives and other image data stores), postprocessing, communication, visualization, image database management, and client application workstations.

Data sources

Patient data come from PACS and associated medical information systems. Data types include patient demographics, medical history, still and moving images, diagnostic reports, voice dictation, video, and other clinical data. Most of these are archived as flat files (such as PACS images) or in nonrelational textual databases (such as the hierarchical data model used in most hospital information systems). These can be archived and shared using recognized data exchange standards and protocols such as Dicom (Digital Imaging and Communication in Medicine) for medical images[4] and HL7 (Health Level 7) for clinical text.[5] With raw images and other medical information in digital media, we can postprocess, create, and present image contents for new multimedia medical imaging applications.

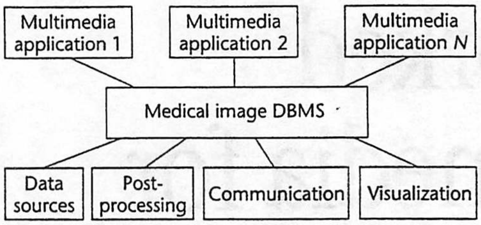

Figure 1. The networked multimedia medical imaging framework and its logical components.

Table 1. Medical image sizes. [illegible]

Modality	Image Dimension (pixels)	Gray Level (bits)	Avg. Size/Exam (Mbytes)
Nuclear medicine (PET/SPECT)	128 × 128	12	1-2
Magnetic resonance imaging	256 × 256	12	8-20
Ultrasound	512 × 512	8	5-10
Computed tomography	512 × 512	12	20-40
Spiral or helical CT	512 × 512	12	80-160
Digitized electronic microscopy	512 × 512	8	Varies
Digitized color microscopy	512 × 512	24	Varies
Digital subtraction angiography (per run)	512 × 512 or 1,024 × 1,024	8	100-500
Digitized X-rays	2,048 × 2,048	12	8
Computed radiography	2,048 × 2,048	12	8
Digitized mammography	4,096 × 4,096	12	128 (4 images)

Table 1 lists the average amount of data per examination generated by a spectrum of medical imaging technologies. The image size and number of images taken in one patient examination vary by modality. Except for digitized electronic microscopy and digitized color microscopy, which are pathologic and histologic images of microscopic tissues, we classify the modalities as radiologic images and use them for diagnosis and treatment planning. In contrast with most other true-color biomedical image types (such as DCM), a radiologic image is monochrome, and each radiologic examination follows a well-defined procedure. For example, one X-ray CT examination (about 40 image slices) with each image slice size of 512 × 512 × 12 bits generates 20 to 40 Mbytes, whereas one digital mammography image may generate 32 Mbytes of data. (X-ray films requiring higher resolution can be digitized using 4,000 × 4,000 × 12-bit digitizers.) Note that dynamic medical images such as digital subtraction angiography for cardiac catheterization generate multiple runs of video data per study. Each run lasts a few seconds to tens of seconds and can generate half a gigabyte of digital data.

Image postprocessing

Images ignore semantic contents and exist as bitmaps consisting of individual pixels, each coded with a fixed number of bits. Imaging specialists must interpret medical images qualitatively. For the past three decades, the medical image processing community has actively pursued efficient algorithms that can extract and quantify semantic objects from plain image files.[6] We can readily integrate established algorithms into the networked multimedia framework to process existing digital images for new applications. Typical tasks include image segmentation, texture analysis, content extraction, and image registration. These can be performed automatically or interactively depending on the difficulty of segmenting and extracting semantic structures.

Communication

Enabling technologies with high-resolution images include networking, data security, image compression, and groupware. Networking employs asynchronous and synchronous communication modes. The former includes image acquisition and exchange, while the latter refers to group teleconferencing and interpersonal communication. Most hospital image networks use Ethernet, Fiber Distributed Data Interface (FDDI), or Asynchronous Transfer Mode (ATM). Medical image communication occurs almost universally over transmission-control protocol/Internet protocol (TCP/IP), but real-time protocols for ATM-based multimedia networks remain an unresolved issue.

We must consider security when implementing both data integrity and access protocols. Wong recently discussed medical image security.[7] After postprocessing, mechanisms such as key-based encryption and digital time stamping will ensure the completeness and authenticity of medical images. Data access systems determine who can access what type of data and when.

Image compression reduces digital medical image data volume and achieves a low bit rate without perceived loss of image quality. Demands for transmission bandwidth and storage space, however, continue to outstrip existing technological capabilities. Furthermore, lossy coding techniques for clinical use raise many complex legal and regulatory issues. Wong focused on progress in lossless and lossy medical image compression and the legal challenges of using lossy compression for medical records.[8]

Groupware designates the computer-based software and systems that support collaborative work among remote sites.[9] Multimedia medical imaging requires shared computer workspace that can accommodate 3D images of 10 to 12 bits per pixel, videoconferencing that can display high-resolution medical images (see Table 1), and the ability to access remote medical databases.

Data visualization

The need to improve tools for volume visualization of medical images has become a bottleneck in multimedia medical applications. This affects the combined interpretation or correlation of 3D anatomic and physiologic or metabolic data. The challenge lies not only in handling large medical images but also in representing complex relationships among the data. Current visualization techniques for biomedical data analysis include surface-rendered anatomical displays with rotation and shading, volume-rendered cutouts with emphasis on particular objects, transparent surfaces within surfaces with color shading and rotation, superimposition of multiple image data sets of the same organ, and reprojection techniques such as maximum-intensity projection (MIP) and weighted-integrated projection, which use various weightings of pixels of interest.

An example already in routine use is the cine CT angiogram, visualized in 3D by projecting at multiple different angles to form a sequence of images that can be played back in "cine" mode to simulate the rotation of blood vessels. Recent advances in 3D graphics accelerators also let us volume-render tens of megabytes of image data on the fly; this is critical for real-time image-guided therapy and surgery procedures.

Medical image database management

This middleware component integrates and organizes images and other patient data, selected image features, and clinical decision rules into a database management system (DBMS). It supports multimedia database management, content-based indexing, formatting and distribution for visualization, and image processing. A medical image database server thus pools hospital network resources in a uniform and easily accessible manner for client application development. Because no existing DBMS can manage medical images and their contents, we must develop such a server using customized object software or some middleware specifications such as the common object resource broker architecture (Corba) that will interact with the underlying databases.

Application client workstations

Once the infrastructural components are in place, we can design client workstations that integrate imaging applications for clinical services, research, and education. The application software also optimizes workstation design for information retrieval, presentation, and visualization with minimal user effort. User acceptance depends on a well-designed graphical user interface (GUI). GUIs for today's medical imaging workstations are mostly Unix-based. Soon, however, the World Wide Web and associated programming languages such as Java and HTML combined with greater PC processing power will let us deploy Web browsers and PCs even for demanding medical imaging operations.[10] Because most of its components are sharable and reusable, the networked multimedia framework enables rapid prototyping and reduces development costs.

Multimedia medical imaging applications

For the past three years, we have been developing a networked multimedia system testbed. We started with the existing storage and networking infrastructure of the UCSF hospital integrated picture archiving and communication system (HI-PACS). We then implemented a middleware image database server (IDBS) to manage multiple medical image databases and interact with data visualization, postprocessing, and other communication utilities.[11,12] HI-PACS connects imaging scanners of the UCSF Medical Center and affiliated hospitals in the San Francisco Bay Area using 155-Mbps ATM wide and local area links. The system stores automatically generated images in its 1.3-terabyte optical jukebox together with relevant patient data from radiology and other hospital information systems.

This article focuses on some of our ongoing applications to demonstrate the uses and benefits of such a multimedia information infrastructure. We discuss four medical imaging applications built on the networked multimedia information system testbed. For each application we present the underlying hypothesis, conventional methods and their shortcomings, the new approach using networked multimedia techniques, and specific components required.

Medical Imaging Acronyms

CR	computed radiography
CT	computed tomography
DCM	digitized color microscopy
DEM	digitized electronic microscopy
DSA	digital subtraction angiography
EEG	electroencephalography
MEG	magnetoencephalography
MRI	magnetic resonance imaging
MRS	magnetic resonance spectroscopy
MSI	magnetic source imaging
PET	positron emission tomography
SPECT	single photon emission computed tomography
US	ultrasound

Bone age assessment

Physicians frequently perform bone age assessment in pediatric patients to evaluate the normality of their skeletal growth.

Hypothesis. Bone age can be assessed by automatically comparing a left hand and wrist digital X-ray image with a comprehensive hand digital atlas.

Conventional approach. Physicians perform radiological examination of the child's left wrist because it offers simplicity, minimal radiation exposure, and multiple ossification centers to evaluate maturity. This provides important information for the diagnosis and management of endocrine disorders and diagnostic evaluation of metabolic and growth abnormalities, acceleration or decrease of a variety of syndromes, malformations, and bone dysplasias. Doctors also actively consult this record in planning an orthopedic procedure because childhood is the best time to correct scoliosis or limb length abnormalities.

Conventional bone age assessment compares a hand radiograph with a reference set of hand X-ray film data developed in the 1930s and published in the Greulich and Pyle atlas.[13] This method, although used for more than thirty years, is inaccurate and not fully applicable to today's children because of its limited sample size and the data set's regional nature.

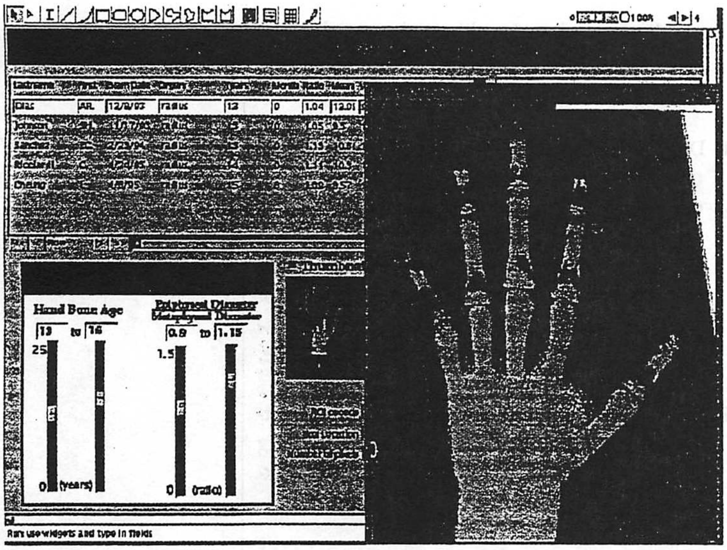

Figure 2. Query user interface developed for bone age assessment application. We have changed all names for confidentiality. The image on the right is the hand digital radiograph to be assessed.

Networked multimedia approach. We need to establish a digital atlas with a large standard set of normal hand and wrist radiographs and associated measurements. This will form the basis for computer-assisted bone age assessment. The tasks include

1. developing a new large reference set of clinically normal hand images that will serve as a digital hand atlas;
2. providing computer-assisted assessment of skeletal development by extracting relevant features from a patient image and comparing these with corresponding values extracted from the digital atlas, thus creating an updated set of reference images;
3. creating a database system that organizes atlas images, extracted features, patient age and sex, and clinical findings; and
4. allowing remote access to the bone image database from physician workstations.

The multimedia components include (see Figure 1):

- Data source: Use computed radiography (CR) images and related data from the PACS image file archive to generate the atlas.
- Postprocessing: Develop edge enhancement and morphological filtering software to extract parameters from CR images for bone age assessment.[14] The features of interest include distal, middle, and proximal phalange lengths, epiphyseal and metaphyseal diameters, and other carpal and metacarpal bone geometry.
- Database management: Implement a relational database to organize and store the digital atlas and associated data. The IDBS manages this bone age database.[12]
- Communication: Use existing PACS networks to connect the IDBS, bone age database, PACS archive server, and client workstations.
- Application software: Design a client workstation that lets users query the bone age database and evaluate the computerized bone age assessment. Query can be by image content (hand bone age or epiphyseal and metaphyseal diameter ratio), patient attributes (name, age, and examination date), or a combination of image and text features.

Figure 2 illustrates the implemented GUI. The sliders in the bottom left "Query by Image Attributes" window specify the range of image attributes for data retrieval. The IDBS returns a list of five patients (upper left window) and thumbnail pictures satisfying the combined image and patient attribute constraints. The user can then click on any thumbnail image to retrieve and analyze the original hand radiograph.

Temporal lung nodule analysis

Quantifying nodule features, especially size and temporal progression, permits clinicians to assess the effectiveness of therapeutic measures or determine the characteristics of particular lesions in the lung. For instance, the volume-doubling time interval of a solitary nodule indicates whether the nodule is benign or malignant. Also, determining whether a small nodule located deep in a lung is benign involves detecting whether its volume doubles within a short (less than 30 days) or long (more than 490 days) period. For metastasis, nodule volume variations reflect drug treatment efficacy. An effective drug reduces or halts cancer cell division; the volume of the malignant nodules thus should not increase during the treatment period.

Hypothesis. Physicians can track and analyze the progression of lung nodules over time with spiral CT scans and use the results to determine the effectiveness of a treatment plan.

Conventional approach. Physicians use serial CT scans to monitor the progression of lung nodules over time. Since metastatic lung nodules are nearly spherical lesions that contrast sharply with their surroundings, we can identify them visually on a monitor screen or film and distinguish them from blood vessels, which are cylindrical branching structures.

Conventionally, a radiologist infers a lesion's size by measuring its typical dimension manually and estimating its volume using certain rough assumptions of its geometrical shape. This approach is time-consuming and often does not provide reliable quantification data. Furthermore, no electronic database exists to organize a large volume of serial imaging studies for comparing lesion changes over time.

Networked multimedia approach. We developed a temporal image DBMS to provide clinicians with necessary image processing tools to collect chest imaging data for outcome analysis. This multimedia system is organized as follows:

- Data source: Use spiral CT images, diagnostic reports, and patient data in the image header files. These are available on line in PACS's file archive. Spiral CT generates higher precision data than conventional CT and more accurately quantifies small lesion structures.[15] Examining the chest with spiral CT generates 80 to 160 Mbytes of image data per study, compared to about 20 Mbytes from conventional CT (see Table 1).
- Postprocessing: Develop image processing tools to segment and quantify lung nodule features from 3D CT images.[16] These features include volumes, locations, nodules surface areas, and total number of nodules. For lung metastases, cancer nodules have relatively high CT numbers, in the range of Hounsfield unit 0 or above, compared with their air-like surroundings (–900). The pixel values thus provide adequate information to segment a lesion from its surroundings. Complication occurs, however, when a nodule attaches to other high-density tissue such as a blood vessel, the thoracic wall, or another nodule; these all have similar CT numbers. Such cases require a mechanism to edit out the connection manually. Two independent radiologists calibrated and validated our algorithms' quantification accuracy with phantom studies.
- Database management: Implement a structured query language-based temporal database to organize and store the CT images, radiologic reports, and extracted data as a timeline. Implicit time markers such as examination date and study number order serial imaging studies. The IDBS for the automated bone age assessment also manages the chest imaging database.
- Communication: Use the PACS local area network to connect the IDBS, the chest imaging database, PACS file archives, and client workstations.
- Application software: The Motif-based client workstation lets users query the chest imaging database. Figure 3 shows some of the GUI features, and Figure 3a illustrates two consecutive CT image slices retrieved (lesions are marked red). The lower right window shows the list of nodule parameters extracted from this CT image data set, including patient ID, study

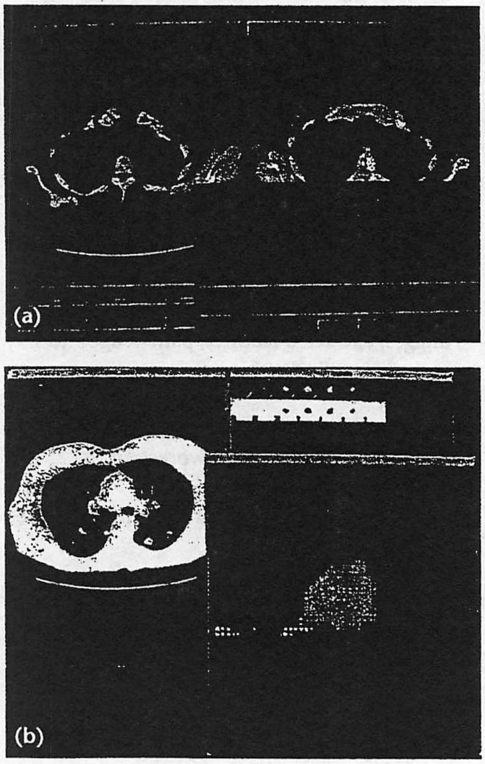

Figure 3. (a) Display of two consecutive CT image slices from the temporal chest imaging database (red denotes segmented nodules). The user can query other attributes of the study. (b) The left pop-up window displays the segmentation results. The top right window shows consecutive slices of the selected nodule within the same region of interest. The bottom window allows manual correction of the segmentation result.

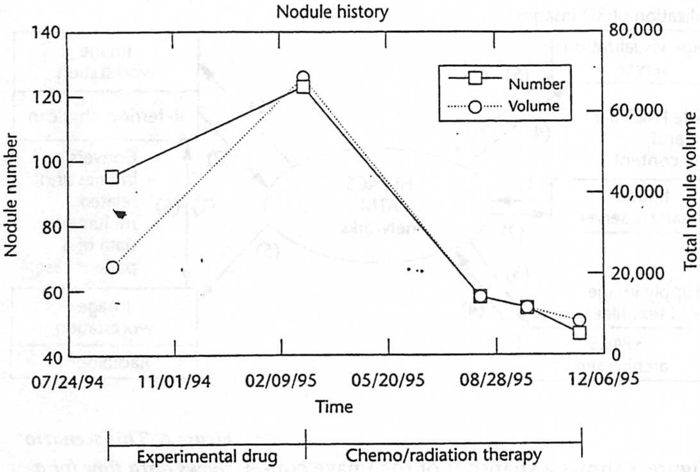

Figure 4. History of the patient nodule number and the total nodule volume. The volume is measured in mm³ (from Zhu et al.[16]).

number, nodule coordinates, volume, surface area, and associated nodule in the previous and follow-up studies. Figure 3b shows the GUI, which lets users correct the segmentation result pixel by pixel, including or excluding pixels with a simple mouse click.

Figure 4 illustrates a case of lung metastases that demonstrates the usefulness of the temporal image database system. The patient is a female diagnosed with breast cancer that has spread to her chest. The horizontal axis marks the periods of the five spiral CT scans taken of her. Below the horizontal axis we drew two lines to denote the different treatment plan intervals. You can see that total nodule number tripled during the early drug treatment procedures. This triggered a treatment protocol change to a combination of radiation therapy and chemotherapy, which proved effective. The total volume of the cancer reduces by a factor of five from its peak value in March 1995. The system also lets physicians track the progression of individual nodules over time.[16]

Collaborative image consultation

Referring physicians and imaging specialists such as radiologists, pathologists, and cardiologists often communicate their findings to each other and consult regarding diagnoses, further studies, and treatment plans.

Hypothesis. We can integrate communication and visualization tools with image databases to enable collaborative consultation among radiologists and referring physicians at various sites, resulting in better health care delivery.

Conventional approach. A physician orders an imaging procedure. Four to 24 hours later, a radiologist—if in the same hospital—issues the diagnostic report; otherwise, the set of screen films must be sent to an outside image consultation group for review. The referring physicians sometimes call or walk to the local radiology department for immediate interpretation or follow-up questions. This is time-consuming and disrupts their work schedule.

Meanwhile, the medical imaging market is moving toward teleradiology, that is, connecting peripheral imaging centers to a major radiology consultation center. This delivers the best possible radiology service to patients: The peripheral imaging centers provide a convenient, local examination site, and specialists provide the necessary expert care by remote diagnosis.

Teleradiology also serves remote and rural areas where radiologists are scarce. Currently, a radiologist contracts to review images from various rural clinics within a certain radius, sometimes traveling among these centers to read cases. A rural patient may wait days for a radiologist to review the examination. Teleradiology permits rural clinics to transmit images to a metropolitan medical center for diagnosis and thus speeds up the reading turnaround time. US military bases use this application. Most current teleradiology systems, however, operate in store-and-forward mode and lack real-time

Figure 5. The functional architecture of our collaborative image consultation system based on the existing storage and communication infrastructure of UCSF's HI-PACS.

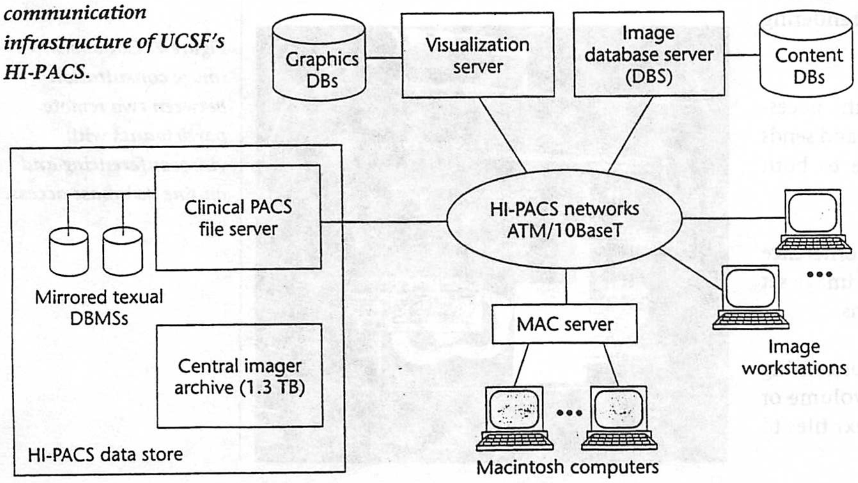

image consultation support and access to other relevant images and databases.

Networked multimedia approach. We have been experimenting with a collaborative image consultation system that enhances the UCSF PACS with 3D visualization and database management capabilities for high-resolution medical images.[17] These can provide resolutions as high as 4 Kbytes × 4 Kbytes per slice for images such as mammograms.

Figure 5 shows this collaborative consultation system's architecture and components. The PACS image archive and mirrored text database appear at left; the computation and 3D rendering node is shown at the top, connected to the HI-PACS networks with ATM and with 10BaseT as backup. The Macintosh server connects physicians' office Macs to PACS, and the Unix-based image workstations provide clinical access.[11]

Now suppose that a referring physician at an image workstation requests a videoconference on a patient image case with a radiologist located elsewhere. Figure 6 shows the data flow, which follows these steps:

1. Establish a videoconference between two image workstations.
2. From an image workstation, the referring physician queries the IDBS to view a particular patient case in 3D space.
3. IDBS identifies the patient case in PACS and asks the PACS server to transmit the data to the visualization server.
4. IDBS issues a command to the visualization server to perform the appropriate rendering tasks once it receives the data.
5. The visualization server performs the necessary computation and 3D rendering and sends the results back in near-real time to both image workstations.
6. The results permit a real-time videoconference concerning the 3D high-resolution image set and related data at both workstations.

The IDBS also provides information concerning image content (for example, nodule volume or phalange length) and other clinical text files to augment the consultation.

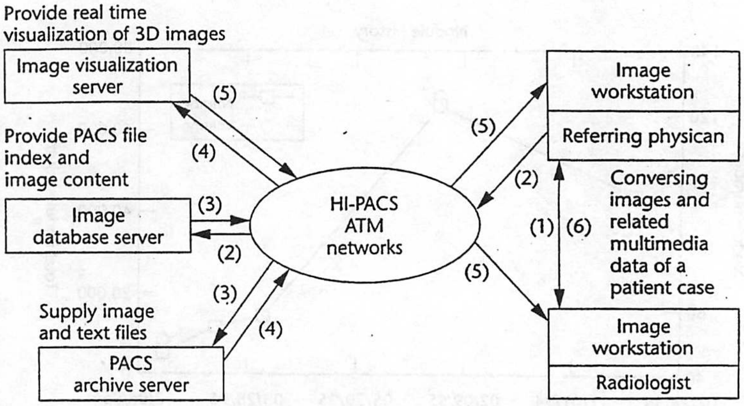
Provide real time visualization of 3D images
Image visualization server
(5)
Provide PACS file index and image content
(4)
Image database server
(3)
(2)
HI-PACS ATM networks
(3)
Supply image and text files
(4)
PACS archive server
(5)
Image workstation
Referring physican
(2)
(1) (6)
Conversing images and related multimedia data of a patient case
(5)
Image workstation
Radiologist

Figure 6. This scenario shows data flow for a collaborative image consultation.

Figure 7 shows a snapshot of the image consultation workstation prototype involving two participants discussing a chest imaging case (upper left corner). The videoconferencing software is based on Silicon Graphics' In-Person package. It integrates access to an image database server (the rightmost window) and a visualization server on an SGI Onyx computer with multiple Reality Engine boards. Figure 8 (next page) shows a volume rendering series done on an MRI brain data set and displayed at the medical workstation.

Noninvasive neurosurgical planning

Despite the advances made in anti-epileptic drugs, about 25 percent of epilepsy patients have seizures not controllable by medical treatment. Approximately half of these patients are candidates for surgical treatment. Surgery planning requires accurately identifying a localized site of seizure onset or a disconnection between epileptogenic zones so that palliative surgical procedures

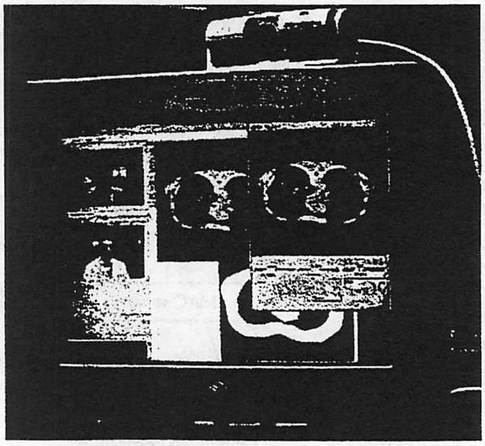

Figure 7. Collaborative image consultation between two remote participants with videoconferencing and on-line database access.

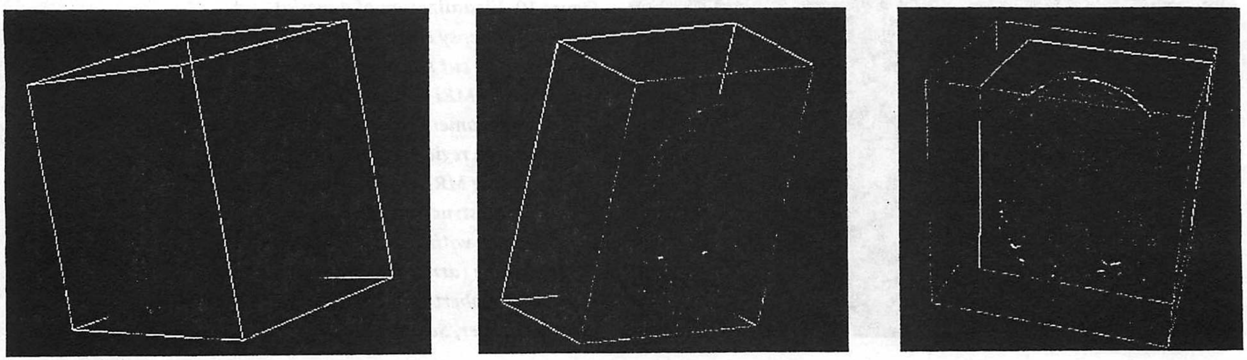

Figure 8. An example of real-time volume rendering using textual mapping techniques of an MRI data set retrieved from the PACS archive, rendered at the visualization server, and transferred to a client videoconferencing workstation through a high-speed link. The 3D rendering is built on top of Volren, a visualization package developed by Brian Cabral of Silicon Graphics.

can interrupt the seizure spread. This provides accurate noninvasive localization of epileptogenic tissue for surgical resection and resolves discordant or inconclusive imaging evaluations.

Hypothesis. Multimodal neuroimages can be fused to aid on-line noninvasive planning of epilepsy surgery.

Conventional approach. The current standard for evaluating medically refractory epilepsy surgical candidates is intracranial electroencephalography (EEG) recording. An intracranial EEG study requires invasive surgery to place electrodes that record brain electrical activity during spontaneous seizures. These electrodes remain in the patient for a week or more for seizure onset monitoring. Intracranial EEGs impose definite risks (6- to 8-percent morbidity rate) and considerable costs due to long-term hospital-based EEG monitoring.

Neuroimaging advances bring forth many new noninvasive techniques that help to lateralize the epileptogenic region with reasonable certainty. These provide useful data prior to invasive EEG recording and can eliminate or reduce the frequency of such invasive testing. These imaging studies include not only established MRI and PET but also new experimental techniques such as MR spectroscopy and magnetoencephalography (MEG). Ideally, the various preoperative localizing examinations produce concordant results that implicate a single brain region as epileptogenic. Unfortunately, these independent imaging studies give discordant or inconclusive imaging data for many patients.

Networked multimedia approach. To investigate image-assisted surgical planning, we developed a neuroimaging client workstation on top of the UCSF networked multimedia infrastructure.[18] This medical workstation provides, first, access to medical data stored in the PACS archive and the neuroimaging database and, second, registration and correlation of different brain images for noninvasive surgical planning.

The multimedia components include

- Data sources: Use MRI, PET, magnetic resonance spectroscopy, and magnetic source imaging, and diagnostic reports, patient history, surface and intracranial EEG readings, neurophysiologic data, and surgery outcome. MRI provides anatomical details; the other three modalities present functional information of glucose

Figure 9. Left: A scalp EEG recording of the patient's epileptiform spike activity recorded over the left temporal region. Middle: T2-weighted coronal MRI slice with dipole sources (yellow triangles), which correspond to EEG spikes, localized adjacent to a focal area of increased T2 in the left middle temporal gyrus. Right: Co-registered FDG-PET slice reveals focal relative hypometabolism (white arrow) in the same region of the left middle temporal gyrus. (Data courtesy of UCSF Dept. of Radiology and Northern California Comprehensive Epilepsy Center.)

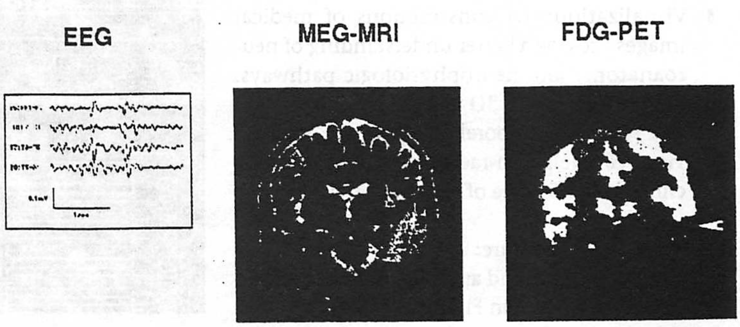

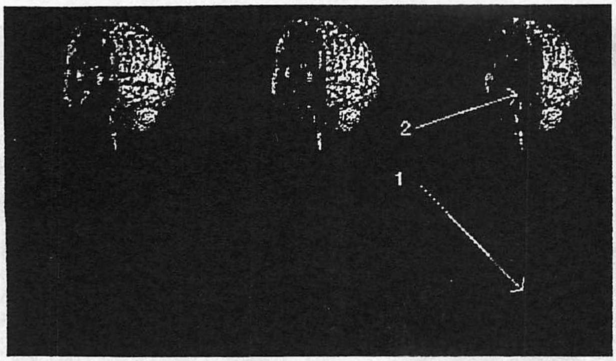

Figure 10. Visualization of a mesial temporal epilepsy case. Top: PET viewed on the cut surface of a registered 3D MRI volume. Arrow 2 indicates hypometabolism in the left temporal lobe region. Bottom: The corresponding MRI coronal slice shows subtle structural atrophy of the hippocampus within the left mesial temporal lobe (arrow 1). (Data courtesy of Robert Knowlton, Swedish Medical Center, Seattle, Wash.)

uptake, in vivo neurochemicals, and electrical spikes through dipole localization. These data come from the PACS image archive or from file transfer through hospital networks.

- Postprocessing: Develop a suite of image processing tools for 3D co-registration, image segmentation, and extraction of functional and structural information on brain regions of interest.[18] Relevant features include volumes, glucose uptakes, neurochemical spectra, and dipole locations. Segmentation of fine anatomical structures such as the hippocampus can be done interactively. Figure 9 illustrates the registration of MSI, PET, and EEG for planning an epilepsy case.

- Database management: Implement a neuroimaging database to organize PACS image indices, annotated pictures, extracted features, clinical text, and outcome data. Use IDBS to manage this neuroimaging database.

- Communication: Use the PACS network to connect the PACS archive server, IDBS, neuroimaging database, imaging scanners, neurophysiologic and outcome databases, and client workstations.

- Visualization: 3D constructions of medical images provide a better understanding of neuroanatomy and neurophysiologic pathways. Figure 10 shows a 3D view of combined MRI and PET for a temporal epilepsy case. Such 3D views can help non-radiologists appreciate the clinical significance of registration findings.

- Application software: Design an object-oriented GUI to access and analyze image fusion data (see the snapshot in Figure 11). The query can combine keywords and image features such as volume ranges and glucose activities of the hippocampus and amygdala in both brain hemispheres. The thumbnail images of patient records satisfying the constraints will display along with the textual information. The user can click the desired thumbnail to view the full-sized slice or download the entire 3D data set from PACS. The GUI also provides a 3D graphical model of the brain that lets the user generate and compose query panels dynamically, as shown in Figure 12. This provides nav-

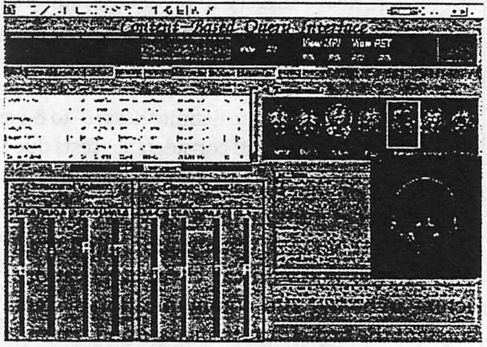

Figure 11. Multimedia GUI of the neuroimaging workstation.[17] The query uses keyword fields (upper left window) and image features relevant to epilepsy diagnosis (lower left window). The retrieved images and diagnostic report appear on the right.

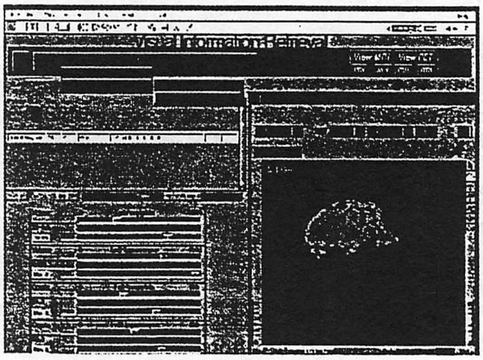

Figure 12. Visual query using a 3D digital brain atlas. The user generates the image feature query panels (bottom left) by pointing to the hippocampus and amygdala regions of the graphics model and selecting the desired features. (Brain atlas courtesy of Ellen Grant, UCSF.)

Table 2. The attributes of multimedia components involved in the four clinical applications discussed in this article.

Application	Data Type	Image Type	Image Content	Networks	Database	Graphics	Area of Care
Bone age assessment	2D image, formatted data	CR	Structural	Departmental	PACS, digital hand bone atlas, RIS, HIS	No	Pediatric diagnosis
Chest nodule analysis	3D image, plain text	CT	Structural, temporal	Departmental	PACS, chest imaging DB, RIS, HIS	No	Therapy monitoring
Collaborative image consultation	2D/3D image, video, audio, formatted data, plain text	General	Manual annotation	Hospital and regional	PACS, RIS, HIS, local databases	Yes	Care delivery
Epilepsy image fusion	3D image, 3D graphic, 2D picture, 1D signal, formatted data, plain text	MRI, PET, MRS, MSI	Structural, functional	Hospital	PACS, RIS, HIS, imaging scanners, neuroimage and outcome DBs	Yes	Surgical planning

HIS: hospital information system
RIS: radiology information system

igational access to information at different levels of anatomical abstraction.

Conclusions

Medical imaging developments have revolutionized medical practice and patient care techniques. The cross-fertilization of medical imaging and networked multimedia will open up new avenues in clinical services and improve health care delivery, education, and research.

When we build something new, however, we have to build the infrastructure to support it. Our medical imaging information infrastructure model includes multimedia data access, content management, volume visualization, high-speed connectivity, and clinical client applications. Picture archiving and communication systems represent the first efforts to manage and transmit large volumes of medical images. PACSs do not, however, transform images and add value—they simply transmit the plain image files for expert interpretation. To add value to the existing systems and make them useful for medicine in general, we must integrate medical images with other data types, process and create content, and deliver new knowledge to the end users in a cost-effective and efficient manner.

Table 2 summarizes key attributes of our networked multimedia framework for medical imaging applications.

Networked multimedia provides the ability to create valuable contents from medical images and associated data—whether anatomic, metabolic, physiologic, temporal, geometric, or spatial. It also lets us manage images by one or more content servers and makes them available electronically to physicians and researchers from a broad spectrum of biomedical disciplines, either in local hospitals or across different regions. Since medical images are complex and large, users normally extract image features after storing the images digitally. Today's large-capacity data archives (such as PACS and RIS, or Radiology Information System) and hospital-wide networks overcome many technological and administrative barriers by gathering image data for postprocessing and constructing medical content servers such as IDBS in our implementation. On the other hand, though now available, multi-megabit broadband technology for real-time (or near-real-time) and long-distance applications is still prohibitively expensive.

Health care applications tend to be problem-specific, which conventionally prompted the development of an entire new solution for each application. Once implemented, a networked multimedia infrastructure would allow sharing and optimal use of data sources and utilities within an organization, reducing development costs and cycles and improving the productivity of physicians and other health care professionals. This new field's success depends on the continuous improvement of many enabling technologies such as image and video compression, content-based image retrieval, communication protocols, volume visualization, Web-based development environments, image processing, and data security, as well as widespread clinical deployment of PACS and similar digital image management systems. **MM**

References

1. E. Krestel, ed., *Imaging Systems for Medical Diagnosis*, Siemens, Berlin, 1990.
2. F. Fluckiger, *Understanding Networked Multimedia—Applications and Technology*, Prentice Hall, New York, 1995.
3. H.K. Huang, *Picture Archiving and Communication Systems in Biomedical Imaging*, VCH Publishers, New York, 1996.
4. *Digital Imaging and Communication in Medicine (Dicom) Version 3.0*, American College of Radiologists/National Electrical Manufacturers Association, 1993.
5. *Health Level Seven (HL7), An Application Protocol for Electronic Data Exchange in Health Care Environments V. 2.1*, Health Level Seven, Ann Arbor, Mich., 1991.
6. J.K. Udupa and G.T. Herman, eds., *3D Imaging in Medicine*, CRC Press, Boca Raton, Fla., 1991.
7. S.T.C. Wong, "A Cryptologic-Based Trust Center for Authenticating Medical Images," *J. American Medical Informatics Assoc.*, Vol. 3, No. 6, Nov./Dec. 1996, pp. 410-421.
8. S.T.C. Wong et al., "Radiologic Image Compression—A Review," *Proc. IEEE*, Vol. 83, No. 2, Feb. 1995, pp. 194-219.
9. C.A. Ellis, S.J. Giggs, and G.L. Rein, "Groupware: Some Issues and Experiences," *Comm. ACM*, Vol. 34, No. 1, Jan. 1991, pp. 38-58.
10. S.T.C. Wong et al., "Interactive Query and Visualization of Medical Image Data on the World Wide Web," *Proc. SPIE*, Vol. 2707, Feb. 1996, pp. 390-401.
11. S.T.C. Wong and H.K. Huang, "A Hospital Integrated Framework for Multimodality Image Base Management," *IEEE Trans. Systems, Man, and Cybernautics*, Vol. 26, No. 4, July 1996, pp. 455-469.
12. S.T.C. Wong and H.K. Huang, "Design Methods and Architecture Issues of Integrated Medical Image Database Systems," *Comp. Med. Imaging and Graphics*, Vol. 20, No. 4, July/Aug. 1996, pp. 285-300.
13. W.W. Greulich and S.I. Pyle, *Radiographic Atlas of Skeletal Development of the Hand and Wrist*, Stanford University Press, Stanford, Calif., 1959.
14. E. Pietka et al., "Feature Extraction in Carpal Bone Analysis," *IEEE Trans. Med. Imaging*, Vol. 12, 1993, pp. 44-49.
15. W.A. Kalender, A Polacin, and C. Suss, "A Comparison of Conventional and Spiral CT: An Experimental Study on the Detection of Spherical Lesions, *J. Computer Assisted Tomography*, Vol. 18, No. 2, 1994, pp. 167-176.
16. X. Zhu et al., "Quantitative Image Measurements for Outcome Analysis of Lung Nodule Treatment," *Proc. SPIE*, Vol. 2709, Feb. 1996, pp. 480-488.
17. S.T.C. Wong, K.S. Hoo, and H.K. Huang, "Empower PACS with Content-Based Queries and 3D Image Visualization," *Proc. SPIE*, Vol. 2711, Feb. 1996, pp. 569-579.
18. S.T.C. Wong et al., "Multimodal Image Fusion for Noninvasive Epilepsy Surgery Planning," *IEEE Computer Graphics and Applications*, Vol. 16, No. 1, Jan. 1996, pp. 30-38.

Stephen T.C. Wong is a senior technical staff member of Philips Research Palo Alto and a faculty member in radiology, neurology, bioengineering, and medical informatics at the University of California, San Francisco. He is a licensed professional electrical engineer. His research interests include multimedia systems and medical informatics. Wong received a BE with honors in electrical engineering from the University of Western Australia in 1983 and an MS and a PhD in computer science from Lehigh University in 1989 and 1991, respectively.

H.K. Huang is a professor and vice chairman of the Department of Radiology and the director of the Radiological Informatics Laboratory at UCSF; he holds a joint appointment in the UCSF/UC-Berkeley Bioengineering Graduate Program. Huang implemented a PACS at UCLA in 1991 and a second-generation PACS at UCSF in 1994. His current research interests include medical multimedia, high-speed medical image transmission, and image content indexing and retrieval.

Contact Wong at the Department of Radiology, Univ. of California, San Francisco, 530 Parnassus Ave., Room CL-158, San Francisco, CA 94143-0628, e-mail swong@lni.ucsf.edu.

The Perception of Visual Information, Ed.
William R. Hendee, Peter N.T. Wells,
Springer, 2nd edition. 1997

11

Architecture and Ergonomics of Imaging Workstations

Paul S. Cho and H.K. Huang

11.1 Architecture of Imaging Workstation

Display workstations transform the binary representation of an image to visual signals and thus serve as the link between invisible pixels and the eye. The bit pattern stored in computer memory is converted to video signals, which in turn stimulate the light-emitting phosphors on the display screen. Therefore, what the eyes see is ultimately dictated by the display system's ability to faithfully reproduce the original image. Unless it becomes possible to transfer visual information directly from computer memory to the visual cortex, this mode of signal transfer which relies on light photons will remain vital to image presentation.

An imaging workstation consists of three major components: image processing hardware, display monitor, and storage device. The image processing hardware generates and transforms pixel data for their visualization on the display monitor. Different types of storage devices are used to meet the high-capacity, high-performance requirements of imaging applications. These include image memory, magnetic disk drives, and optical disks.

11.1.1 Image Processing Hardware

a. Special-Purpose Image Processing Hardware

For high resolution, high speed image processing and display applications, special-purpose image processing hardware is required. The image processors may be board-level units that plug directly into the computer's general-purpose bus, or they may be chassis-level products that communicate with the computer via a bus adapter. A typical image processing system consists of an image memory (or frame buffer), a pixel processor, and a video output processor (Fig. 11.1). These components usually share a common image transfer bus to realize high speed transfer of data.

To store images, either a part of the CPU memory or a separate image memory can be used. Ideally, the image memory should be addressable in linear, two-dimensional, or three-dimensional modes to eliminate address-calculation overhead otherwise necessary for pixel and voxel data access. The pixel processor performs arithmetic operations on the data copied from the image memory. These operations include point functions such as image addition, subtraction, and

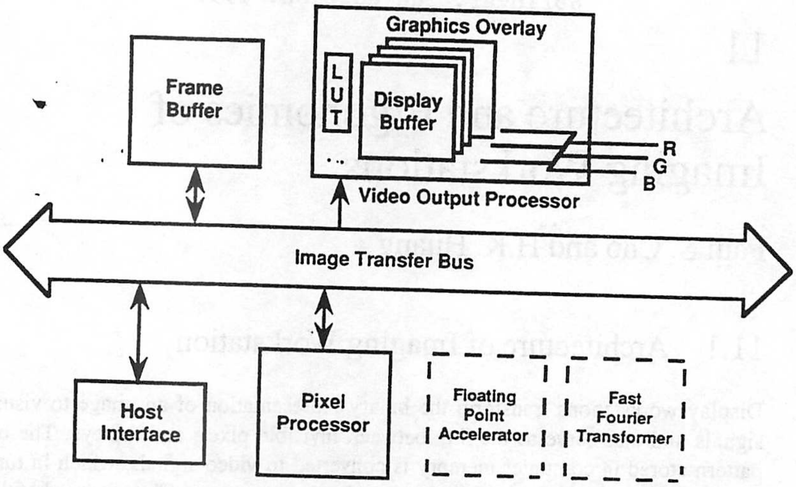

FIGURE 11.1. A simplified hardware configuration of a typical image processing system controlled by a host computer.

merge; geometric functions such as magnification; statistical functions such as histograms; and transformation functions such as lookup table operations. Often, optional hardware components are available to speed up the image processing computation. These components may include a floating-point accelerator, fast Fourier transform coprocessor, and spatial convolver. The video output processor normally contains three channels of image output to provide either one 24-bit full-color image or three 8-bit gray-scale images. In addition to providing the image channels, a well-designed system also supplies an alpha channel for graphics overlay.

b. General-Purpose Hardware Platform

The idea of adding special-purpose imaging hardware to an existing computer is one approach to an imaging workstation, but it has some serious limitations. For instance, the lack of a universal device driver requires the user to learn a new library of subroutines for each new image processing hardware configured. Also, the programmer must become familiar with the way the host-computer's operating system interacts with these special-purpose devices. This use of multiple software can significantly delay the development of application software. In addition, the application software is likely to have a short life span because of its device-dependent nature.

With recent advances in CPU speed, memory size, and the ability of built-in graphics devices to handle large amounts of pixel data, it is possible to design an upper-performance imaging workstation around a standard hardware platform. Application programs are written using the standard software tools such as the X-window library.[11.1–11.2] The X-window has gained popularity because of its portability from one computer hardware to another. It is designed as a network communications protocol and therefore permits network-transparent image transfer and display. This is a powerful concept which has helped usher in the present Internet revolution.

11.1.2 *Display Monitor*

The video output processor generates picture signals which are used to drive a display device. Today, the display monitor using the cathode ray tube (CRT) is still the predominant display device because its overall image quality is superior to other types of display devices such as liquid crystal screens, light valves, and flat-panel displays. Since the image quality of the visualized data can affect the interpretation of the data, CRT display monitors play a crucial role in the formation of visual information. Characteristics of the video display monitor that affect visual quality include scanning technique, resolution, phosphor characteristics, luminance-contrast, color display, and geometric distortion.

a. Scanning Technique

Early vector graphic CRT systems used a random scanning technique in which the electron beam is moved randomly to draw lines. In this method, only the endpoint coordinates of the line segments had to be stored. In the days when computer memory was expensive and slow, this method proved expedient although it was unable to display complex objects.

The emergence of image processing technology in which the data are represented as a rectangular array of pixels has required a raster-scan CRT display. In the raster scanning method the electron beam scans the CRT screen in a fixed pattern of closely spaced parallel lines. These lines are usually horizontal and scanned in succession from the top to the bottom of the screen. The beam current is varied either as "on-off" or continuously to produce a black-white or gray-scale picture, respectively. There are two modes of scanning: interlaced and progressive. In interlace scanning, a complete frame is displayed in two steps. For example, in the American standard the even lines are painted (1/60), then the odd lines fill the gaps (1/60) to comprise a complete picture frame in 1/30. The most common interlaced scanning standards are the American standard of 525 lines at 30 interlaced frames per second and the European standard of 625 lines at 25 interlaced frames per second. It is generally assumed that a 25 to 30 Hz interlaced refresh rate is sufficient to produce a picture without causing the sensation of brightness variation or flicker. Although this assumption may be valid for commercial TV standards, higher refresh rates are often required for imaging workstation applications. In the progressive scan, the entire image is painted continuously from left to right and top to bottom. For this type of scan the trend is to use a monitor that is operating between 60 and 72 frames per second (Hz). It is commonly accepted that in order to eliminate flicker, a 72 Hz progressive scan should be used in medical imaging applications.

b. Phosphor

A visible light image from the monitor screen is produced by the phenomenon of *cathodo-luminescence* in which high energy electrons excite phosphors deposited on the screen plate. As the excited electrons in the phosphor return to the ground state, light is emitted whose intensity is proportional to the electron beam current. Over 50 different types of phosphor are available as listed in the P number register regulated by the U.S. Electronic Industries Association. Crystalline materials most commonly used as phosphors are based on zinc sulphide, although rare earth activated oxides and oxisulphides have been increasingly used. The important factors to consider in selecting phosphors are energy conversion efficiency, decay time, color, and longevity. A large number of phosphors can convert 10% to 20% of electron beam energy into light. These efficiencies are remarkably high, an order of a magnitude above those used in other types of display devices. This is one reason for the continued predominance of CRT technology.

Phosphor decay times may vary from less than a microsecond to a few seconds. Phosphors with longer persistence can be used to reduce flicker by allowing significant integration of temporal variations in luminance. This works well for stationary images but causes smearing in dynamic images. Phosphors of almost any emission color may be selected from the visible light spectrum. The conversion efficiency degrades with the amount of excitation. Most phosphors have a practical lifetime of several thousand hours. To prolong phosphor longevity, the screen-saver feature is often enabled in workstations, in which the electron beam is automatically shut off after a certain period of inactivity.

The selection criteria for the phosphor depend on the imaging applications and involve the following considerations (see Table 11.1).

1. Phosphor steady-state color (color of phosphor during excitation should appear with a slight blue tint to resemble the hue of the radiograph). The C.I.E.[Commission Internationale de l'Eclairage (International Commission on Illumination)] chromaticity diagram can be used to find the relative percentage of the primary colors presented in a given color.

2. Phosphors with fluorescence decay times that are shorter than the field refresh rate of an interlacing scan (16.7 ms), or the frame refresh rate of a progressive scan (33.3 ms), will contribute an annoying flicker effect to the static image. To minimize this flicker fluorescence decay times chosen for the phosphor should be longer than the scanning refresh rate.

3. Light output efficiency provides a scale of efficiency for a given input beam current. A phosphor with a low efficiency (relative to P4) needs a larger beam current to produce the same light intensity. As a result, it reduces the life expectancy of the monitor.

TABLE 11.1. Specifications of three popular phosphors used in display monitors.

Phosphor	Primary	color	percent	Decay time	Efficiency
	(Red	Green	Blue)	(milliseconds)	(relative to P4)
P4	27	30	43	.100	1.00
P40	26	33	41	>100.000	0.76
P164	27	29	44	>100.000	0.60

c. Resolution

The display screen contains a layer of phosphor grains $10\mu m$ or less in size. The pixel size is limited by the spot size of the electron beam. The spot has a Gaussian-like current distribution over a cross-sectional area. It is usually defined as the width between points where the beam current has dropped to a certain fraction such as $1/e$ (about 37%) of its maximum value. The beam spot diameter increases as the square root of the beam current. The minimum diameter to which the spot size can be reduced is dictated by the beam current required to produce an acceptable phosphor brightness. Therefore, there is a tradeoff between resolution and image brightness.[11.3]

The resolution of a display monitor is most commonly specified in terms of the number of scan lines. For example, the term "1k monitor" means that the monitor has 1024 raster lines. In the strict sense of the definition, however, it is not sufficient to specify spatial resolution simply in terms of raster lines because the actual resolving power of the monitor may be less. Consider a digitally generated line pair pattern (black and white lines in pairs). The maximum displayable number of these line pairs on a 1k monitor is 512. However, the monitor may not be able to resolve 1024 alternating black and white lines in the vertical direction if the electron beam spot is out of focus or the contrast/brightness is set too high, causing the adjacent raster lines to overlap. Horizontal resolution has no relation to the number of raster lines; rather, it is limited by the beam spot size and dependent on how quickly the beam current changes according to the driving video signals.

There are several techniques for measuring spatial resolution. The simplest and most commonly used method used a test pattern which consists of varying widths of line pair objects in both vertical, horizontal, and sometimes radial directions. It should be noted that this visual approach measures the resolution of the total display-perception system, including the visual acuity of the observer, and therefore is prone to subjective variations.

Other techniques include the shrinking raster test, the scanning spot photometer, the slit analyzer, and the measurement of the modulation transfer function (MTF).[11.4] Another noteworthy fact is that resolution is a function of the location of the electron beam on the screen. In general, the defocusing effect increases as the beam moves away from the center of the screen. Therefore, resolution specifications must be accompanied by data concerning the location on the screen where the measurement was taken as well as the luminance of the screen.

d. Luminance and Contrast

Luminance measures the brightness in candelas per square meter (cd/m^2) or in foot-lamberts (ft L; 1ft L = 3.426cd/m^2). The concept of luminance applies when the luminous source cannot be treated as a point source, i.e., it has a finite area. Luminance of the display monitor is a function of the electron beam current and the conversion efficiency of the phosphor.

There are various definitions for contrast and contrast ratio. Contrast is most often defined as a ratio: the difference between two luminances divided by one of the two luminances, usually the larger. Thus

$$C = (L_s - L_0)/L_s$$

or

$$C = (L_0 - L_s)/L_0,$$

where L_0 is the luminance of the object and L_s is the luminance of the background. The contrast ratio C_r is frequently defined as the ratio of the luminance of an object to that of the background. This is expressed by

$$C_r = L_{\max}/L_{\min},$$

where $L_{\max}$ is the luminance emitted by the area of greatest intensity and $L_{\min}$ is the luminance emitted by the area of least intensity.

Because of the particulate nature of the phosphor and its optical transparency, the screen acts as a high efficiency reflector such that 25% to 75% of the incident light is scattered back. The light emitted from the phosphor is viewed against this reflected light. The contrast ratio, therefore, depends on both the luminance of the CRT image and the intensity of the ambient light. For instance, in bright sunlight the display surface can have an apparent luminance of 3×10^4cd/m^2. To achieve a contrast of 10, the luminance of the cathodo-luminescence must be 3×10^5cd/m^2, which is extremely high even for a high efficiency phosphor.

Since perceived contrast depends on the human observer, the psychophysical parameter called just-noticeable-difference (JND) is sometimes used to characterize a CRT. JND is the smallest luminance difference that can be perceived by the human observer in the presence of noise caused by temporal fluctuations in luminance output and nonuniformity in the CRT phospor layer. Other sources of noise are found in the observer's visual system, such as the random firings of neurons.[11.5]

e. Color CRT

The oldest and still most widely used design of a color CRT is the shadow mask. It consists of three electron guns, a shadow mask with circular holes, and a phosphor

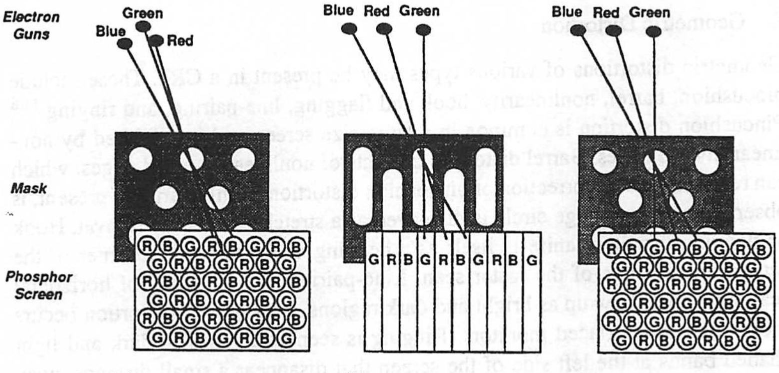

(a) (b) (c)

FIGURE 11.2. (a) Delta gun with circular hole mask. (b) In-line gun with slotted mask. (c) In-line gun with circular hole mask.

screen. The phosphor screen has arrays of "triads," where each triad consists of the phosphors of the three primary emission colors, namely, red, green, and blue. The guns are positioned in a triangular or delta form and therefore are referred to as the delta gun. The geometrical relationship of the gun, shadow mask, and screen is such that the beam from each gun strikes only one type of the phosphor in the triad. The other two types of phosphor are masked from the gun by the shadow mask. The beams are made larger than the holes so that the beam completely fills the hole to transfer maximum energy to the phosphor. Three guns can independently modulate the beam current to produce the desired color mixture for each triad [Fig. 11.2(a)].

In recent years the design of the shadow mask and guns has improved to meet the increasing demands of the high brightness, high resolution market in such applications as large-scale PC board design, detailed CAD/CAM, and computer graphics. The current trend is to place guns in line to achieve better tracking of the beam, thus improving the hit rate of the proper color phosphor. The shadow mask may be either slotted [Fig. 11.2(b)] or circular [Fig. 11.2(c)], with color triads laid down as vertical stripes or as circular dots, respectively.

A classic problem in shadow mask technology is associated with the significant dissipation of electron beam energy by the shadow mask. Apart from the loss of luminance, the absorbed energy can cause local thermal expansion which may result in color distortion by dealigning the geometry between the shadow mask and the phosphor screen. This has led to the development of flat pretensioned shadow masks in conjunction with flat screens as described by Dietch, et al.[11.6]

Advancements in spot shaping and focusing techniques as well as video amplifier technology have enabled the recent development of a large screen (20-inch square), high resolution (2048 × 2048) color CRT which operates at 60 Hz noninterlaced refresh rate. The spot size is 0.5 mm at the center and 0.6 mm at the corner.[11.7]

f. Geometric Distortion

Geometric distortions of various types may be present in a CRT. These include pincushion, barrel, nonlinearity, hook and flagging, line-pairing, and ringing.[11.8] Pincushion distortion is common in a large-size screen and is exhibited by nonlinear inward edges. Barrel distortion consists of nonlinear outward edges, which can result from overcorrection of pincushion distortion. Nonlinearity, if present, is observable when a large circle is displayed as a stretched or flattened oval. Hook or flagging usually manifests itself as a bending of the upper-left corner of the screen on the edge of the raster scan. Line-pairing is a bunching of horizontal scan lines that show up as bright and dark regions. This type of distortion occurs most often in interlaced monitors. Ringing is seen as a series of dark and light shaded bands at the left side of the screen that disappear a small distance away from the edge. Geometric distortion on a monitor may occur from time to time. Calibration during preventive maintenance with a standard phantom such as an SMPTE pattern[11.9] should be performed to detect distortion.

11.1.3 Image Storage Devices

Stringent requirements are placed on the storage device in imaging applications. The sheer volume of data calls for a large capacity in excess of the gigabyte range, and increasing demands for image processing and graphics at interactive speeds, require a very high throughput capacity. There are two categories of image storage. One type is random access memory (RAM), which is directly connected to the image processor or the computer system bus. This type of image storage has a very fast input/output rate but is volatile and expensive. The second type of storage is slower, permanent, and less expensive. Today, high capacity magnetic disk drives dominate the primary storage arena while optical disks are widely used for secondary storage.

a. Random Access Memory

Random access memory is used as a buffer in an imaging workstation. Typically, workstations are configured with 32 to 256 megabytes of RAM. One 2k × 2k × 8-bit image takes up four megabytes of memory. The RAM is used as a buffer in the sense that a set of images is first loaded from disk storage into the RAM. From there, one image at a time is transferred to the video random access memory (VRAM). The VRAM has higher input/output rates than the RAM and is connected to the display monitor through a fast digital-to-analog (D/A) converter. This architecture allows an image to be displayed rapidly on the video monitor.

b. Magnetic Disk Drives

The storage capacity of magnetic hard disk drives has increased dramatically in recent years. For example, the capacity of the 5.25-inch drive, which was first introduced in 1980 (Seagate ST 506), increased from its initial five megabytes to 800 megabytes in 1990 and to 9,000 megabytes (or 9 gigabytes) in 1995.

Currently, the speed of data transfer is dictated by the disk-to-computer interface. The disk drive reads out bit information faster than the interface can accept it. In applications where display speed becomes critical, a parallel transfer disk (PTD) or disk array is used to overcome this limitation. The PTD allows multiple read/write heads to transfer data simultaneously. The disk array, on the other hand, configures multiple conventional disks in parallel. This scheme is often referred to as RAID (redundant array of independent disks). Two common approaches for the disk array are software striping and hardware paralleling. In software striping, the disks are connected to the system bus through traditional controllers. Blocks of data are segmented and moved to and from the disk drives in parallel. Data segmentation and recombination are handled by the software. In the hardware approach, a parallel drive array controller simultaneously manages multiple disk drives.

The useful life cycle of parallel architecture may be nearing an end as the new generation of fast disk-to-computer interfaces emerges. These are Ultra SCSI (small computer system interface), Fiber Channel, and SSA (serial storage architecture) interfaces, all of which exceed the disk drive performance.[11.10]

c. Optical Disk Drives

Optical disks provide a convenient means for storing and archiving a large volume of data. Unlike magnetic tape, which requires sequential data access, the optical disk allows random access of recorded data. There are two types of optical disks: WORM (write once, read many) optical disks and erasable MO (magneto-optical) disks. These disks are available in different sizes: 3.5-inch (WORM and MO), 5.25-inch (WORM and MO), 12-inch (WORM), and 14-inch (WORM), ranging in capacity from 180 megabytes to 10 gigabytes. In addition, the capacity of online storage can be increased to the terabyte range by configuring optical disk jukeboxes.

11.2 Examples of Imaging Workstation

Today, imaging workstations are used in many different fields, including medicine, engineering, scientific visualization, defense, and entertainment. A wide range of specifications are seen. The spatial resolution requirements range from 1k to 3k and the pixel representation can be monochrome, gray scale, or color. The number of configurable monitors is generally limited by the available hardware address space and physical bus slots for video output boards. The examples of imaging workstations presented here are from radiological applications.

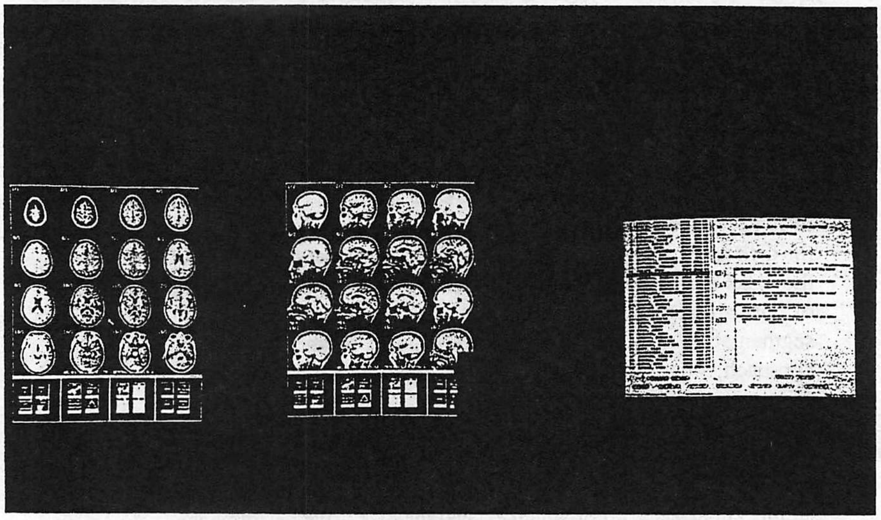

FIGURE 11.3. A dual-monitor 2k imaging workstation showing two sets of MR neuro images. The separate text monitor shows patient directory and study list. Image processing functions are controlled by the icons located at the bottom of the 2k screens and the external dials.

11.2.1 Diagnostic Workstation

The first workstation example is the diagnostic workstation used by radiologists for making primary diagnoses.[11.11–11.12] Components in this type of workstation should be of highest quality. If the workstation is used for displaying projection radiographs, then a number of 2k monitors are needed; if used for CT and MR images, multiple 1k monitors are sufficient. The diagnostic workstation requires a rapid (about 1 to 2 seconds) image display time and a digital dictating phone to report findings. The workstation provides software to append the reports with the images. Figure 11.3 shows a dual-monitor 2k imaging workstation at the University of California, San Francisco (UCSF). This 2k station is based on the SUN SPARCserver 470 computer and two 21-inch diagonal 2k portrait-mode monitors (UHR-4820P MegaScan display system, E-Systems, Littleton, MA). Each 2k station has a parallel transfer disk with 5.2 gigabytes of formatted storage which can display a 2k × 2k × 12-bit image in 1.5 seconds (Storage Concepts, Irvine, CA).

11.2.2 Review Workstation

Review workstations are used by radiologists and referring physicians to review cases in the hospital wards.[11.13–11.14] The transcribed report should be available with the corresponding images. The review workstation does not require 2k mon-

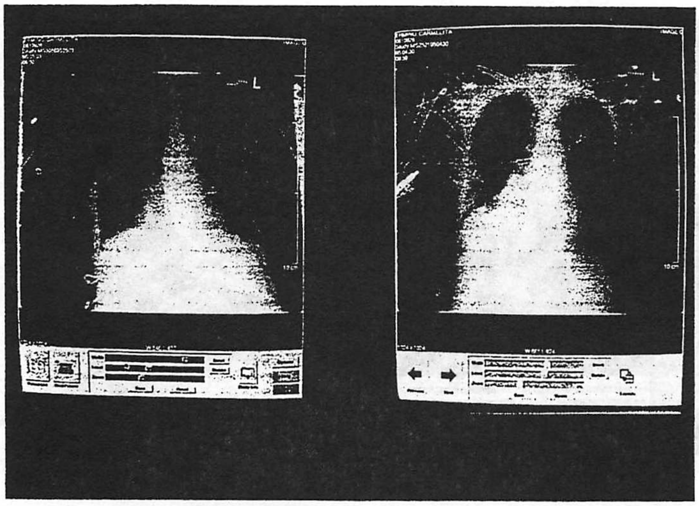

FIGURE 11.4. A dual-monitor 1k (1,600-line) imaging workstation for intensive care units showing two images. The left-hand monitor shows the current image, and the right monitor is used to show previous images by clicking the two lower-left icons (Previous and Next). Image processing functions are controlled by the icons located at the bottom of each screen.

itors because referring physicians are not looking for minute detail. Figure 11.4 shows a dual-monitor 1k (1,600-line) review workstation used at the ICUs (intensive care units) at UCSF. This workstation consists of a SUN SPARC 20 workstation with 2 gigabytes of disk storage, two GXTurbo video display boards and two 1,600 × 1,024 display monitors.

11.2.3 Analysis Workstation

Analysis workstations differ from diagnostic and review workstations in the sense that they are used to extract useful parameters from images. Some parameters are easy to extract from a simple region of interest (ROI) operation. Others such as blood flow measurements from DSA and three-dimensional reconstructions from sequential CT images, are computationally intensive. These operations require an analysis workstation with a more powerful image processor and high performance software. Figure 11.5 shows an analysis workstation, Onyx, developed at Silicon Graphics (Mountain View, CA).

11.2.4 Digitizing and Printing Workstation

Digitizing and printing workstations are designed for radiology department technologists or film librarians to digitize historical films and films from outside the department. The workstation is also used to convert softcopy images to hardcopy.

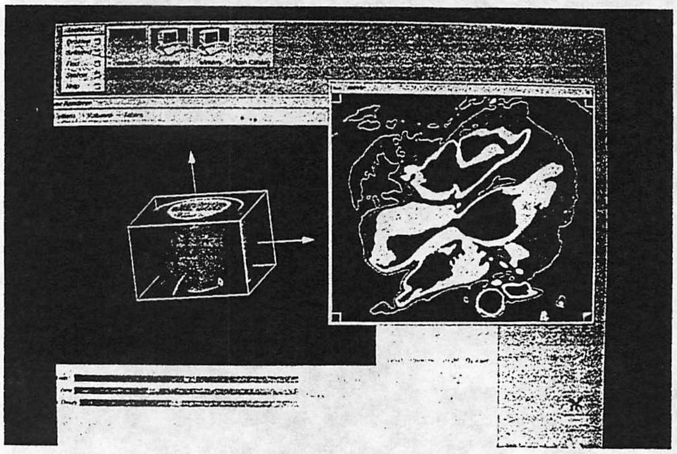

FIGURE 11.5. An analysis workstation (Onyx) at UCSF showing a three-dimensional rendering of a CT examination of a child, on the left, and a simulated blood flow (dark gray) in the four chambers of the heart, on the right. (Courtesy of Silicon Graphics Computer Systems, Mountain View, CA., S. Wong and E. Grant.)

In addition to the standard workstation components, this workstation also requires a laser film scanner, a laser film imager, and a paper printer. The paper printer is used for pictorial report generation from the diagnostic, review, and editorial and research workstations. A 1k display monitor for quality control purposes would be sufficient for this type of workstation.

11.2.5 Interactive Teaching Workstation

The teaching workstation is used for interactive teaching. It emulates the role of a teaching library but has more interactive features. Figure 11.6 shows a digital mammography teaching workstation from VICOM (Fremont, CA).

11.2.6 Editorial and Research Workstation

The editorial and research workstation is used for simple data analysis as well as for generation of slides, teaching materials, and illustrated reports. Macintosh, PC, or UNIX-based workstations with imaging software are commonly used. Figure 11.7 is an example of a Macintosh-based editorial-research workstation. Ideally, the software should include both ready-to-use imaging functions and research development utilities which enable researchers to assemble new research tools in a timely fashion. The latter can be accomplished through the use of object-oriented software modules.[11.15]

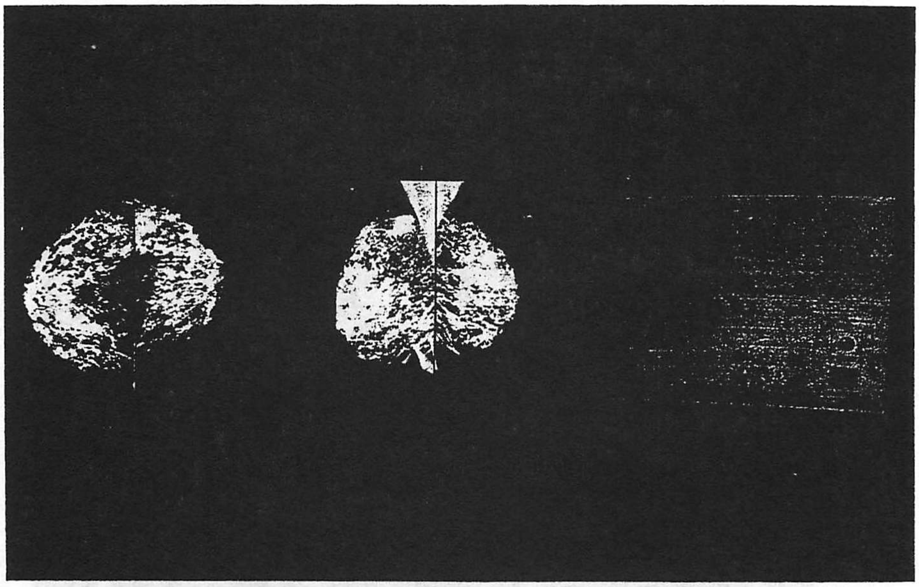

FIGURE 11.6. A 2k digital mammography teaching workstation showing four mammograms. Left: left and right craniocaudal views; Middle: left and right mediolateral oblique views; Right: text monitor with icons for image display and manipulation.

11.3 Ergonomics of Imaging Workstation

The ergonomics analysis of an imaging workstation addresses a variety of human engineering factors, including interactive devices, acoustic noise, lighting conditions, and workstation layout.[11.16] This section focuses on ergonomic issues that affect perceived image quality, including glare, ambient illuminance, user interface, and display monitor configuration.[11.17]

11.3.1 Glare

According to the study conducted by Stammerjohn, et al., glare is the most frequent complaint among workstation users.[11.18] Glare is defined as the sensation produced by luminance within the visual field that is sufficiently greater than the luminance to which the eyes are adapted that can cause annoyance, discomfort, or loss in visual performance and visibility.[11.19]

Glare can be caused by reflections of electric light sources, windows, and light-colored objects such as furniture and clothing. The magnitude of sensation of glare is a function of the size, position, and luminance of a source, the number of sources, and the luminance to which the eyes are adapted at the moment. Glare may be categorized according to its origin as either direct or reflected. Direct

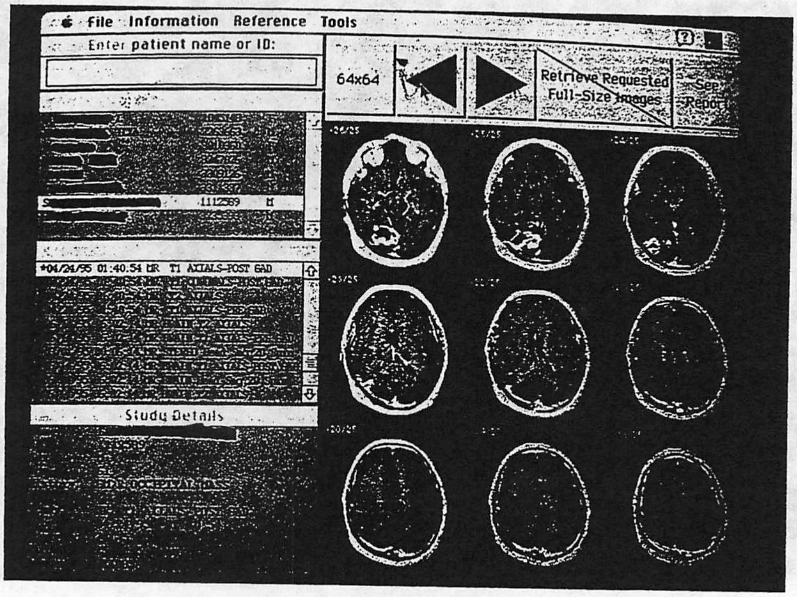
File Information Reference Tools
Enter patient name or ID:
64x64
Retrieve Requested Full-Size Images
See Report
[redacted]
1112589
*04/24/95 01:40.54 MR T1 AXIALS-POST GAD
Study Details

FIGURE 11.7. A Macintosh-based editorial-research workstation. The image window shows a set of MR T_1 images subsampled to 128 × 128 pixels. The text windows contain patient list (top), study list (middle), and demographic information of the currently selected patient (bottom).

glare may be caused by bright sources of light in the visual field of view (e.g., sunlight and light bulbs). Reflected glare is caused by light reflected from the display screen. If the reflections are diffuse, they are referred to as veiling glare.

Image reflections are both distracting and annoying because the eye is induced to focus alternately between the displayed and reflected images. Reflected glare can be reduced by increasing display contrast, wearing dark clothing, correctly positioning the screen with respect to lights, windows, and other reflective objects, and adjusting the screen angle.

Further reduction of glare can be achieved by etching the screen glass, treating the glass with antireflective coatings, or superimposing antireflection filters on the screen, such as micromesh, circular polarizers, and neutral density filters with antireflective coatings.[11.20] Etching the glass reduces reflection by scattering reflected light, thus giving a more diffuse and less conspicuous appearance of reflected objects. Since the light emitted from the display phosphors is also dispersed, image sharpness may be compromised. Coating the screen with a thin film of antireflective agent such as Lambda-4 usually does not diminish image sharpness.[11.21] The coating layer, however, can be easily and permanently smeared with fingerprints. Antireflection filters reduce perceived glare by attenuating reflected light more than the light emitted from the CRT, since the reflected light must pass through the filter twice. Morse[11.22] has evaluated some of these antireflective techniques. Objective measurements were made of luminance, modulation transfer function, contrast, and glare, as well as subjective evaluations of the brightness, sharpness, contrast, color, and glare. On average, the order of preference was: gray antireflection filter, micromesh filter, circular polarizer, blue antireflection filter, etched plastic filter, and no filter.[11.22]

11.3.2 Ambient Illuminance

An important issue related to the problem of glare is the proper illumination of the workstation area. Excessive lighting can increase the readability of paper documents but may also increase reflected glare, while dim lighting can reduce glare but make reading at the work surface difficult. Illuminance refers to the light flux incident on a unit area of surface. A common unit of illuminance is the meter-candle or lux.

Ergonomic guidelines for a traditional office environment recommend a high level of lighting of 700 lux or more.[11.23] According to a study conducted by van der Heiden, et al.,[11.24] among 38 CAD operators allowed to adjust the ambient lighting, median illumination levels were around 125 lux, with 90% of the readings falling between 15 and 505 lux. These levels are optimized for CRT viewing but certainly not for reading documents. An illuminance of 200 lux is normally considered inadequate for an office environment. Cushman recommends a reasonable compromise.[11.23] He suggests a lower range of 150 to 400 lux for tasks that do not involve information transfer from paper documents. At these levels, lighting is sufficiently subdued that good display contrast is usually obtainable. A higher range of 400 to 550 lux is suggested for tasks that require reading of paper documents. Increasing ambient lighting above 550 lux reduces display contrast appreciably. If paper documents contain small and low contrast print, 550 lux may not provide adequate lighting. In such cases, special task lighting directed only at the document surface may be recommended.

In radiology, where optimal viewing conditions are most critical, the level of ambient illuminance should be equal to the average luminance of displayed images. In addition, lighting for the viewing room containing display monitors should be lower than that in a conventional film viewing room. The luminance of the X-ray film placed on the lightbox ranges from 3 to 200 cd/m^2, while that of a display monitor varies from 0.1 to 50 cd/m^2.[11.25]

11.3.3 User Interface

The main goal of the user interface is to provide efficient tools with which the user can call up and manipulate images. This is accomplished through software switches that appear on the screen as graphic icons and menus. The mouse is widely used in today's workstations as the point-and-select input device. A well-designed user interface should provide ergonomic efficiency to a degree that the interaction becomes second nature to the user.

One design aspect of the user interface that can seriously affect image viewing is the window format. In applications where only a single image needs to be displayed, this may be straightforward, but the window design becomes complicated for applications where multiple images must be displayed. This situation is prevalent in medical imaging applications such as examination of CT/MRI slices, side-by-side comparison of projection radiographs, and movie loops of dynamic studies. The image windows can be formatted to display images in a tiled format in which all the windows are fully visible simultaneously or as stacked images which require the user to select one window to be placed on top of the stack for full, unobstructed display.[11.26]

The windows may or may not have a frame or scroll bars. If they do, they should not interfere with the task of image viewing. The width of the frame bars should be narrow and dark so that potential sources of glare and distraction are minimized.

11.3.4 Multiple Display

Depending on the size of the image set to be displayed, it may be necessary to configure multiple monitors. Comfortable viewing with a single imaging workstation is provided by tilting the monitors to form a mosaic of concave surfaces focused at the user while maintaining a viewing distance of 50 to 90 cm. For group viewing, a flat arrangement is preferred since this provides fewer restrictions for people located peripherally.[11.25]

To facilitate the visual integration of images displayed on multiple monitors, the idle space between screens should be minimized. It may be necessary to remove each CRT from its original chassis which tends to add extra width around the screen. The bare CRTs can then be spliced more closely together, and a custom face plate installed to form a multiple-display workstation.

Because the lifetime of the phosphor is a function of active use, a set of CRTs commissioned at the same time may degrade at different rates over time. Therefore, it is important to maintain equality among the monitors in terms of contrast, brightness, and dynamic range. It is a good policy to bring up a test pattern on a daily basis to ascertain that all the monitors are optically in tune. Adjustments can be made using the analog brightness-contrast controls. The brightness control adjusts the beam current and provides a means to offset brightness loss. The contrast control changes the gain of the video amplifier. A comprehensive quality control program of CRT displays is provided by Roehrig, et al.[11.26]

11.4 References

[11.1] Jones O. *Introduction to the X Window System.* Englewood Cliffs, NJ: Prentice Hall; 1989.

[11.2] Weinberg W.S., Hayrapetian A.S., Cho P.S., Valentino D.J., Taira R.K., Huang H.K. X-window based 2k display workstation. *Proc. SPIE* 1991; 1446: 35–39.

[11.3] Glasford G.N. *Fundamentals of Television Engineering.* New York: McGraw-Hill; 1974: 64–74.

[11.4] Sherr S. *Fundamentals of Display System Design.* New York: Wiley; 1970: 399–411.

[11.5] Ji T., Roehrig H., Blume H., Seeley G., Browne M. Physical and psychophysical evaluation of CRT noise performance. *Proc. SPIE* 1991; 1444: 136–150.

[11.6] Dietch L., Palac K., Chiodi W. Performance of high-resolution flat tension mask color CRTs. *SID Dig.* 1986; 322–323.

[11.7] Awata Y., Sumiya H., Shibata Y., Umemura S. A new large-screen high-resolution Trinitron color display monitor for computer graphics application. *SID Dig.* 1986; 459–462.

[11.8] Keller P.A. Cathode-ray tube displays for medical imaging, *J. Dig. Imag.* 1990; 3: 15–25.

[11.9] Lisk K.G. SMPTE test pattern for certification of medical diagnostic display devices. *Proc. SPIE* 1984; 486: 79–82.

[11.10] Mayer J.H. Revolutionizing mass storage. *SunExpert* 1995; 6: 45–50.

[11.11] Dwyer S.J., Cox G.G., Cook L.T., McMillan J.H., Templeton A.W. Experience with high resolution digital gray scale display systems. *Proc. SPIE* 1990; 1234: 132–138.

[11.12] Taira R.K., Simons M., Razavi M., Kangarloo H., Boechat M.I., Hall T., Chuang K.S., Huang H.K., Eldredge S. High resolution workstations for primary and secondary radiology readings. *Proc. SPIE* 1990: 1234: 18–25.

[11.13] Arenson R.L., Seshadri S.B., Kundel H.L., DeSimone D., Van der Voorde F., Gefter W.B., Epstein D.M., Miller W.T., Aronchick J.M., Simon M.B., Lanken P.N., Khalsa S., Brikman I., Davey M., Brisbon N. Clinical evaluation of a medical image management system for chest images. *Am. J. Roentg.* 1988; 150: 55–59.

[11.14] Cho P.S., Huang H.K., Tillisch J., Kangarloo H. Clinical evaluation of a radiologic picture archiving and communication system for a coronary care uinit. *Am. J. Roentg.* 1988; 151: 823–827.

[11.15] Ehricke H-H., Grunert T., Buck T., Kolb R., Skalj M. Medical workstations for applied imaging and graphics research. *Comp. Med. Imag.* 1994; 18: 403–411.

[11.16] Horii S.C., Horii H.N. An eclectic look at viewing station design. *Proc. SPIE Med. Imag. II* 1988; 914: 920–928.

[11.17] Horii S.C. Electronic imaging workstations: ergonomic issues and the user interface. In: *Syllabus: Special course in computers for clinical practice and education in radiology.* Radiological Society of North America; 1992: 125–134.

[11.18] Stammerjohn L.W., Smith M.J., Cohen B.G.F. Evaluation of work station design factors in VDT operations. *Hum Fact.* 1981; 23(4): 401–412.

[11.19] Kaufman J.E., ed. *IES Lighting Handbook.* (5th ed.). New York: Illuminating Engineering Society; 1972: 1-9.

[11.20] Rancourt J., Grenawalt W. Approaches to enhancing VDT viewability and methods of assessing the improvements. *Proc. SPIE* 1986; 624: 8–13.

[11.21] Grandjean E. Design of VDT workstation. In: Salvendy G., ed. *Handbook of Human Factors.* New York: Wiley; 1987: 1359–1397.

[11.22] Morse RS. Glare filter preference: influence of subjective and objective indices of glare, sharpness, brightness, contrast, and color. *Proc. Hum. Fact. Soc.* (29th Ann. Mtg.); 1985: 782–786.

[11.23] Cushman W.H. Illumination. In: Salvendy G., ed. *Handbook of Human Factors.* New York: Wiley; 1987: 670–695.

[11.24] van der Heiden G.H., Brauninger U., Grandjean E. Ergonomic studies on computer-aided design. In: Grandjean E., ed. *Ergonomics and Health in Modern Offices.* London: Taylor & Francis; 1984: 119–128.

[11.25] Arenson R.L., Charkraborty D.P., Seshadri S.B., Kundel H.L. The digital imaging workstation. *Radiology* 1990; 176: 303–315.

[11.26] Ho B.K.T., Ratib O., Horii S.C. PACS workstation design. *Comp. Med. Imag.* 1991; 15: 147–155.

[11.27] Roehrig H., Blume H., Ji T-L., Browne M. Performance tests and quality control of cathode ray tube displays. *J. Dig. Imag.* 1990; 3: 134–145.

**RSNA EJ 1 (1997): 26 pars. Online. Available HTTP:
http://ej.rsna.org/EJ_0_96/0037-97.fin/mammo.html. 18 July 1997.**

Interactive Digital Breast Imaging Teaching File

Fei Cao, Edward A. Sickles, H. K. Huang

Abstract

The authors present the University of California, San Francisco (UCSF), digital breast imaging teaching file. The teaching file is implemented on a high-resolution display station that is capable of viewing and manipulating 2K images at near real-time speed. The teaching file is also built on a sophisticated computer-aided instruction (CAI) model that simulates the management sequences used in image interpretation and work-up. Each user can be prompted to respond by making his/her own observations, assessments, and work-up decisions, as well as the marking of image abnormalities. This effectively replaces the traditional "show-and-tell" teaching file experience with an interactive, response-driven type of instruction. The display station is found to be adequate for fast display of high-resolution digital mammograms. The CAI model integrates vast quantities of image and textual data with visualization software into an interactive mammography teaching file. This digital teaching file has been used successfully at UCSF as a routine teaching tool for training radiologists in breast imaging.

Back to Contents
Send Letter

Interactive Digital Breast Imaging Teaching File

Fei Cao, PhD, Edward A. Sickles, MD, H. K. Huang, DSc

Department of Radiology, University of California, School of Medicine, San Francisco, CA 94143-0628

Author information:
F.C.(correspondence): fcao@lri.ucsf.edu, http://www.lri.ucsf.edu/~fcao, 415-502-4288, 415-502-3217 (fax)
E.A.S.: edwards@email.his.ucsf.edu, 415-885-7417, 415-885-7829 (fax)
H.K.H.: bernie_huang@radmac1.ucsf.edu, http://www.lri.ucsf.edu/bernie, 415-476-6044, 415-502-3217 (fax)

Received April 17, 1997; revision requested June 5; revision received and accepted July 7; posted July 18.

©RSNA, 1997

Index terms:

- Breast neoplasms, diagnosis
- Computers, educational aid
- Education
- Images, display

Contents

- Abstract
- Introduction
- Mammography Display Station
- Teaching File Data Collection
- Graphical User Interface (GUI) and an Online Demonstration
- Computer-aided Instruction (CAI) Model
- Clinical Application
- Summary
- Acknowledgment
- Appendix: Teaching File Script

- List of tags and keywords

- References

Introduction

Routine screening with periodic mammography has proved to be effective for early detection of breast cancer and in lowering the death rate due to this disease (1-2). Because of limited resources and facilities for providing hands-on instruction in breast imaging interpretation, there is a need to develop an alternative method to supplement or replace the current film-based teaching file method of training. A digital-based system can alleviate this shortage because a digital teaching file can be duplicated easily and disseminated widely, to be used simultaneously by many individuals at different sites for continuing medical education. This promises to improve the quality of breast imaging interpretation, and thereby facilitate mass screening with mammography and the problem-solving imaging evaluation of screening-detected abnormalities.

To our knowledge, no currently available digital mammography teaching file is fully adequate for clinical use. This is due in part to the relatively low resolution of currently affordable display monitors and to the relatively high speed required to manipulate large digital mammograms (10 Mbytes for each image). The basic requirement for the general use of a mammography display station is the ability to show an entire breast with such fine detail that tiny structures are readily visible. Furthermore, since routine mammographic interpretation involves four images of a current examination compared with four images from a previous examination, digital display workstations must be able to utilize monitors so that two or more whole-breast mammograms are displayed per monitor and can be manipulated at nearly real-time speed. There has been only limited success in applying computer-aided instruction (CAI) to mammography teaching files, in part because of difficulties in handling high-resolution images and in simulating an interactive teaching session (3). Furthermore, previous CAI models have not required the user to identify abnormalities by marking displayed images, a substantial deficiency because this represents one of the key elements in breast imaging interpretation. In addition, CAI models should be designed to allow the user to follow more than one suitable approach to working up a specific breast imaging problem for cases in which several such approaches are valid. These features should all be incorporated into a successful, clinically relevant CAI model. To serve as a useful instructional tool, a digital teaching file should also contain a large set of cases, selected and prepared by expert radiologists.

We use a high-resolution (50-micrometer spot size) laser film digitizer for mammogram digitization and a high-resolution (2,000 pixels by 2,500 lines) multimonitor display workstation for viewing digital mammograms. The quality of the digital images produced and subsequently read has been found to be adequate for clinic applications(4,5). Our CAI model specifies the sequence of questions, image display, instructions, and explanations of cases dynamically, based on user responses during the interactive teaching session. It not only gives answers to questions but also provides follow-up questions. It also requires the user to detect imaging abnormalities by pointing. With carefully structured questions, each user is prompted to respond by making his/her own observations, assessments, and work-up decisions just as if the patient were being examined at that time. This effectively replaces a "show-and tell" teaching experience with the interactive, response-driven type of instruction that currently must be taught in person. We also developed a simple teaching file script that integrates text/image data with the CAI and makes it possible for radiologists to create and modify case presentations without the aid of a computer programmer. The digital teaching file is now available to all radiology residents, fellows, staff radiologists, and visiting radiologists for continuing medical education at the University of California, San Francisco (UCSF).

Mammography Display Station

Our 2K mammography display station is sketched in Figure 1. The 2K station is based on a Sun SPARC 470 workstation (Sun Microsystems, Mountain View, Calif), two 21-inch (53.3 cm) diagonal 2K MegaScan monitors (Gatan, Pleasanton, Calif) (Fig 2), Pixar (Richmond, Calif) image processing hardware (Fig 3), and a 7-Gbyte fast storage disk (Vicom, Fremont, Calif) .

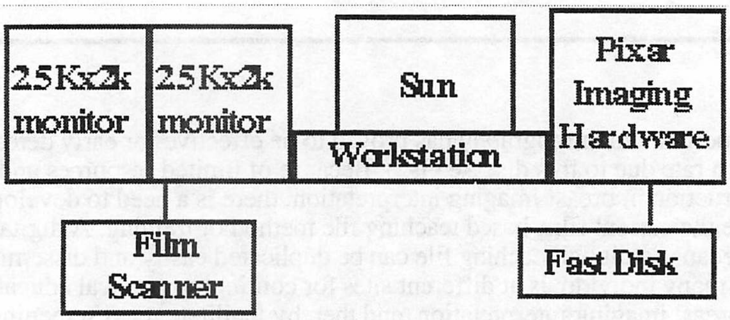

Figure 1. Configuration of mammography display station.

The Sun 470 workstation (64-Mbyte system memory) serves as a host for the display station. Each of two gray-scale monitors has 10-bit resolution and is able to display 2,560 scan lines, each with 2,048 pixels. The Pixar imaging hardware comes with two 32-Mbyte frame buffers and optimized image processing routines. The 7-Gbyte Fast-Disk subsystem is capable of storing 1,000 digital mammograms for fast retrieval by the Pixar system. A common thread in digital mammography applications is the need to deal with large amounts of data quickly. The transfer of image data between disk storage and the image computer accounts for a substantial percentage of the total time consumed during an imaging job. The principal difference between the Fast-Disk subsystem and a conventional hard disk is the high data throughput rate. The Fast-Disk subsystem achieves its speed by distributing each input/output operation over the four drives within the system. In addition to the high data transfer rate, the Fast-Disk subsystem can also operate in conjunction with the Pixar imaging system to deliver data directly to the frame buffers without a layover in the memory of the host (Sun 470). A 10-Mbyte digital mammogram takes less than 2 seconds to retrieve from the Fast-Disk and display on the 2K monitors. This makes it possible for four mammograms (<10 Mbytes each), in a typical display mode, to be easily manipulated on screen in nearly real time.

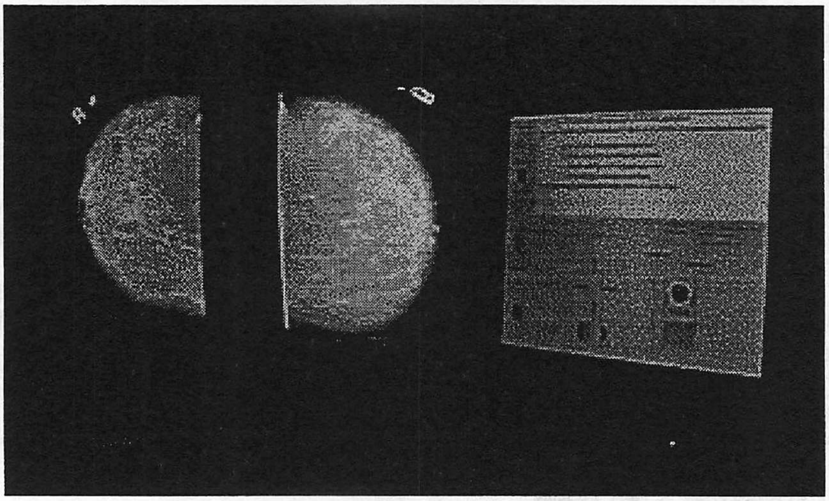

Figure 2. Two mammograms displayed on the two 2K monitors, with the user interface shown on the Sun console monitor on the right.

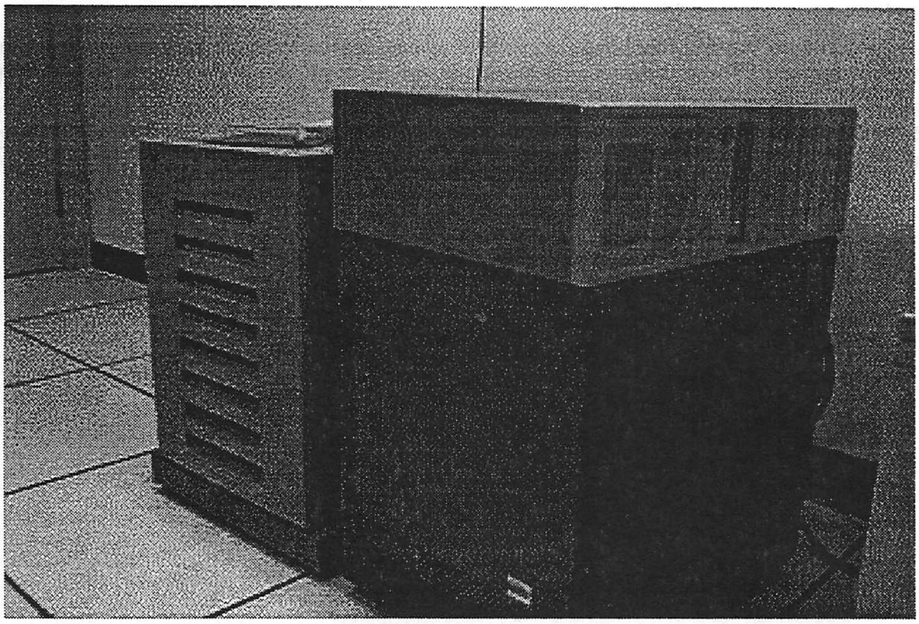

Figure 3. Sun SPARC 470 (left), Pixar imaging hardware (right), and 7-Gbyte Fast-Disk (top).

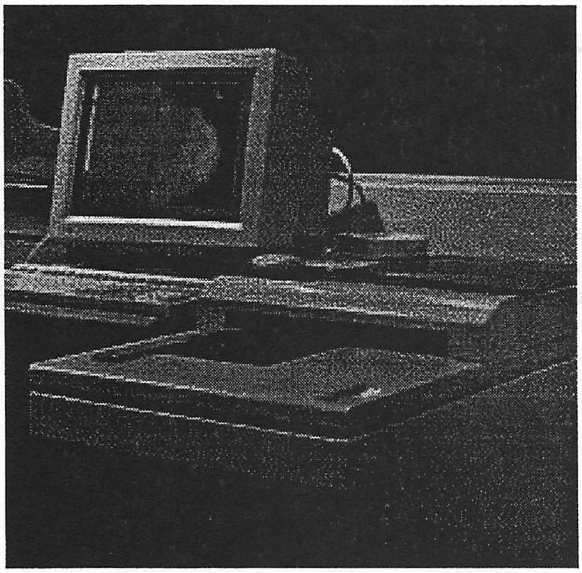

Figure 4. 5K &times; 4K laser film digitizer, specially made for mammogram digitizing by Abe Sekkei (Tokyo, Japan). On the left is a Sun console monitor displaying a digitizing user interface.

The laser film digitizer, shown in Figure 4, is provided by Abe Sekkei (6). It is a high-resolution scanner especially designed and developed for mammograms, with a 50-micrometer spot size, a 50-micrometer sampling distance, and 12-bit resolution. This scanner also has the capability of minimizing scanning artifacts due to grid lines (7,8). An 8 &times; 10-inch (20.3 &times; 25.4-cm) mammogram yields 2,500 lines &times;

Routine mammographic interpretation requires displaying four or eight images. A special display mode therefore has been developed for the digital teaching file, taking advantage of the fact that most breast images can be fitted into a narrow rectangle. Thus, we can split the 2.5K &times; 2K monitor into two 2.5K &times; 1K display areas. An example is shown in Figure 5, where the left monitor displays craniocaudal (CC) views of both breasts, and the right monitor displays mediolateral oblique (MLO) views of both breasts. A toggle button is used for alternative display of the current and previous four mammograms.

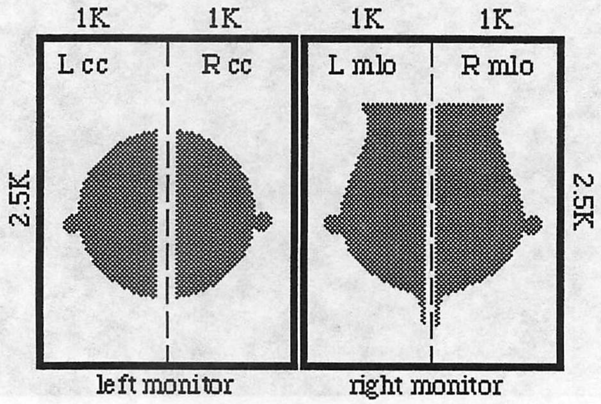

Figure 5. Display of four mammograms on the two 2K monitors. Each screen is split into two 2.5K &times; 1K regions to accommodate two mammograms.

Teaching File Data Collection

The UCSF film-based breast imaging teaching file has been in constant use since 1976 by radiology residents and fellows. The teaching file consists of over 1,000 pathologically proved cases, each of which begins with a screen-film mammography examination no more than 7 years old. The case material demonstrate the various problem-solving imaging approaches available in reaching accurate imaging diagnoses. One thousand cases from this teaching file have been selected by Dr Sickles and his staff for conversion to digital images.

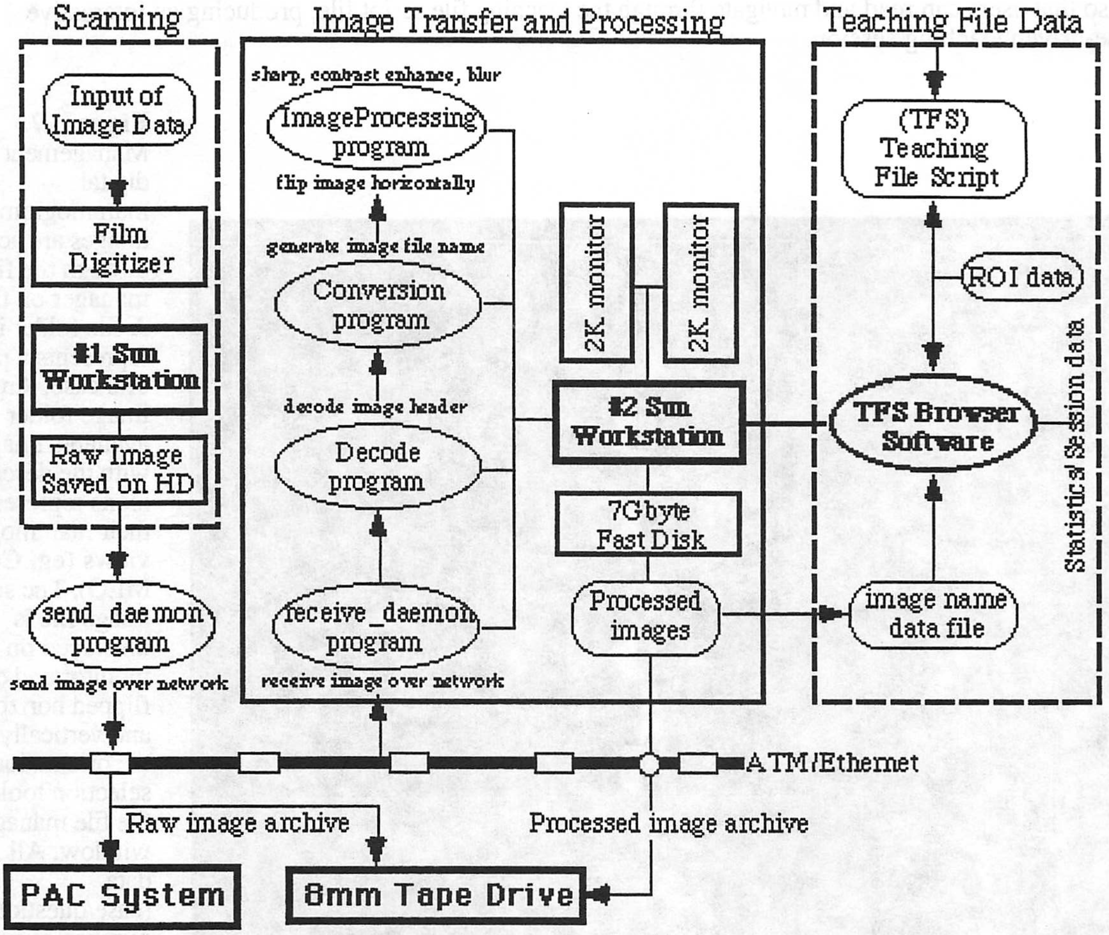

Figure 6. Diagram for digitization process and teaching file database establishment.

Figure 6 summarizes the processes for image digitization and teaching file data collection. Mammograms, as well as breast sonograms amd computed tomographic and magnetic resonance images (if they are included in the case), are digitized with the high-resolution film scanner connected to Sun Workstation #1. Related medical system so that users can read and navigate through the teaching file script file, producing an interactive response-driven teaching session.

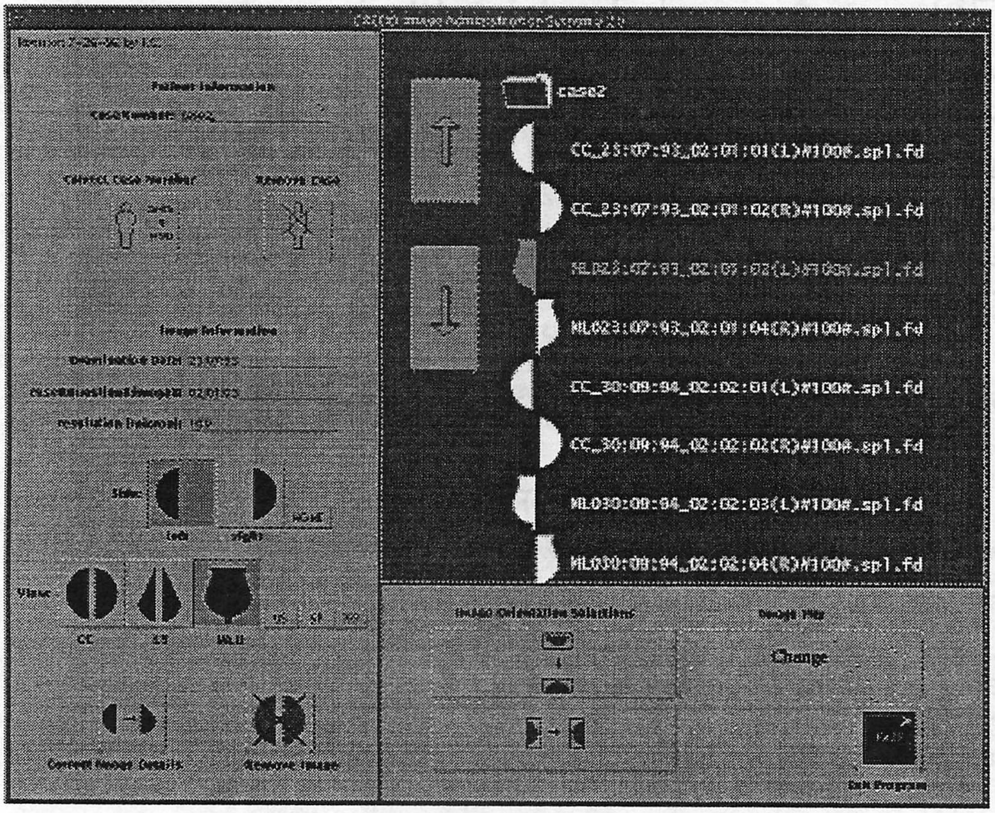
case2
CC_23:07:93_02:01:01(L)#100#.spl.fd
CC_23:07:93_02:01:02(R)#100#.spl.fd
MLO23:07:93_02:01:03(L)#100#.spl.fd
MLO23:07:93_02:01:04(R)#100#.spl.fd
CC_30:09:94_02:02:01(L)#100#.spl.fd
CC_30:09:94_02:02:02(R)#100#.spl.fd
MLO30:09:94_02:02:03(L)#100#.spl.fd
MLO30:09:94_02:02:04(R)#100#.spl.fd
Patient Information
Image Information
Side:
View:
CC
MLO
Change
Exit Program

Figure 7. Management tool for digital mammograms. All images are accessible through the file manager on the right. A file folder icon represents a patient or a case. An open image folder displays available image files with the descriptive icons representing their mammographic views (eg, CC, MLO). The selected image file is displayed on a 2K monitor and can be flipped horizontally and vertically with the orientation selection tools under the file manager window. All relevant data (case/question/image number, examination date, and breast side and view) for the selected image are editable and listed on the left. (Full-size image)

Figure 7 shows the main control screen of our image management tool. The tool is specially developed for radiologists to manage and manipulate digital mammograms and teaching file image data records. The tool is capable of viewing and flipping images and changing the image index, examination type, and date. With this management tool, it is easy to organize and index digital mammograms for use in the teaching file.

Our development of the teaching file script, coupled with the image management tool, makes it possible for radiologists who are unfamiliar with computer operating systems to create, update, and manage their own teaching sessions. The teaching file script is a plain-text file, easy to edit and to port to other systems. All tags used in the teaching file script are described in the Appendix, while the graphical user interface (GUI) of the teaching file navigation browser is shown and explained in the next section.

Graphical User Interface (GUI) and an Online Demonstration

An easy-to-use GUI has been designed for our interactive teaching file. It responds dynamically with detailed instruction to every action of the user. Combined with online help, the GUI makes it easy for the user to manipulate digital mammograms and navigate through the teaching session.

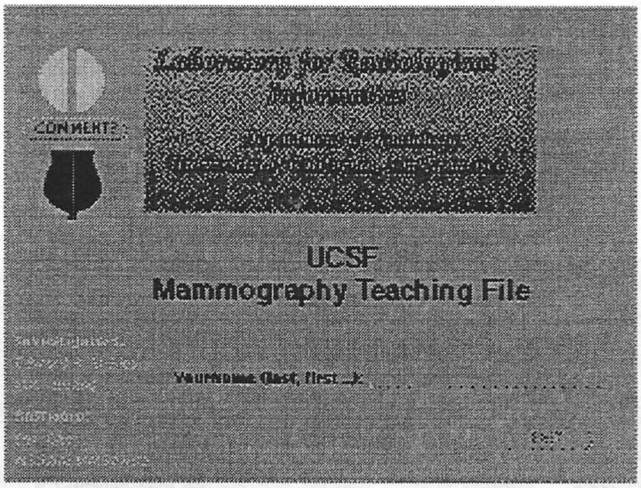
COMMENT?
Laboratory for Radiological Informatics
UCSF
Mammography Teaching File
Yourname (last, first ...):

Figure 8. Screen shot of the login screen. (Full-size image)

Each user must first type his/her name on the login screen displayed in Figure 8. The login process then captures the user name and starts the teaching file. User performance scores are time-stamped and recorded in a log file. Users also can click the "COMMENT?" button to get a pop-up text editor window in which they can write their comments and suggestions on how to improve the teaching file.

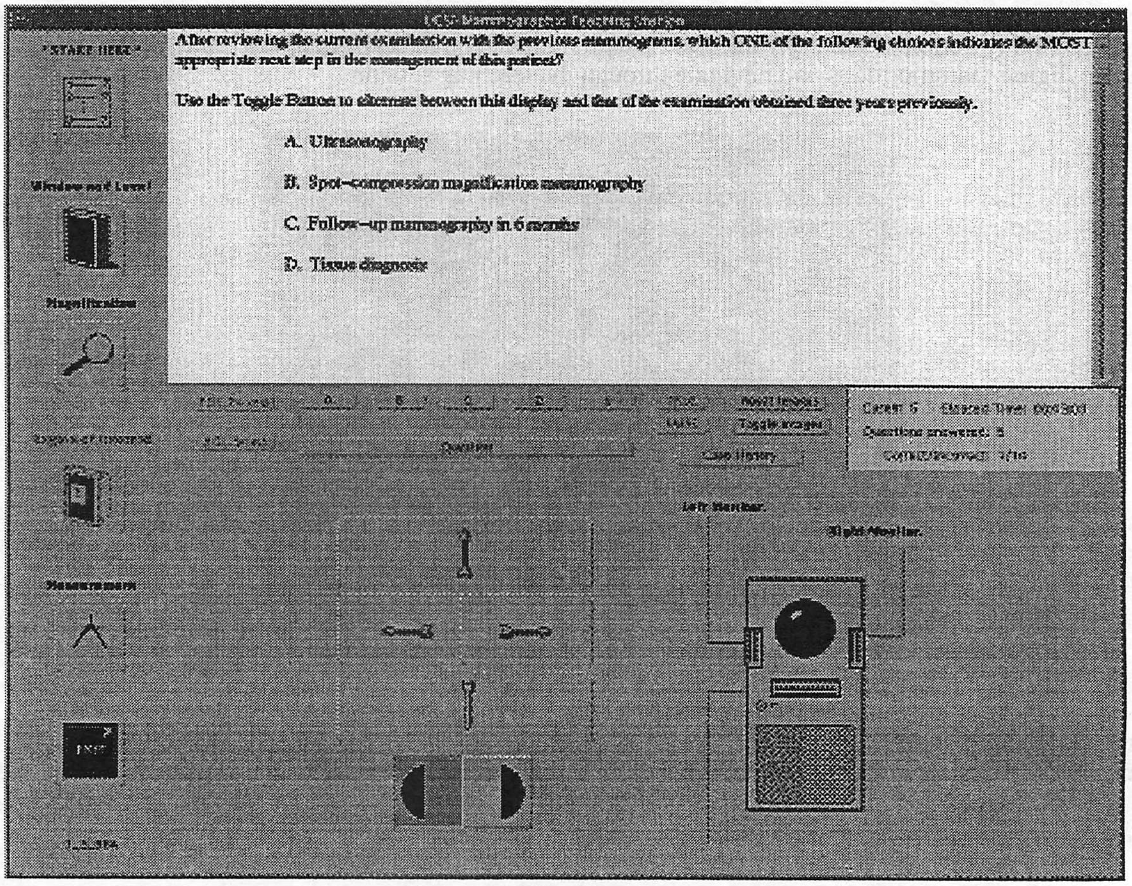

After reviewing the current examination with the previous mammograms, which ONE of the following choices indicates the MOST appropriate next step in the management of this patient?

Use the Toggle Button to alternate between this display and that of the examination obtained three years previously.

A. Ultrasonography

B. Spot–compression magnification mammography

C. Follow–up mammography in 6 months

D. Tissue diagnosis

Figure 9. Main control screen of the interactive teaching file (see text for explanation).
(Full-size image)

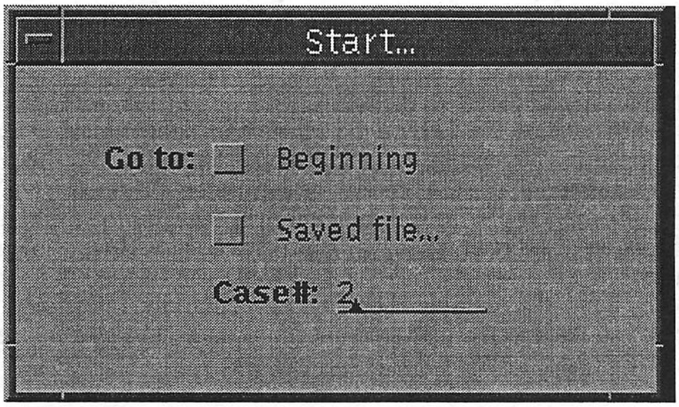

Start...

Go to: ☐ Beginning

☐ Saved file...

Case#: 2

Figure 10. Choices of start-up pointer (top to bottom): starting a new session from the beginning, resuming a previous session, or starting a specific case.

Computer-aided Instruction (CAI) Model

Our CAI model specifies the sequence of questions, image display, instructions, and explanations of cases dynamically, based on user responses during an interactive teaching session. It permits image visualization, allows the user to detect imaging abnormalities by pointing and clicking on the 2K monitors, provides questions and displays both correct and incorrect answers, and leads the user through the analysis and management of each case in a clinically relevant sequence. Follow-up questions are also included in most cases, once the correct diagnosis and treatment are determined by the user.

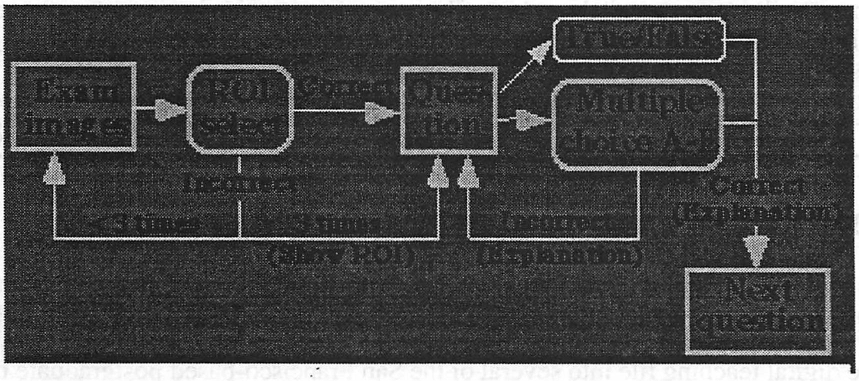

Figure 11. A general algorithm for the CAI model and basic work-up sequences.

Figure 11 shows the general flow of control in this model and the imaging work-up sequences. At the start of each case, the system first gives a brief description of the case history and then presents to the user a set of initial screening mammograms. After examination of those images, the user is asked to use a mouse pointer to identify on the 2K monitors any mammographic abnormalities. The user's selection is compared with prerecorded ROI data. If the user succeeds in identifying the ROI, he/she proceeds to a multiple choice or true/false question that is relevant to his/her findings, or the user must try again. If a user has not marked the abnormality after three tries, the system displays the ROI on the 2K monitor, accompanied by an explanation. The user then proceeds to the next question. Depending on user response to a question, the computer system presents different work-up sequences defined in the CAI model, as illustrated in Figure 11. The system provides instructions, explanations, and answers to the question, guiding the user toward the next question. During this process, additional images are displayed whenever appropriate. This flow of control serves, in a structural way, to aid the user in navigating through the medical knowledge embedded in the teaching file cases. Note that a user cannot proceed beyond a multiple choice question until the question is answered correctly. The immediate repetition of an incorrectly answered question serves as a powerful educational device for reinforcing correct answers.

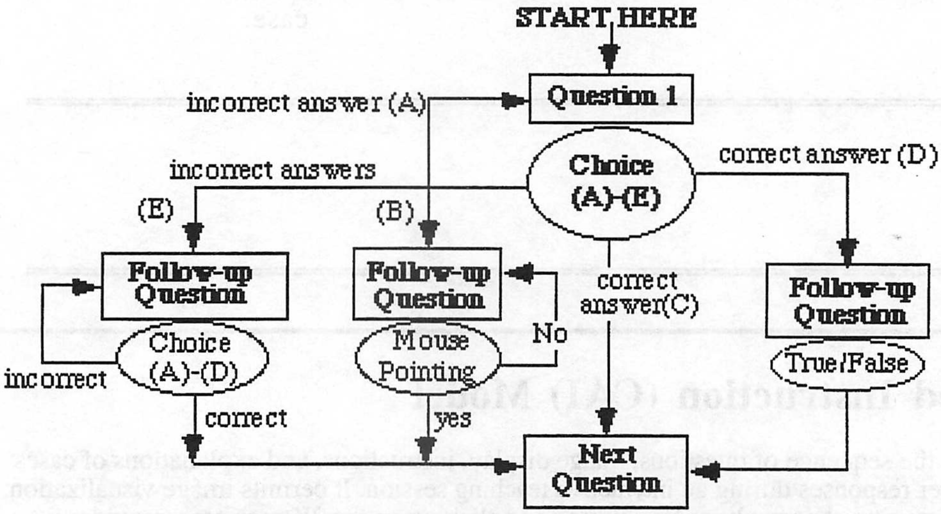

Figure 12. An example of nested building blocks and different work-up sequences, based on five possible choices, *(A)*-*(E)*, for a hypothetical Question 1.

There is often more than one suitable approach to working up a specific breast imaging problem. The questions and instruction sequences built into our digital teaching file system support this by accepting more than one choice as correct and by providing different pathways with tailored follow-up questions. Figure 12 shows, as an example, how the system can call up different work-up sequences and follow-up questions in responding to user choices. Marking the abnormality and the multiple choice and true/false questions are the three basic building blocks of our interactive teaching file. Nesting them together creates an effective teaching tool.

Clinical Application

The digital teaching file is available to all radiology residents, fellows, staff radiologists, and visiting radiologists for continuing medical education at UCSF. All radiology residents are now required to complete a set of 25 cases in the digital teaching file during each 4-week breast imaging rotation at UCSF. We also have incorporated use of the digital teaching file into several of the San Francisco-based postgraduate breast imaging courses given at UCSF.

The digital teaching file currently contains 50 active cases, with approximately 500 digital mammograms and approximately 800 questions. It takes about 10 hours for an average user to complete a 50-case set. Using the teaching file script and the image management tool described in "Teaching File Data Collection" above, Dr Sickles and his associates are constantly adding new cases, thereby replenishing the teaching file with new material. Mammograms of 1,000 carefully selected cases will be maintained in digital format, from which active case sets will be updated periodically.

We have developed a comprehensive user-log mechanism to record user activities. This system documents user progress and performance by time-stamping user activity and recording of the user's correct/wrong answers. The user is allowed to log off anytime in the middle of a session. The system automatically saves an unfinished session so that the user can resume at the point he/she logged off. The user log provides performance evaluation feedback for users and can be used to test the effectiveness of the digital teaching file compared with traditional film-based methods of teaching file instruction.

Two identical display stations, as described in "Mammography Display Station" above, have been set up at UCSF, in the Laboratory for Radiological Informatics at our Parnassus campus and at UCSF/Mount Zion Breast Imaging Center, located 2 miles away. The two sites communicate via an asynchronous transfer mode (ATM) wide-area network. The OC3 (155 Mbits/sec) ATM switches connected at both sites provide a realization speed of 60 Mbits/sec (9). With this high-speed ATM connection, the mammograms digitized at one site can be sent to and displayed at the other site at near real-time speed. Integration of mammogram digitization, high-resolution display, and the ATM connection can be used for developing not only the digital teaching file but telemammography applications. A general radiologist at one site can digitize mammographic images and then transmit them to the expert mammographers at the other site for online consultation and diagnosis.

Building on the success of our digital breast imaging teaching file developed during the last two years at UCSF, we are going to port the teaching file from the Pixar imaging/Sun SPARC 470 display system to our newly designed telemammography display workstation (Ultra SPARC 2 platform with two DOME [Waltham, Mass] Md5/SBX display boards). The old Pixar/Sun 470 system, although adequate for fast and high-resolution image display, is 4-year-old technology, expensive to maintain and difficult to upgrade. The new telemammography workstation is more cost-effective and is also compatible with the digital image format from a full-field direct digital mammography system (10). This system has been installed recently at UCSF/Mount Zion Breast Imaging Center, which generates mammograms that are already in digital format.

Summary

We have implemented a high-resolution display system for viewing digitized mammograms at near real-time speed. This display system, combined with a sophisticated CAI model, has been used to create an interactive breast imaging teaching file for training radiology residents, fellows, staff radiologists, and visiting radiologists.

A mammography display must be able to portray the entire breast with such fine detail that tiny structures are readily visible. This must be done at near real-time speed. The quality of digital mammograms is highly dependent on the film digitizer and display system, while the speed of image display and on-screen image manipulation is determined by system hardware architecture and image processing software. With a two-monitor 2K display station and a high-resolution film digitizer, the image quality of digitized and displayed mammograms has been found to be adequate and acceptable for clinical applications. Pixar image hardware with two large frame buffers and optimized processing software, combined with rapid retrieval of images from a hard disk, makes nearly real-time mammogram viewing and on-screen image manipulation possible. We also have developed a special display mode to simultaneously show on two 2K monitors a set of four mammograms (eight mammograms with the use of a toggle switch). Such a display mode is needed for efficient mammogram interpretation.

Using our high-resolution display station, we have created a large interactive breast imaging teaching file. The teaching file has been designed on a sophisticated CAI model to simulate clinically relevant work-up sequences. Our CAI model not only provides answers to questions but allows users to identify abnormalities by pointing and clicking on displayed digital images. Development of a simple teaching file script, which integrates vast teaching file data with the CAI, makes it feasible for breast imaging experts to create and maintain a digital teaching file without the assistance of a computer programmer. These several features, in conjunction with an easy-to-use GUI, make our interactive teaching file a powerful tool for providing breast imaging training for radiologists.

Acknowledgment

This work is supported by the U.S. Army Medical Research and Materiel Command under contracts DAMD17-94-J-4338 ("A Digital Breast Imaging Teaching File") and DAMD17-96-C-6111 ("Real-Time Full-Field Direct Digital Telemammography") and the California Breast Cancer Research Program, "Real-Time Telemanagement of Mammography Examination" under grant IRB-0148. Many people contributed to the success of this project, especially in its early stages. Among them are Jun Wang, PhD, Michael J. Moskowitz, PhD, Jeffrey Allen, PhD, Andrew Lou, PhD, Anthony Giles, and David Hoogstrate. Thanks also to Faye Dalessio and Tianrao Jiang, who spent many hours at film digitization and text data entry.

The views, opinions, and findings contained in this report are those of the authors and should not be construed as an official Department of the Army position, policy, or decision unless so designated by other documentation.

Appendix: Teaching File Script

A key issue when creating a large digital teaching file is how to integrate vast teaching file text/image data with a CAI model. Few breast imaging experts are able to do computer programming or make use of the Unix operating system. Our teaching file script (TFS) was created to overcome these difficulties and provide an easy way for radiologists to create, update, and maintain the digital breast imaging teaching file.

TFS files are ordinary text files, together with tags, that tell the computer how to identify each of the elements in the file, how to query and display images, and how to respond to user actions. Since TFS files are plain-text files, they can be created on any computer platform with any text editor.

TFS tags consist of a left angle bracket (<), followed by the name of the tag and some attributes, and then closed with a right angle bracket (>). Tags are generally written as

<tag_name attributes ...>Affected text.

Therefore, to make a question, one would use the following TFS text:

<Question 2> Which one of the following choices BEST describes the location of the mammographic abnormality in this case?

The computer will identify the above text as the second question in the current case and display the text accordingly.

List of Tags and Keywords

<Section number> *text*
Beginning of the number'th case; with text describing the case history
<Question number> *text*
Identifies text as the number'th question
<Image number1 (number2) (yes)> ***(pointers to images)***

Displays images

"Number1" is the number of images to be shown (maximum of four). The images will be displayed on the two 2K monitors according to the display mode in Figure 5.

"Number2" is the number of images to be toggled, if any (maximum of four, optional).

If "yes" (optional) is specified, the images will not be shown until a correct answer is given.

"Pointers to images" (optional): Image file names will be read in automatically from an image data file indexed by case, question, and image number. Normally, one does not have to specify image pointers, since these are entered when films are digitized. However, if one wants to show again the images from a previous question or case, one has to specify the image pointers (which can be either an image file name or an index).

<A (yes) (x)>...<E (yes) (x)>

Text answers to the multiple choices (A)-(E). The keyword "yes" is used to indicate a correct answer (eg, **<B>** is used for a wrong choice while **<B yes>** is used for the correct answer). The keyword "x" (optional) indicates the existence of a follow-up question specified by the tag **<Xstem>**.

<T (yes) (x)> and **<F (yes) (x)>**

Text--similar to that for **<A>...<B>** but used to provide answers to true/false questions.

<Mouse (no) (x)> text1 and **<Mouse yes (x)>** text2

Requires the user to operate a mouse pointer to identify any important finding on the displayed image. The answer "text2" will be shown if the user selects the correct region on the display; "text1" will be shown if an incorrect region is selected. The keyword "x" (optional) indicates the existence of a follow-up question specified by the tag **<Xstem>**.

<Xstem number1 number2>

Follow-up question that stems from question "number1" and answer "number2."

{ } : Braces are used to contain a block of physicians'/programmers' comments, ignored by the computer system.

References

1. Smart CR, Hendrick RE, Rutledge JH, Smith RA. Benefit of mammography screening in women ages 40 to 49 years: current evidence from randomized controlled trials. Cancer 1995; 75:1619-1626.

2. Tabar L, Larsson LG, Anderson I, et al. Breast-cancer screening with mammography in women aged 40-49 years. *Int J Cancer* 1996; 68:693-699.

3. Chew FS, Smirniotopoulos JG. Educational efficacy of computer-assisted instruction with interactive videodisc in radiology. Invest Radiol 1993; 28:1052-1058.

4. Lou SL, Sickles EA., Wang J, Huang HK. A high resolution display system for mammograms (abstr). Radiology 1994; 193(P):474.

5. Moskowitz M, Wang J, Huang HK, Sickles E, Allen J, Giles A. High resolution display system for mammograms. Proc SPIE Med Imaging 1995; 2431-2444.

6. Andriole K, Wang J, Gould RG, Huang HK. Digital image quality comparison between a 50-micrometer laser digitizer and a high-resolution CR imaging plate (abstr). Radiology 1994; 193(P):250.

7. Ishimitsu Y, Arai K, Taira RK, Huang HK. Radiological laser film scanner sampling artifact. Comput Med Imaging Graphics 1990; 14:25-33.

8. Wang J, Huang HK. Film digitization aliasing artifacts caused by grid line patterns. IEEE Trans Med Imaging 1994; 13:375-385.

9. Huang HK, Arenson RL, Dillon WP, Lou SL, Bazzill T, Wong AWK. Asynchromous transfer mode (ATM) technology for radiologic image communication. AJR 1995; 164:1533-1536.

10. Lou SL, Sickles EA, Huang HK, Cao F, Hoogstrate D, Jahangiri M. Full-field direct digital telemammography--preliminary. Proc SPIE Med Imaging 1997; 3035:369-379.

Back to **Table of Contents** | **Online Demo** | **Author Information** |

Back to Contents

Automatic Background Recognition and Removal (ABRR) in Computed Radiography Images

Jianguo Zhang* and H. K. Huang, *Senior Member, IEEE*

Abstract— **A novel method to automatically recognize and remove background signals in computed radiography (CR) images caused by X-ray collimation during projection radiographic examinations is presented. There are three major steps in this method. In the first step, a statistical curve is derived based on many hierarchical CR sample images as a first approximation to loosely separate image and background pixels. Second, signal processing methods, including specific sampling, filtering, and angle recognition, are used to determine edges between image and background pixels. Third, adaptive parameter adjustments and consistent and reliable estimation rules are used to finalize the location of edges and remove the background. In addition, this step also evaluates the reliability of the complete background removal operation. With this novel method implemented in a clinical picture archiving and communication system (PACS) at the University of California at San Francisco, we achieved 99% correct recognition of CR image background, and 91% full background removal without removing any valid image information.**

Index Terms— **Background removal, computed radiography, pattern recognition, statistical image processing.**

I. INTRODUCTION

PROJECTION radiography accounts for more than 60% of procedures in diagnostic radiology. As digital imaging becomes more important in daily radiology practice, the need for converting images from projection radiography to digital format becomes apparent. Currently three digital methods are being used: digital fluorography (DF), film digitization, and computed radiography. Digital fluorography uses a vidicon camera to capture X-ray images and convert them to digital images through a frame grabber. One type of film digitizer uses a laser beam to convert the optical densities on film to a digital image. Computed radiography (CR) aims to replace screen/film analog radiographs with direct digital images [1]. The imaging plate (IP) used in CR is based on the principle of laser stimulable phosphor technology. During the past ten years, CR has been gradually replacing the screen/film system.

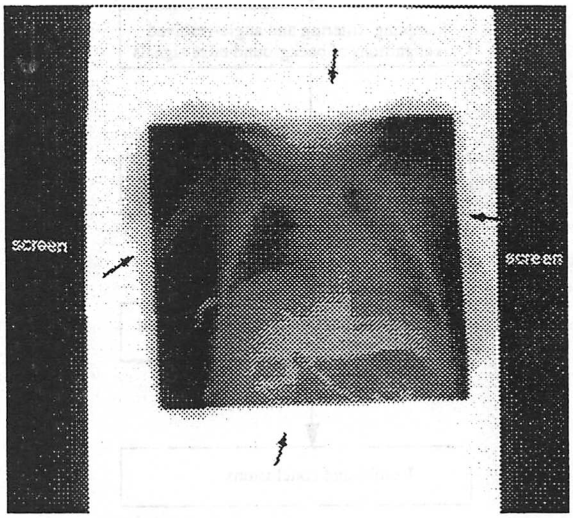

Fig. 1. A CR image with background, marked by arrows as seen on a display monitor. This picture shows three regions: the image, the background, and the black screen which is the result of a small image on a large display surface.

Under normal operating conditions, images obtained by projection radiography contain unexposed areas due to X-ray collimation: for example, areas outside the circle of the imaging field in DF, and areas outside the collimator of CR for skeletal and pediatric radiology. In digital images, unexposed areas appearing white on a display monitor will be called background in this context. Fig. 1 is a pediatric CR image with white background as seen on a monitor. Background removal in this context means that the brightness of the background is converted from white to black.

There are three major advantages gained by performing background removal in digital projection radiography. First, background removal immediately provides lossless data compression, an important cost-effective parameter in digital radiography when dealing with large-size images. Second, a background-removed image has better image visual quality for the following reason. Diagnosis from radiography is the result of information processing based on observation with the eye. Since the contrast sensitivity of the eye is proportional to the Weber ratio $\Delta B/B$, where B is brightness of the background, and ΔB is brightness difference between the region of interest in the image and the background [2], removing or decreasing the unwanted background in projection radiography images make these images more easily readable and greatly improves their diagnostic effects. Once the background in a CR image is

---

Manuscript received February 28, 1996; revised February 17, 1997. This research was supported in part by the National Natural Science Foundation of China. The Associate Editor responsible for coordinating the review of this paper and recommending its publication was C. Roux. *Asterisk indicates corresponding author.*

J. Zhang is with the Laboratory for Radiological Informatics, Department of Radiology, 530 Parnassus Ave., Rm. CL-158, University of California, San Francisco, CA 94143-0628 USA (e-mail: jianguo-zhang@radmacl.ucsf.edu).

H. K. Huang is with the Laboratory for Radiological Informatics, Department of Radiology, 530 Parnassus Ave., Rm. CL-158, University of California, San Francisco, CA 94143-0628 USA.

Publisher Item Identifier S 0278-0062(97)08957-X.

0278–0062/97$10.00 © 1997 IEEE

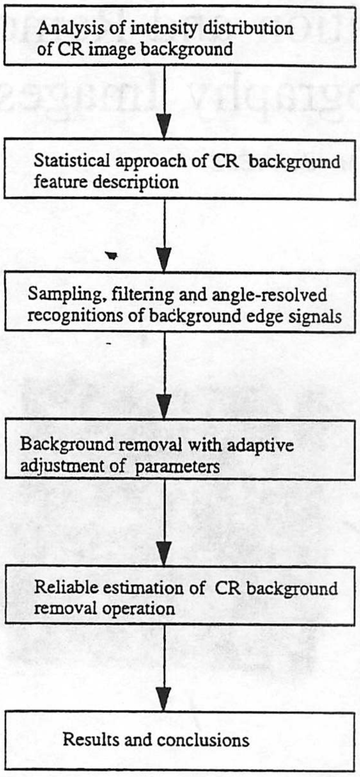
Analysis of intensity distribution of CR image background
Statistical approach of CR background feature description
Sampling, filtering and angle-resolved recognitions of background edge signals
Background removal with adaptive adjustment of parameters
Reliable estimation of CR background removal operation
Results and conclusions

Fig. 2. A block diagram of the background recognition and removal procedure.

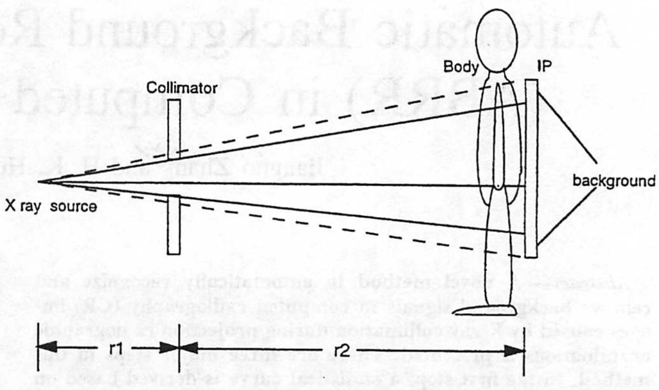

Fig. 3. A diagram showing the radiography procedure of a pediatric patient. Usually, $r1 = 1$ ft, $r2 =$ 2–6 ft. IP: imaging plate.

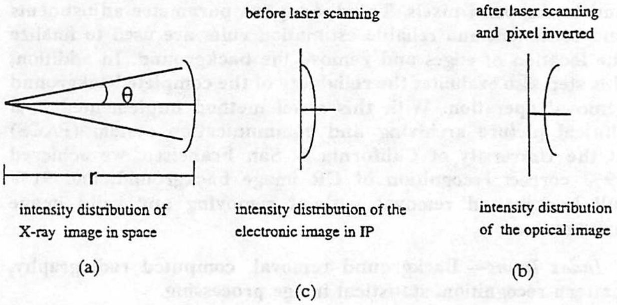
before laser scanning
after laser scanning and pixel inverted
θ
r
intensity distribution of X-ray image in space
intensity distribution of the electronic image in IP
intensity distribution of the optical image
(a)
(b)
(c)

Fig. 4. (a) Intensity distribution of X-rays in space. IP: imaging plate. (b) intensity distribution of electronic image in the IP, and (c) intensity distribution of the optical image.

removed, a more representative look-up table pertinent to only the range of gray scales in the image and not the background can be assigned to the image. Thus, it can improve the visual quality of the images [3], [4]. Third, background removal is a crucial preprocessing step in computer-aided-diagnosis (CAD). A background-removed image can improve the diagnostic accuracy of CAD algorithms as the cost functions in the algorithms can be assigned to the image only, rather than to the image and its background combined [5]–[9].

In the cases of DF and the film digitizer, the background removal procedure is straight forward. In the former, since the size of the image field is a predetermined parameter, the background can be removed by converting every pixel outside the diameter of the image field to black. In the latter, since the digital image is obtained in a two-step procedure (first a film is obtained and then the film is digitized), the boundaries between the background and the exposed area can be determined interactively by the user, and the corner points may be input during the digitizing step.

In the case of CR, background removal is a more complex procedure since it has to be done automatically during image acquisition or preprocessing time. Automatic removal of CR background is difficult because the algorithm has to recognize different body part contours as well as various collimator sizes and shapes. Since the background distribution in CR images is complex and the removal is an irreversible procedure, it is difficult to achieve a high successful ratio of full background removal and yet ensure that no valid information in the image is removed. Some methods developed to remove the background of CR images can only achieve 42% background removal [10]. Here, we present a novel theoretical method to recognize and remove the background in CR images. The method is based on statistical description of intensity distribution of CR background, signal processing, and consistent and reliable estimations of background removal operations. Fig. 2 is a block diagram of the background recognition and removal procedures. With this method implemented in the CR preprocessing unit, we achieved very high ratios of full background removal without deleting valid information from the image.

II. INTENSITY DISTRIBUTION FEATURES OF CR BACKGROUND

Usually, the background in CR images is created due to the X-ray collimator. Fig. 3 shows the X-ray imaging procedure of a pediatric patient. Most collimators may be considered as attenuators of X-rays. Depending on the sensitivity of the imaging plate (IP), the background may not be of uniform intensity due to various body parts covered by the collimator. First, let us ignore the anatomical information in the CR background, and assume that the X-ray beam is a point source as shown in Fig. 4(a). Then the intensity distribution, I, is spherical function and can be described by

$$I(\theta, r) = a_0 \cdot \cos^2 \theta / r^2 \qquad (1)$$

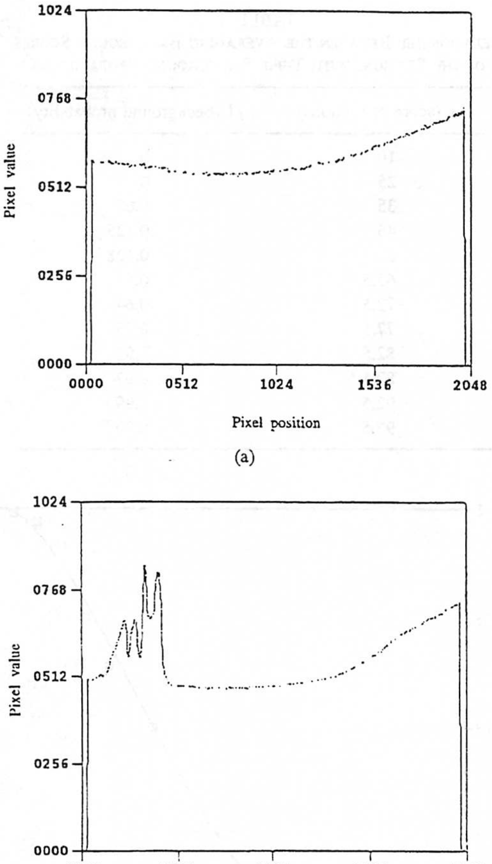

Fig. 5. (a) An intensity trace (or distribution) of a CR image with pure background in the direction pointed by "arrow a" in Fig. 6. The black area outside of "a" is the result of a small image on a large display surface. (b) an intensity trace of a CR image with combined external objects covered by the collimation and background in the direction pointed by "arrow b" in Fig. 6, and (c) An intensity trace of a CR image with partial background and partial anatomy in the direction pointed by "arrow c" in Fig. 6.

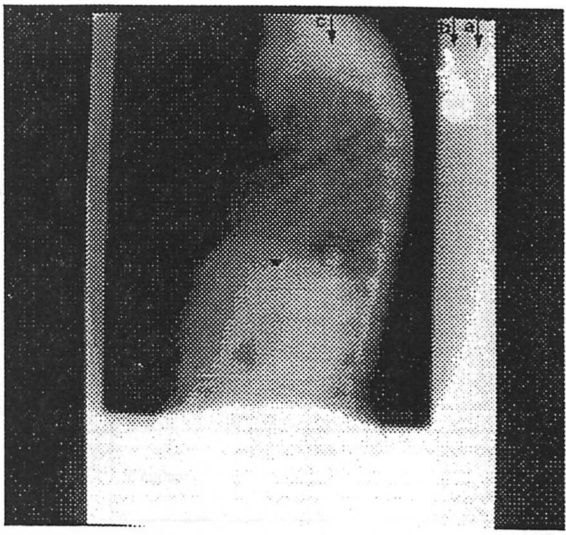

Fig. 6. The locations of the three intensity traces described in Fig. 5(a)–(c) from the same CR image. Arrows **a**, **b**, and **c**, point the direction and position of intensity trace curves shown in Fig. 5(a)–(c), respectively.

where r is distance between the source and IP center. θ is the angle between the pixel under consideration and the center line in the plane defined by the pixel under consideration and the center line, and a_0 is a constant, as shown in Fig. 4(a). The intensity distribution of uniform latent image stored in IP is shown in Fig. 4(b). After laser scanning the IP, the optical image generated from the latent image is converted to a digital image, and the intensity distribution is shown in Fig. 4(c).

Sometimes, parts of anatomy combined with other external objects such as prostheses, and markers, are projected onto the background due to insufficient thickness of the collimator, high sensitivity of the IP, or the collimator center being not aligned with the center of the IP. The shapes and intensity (or pixel value) distributions of the background in CR images are usually asymmetrical and complex. Fig. 5(a)–(c) shows examples of background intensity distribution curves at three different locations marked by arrows a, b, and c in the CR image shown in Fig. 6. Fig. 5(a) is a pure background distribution; Fig. 5(b) is a background distribution combined with external marker information; Fig. 5(c) is a distribution of part background and part anatomy.

III. STATISTICAL APPROACH OF CR BACKGROUND FEATURE DESCRIPTION

The first step in the background recognition algorithm is to determine the background probability of a pixel in a CR image. Background probability of a pixel is defined as the chance of this pixel belongs to the background of the CR image. To do this, we need to compute the background score of this pixel based on some background characteristics of CR images and relates this score to the background probability. This relationship can be derived from statistics based on many CR images. This section describes this step.

The intensity distribution of CR background can be computed by (1). Because gray levels of CR image background are normally very high compared with the anatomical parts

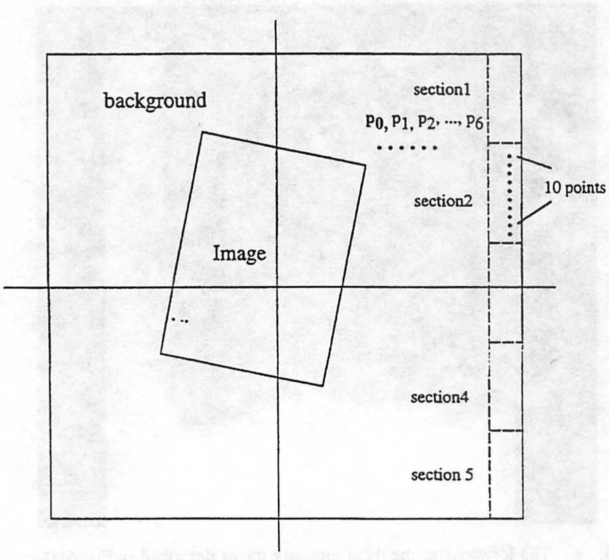

Fig. 7. Schematic showing a CR image with background; locations of six consecutive pixels with respect to P_0; and five sections on the right-hand side of the background, each with ten pixels selected to calculate the background scores.

in the image, any three consecutive points P_0, P_i, P_{i+1} in the background and away from the center of the image should satisfy the following two conditions:

$$I_0 \geq T_p \tag{2}$$

$$I_0 \leq I_i \leq I_{i+1} \tag{3}$$

where T_p is a threshold (given empirically), I_0, I_i, I_{i+1} are average intensities of points located at P_0, P_i, P_{i+1}, respectively, as shown in Fig. 7, I_i is obtained by averaging the pixel values of P_i and its neighbors.

We first define a parameter, called background score, for every pixel in a CR image. Consider the right side of a CR image and an arbitrary background point P_0 as shown in Fig. 7. Six consecutive pixels P_1, P_2, P_3, P_4, P_5, and P_6 from left to right next to P_0 are chosen. If P_0 satisfies (2), and if any of two consecutive pixels satisfy (3), the background score of P_0 is two, otherwise its score is zero. Since there are five possible consecutive pairs, the background score P_0 can be one of 10, 8, 6, 4, 2, 0. The higher the score is, the higher the probability that P_0 belongs to CR image background.

Now, we use statistical approach to find the relationship between the background score of a pixel with its background probability. On one side of the CR image, say, the right-hand side, we divide this side into five equal sections and from each section we select ten equal distant points in the vertical direction next from the right edge, shown in the right side of Fig. 7. Using the same score scheme defined above for each of these ten points, then each section can get a maximum score of 100, or less.

In order to compute the statistic, we randomly selected 50 CR images some of which have background and some do not. The total number of sections examined is $m = 1000$ (= 50 CR images × 4 sides × 5 sections). The possible score of each of these sections ranges from 0–100. Suppose there are l sections in m the scores of which range from 40–50 with an average $s = 45$; and of these l sections, k sections contain background, which gives a background probability equal to k/l. Table I gives the relationship between the averaging background scores of the 1000 sections with their background probabilities based on these 50 CR images.

TABLE I
RELATIONSHIP BETWEEN THE AVERAGING BACKGROUND SCORES OF THE SECTIONS WITH THEIR BACKGROUND PROBABILITIES

s (score of sections)	k/l (background probability)
10	0
25	0
35	0.08
45	0.125
55	0.428
63.5	0.5
72.5	0.64
77.5	0.75
82.5	0.92
87.5	0.97
92.5	0.99
97.5	0.99

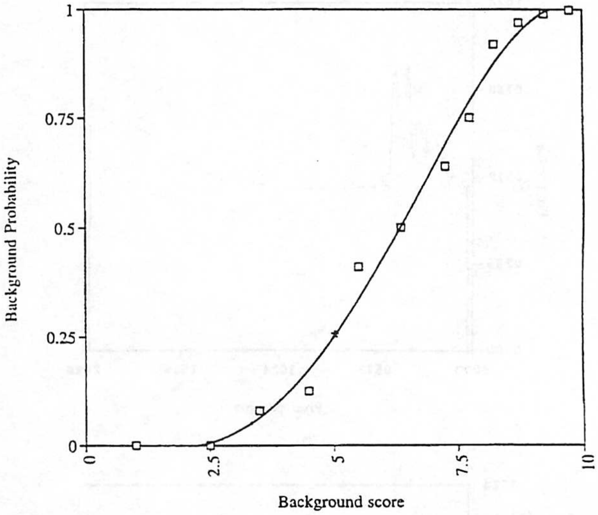

Fig. 8. The curve of background probability versus its background score of a pixel. The curve was obtained by using 10 000 points from 50 CR images. The "□"s are real data and the curve is the "best fit" curve from these "□"s.

Since we sampled ten pixels in a section, the normalized background score of a pixel in these sections is $s_p = s/10$. Fig. 8 shows the relationship between k/l and s_p. The "□"s in Fig. 8 are the normalized data from Table I and the curve is the "best fit" from these "□"s. Because this curve is the statistical result of 10^4 (= 50 × 4 × 5 × 10) pixels from 50 different CR images, we can apply this curve to every pixel in an image to describe the relationship between its background probability and its score. For example, the background probability of a pixel with score 5 is 0.25, as shown by "*" in Fig. 8; and the background probability of a pixel is approximately 1 when the score is greater than eight. This curve can be used to estimate the probability of a pixel being in the background based on its background score.

IV. Recognition of Background in CR Images

A. Sampling of Potential Pixels to Determine the Background Edge

The key step of recognition or removal of CR background is to locate the background edges. In order to find out the position and direction of every edge, we need to use the angle and the value of the pixels under consideration. Because the value of pixels at the edges normally varies greatly, there are many methods to detect this variation, for example, finding the points with a gradient which is larger than a threshold, or those points whose standard deviation of pixel values exceeds an empirically determined threshold, etc. Here, we use the gradient method.

We first differentiate the CR image, $I(x, y)$, and obtain a vector $V(x, y)$ for every pixel as follow:

$$V(x, y) = \rho(x, y) \cdot e^{-i\cdot\theta(x, y)} \tag{4}$$

where

$$\rho(x, y) = [(\partial I/\partial x)^2 + (\partial I/\partial y)^2]^{1/2} \tag{5}$$

$$\theta(x, y) = \tan^{-1}\,[(\partial I/\partial y)/(\partial I/\partial x)]. \tag{6}$$

Consider the collection of all $V(x, y)$ which form a gradient image. We scan the right side of the image from right to left for every line in the horizontal direction, and select one pixel on every line based on three criteria:

1) the gradient $S_d[= \rho(x, y)]$ of the pixel is greater than a threshold T_g (empirically determined), or

$$S_d > T_g \tag{7}$$

2) the position of this pixel is in the right side of $V(x, y)$;
3) it is closest to the right boundary of the image.

Some lines may have a pixel satisfying these conditions, and some may not because there is no pixel satisfying all these three conditions in that line.

Now, we have a pixel array $\{E_i(x, y), i = 1, 2, 3, \cdots, n\}$ where n is the total number of pixels satisfying the conditions. Some of these pixels may be at the edge of CR image background and some may not. Similarly, we form pixel arrays for the left, top, and bottom sides of the image. The procedure of selecting these pixel arrays is similar to that of the right side, the only differences are the scanning direction and changing the "right" to the appropriate location.

B. Filtering and Angle Recognition of Background Edge Pixels

Next, we filter out those pixels in $\{E_i\}$ which belong to CR background and at the edge. Let us again consider the right side of the image. This can be accomplished in two steps by using the pixel background probability, and the angle information. First, we calculate the score on the right side of every pixel of $\{E_i, i = 1, 2, \cdots, n\}$, using the method described in Section III. Once the score of a pixel is obtained we use the curve in Fig. 8 to determine this pixel's background probability. If the score is greater than eight (full score is ten for every point), the probability that it is a background pixel is almost one. Then, this pixel is filtered out as a potential candidate belonging to the background. After applying this algorithm to $\{E_i\}$, a new pixel array $\{E'_j, j = 1, 2, 3, \cdots, n'\}$ is obtained and most pixels in $\{E'_j\}$ should belong to the background.

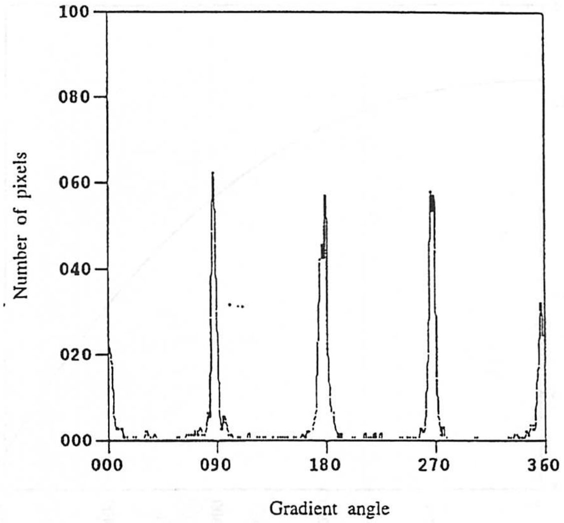

Fig. 9. The angle distribution curve of background pixels at four edges of the CR image shown in Fig. 1; X-axis: angle in degree, Y-axis: no. of pixels.

In order for the pixels in $\{E'_j\}$ to be on a background edge, it should satisfy two other conditions. First, the pixel values should satisfy the background edge condition. This can be determined as follows: Consider the right-hand edge, if the difference of the average intensity of a pixel in $\{E'_j\}$ with its left nearest neighboring pixel average intensity is larger than that of this pixel with its right nearest neighbor, then this pixel is on the edge. Mathematically, if I_1 is the average pixel value of P_1 in $\{E'_j\}$, I_L is the average pixel value on the left side P_1, I_R is that on the right side, the condition is $I_1 - I_L > I_R - I_1$.

Second condition is that the gradient angles of all pixels in $\{E'_j\}$ which satisfy the first condition should have almost same values. Since most collimator edges are straight, the background edges should be straight lines. Because the gradient direction of pixels in $\{E'_j\}$ at the edge should be almost the same and perpendicular to the edge, the distribution (or the number of pixels) of their gradient angles $\theta(x, y)$ should attain a maximum value (or a peak). All the gradient angles at the edge should be closed to θ_m which is corresponding to the maximum value. For the array $\{E'_j\}$, we can draw a curve, called angle distribution curve. the horizontal axis of this curve represents gradient angle and vertical axis represents the number of pixels having same gradient angle in $\{E'_j\}$. Fig. 9 shows angle distribution curves for four sides of the image as shown in Fig. 1. There are four peaks (maxima) in Fig. 9, and the location of a peak represents a background edge direction in the CR image in Fig. 1. The pixels in $\{E'_j\}$ which are not in the half width of the location of the peak of the gradient angle distribution curve are deleted. The remaining pixels $\{E''_k, k = 1, 2, 3, \cdots, n''\}$, the angles of which are

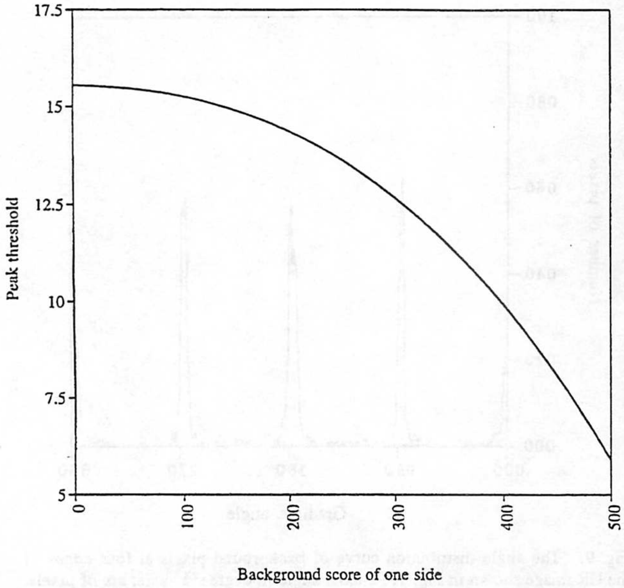

Fig. 10. The curve showing the peak threshold of the number of pixels having the same gradient angle versus the total background score of one side of a CR image based on (9) with $H = 500, U = 250, B = 6$, and $C = 10$.

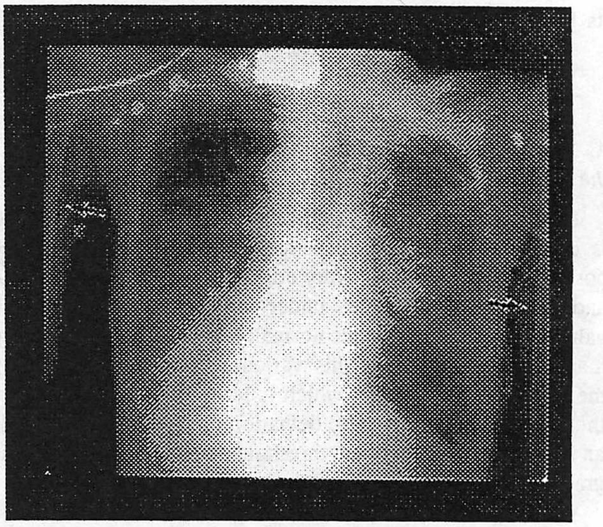

Fig. 11. The gaps between the arms and the body of this CR image create two false edges because they satisfy the background recognition conditions, see arrows. These two false edges were detected by histogram checking. As a result, the two false edges were ignored and the two arms were not deleted.

within the half width of the location of the peak, are used to fit a line which should coincide with the background edge.

During line fitting, the contribution of every pixel selected to fit the line is different with varying weights. The weight (w) can be determined by the following formula:

$$w = A \cdot e^{-k_0 \cdot \Delta\theta} \tag{8}$$

where A and k_0 are positive constants, and $\Delta\theta$ is the angle difference between the angle θ_m of maximum distribution and the gradient angle of that pixel. A large $\Delta\theta$ results in a small w.

V. REMOVAL OF BACKGROUND IN CR IMAGES

A. Adaptive Adjustment of Parameters

Before using pixels $\{E_k''\}$ to fit a line, we have to determine a peak threshold T_s as a basis for whether a line fitting should be performed. This threshold is based on how many pixels in $\{E_k''\}$ which have the angle close to the peak value θ_m. If $P_m \geq T_s$ (P_m is the peak value of angle distribution, or number of pixels), we will do the line fitting because there are enough pixels in $\{E_k''\}$ to make the fitted line more trustworthy, otherwise, the complete set $\{E_k''\}$ will be discarded because this set of pixels may be noise or artifacts.

Since some background edges are very long and distinct and some are not, the P_m for a long distinct edge is very large and for an unclear edge is very small. Meanwhile, some angle distribution curves of images with no background may also have peaks with small P_m value which are created by some objects or anatomy with straight line segments. If T_s is set high, the probability of fitting a line as an edge is high, but the ratio of full background removal would be low. In order to solve this problem, we develop an algorithm to adjust T_s dynamically based on the background characteristic of the image under consideration.

Since all pixels are selected based on their high background scores from the statistical curve shown in Fig. 8, we establish a relationship between T_s and the total score of one side of the image by using the following equation:

$$T_s = B + C \cdot \left[1 - e^{-(H-X)/U}\right] \tag{9}$$

where B and C are constants determined empirically, H is the full score of one side (in our situation $H = 500$, $U = H/2$), and X is the total score of the five sections in one side of the image. Fig. 10 is the curve of (9), where $B = 6$ and $C = 10$.

With (9), the threshold T_s can be changed dynamically according to the total score in one side of the image. So, although the peak values of angle distribution curves of unclear edges, segments of objects or, some anatomy may be the same, their thresholds may be different.

One side of an image with background may have a low threshold T_s, and there can be a background removal operation because that side of the image has a high score. On the other hand, one side of an image can have a high threshold, but there may not be a background removal process because the background score is low. The adaptive adjustment of parameters balances the reliability of background removal operation and the percentage of full background removal before the line fitting. In our experience, the fraction of full background removal without cutting off any pertinent image data is 72% before the adaptive parameter adjustment and 91.7% after the adjustment.

B. Reliable Estimation of Background Removal

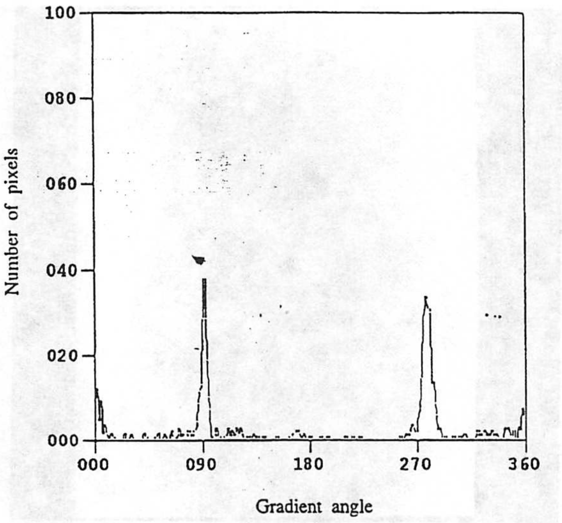

Fig. 12. The angle distribution curve of the two false-background edges in Fig. 11 (90° and 270°) shows definite signals of background edges. These two false edges were detected by histogram checking and were ignored.

C. Implementation

All operations discussed were performed on subsampled 512 × 512 CR images from $2K \times 2K$ images for computational efficiency. If all reliable estimations are passed, the background on the original $2K \times 2K$ CR image is removed according to the parameters calculated from (10).

Before and after background removal operation, there should be some necessary steps to examine the reliability of this operation because automatic background recognition and removal (ABRR) is an irreversible procedure and the image can not be recovered once the valid image data had been discarded. Here, we give a reliable estimation before and after background removal.

Next page

Assume the equation of the fitted line is given by

$$y = a \cdot x + b \tag{10}$$

where a and b are constants. In order to estimate the goodness-of-fit of the points $\{E_k''\}$ to the line [11], we apply Chi-square fitting to these points and estimate the goodness-of-fit by use the Q value calculated from the incomplete gamma function, and the coefficients of probable uncertainties (Δa and Δb). If $Q \geq 0.001$, and $\Delta a/a \leq 0.001$, $\Delta b/b \leq 0.01$, the fitting is acceptable. Another estimation is to compare the angle of fitted line $\theta_b = \tan^{-1}(b)$ with θ_m (for example, one of the four angles of distribution maximum in Fig. 9). If θ_b is equal or approximately equal to θ_m, this fitting is consistent with the edge angle determination procedure. The background removal will be applied to the image according to the parameters of (10). The acceptable angle difference ($\theta_m - \theta_b$) is chosen to be about 6°.

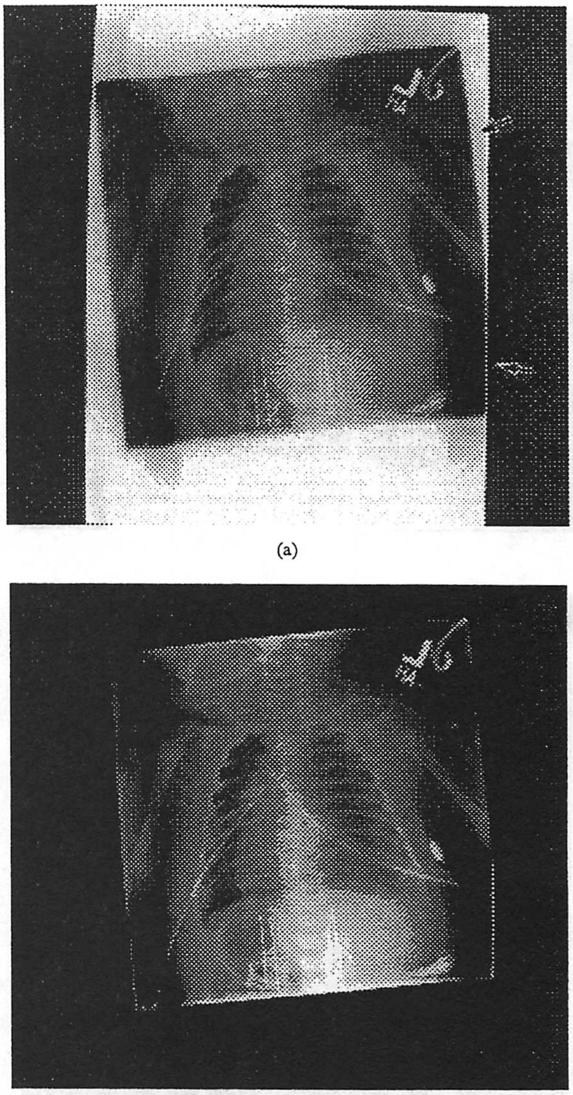
(a)

(b)

Fig. 13. (a) Original image and (b) background removed image. Characteristics: more than two edges on the right side, marked by arrows.

TABLE II
MEASURE OF SUCCESS OF THE AUTOMATIC BACKGROUND RECOGNITION AND REMOVAL ALGORITHM (TOTAL IMAGES = 330, WITH BKGD = 246, NO BKGD = 84)

Recognition of BKGD	243 (BKGD) 87 (no BKGD)	99.0%
Full Removal	223	91.0%
Partial Removal	21	8.8%
No Removal	2	0.2%
Removal of valid inform	0	0.0%

After background removal, we still can estimate the reliability by comparing the histograms between the original CR and the background removed image. Since the gray levels of the background are normally higher than T_p in (2), most portions of the histogram lower than T_p should be unchanged before and after background removal. With this comparison, we can know whether the image has been trimmed too much after background removal. Fig. 11 is an example of a CR image, the left and right sides of which show strong background signals (see Fig. 12, 90°, and 270°). This image did not pass the

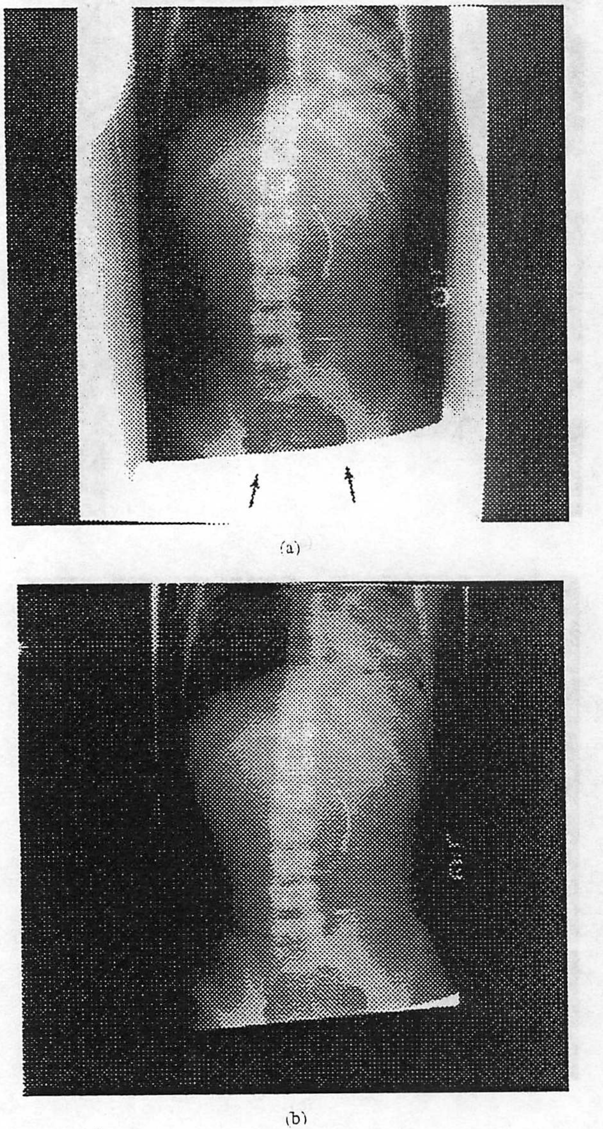

(a)

(b)

Fig. 14. (a) Original image and (b) background removed image. Characteristics: with an odd-shaped abdominal collimator, marked by arrows.

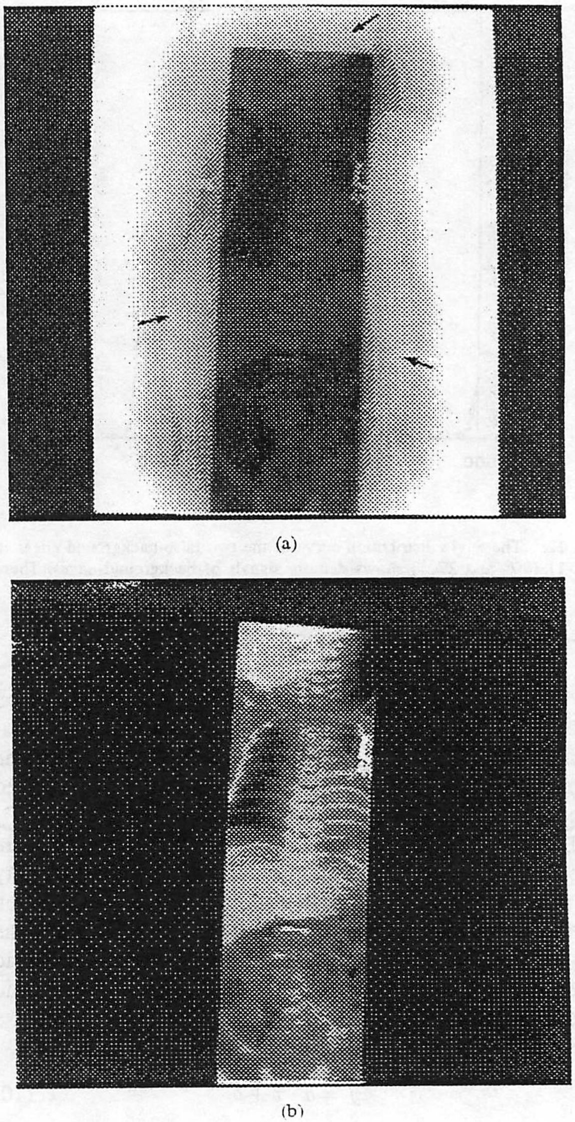

(a)

(b)

Fig. 15. (a) Original image and (b) background removed image. Characteristics: with a longitudinal collimator. Background shows anatomical structures, marked by arrows.

histogram-checking stage because the two false edges cut away some of the anatomical structures lateral to both shoulders changing the shape of the lower portion of the histogram. The algorithm detects the shape change in the histogram and ignores the background removal operation.

VI. RESULTS

Figs. 13–16 show some examples of CR images before and after ABRR. The characteristic of Fig. 13. is that there are more than two edges on the right side of the original image; Fig. 14. is that odd-shaped abdominal collimator is on the bottom side; Fig. 15 is that there are anatomical structures on both sides of the background of an elongated pediatric spine CR image; and Fig. 16. is that there is a prosthetic device at the left side. These images show that the visual contrast of background-removed images (b) is much better than that of the original images (a) because a higher portions of each histogram is shifted after background removal which renders a better look-up table determination. Also, image sizes are reduced without loss of image information.

The method of ABRR was implemented in a clinical picture archiving and communication system (PACS) at the University of California, San Francisco. We sampled 330 consecutive intensive care unit (ICU) CR images over a period of five days, of which 246 have background and 84 do not. The evaluation of the success of this method using this sample was based on the following measures: 1) correct recognition of background; 2) full background removal (see Figs. 13–16); 3) partial background removal [see Fig. 17(b), bottom]; 4) little or no background removal (see Fig. 18); 5) removal of valid

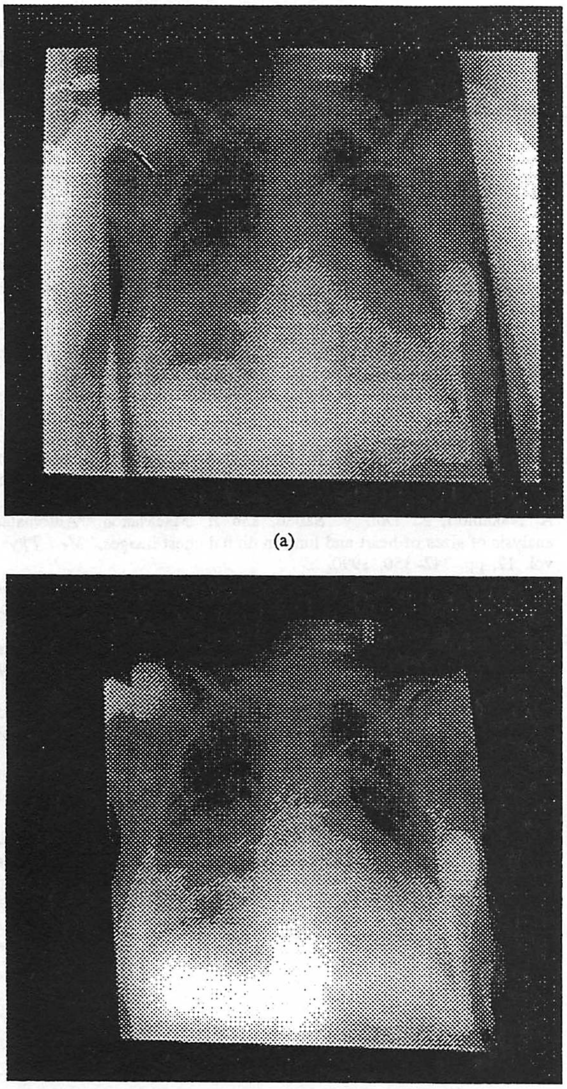

(a)

(b)

Fig. 16. (a) Original image and (b) background removed image. Characteristics: with a prosthetic device at the left side of the image, marked by arrow.

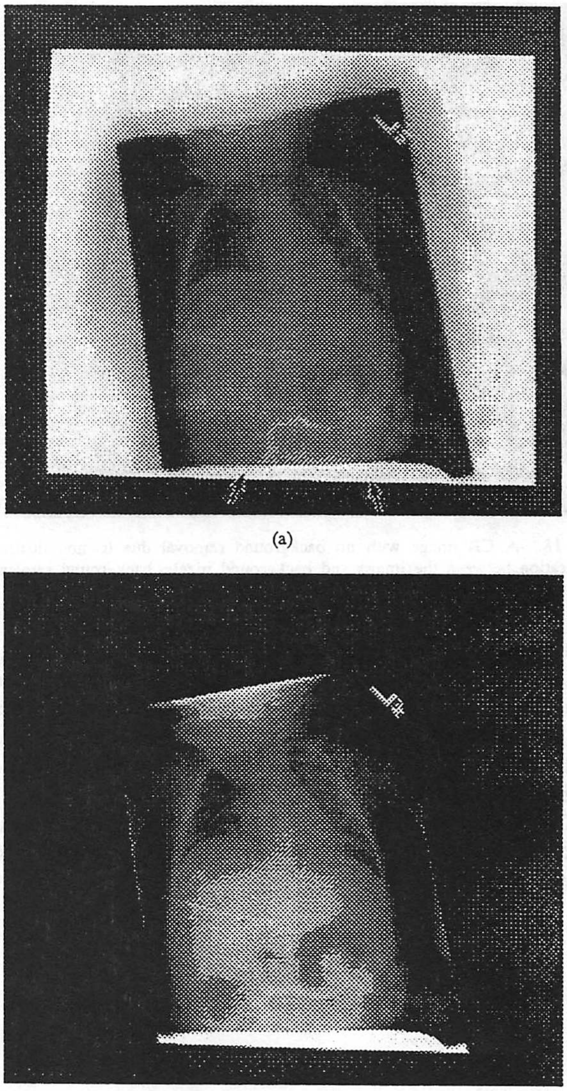

(a)

(b)

Fig. 17. (a) A CR image with an odd-shaped abdominal collimator, marked by arrows and (b) the partial background removed image.

image data. Table II shows the result after applying ABRR to these images.

This result shows that the ABRR has 99% correct background recognition. In this sample set, the algorithm achieves 91, 8.8, and 0.2% full, partial, and no background removal, respectively. Most importantly, no valid data were removed from any of these images. We observe that the percentage of full background removal is less than that of correct recognition. This means that even though the recognition is correct, several built-in checking mechanisms prevent the removal of background with certain degrees of uncertainty. These mechanisms safeguard the irreversible process of deleting valid image data, provide a trade-off between sensitivity and specificity.

VII. CONCLUSIONS

The ABRR method developed is novel to automatically recognize and remove background signals in CR images caused by X-ray collimation during projection radiographic examinations. This method is based on several innovative concepts including: 1) the statistical approach description of intensity distribution features of background signals in CR images, 2) special sampling, filtering, and edge angle recognition methods, 3) continuously adaptive parameter adjustment, and 4) consistent reliability estimation rules.

The results show that ABRR has an excellent performance (99%) of correct recognition for background signals in CR images, a very high ratio (91%) of full background removal, and it is extremely reliable in that no valid image information is removed from this operation even with asymmetrical and complex background signals. Three immediate benefits to CR

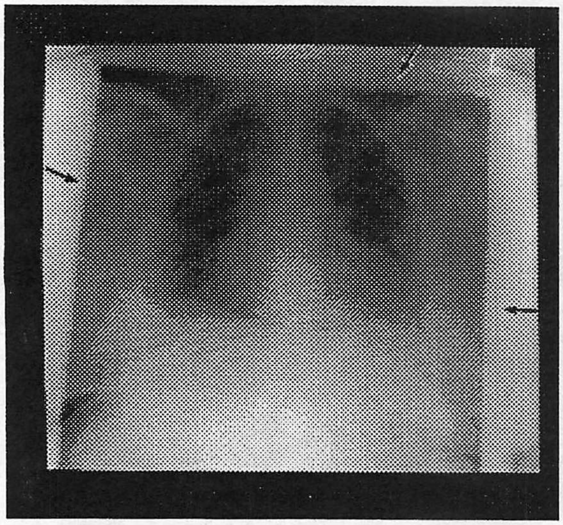

Fig. 18. A CR image with no background removal due to non distinct separation between the image and background pixels, background remains marked by arrows.

images after they are processed with the ABRR method are: 1) the image visual quality for the eye in reading these processed images can be improved greatly, 2) the ABRR images offer an immediate lossless data compression, and 3) the images facilitate some computer-aided diagnosis methods applied to digital projection radiography.

The ABRR is an important step contributing to the implementation of automatic soft copy display in PACS and teleradiology.

ACKNOWLEDGMENT

The authors would like to thank K. Andriole, A. Wong, and S. Wong for acquiring CR images, testing software, and discussing results.

REFERENCES

[1] T. L. Takano, Ed., *Computed Radiography*. Springer-Verlag, 1987, pp. 1–6.

[2] R. C. Gonzalez and R. E. Woods, *Digital Image Processing*. New York: Addision-Wesley, 1993, p. 27.

[3] M. I. Sezan, A. M. Tekalp, and R. Schaetzing, "Automatic anatomically selective image enhancement in digital chest radiography," *IEEE Tran. Med. Imag.*, vol. 8, pp. 154–162, 1989.

[4] R. H. Sherrier and G. A. Johnson, "Regionally adaptive histogram equalization of the chest," *IEEE Trans Med. Imag.*, vol. MI-6, pp. 1–7, 1987.

[5] M. L. Giger, K. Doi, and H. MacMahon, "Automatic detection on nodules in peripheral radiography," *Med. Phys.*, vol. 15, pp. 158–166, 1988.

[6] A. Nakamori, K. Doi, V. Sabeti, and H. MacMahon, "Automated analysis of sizes of heart and lung in digital chest images," *Med. Phys.*, vol. 17, pp. 342–350, 1990.

[7] E. Pieka, M. F. McNitt-Gray, and H. K. Huang, "Computer-assisted phalangeal analysis in skeletal age assessment," *IEEE Trans. Med. Imag.*, vol. 10, pp. 616–620, 1991.

[8] E. Pieka, L. Kaabi, M. L. Kuo, and H. K. Huang, "Feature extraction in carpal-bone analysis," *IEEE Trans. Med. Imag.*, vol. 12, pp. 44–49, 1993.

[9] M. F. McNitt-Gray, H. K. Huang, and J. W. Sayre, "Feature selection in the pattern classification problem of digital chest radiograph segmentation," *IEEE Trans. Med. Imag.*, vol. 14, pp. 537–547, 1994.

[10] M. F. McNitt-Gray, E. Pietka, and H. K. Huang, "Image preprocessing for a picture archiving and communication system," *Invest Radiol.*, vol. 27, pp. 529–535, 1992.

[11] **<Author: Please provide all authors, if available>** H. W. Press *et al.*, *Numerical Recipes in C*, 2nd ed. New York: Cambridge Univ. Press, 1992, pp. 661–666.

Min Invas Ther & Allied Technol 1997: 6: 000–000

Telemedicine and teleradiology technologies and applications

H.K. HUANG

Laboratory of Radiological Informatics, Department of Radiology, School of Medicine, University of California, San Francisco, CA, USA

Summary. Telemedicine and teleradiology hold the key for improving future health care delivery. In this paper we first review current communication and computer technologies used in telemedicine and teleradiology. Five examples in teleradiology applications are given including hospital-integrated picture archiving and communication systems, tele-neuro-imaging, telemammography, university consortium teleradiology service, and teleradiology for second opinion. Parameters important to teleradiology applications like costs, image quality, system reliability, and turn around time are considered. Data security is discussed, including patient confidentiality and image authenticity–which will be a major issue in future teleradiology applications.

Keywords: telemedicine, teleradiology, wide area network

Introduction

Telemedicine and teleradiology have become increasingly important in the USA as the country's health care delivery system gradually changes from fee-for-service to managed, centralized care. During the past several years, we have seen the trend of primary care physicians joining health maintenance organizations (HMOs). HMOs purchase smaller hospitals and form hospital groups under one organizational umbrella. Also, academic institutions form consortia to compete with other local hospitals and HMOs. This consolidation allows the elimination of duplication and the streamlining of health care services among hospitals. As a result, costs are reduced, but at the same time, the number of experts available for service also is decreased. Utilization of telemedicine and teleradiology is a method of cost saving and compensating for the loss of expertise.

One of the most comprehensive reviews in assessing telecommunications in health care was a study reported by the Institute of Medicine, Committee on Evaluating Clinical Applications of Telemedicine in 1996 [1]. In this report, various issues in telemedicine including the technical and human context, policy, and methods of evaluation are discussed in detail. It is an excellent source for future reference.

Telemedicine, in terms of applications, can be simply defined as the delivery of health care using telecommunications and computer technologies. The well-established consultation by means of telephone conversation would not alone qualify as telemedicine since it only uses telecommunication and not computer technology. There are two models in telemedicine and teleradiology: the referring physician or health care provider can either consult an individual specialist at various places through a network, or, can request opinions from a consolidated expert centre where different types of consultation services are provided. In this paper we will concentrate on the expert centre model as this is the trend in the health care delivery system. In the expert centre consultation process, three modes are possible: telediagnosis, teleconsultation, and telemanagement. For telediagnosis, the patient's examination results and imaging studies are done at the referring physician's remote site and data and images are transmitted to the expert centre for diagnosis. The urgency of this telediagnostic service is nominal and turn around can take between 4 h and a day. For teleconsultation, the patient may be still waiting in the examination site, and the referring doctor would like to have a second opinion or a diagnosis result from the expert centre within half an

Correspondence: Professor H.K. Huang, Director, Laboratory of Radiological Informatics, Department of Radiology, School of Medicine, University of California, San Francisco, 530 Parnassus Avenue, San Francisco 94143-0628, USA.

© 1997 Blackwell Science Ltd

hour. For telemanagement, the patient may still be on the gantry or in the examination room at the remote site, and the expert is supposed to provide immediate management care to the patient *in situ*. Because of these three different operational modes, the technology requirements and time constraints in the three expert centre modes are different.

Telemedicine and teleradiology technologies

Teleradiology is a subset of telemedicine dealing with the transmission and display of images in addition to other patient-related information between a remote site and an expert centre. The technology requirement for teleradiology is more stringent than that of general telemedicine, because the former involves large amounts of data.

Telemedicine

Basically, telemedicine without teleradiology requires only very simple technology: a computer gathering all necessary patient information, examination results, diagnostic reports, arranging them in proper order at the referring site, and transmitting them through telecommunication technology to a second computer at the expert centre where this information is displayed as soft copy on the monitor. In modern hospitals or clinics, the information gathering, and the arrangement of the information in proper order can be handled by the hospital information system (HIS). In a private practice group or an individual physician's office, these two steps can be contracted out to a computer application vendor. Another requirement of telemedicine is to design communication protocols for sending this pre-arranged information to the expert centre. This requirement needs special hardware and software components.

Hardware and telecommunication choices vary according to required data thoughput. The hardware component includes a pair of communication boards and/or modems connecting the two computers, one at the referring site and the other at the expert centre through a telephone line. The type and cost of such hardwarre depends on which telecommunication service is selected. Depending upon the transmission speed required, the line can be either a regular telephone line, a DS-0 (Digital Service, 56 Kbits/s, an ISDN (Integrated Service Digital Network, from 56 Kbits/s to 1.544 Mbits/s), or a DS-1 or Private Line (T-1) with 1.544 Mbits/s. The cost of these lines is related to their transmission speed, and the distance between sites. For telemedicine applications without images, a regular telephone line, DS-0, or a single ISDN line would be sufficient. A local ISDN line within the San Francisco Bay area costs between $30–$40 per month.

The software component includes the information display, some quality assurance and communication protocol programs. All software programs can be supported by either the HIS department or from a vendor. Efficient information gathering and selecting proper subsets of information for timely transmission are critical to the success of the telesystem. Once diagnostic results are available from the expert centre, they can be transmitted back to the referring site with the same communication chain or through a standard FAX machine. Figure 1 shows a generic telemedicine communication chain.

Teleradiology

In teleradiology, since it involves images, the technologies required are more demanding. Figure 2 shows a generic schematic of a teleradiology connection between a referring site and an expert centre. At the referring site, imaging devices generate images for teleradiology applications including computed tomography (CT), magnetic resonance imaging (MR), computed radiography (CR), ultrasound (US), nuclear medicine (NM), digital subtraction angiography, digital fluorography (DS, DF), and film digitization. Images from these acquisition devices are first acquired at the examination site and then sent through the communication network to the expert centre if they are already in digital format (Direct Digital). Alternatively, if these images are printed on film, first they need to be digitized by a film digitizer (either with a low resolution vidicon or a high quality laser scanner) at the examination site.

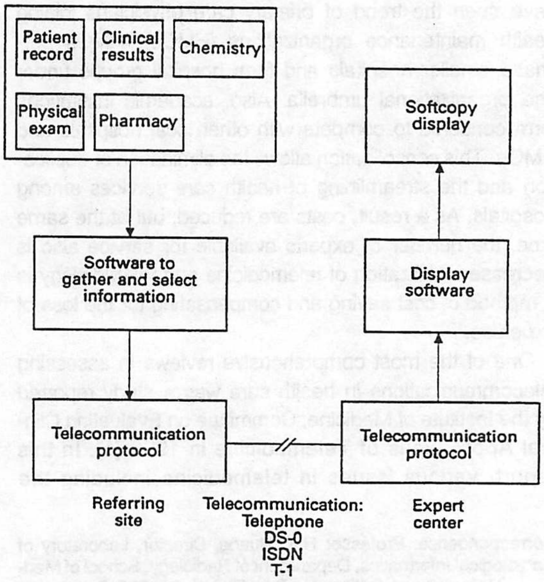

Figure 1. A generic telmedicine communication chain.

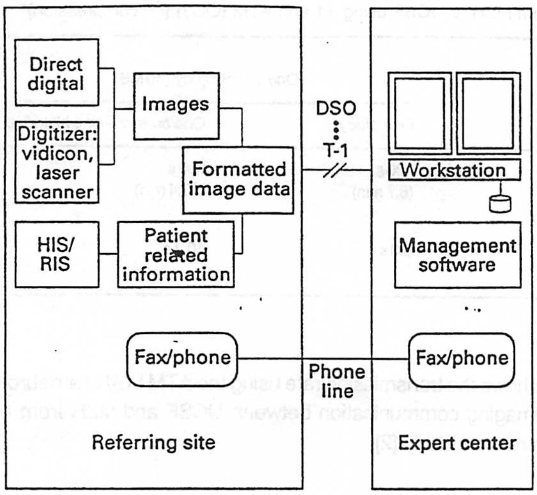

Figure 2. A generic teleradiology set-up.

Unlike telemedicine, at the referring centre a local storage device attached to the computer is needed for storing the transmitted images. The capacity of this device can range from several hundred Mbytes to 5–10 Gbytes depending on the type and number of radiological examinations. For an inexpensive teleradiology system for screening at night or for weekend on-call purposes, a low cost 512-line single monitor workstation would be sufficient for displaying the images. However, for primary diagnosis, high quality 2000 or 1600 line dual-monitor display workstation is needed. This type state-of-the-art workstation usually includes over 2 Gbyte disks for image storage, and can display images and reports within 1–2 s. User-friendly software is required for easy and convenient use by the radiologist and clinician. A 2000 line workstation costs between $50 000 and $60 000, and a 1600 line costs between $30 000 and $40 000.

Teleradiology requires high bandwidth wide area telecommunication networks (WAN) for image communication between the referring site and the expert centre. Regular telephone lines, DS-0 and even 56 Kbits/s. ISDN would be too slow for effective image communication especially in the cases of teleconsultation and telemanagement. T-1 is the preferrred method for teleradiology application.

Table 1 compares the costs of a DS-0 with a T-1 line, between UCSF and Mt. Zion Hospital (MZH), respectively, which are located about two miles (3.3 km) apart in the San Francisco Bay area. The initial investment for the DS-0 is $500. The monthly cost is a $30 fixed fee plus per local call charge. For the T-1 service, the up front investment is $14 500 and the monthly cost is $554 but with no extra charge per call to use the line. The up front investment for the T-1 is much higher than the DS-0. For longer distances, the T-1 monthly charge is very expensive. For example, the monhtly charge between San Francisco and Washington, DC. could be as high as $10 000 per month. However, the transmission rate using the T-1 is 30 times higher than the DS-0. The T-1 line is a very popular choice for teleradiology. Some larger companies lease several T-1 lines from telephone carriers and sub-lease time portions to smaller companies for teleradiology applications.

Table 1. WAN cost using DSO (56 Kbits/s) and T-1 (1.5 Mbits/s) between UCSF and MZH, two miles apart

DSO		T-1	
● Up front investment	$500	● Up front Investment	$14 500
Modems (2)	$400	Modems (2)	$12 000
Installation (2)	$100	Ethernet Converter (2)	
● Monthly fee $30 + per call		T-1 installation	$2 500
(30 times slower than the T-1)		● T-1 monthly charge	$554

The most up-to-date technology standard is the ATM (asynchronous transfer mode, OC-3) which provides a transmission rate of 155 Mbits/s [2]. ATM currently is still very expensive due to the charge imposed by long distance carriers. Table 2 shows the transmission rates between using T-1 and ATM for tele-imaging communications.

One method for increasing the transmission rate of images is to use image compression, where the image data is compressed before the transmission and then reconstructed at the expert centre before being displayed. Lossless compression ratios of 2 : 1 (original size : compressed size) are typical and all image information is restored when the image is decompressed. Lossy image compression, however can potentially degrade the image quality and create some legal issues, especially for the current (unreported) image and mammography [3].

Some current clinical applications

In this section, we describe some current technology clinical applications at the University of California, San Francisco (UCSF).

Hospital-integrated PACS

Technologies used for Picture Archiving and Communication Systems (PACS) are very similar to that of teleradiology [4]. At UCSF, we developed an in-house hospital-integrated HI-PACS connecting four CT scanneers, four MR scanners, two CRs, two film digitizers, one ultrasound (US) PACS module, the hospital information system (HIS), and the radiology information system (RIS). Relevant data from HIS and RIS are automatically incorporated into the

Table 2. Time required to send a 10 MB radiography, 40 MB CT study from MZH to UCSF using T1 and ATM (OC3) (no compression)*

	One radiograph Exam 2K×2.5K×2 byte (10 MB)		One CT of Study (40 MB)	
	One image	Two images	One study	One current + one historical
T1 (1.5 Mbits/s) Realization 100 Kbits/s	100 s (1.6 min)	200 s (3.9 min)	400 s (6.7 min)	800 s (13.4 min)
ATM (155 Mbits/s) Realization 60 Mbits (7.5 MB/s)	1.3 s	2.7 s	5.3 s	10.7 s

* Adopted from Table 3 [2].

PACS using HL7 (Health Seven) data format [5] and the TCP/IP (Transmission control protocol/Internet protocol) communication protocol [6]. Images and related patient data are distributed to 2000 line and 1600 line two-monitor workstations located in both the radiology department and Intensive Care Units (ICUs) [7].

The HI-PACS uses state-of-the-art communication, storage, and software technologies including ATM, multiple storage media, automatic programming, and multilevel process control for a better cost-performance system. The primary PACS local area network (LAN) is the 155 Mbits/s OC3 ATM with Ethernet as a back-up. The system connects Mt Zion Hospital (MZH) via an ATM wide area network (WAN) with a T-1 line as the back-up. An ATM connection has also been established between UCSF and San Francisco VA Medical Center (SFVAMC). The ATM connections between UCSF, MZH, and SFVAMC were supported through a HPCC (High Performance Computing and Communication) contract from the National Library of Medicine, and a grant from CalREN (California Research and Education Network) of Pacific Bell.

Four teleradiology projects

There are currently four teleradiology projects at UCSF, they are teleneuro-imaging, telemammography, Telequest, and Second Opinion.

Tele-neuro-imaging. In April 1994 we started a tele-neuro-imaging project funded by the CalREN and HPCC. This project transmits direct digital neuro-images from one CT and one MR scanner at MZH through the ATM WAN. Images go through the HI-PACS at UCSF and are distributed to two 2000 line two-monitor workstations located at the in- and outpatient neuro reading areas. This tele-neuro-imaging application has been on-line since early 1995. All neuro-images from MZH are now read from these two workstations. We have documented the cost saving [8] and improvement of health care in terms of turn around time [9] with the teleradiology service. Table 2 shows the transmission rate using the ATM WAN for neuro-imaging communication between UCSF and MZH from a previous study [2].

Telemammography. Among other technologies developed for improving the diagnostic value of mammography, telemammography emerges as a primary candidate because it can alleviate the shortage of trained mammographers for mass screening. In July 1995 we started a telemammography project funded by the California Breast Research Program, and the US Army Medical Research and Development Command. In this project, the expert centre is MZH, where the breast imaging section is located, and the ambulatory care center (ACC) at UCSF is the referring site. A full-field direct digital mammography (FFDDM) system which can generate a 3100×3870×12 bit digital mammogram has been installed at MZH. The images are displayed on a 2500 line two-monitor workstation specially designed for the digital mammogram [10]. Since mammography requires very high spatial resolution, we first tested the system with 25 teaching cases read by over 20 radiologists and residents. They were then asked for their opinions of the digital display on both image quality and the system's ease-of-use. The responses were overwhelming positive [11]. We are in the second phase of the project connecting the telemammography system between these two sites with the ATM WAN. The third phase is to install the second FFDDM at ACC. The study is expected to extend until the end of 1999. Figure 3 shows the concept of using the telemammography for telediagnosis, teleconsultation, and telemanagement between the ACC at UCSF and MZH. The ultimate goal is to validate a standard telemammography operating procedure involving the real-time off-site management and interpretation of a community-based general radiologist mammography practice by mammography specialists.

Telequest. A commercial organization named Telequest was formed by a university consortium which provides a

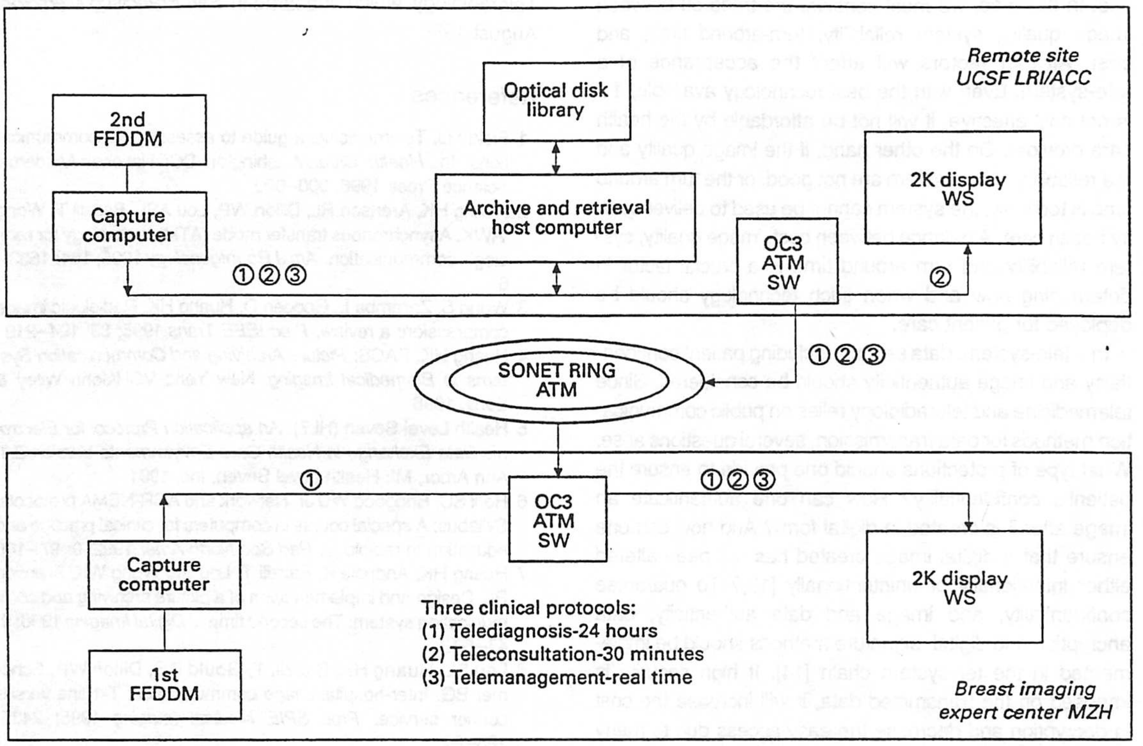

Figure 3. A telemammography system being developed for telediagnosis, teleconsultation, and telemanagement. The expert site is located at the breast imaging centre, MZH, and the remote site is at ACC, UCSF. (1) Telediagnosis: Images sent from FFDDM at MZH or ACC to 2K WS at MZH for interpretation. (2) Teleconsultation: Images sent from FFDDM at ACC to 2K WSs at both MZH and ACC. Referring physician at ACC and expert at MZH uses the WSs for consultation. (3) Telemanagement: Images sent from FFDDM at ACC to 2K WS at MZH. Expert at MZH telemanages the patient who is still at ACC based on the reading.

turn-key teleradiology operation for the customer (e.g., an imaging centre, a HMO, etc.) to transmit images to an imaging expert centre belonging to the consortium for reading [1,12]. Telequest handles all the marketing, service, communication connections, billing, and management. At the customer site, Telequest provides a turn-key operation, assists the site to interface with the radiology information system and the image acquisition devices, and provides the customer site around-the-clock service coverage. The communication connection is from a third party vendor. At the expert centre, a 1600 line workstation is used for the reading, and a rapid turn-around report is provided with a FAX or telephone conversation. Currently, our radiologists are reading tele-images for a Telequest customer from an Imaging Center in Ohio.

Teleradiology service for second opinion. [12] Second Opinion is an Israel-based health insurance company which sells an add-on benefit to its policy holders. The add-on subscriber has the right to request a second opinion on an existing medical diagnosis from UCSF at his/her own expense. The current enrollment of this add-on policy is about 800 000 in a country of 5 million people. Second Opinion consultation provides patients in a country where experts are in great demand with an easy access to a premier medical centre in the United States for consultation. From the policy holder's viewpoint, a minimal add-on cost on top of an existing health insurance policy is a small amount to pay for the peace of mind gained from a second opinion consultation if necessary.

The physical communication connection between the customer and expert site is through international ISDN lines. Images from an Israeli site are digitized and sent to UCSF through these ISDN lines. Radiologists at UCSF read the tele-images with a 1600 line two-monitor workstation.

Discussion

Technologies needed for both telemedicine and teleradiology are mature now and ready for deployment in clinical use. In doing so, we must consider the trade-off between image quality, system reliability, turn-around time, and cost. All four factors will affect the acceptance of a tele-system. Even with the best technology available, if it is not cost-effective, it will not be affordable by the health care provider. On the other hand, if the image quality and the reliability of the system are not good, or the turn around time is too slow, the system cannot be used to deliver quality health care. A balance between cost, image quality, system reliability and turn around time is a crucial factor in determining how and when such technology should be deployed for patient care.

In a tele-system, data security including patient confidentiality and image authenticity should be considered. Since telemedicine and teleradiology relies on public communication methods for data transmission, several questions arise. What type of protections should one provide to ensure the patient's confidentiality? How can one authenticate an image after it is created in digital form? And how can one ensure that a digital image created has not been altered either intentionally or unintentionally [13]? To guarantee confidentiality, and image and data authenticity, data encryption and digital signature methods should be implemented in the telesystem chain [14]. If high security is imposed on the transmitted data, it will increase the cost in decryption and decrease the easy access due to many layers of passwords. The trade-off between cost and performance, confidentiality and reliability will become a major future debatable socio-economic issue in telemedicine and teleradiology. We foresee a trend to integrate telemedicine and teleradiology as an important component into the health care delivery system.

Acknowledgments

This work is partially supported by the National Library of Medicine Contract No. N01-LM-6-3547, and the US Army Medical Research Materiel Command Contract No. DAMD-96-C-6111. The content of this paper is an extension of the author's short article 'Telemedicine and Teleradiology' which appeared in *San Francisco Medicine*, August 1996.

References

1 Field MJ. Telemedicine: a guide to assessing telecommunications. In: *Health Care*. Washington DC: National Academic Science Press 1996: 000–000

2 Huang HK, Arenson RL, Dillon WP, Lou ASL, Bazzill T, Wong AWK. Asynchronous transfer mode (ATM) technology for radiologic communication. *Am J Roentgenology* 1995; **164: 1533–6**

3 Wong S, Zaremba L, Gooden D, Huang HK. Radiologic image compression: a review. *Proc IEEE Trans* 1995; **83: 194–219**

4 Huang HK. PACS: *Picture Archiving and Communication Systems in Biomedical Imaging*. New York: VCH/John Wiley & Sons, 1996

5 Health Level Seven (HL7). *An application Protocol for Electronic Data Exchange in Health Care Environments Version 2.1*. Ann Arbor, MI: Health Level Seven, Inc. 1991

6 Horii SC, Bridgood WD Jr. Network and ACR-NEMA protocols. Syllabus: A special course in computers for clinical practice and education in radiology. *Rad Soc North Amer* 1992; **0: 97–106**

7 Huang HK, Andriole K, Bazzill T, Lou SL, Wong WK, Arenson RL. Design and implementation of a picture archiving and communication system: The second time. *J Digital Imaging* 1996; **9: 47–59**

8 Lou SL, Huang HK, Bazzill T, Gould RG, Dillon WP, Schomer BG. Inter-hospital image communication: T-1 line versus courier service. *Proc SPIE Medical Imaging* 1995; **2435: 188–94**

9 Huang HK, Wong AWK, Lou SL, Bazzill TM, *et al*. Clinical experience with a second generation PACS. *J Digital Imaging* 1996; **9: 151–166**

10 Lou SL, Sickles E, Huang HK, Cao F, Hoogstrate D, Jahangiri M. Digital mammography: preliminary. *Proc SPIE Med Imaging* 1997 (in press)

11 Moskowitz MJ, Wang J, Allen JD, Huang HK, Sickles EA, Allen J *et al*. High-resolution display system for mammograms. *Proc SPIE Medical Imaging* 1995; **2431: 447–54**

12 Huang HK. Teleradiology technologies and some service models. *Comp Med Imag Graph* 1996; **20: 59–68**

13 Mitchell W. When is seeing believing? *Sci American* 1994; **270: 68–73**

14 Wong STC, Abundo M, Huang HK. Authenticity techniques for PACS images and records. *Proc SPIE Medical Imaging* 1995; **2435: 68–79**

11 AS T1446.
P04164.

(P.)

MED. INFORM. (1997), VOL. 00, NO. 0, 000–000 100135

Medical image informatics infrastructure design and applications

H. K. HUANG†, S. T. C. WONG† and E. PIETKA†‡
† Laboratory for Radiological Informatics, Department of Radiology, University of California, San Francisco, California 94143-0628, USA
‡ University of Silesia, School of Medicine, Department of Nuclear Medicine, ul.Medykow 18, PL-40 752, Katowice, Poland

Abstract. Picture archiving and communication systems (PACS) is a system integration of multimodality images and health information systems designed for improving the operation of a radiology department. As it evolves, PACS becomes a hospital image document management system with a voluminous image and related data file repository. A medical image informatics infrastructure can be designed to take advantage of existing data, providing PACS with add-on value for health care service, research, and education. A medical image informatics infrastructure (MIII) consists of the following components: medical images and associated data (including PACS database), image processing, data/knowledge base management, visualization, graphic user interface, communication networking, and application oriented software. This paper describes these components and their logical connection, and illustrates some applications based on the concept of the MIII.

Keywords: Picture archiving and communication systems (PACS); Image informatics; Image content retrieval; Infrastructure design.

1. Introduction

Picture archiving and communication systems (PACS) is a concept perceived in the early 1980s by the radiology community as a future method of practicing radiology. PACS consists of image acquisition devices, storage archiving units, display workstations, computer processors, and database management systems. During the past ten years, PACS have been installed throughout the world for tailored special clinical applications as well as for large-scale, hospital-wide operations [1]. The result is the accumulation of an enormous volume of images and related data allowing for new levels of clinical, research, and education applications which could not be performed before due to insufficient data. A medical image informatics infrastructure (MIII) is a design taking advantage of these voluminous data generated by PACS for facilitating the aforementioned applications.

2. Medical image informatics infrastructure (MIII) architecture and components

Medical image informatics infrastructure (MIII) comprises the following components: medical images and associated data (including PACS database), image processing, data/knowledge base management, visualization, graphic user interface, communication networking, and application oriented software. These components

0307–7640/97 $12·00 © 1997 Taylor & Francis Ltd

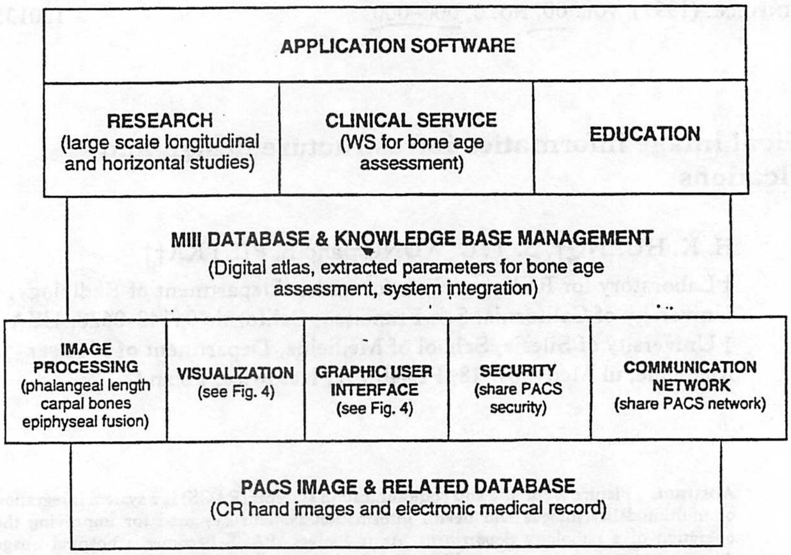
APPLICATION SOFTWARE
RESEARCH (large scale longitudinal and horizontal studies)
CLINICAL SERVICE (WS for bone age assessment)
EDUCATION
MIII DATABASE & KNOWLEDGE BASE MANAGEMENT (Digital atlas, extracted parameters for bone age assessment, system integration)
IMAGE PROCESSING (phalangeal length carpal bones epiphyseal fusion)
VISUALIZATION (see Fig. 4)
GRAPHIC USER INTERFACE (see Fig. 4)
SECURITY (share PACS security)
COMMUNICATION NETWORK (share PACS network)
PACS IMAGE & RELATED DATABASE (CR hand images and electronic medical record)

Figure 1. Medical Image Informatics Infrastructure Components and their logical relationship. The bottom layer is image data and related data from PACS and other databases. The middle two layers are described in §2. The top layer software is application specific. Contents inside (...) is specific for bone age assessment application described in §5.

are logically related as shown in figure 1 and their functions are summarized as follows.

2.1. *PACS and related data*

PACS databases and other related health information systems containing patient demographic data, case history, medical images and corresponding diagnostic reports, and laboratory test results constitute the data source in the MIII. This data is organized and archived with standard data formats and protocols, such as DICOM (Digital Imaging and Communication in Medicine) [2] for image and HL7 (Health Level 7) [3] for text. In addition, controlled health vocabulary can be based on standards for medical identifiers, codes, and messages proposed by the American Medical Informatics Association [4].

2.2. *Image processing*

retrieval mechanism. Its functions include segmentation, region of interest determination, texture analysis, content analysis, morphological operations, and image registration. The output from image processing can be a new image or some features which describe some characteristics of the image. Image processing functions can be performed automatically or interactively on image data from the PACS database by an input server. Data extracted by the image processing functions can be appended to the image data file.

Rom

☐ Image processi
Software allows
Setting up the i
Content indexing
and

2.3. *Database and knowledge base management*

The database and knowledge base management component software has several functions. First, it integrates and organizes PACS image and related data, extracted image features and keywords from image processing, and derives medical heuristics rules and guidelines into a coherent multimedia data model [5]. Second, it supports on-line database management, content-based indexing and retrieval, formatting and distribution for visualization and manipulation. This component can be developed on top of a commercial database engine with add-on application software.

2.4. *Visualization and graphic user interface*

Visualization and graphic user interface are output components. Both components are related to workstation design. Visualization includes 3D rendering, image data fusion, static and dynamic imaging display. Visualization utilizes extracted data from image processing, for example segmentation, enhancement, and shading for output rendering. Visualization can be performed on a standard workstation (WS) or with high performance graphic engines. For low performance WS, the final visualization can be pre-computed and packaged at the WS; with high performance graphic engines, the rendering can be in real-time at the WS. Section 3.2.3 shows an example of a high performance graphic engine used in the MIII.

Graphic user interface (GUI) considers optimization of workstation design for information retrieval and data visualization with minimal effort from the user. A well-designed GUI is essential for effective real-time visualization and image content retrieval. GUI can also be used for extraction of additional parameters for non-standard interactive image analysis.

2.5. *Communication networks*

Communication networks include network hardware and communication protocols required to connect MIII components together. The MIII communication networks can have two architectures: a network of its own with a connection to the PACS's networks, or it can share the communication networks with the PACS. In the former, the connection between the MIII and the PACS networks should be transparent to the users and provide the necessary high speed throughout for the MIII to request PACS images and related data and to distribute results to a user's workstation. In the latter, the MIII should have a logical segment isolated from the PACS networks so that it would not interfere with the PACS daily clinical functions.

2.6. *System integration*

System integration includes system interface and shared data and workspace software. System interface software utilizes existing communication networks and protocols to connect all infrastructure components into an integrated information system. Shared data and workspace software allocates and distributes resources including data, storage space, and workstation to the on-line users.

2.7. *Security*

Security includes data integrity and data access. The former considers image authenticity and the completeness of data. After PACS images have been processed, some validation mechanisms are needed to assure its accuracy, completeness, and authenticity. Data access considers who can access what type of data and when.

Once the aforementioned components are implemented in the MIII, application oriented software can be designed and developed to integrate necessary components for a specific clinical, research, or education application. This provides rapid prototyping and reduces costs required for the development of every application. It is in this application layer component that the user encounters the advantages and power of the MIII.

3. An example of MIII

In this section, we describe the MIII developed in our laboratory based on an existing hospital-integrated PACS.

3.1. *Hospital-integrated (HI) PACS at UCSF*

The HI-PACS at UCSF is an integrated hospital imaging system, the details of which have been described elsewhere [6, 7]. The system consists of a 2·6 terabyte optical disk library as the long term archive, and a two-tier communication network with the ATM (asynchronous transfer mode) technology as the primary [8] and the Ethernet as the secondary network. It interfaces the hospital information system (HIS) and the radiology information system (RIS) with TCP/IP communication protocols and HL7 data format. Various types of workstations are distributed in both the radiology department and intensive care units. Figure 2 shows the architecture and table 1 lists the image acquisition devices and databases connected to the HI-PACS.

(AQ: pls provid
table 1 as it
was missing

3.2. *MIII based on the HI-PACS*

The MIII based on the UCSF HI-PACS includes the components given in §2 as well as some additional special features described in the following.

3.2.1. *Communication networking.* The communication of the HI-PACS consists of a two-tier wide area network (WAN), and local area network (LAN). The WAN connects UCSF, San Francisco VA Medical Center, San Francisco General Hospital, and Mt. Zion Hospital, all in the San Francisco Bay area with a 155 Mbits s^{-1} ATM as the primary and a 1·5 Mbits s^{-1} T-1 as the secondary network. The LAN (see figure 2) consists of a 155 Mbits s^{-1} ATM as the primary and a 10 Mbits s^{-1} Ethernet as the secondary network. The MIII shares these communication networks with the PACS which guarantees high bandwidth image delivery for clinical service, education, and research requirements.

3.2.2. *Content-based image indexing.* The PACS database is designed to retrieve information by artificial keys, such as patient name and hospital ID. This mode of operation is sufficient for traditional radiology operations, but not adequate to fully utilize the image data store for large scale research and clinical applications. Therefore, in the MIII we have been developing a separate database which contains keywords of diagnostic reports, patient history, and imaging sequences, as well as certain features of images for content-based indexing of underlying MR/CT/CR images in the PACS database. As an example, the user can request a search in the PACS database to retrieve only those MR images of a patient which contains tumours with the size over one centimetre. Instead of bringing back all MR images, only those which satisfy the search criterion are retrieved. The content-based image

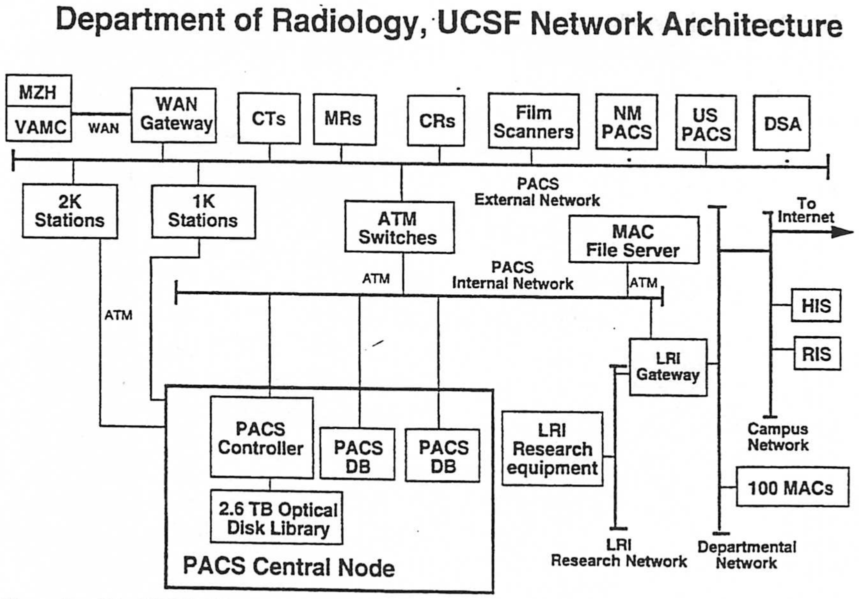

Figure 2. The UCSF HI-PACS infrastructure. The HIS/RIS (middle right) are connected to the infrastructure through the campus and departmental networks. The WAN gateway (top left) connects the infrastructure to Mt. Zion Hospital (MZH) and VA Medical Center (VAMC) through an ATM OC-3 ring. The PACS external network is standard Ethernet. PACS internal network is ATM with Ethernet as a back-up. LRI: Laboratory for Radiological Informatics can access PACS data for large scale clinical studies described in §§4 and 5. Research workstations can access PACS and related data through the ATM research network (bottom middle). Macintosh users can access PACS data through the Mac file server. '------': not yet connected. Adapted from figure 2 of [6].

indexing allows for efficient image storage and retrieval and are used in applications described in §4.

3.2.3. *Volumetric visualization of 3D images.* In visualization, we have been developing a volumetric visualization node as a computing resource for the MIII. The user at a satellite site who wishes to view fusion volumetric images from different imaging modalities, e.g. MRI and CT, in the PACS database from a workstation can use the visualization node. Figure 3 shows the steps to accomplish this task through the central visualization node consisting of a high end graphic computer:

(1) From the image workstation, the request is sent to either the PACS database or the MIII server to retrieve the volumetric image sets.
(2) The image set is sent to the visualization node (Onyx, SGI, Mountain View, CA).
(3) The visualization node performs necessary 3D computation and rendering functions.
(4) Results are sent back to the workstation for viewing after the task is completed.

In step (4), the user can also communicate with the visualization node directly for further instructions or manipulation.

Table 1 missing, ½ page allowed.

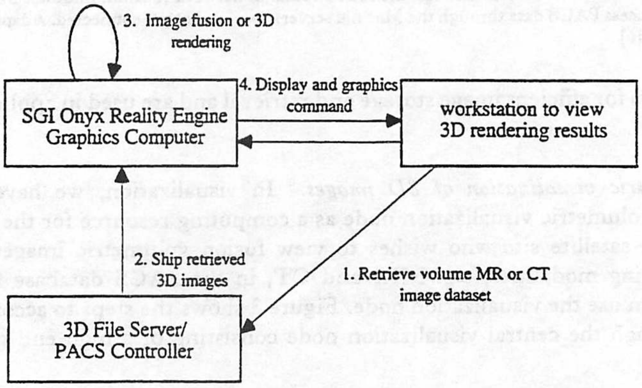
3. Image fusion or 3D rendering
4. Display and graphics command
SGI Onyx Reality Engine Graphics Computer
workstation to view 3D rendering results
2. Ship retrieved 3D images
1. Retrieve volume MR or CT image dataset
3D File Server/ PACS Controller

Figure 3. Visualization of volumetric images using the client–server visualization node for high speed image processing with a SGI Onyx Reality Engine Graphic Computer in the MIII.

4. Some applications using the MIII

In the following, we briefly discuss four on-going projects in our laboratory based on the concept of the MIII. In each of these projects, we describe the utilization, hypothesis, conventional method and its drawback and the MIII approach. We also mention components required in the MIII and their utilization. In §5 we elaborate one of these projects: 'Bone Age Assessment' in greater detail.

4.1. *Bone age assessment with a digital hand atlas* [*9, 10*]

UTILIZATION: Research and clinical service

HYPOTHESIS: Bone age of children can be assessed by comparing a left hand and wrist digital X-ray image with a comprehensive hand digital atlas automatically.

CONVENTIONAL METHOD: Compare a hand X-ray film with an atlas developed in 1930s with a limited number of films. Thus, the conventional method is inaccurate and has bias because of the limited data available for comparison.

I/ ...

MIII APPROACH: Use computed radiography (CR) images and related data from the PACS database to generate a digital atlas. Image processing software is used to extract parameters from CR images for bone age assessment. Visualization engine is used to match the image with extracted parameters with those from the digital atlas. Specific application software based on the match can be developed for bone age assessment.

4.2. *Effectiveness of therapy treatment planning using spiral CT images* [*11*]

UTILIZATION: Research and clinical service

HYPOTHESIS: Progression of lung nodules over time can be tracked and analysed using spiral CT scans. The results can be used to determine the effectiveness of a treatment plan.

CONVENTIONAL METHOD: It is tedious to track down temporal CT images alone with patient's records through time without the PACS database. It is difficult to append the extracted nodule data with the images to perform longitudinal comparison.

MIII APPROACH: Quantitate nodules attributes from spiral CT images with relevant patient records can be obtained from PACS database. Image processing can be used to extract sizes and shapes of lung nodules from longitudinal sequential CT images. MIII database, knowledge base, and special application software organizes the extracted data with therapeutic treatment planning results to determine the effectiveness of the plan.

4.3. *Collaborative consultation with high resolution images* ([*1*] chapter *11*)

UTILIZATION: Clinical service

HYPOTHESIS: Communication and visualization tools can be integrated with PACS database to enable collaborative consultation among radiologists and referring physicians at various sites resulting in a better health care delivery system.

CONVENTIONAL METHOD: Referring physicians use telephones or walk to radiology department for consultation or reviewing images.

MIII APPROACH: Utilize PACS database, communication protocols, user graphic interface, visualization engines, and specific application software for interactive collaborative consultation with high resolution images from PACS as needed.

C/

4.4. *Non-invasive surgical planning using multimodel neuro-images* [12]

UTILIZATION: Research and clinical service

HYPOTHESIS: Multimodality neuro-images can be fused to aid non-invasive planning of epilepsy surgery.

CONVENTIONAL METHOD: It is tedious to assemble necessary neuro-images and related data from various modalities to locate the epileptic site and to determine its extent in the patient. To perform image fusion requires off-line computing and on-line visualization from non-interconnected computing resources.

MIII APPROACH: Use the MIII input server to acquire neuro-images from the PACS database, the image processing software for segmentation and registration, and the visualization engine for 3D rendering. Special application software can be developed to aid non-invasive planning of epilepsy surgery based on derived results.

5. Bone age assessment with a digital hand atlas [9, 10]

BQd

5.1. *Background*

In this section we elaborate the bone age assessment project as a means to illustrate how it utilizes the MIII. Bone age assessment based on a radiological examination of a left hand and wrist is a procedure frequently performed in pediatric patients to evaluate their growth. It is universally used due to the advantage of simplicity, a minimum of radiation exposure, and the availability of multiple ossification centres for evaluation of maturity. The main clinical uses of this examination include: (1) evaluation of growth disorders due to endocrine abnormalities in the thyroid, pituitary, or gonads; (2) determination of growth potential in children with abnormal stature and in children with a various bone dysplasias, syndromes, and nutritional abnormalities; (3) monitoring of therapy effects such as administration of growth or sex hormones; and (4) determination of the best time for intervention to correct scoliosis or limb length discrepancies.

Atlas matching methods currently used in radiological diagnosis compare the diagnosed image with a set of atlas patterns that in most cases includes one hand image pattern per year of age. A reference set of data, developed in the 1930s and published in the Greulich and Pyle atlas [13] is not fully applicable for children of today. It does not reflect the standard development particularly in black girls and white boys. The discrepancy in these two groups can range from 0·4 to 0·9 years.

In order to increase the accuracy of the bone age assessment an upgraded set of reference radiographs need to be collected. For each age group various images should be available. Moreover, the diagnosis ought to be based on quantitative features extracted from the diagnosed image and their comparison with the corresponding values of an upgraded reference set. The goal of the digital atlas is to collect a large standard set of normal hand and wrist radiographs associated with automatically extracted measures which forms a basis for computer-assisted bone age assessment. This project tests three hypotheses:

(1) A reference set of clinically normal radiographs can serve as a digital atlas used in clinical diagnosis, teaching, and research.
(2) Computer-assisted assessment of skeletal development can extract radiological findings from a patient image and allow for their comparison with corresponding values extracted from the digital atlas.
(3) The database system can archive image data and radiological findings and allow their access from clinical workstations for automatic comparison.

5.2. *Methodology*

5.2.1. *Selection of reference images and related data for the digital atlas.* This is the first step in setting up the MIII using images and related data from PACS. Collection of normally developed hand and wrist computed radiography (CR) images from children can be obtained by searching the PACS database. This collection of hand images and related data can be used as a component of the digital atlas.

5.2.2. *Image processing and bone age assessment methodology.* Image processing functions are used to extract attributes from hand images which are related to bone age. These extracted attributes, obtained from three regions of interest, namely phalangeal, carpal, and epiphyseal, include phalangeal length and diameter, number and size of carpal bones, and degree of epiphyseal fusion. Based on these extracted attributes, derived parameters can be computed to compare with those extracted from images with known chronological age. From these comparisons, heuristic rules can be derived to assess bone age of a patient from a CR hand image.

5.2.3. *Database and knowledge base management component.* The database in this component is the computerized or digital hand atlas. The atlas comprised two types of data: CR hand images and related data from various ethnic origin, sex, and age group obtained from PACS, and extracted attributes and derived parameters from these images. The knowledge base consists of heuristic rules for bone age assessment. These rules are derived by correlating the patient chronological age from PACS related data with extracted parameters from the hand image. Software integration permits the digital atlas associating with the knowledge base to allow for bone age assessment.

5.2.4. *User graphic interface and interactive communication.* The user graphic interface and interactive communication is located at the user workstation. Its major function is to assist the user to perform an automatic bone assessment of a CR image from a patient based on the digital atlas. Other functions include requests to the database and the knowledge base to retrieve, compare, manipulate, analyse, and update of related information concerning the patient under consideration. Figure 4 shows a page of the user graphic interface in a SUN SPARC workstation. A user-friendly environment, allowing additional findings to be extracted interactively, is the key to success of such a workstation.

5.2.5. *Operational procedure.* When a patient is required to have the bone age assessed, the first step is to obtain a hand/wrist CR image from the patient. The physician retrieves this image from the PACS database and requests the digital atlas for an automatic bone assessment from the workstation. The system returns the bone age and the physician can request comparisons among patients with similar symptoms and age group. If the user is satisfied with the result, both image and extracted data will be automatically appended in the atlas to increase its statistical power. If the result is doubtful, different queries can be invoked to the atlas for other alternatives. Figure 5 shows the bone age assessment procedure using the digital atlas.

5.2.6. *Clinical evaluation of the digital atlas base bone age assessment.* A digital atlas approach for bone age assessment permits the diagnosis to be standardized and become more objective and reproducible. All findings (radiological and clinical) can be stored to enrich the atlas for future reference. An advantage of using the MIII approach for large scale longitudinal and horizontal clinical study and application is

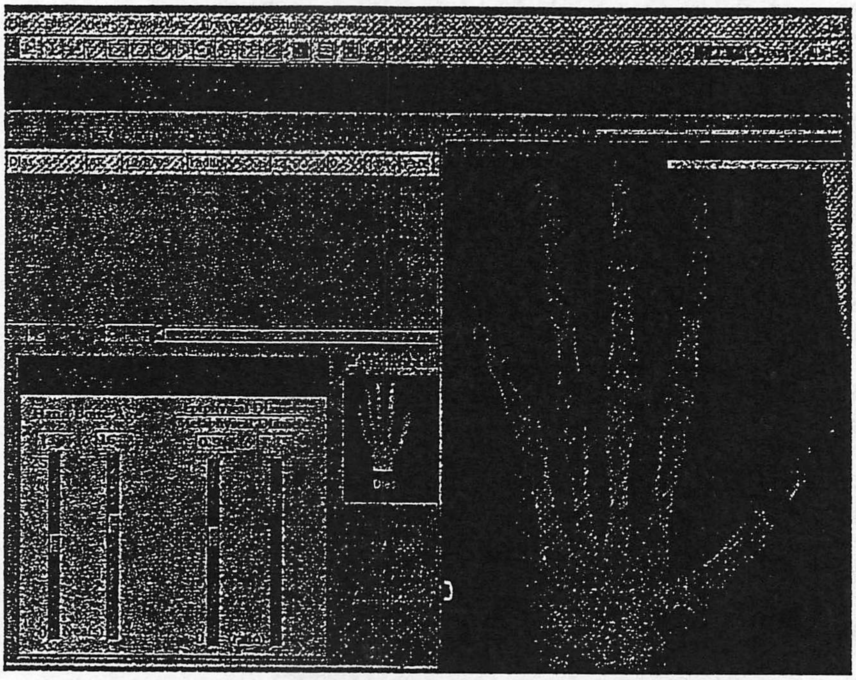

Figure 4. Graphic user interface developed for bone age assessment in a SUN SPARC workstation. Top left window shows five previous records retrieved based on heuristic rules by comparing the current patient image shown in the right window with images in the digital atlas. Bottom left window shows query by image attributes, a form of image content retrieval. Middle thumb nail image is from the first patient record, and the other four are hidden by the large hand image. Bottom middle window partial hidden by the large hand image shows quantitative data extracted from the hand.

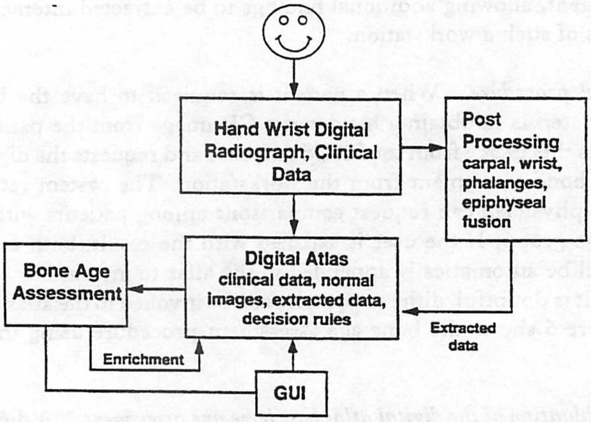
Hand Wrist Digital Radiograph, Clinical Data
Post Processing
carpal, wrist, phalanges, epiphyseal fusion
Digital Atlas
clinical data, normal images, extracted data, decision rules
Bone Age Assessment
Extracted data
Enrichment
GUI

Figure 5. Procedure involved in bone age assessment using a digital atlas.

the ease of developing evaluation criteria and improving the performance of the digital atlas. The accuracy of each assessment can be automatically logged and scored. The results can be used to improve the performance of the atlas.

6. Summary

Implementation of the medical image informatics infrastructure is the next logical step after the PACS is in place. In this paper, we describe the concept of, and the components in, the MIII and their logical relationship. The MIII we discussed here is different from the Health Care Information Infrastructure (HII) adopted by many in the sense that the MIII emphasizes image analysis and content retrieval with image data from the PACS database. Another difference is the design of the graphic user interface in which the MIII relies on image data sets instead of textual information. However, data retrieved from the MIII can be reformatted to become part of the Health Care Information Infrastructure.

We also give four examples to illustrate how the MIII can be used for various applications in research, education, and clinical service. With the MIII, we can advance our biomedical knowledge to new levels of application in large-scale longitudinal and horizontal clinical studies, and to initiate novel research and education programs. All these would result in a better health care delivery system.

Acknowledgement

This work is partially supported by the National Library of Medicine under the HPCC Program: Contract No. N01-LM-4-3508 and N01-LM-6-3547, and the NIH Grant No. R01 LM06270.

References

1. Huang, H. K., 1996, *PACS—Picture Archiving and Communication Systems in Biomedical Imaging* (New York: VCH/Wiley & Sons).
2. ACR/NEMA, 1994, Digital Imaging and Communications in Medicine Standard (DICOM), (Washington, DC: ACR/NEMA.
3. Health Level Seven Inc., 1991, *Health Level Seven: An Application Protocol for Electronic Data Exchange in Healthcare Environments* (Ann Arbor, MI: Health Level Seven Inc.)
4. Board of Directors, American Medical Informatics Association, 1994, Standards for medical identifiers, codes, and messages needed to create an efficient computer-stored medical record. *Journal of American Medical Informatics Association*, 1, 1–7.
5. Wong, S. T. C., and Huang, H. K., 1996, A hospital integrated framework for multimodality image base management. *IEEE Transactions on System, Man and Cybernetics*, 26, 455–469.
6. Huang, H. K., Andriole, K., Bazzill, T., Lou, A. S. L., and Wong, A. W. K., 1996, Design and implementation of PACS—the second time. *Journal of Digital Imaging*, 9, 47–59.
7. Huang, H. K., Wong, A. W. K., Lou, S. L., Bazzill, T. M. *et al.*, 1996, Clinical experience with a second generation PACS. *Journal of Digital Imaging*, 9, 151–166.
8. Huang, H. K., Arenson, R. L., Dillon, W. P. *et al.*, 1995, Asynchronous transfer mode (ATM) technology for radiologic communication. *American Journal of Roentgenology*, 164, 1533–1536.
9. Pietka, E., Kaabi, L., Kuo, M. L., and Huang, H. K., 1993, Feature extraction in carpal bone analysis. *IEEE Transactions on Medical Imaging*, 12, 44–49.
10. Pietka, E., and Huang, H. K., 1996, Epiphyseal fusion assessment based on wavelets decomposition analysis. *Journal of Computerized Medical Imaging & Graphics*, 19, 465–472.
11. Zhu, X. M., Lee, K. N., and Levin, D. L., 1996, Temporal image database design for outcome analysis. *Journal of Computerized Medical Imaging & Graphics*, 20, 347–356.
12. Wong, S. T. C., Soo Hoo, K., and Knowlton, R. C., 1996, Use of image coregistration and visualization techniques to study relationships between MEG neurophysiology and FDG-PET metabolism in epilepsy imaging. *Proceedings of Medical Imaging, SPIE*, 2709, 280–289.
13. Greulich, W. W., and Pyle, S. I., 1959, *Radiographic Atlas of Skeletal Development of Hand Wrist* (Stanford, CA: Stanford University Press).

(Au: et al in full please)

Pergamon

Computerized Medical Imaging and Graphics, Vol. 21, No. 5, pp. 000-000, 1997
© 1997 Elsevier Science Ltd. All rights reserved
Printed in Great Britain
0895-6111/97 $17.00 + .00

PII: S0895-6111(97)00029-3

NEURORADIOLOGY WORKSTATION READING IN AN INTER-HOSPITAL ENVIRONMENT: A NINETEEN MONTH STUDY

H. K. Huang,* S. L. Lou and William P. Dillon
Department of Radiology, University of California, San Francisco, 530 Parnassus Ave., San Francisco, CA 94143-0628, U.S.A.

(*Received* 12 *May* 1997)

Abstract—Two workstations (WS) each with two, 2500 line display monitors were installed in the in-patient and the out-patient neuroradiology reading areas for inter-hospital workstation readings. These WSs are part of the display component of a hospital-integrated picture archiving and communication system (PACS). Direct digital neuro images from 10 CT and MR scanners located at various buildings from two medical centers are first transmitted to the PACS database and then distributed to these two WSs automatically. This paper attempts to answer two questions. First, do the WSs facilitate neuroradiology operation? Second, does it cost less for preparing WS reading than that for the traditional film reading?

Two parameters, the "time required before images become available for reading after the examination" and a "workstation utilization index" were derived as a means for answering these two questions. Nineteen months of clinical data were collected and analyzed. The results demonstrate that the workstation utilization index goes up from 40% in September 1994 when the WS was first introduced to over 80% in March 1996. This upward trend substantiates the hypothesis that these WSs do facilitate the neuroradiology operation. The derived results also exhibit that it costs much less to prepare images for WS reading than for film reading. Other indirect results derived from this study including the WS utilization hours, WS functions used, and the time duration of each WS session are also presented. © 1997 Elsevier Science Ltd

Key Words: picture archiving and communication system (PACS), teleradiology, softcopy reading, display workstation

INTRODUCTION

In March 1994, we installed a hospital integrated picture archiving and communication system (PACS) infrastructure which provides intra-hospital as well as inter-hospital digital image communication and management (1,2). For inter-hospital communication between the main campus (UCSF Medical Center) and the Mt Zion Medical Center (MZH), 2 km apart, a two-tier communication network with the 155 Mbits/sec ATM (asynchronous transfer mode) (3) as the primary and the T-1 line as the secondary is used. Currently, five MR and five CT scanners (CT: 3 GE Spiral, Milwaukee, WI; 1 GE 9800 Quick; 1 Imatron, South San Francisco, CA; MR: 4 GE Signa 5X, 1 Siemens Vision, Erlangen, Germany) located at different buildings of both medical centers have been digitally connected to the PACS network for clinical application. The image formats used are either the American College of Radiology/National Electrical Manufacturers' Association (ACR/NEMA) 2.0 or the DICOM 3.0 (4,5) In addition, data from the hospital information system (HIS) and the radiology information system (RIS) are also available in the PACS network.

The neuroradiology section with five neuroradiologists and five fellows provides clinical service for both radiology departments at the two campuses. At UCSF's neuroradiology section, two 2K workstations (WS), one in the in-patient reading area, and the second in the out-patient reading area were deployed in September 1994, and May 1995, respectively.

The two reading areas are located in two different buildings across the street from each other. Both workstations have an identical database, each with a local storage for more than one week of all current neuro CT and MR studies performed at both UCSF and MZH, as well as some comparison examinations.

The neuroradiology section is currently running a dual reading system with both film alternators and workstation display. Neuroradiologists are free to use either display mode or both for their daily clinical practice. This paper describes our 2 year experience of using these two workstations for inter-hospital neuroradiology workstation reading.

---

*Author to whom correspondence should be addressed.

MARKED SET

METHODS

Although workstation viewing can have various impacts to the operation in a radiology department, the objectives of this paper is to focus on two questions: (1) Do the two workstations placed in the neuroradiology in-patient and out-patient reading areas facilitate the inter-hospital reading? (2) Does the inter-hospital reading of images performed at MZH from UCSF save operational costs?

Two parameters

Answers to question 1 can be complex because the word "facilitate" can be interpreted differently. For this reason, we choose two parameters as a measure of "facilitation". The first parameter T is the "time required before images become available for viewing after the examination" (6,7). This parameter can be used to measure when images will become available for film and workstation readings.

The second parameter called "**workstation utilization index**" is defined as the percentage of neuro examinations performed which are read via the workstation. To measure this parameter, we select a passive approach which is to allow neuroradiologists to choose either the film or the workstation they prefer to read a case. If the workstation is used, then relevant data needed to compute this index are recorded automatically and will count as one entry even though films of the same patient may also be used at a certain time during the diagnostic process. Since both the film and the workstation reading are available and the neuroradiologists are free to select the reading method for their convenience, a steadily increase of workstation usage through time means that neuroradiologists find the WS useful and are using them more frequently. This upward trend can be interpreted as a "facilitation" of the neuroradiology section operation.

In doing this analysis, some by-products of the WS utilization can also be generated. These include user habits, WS functions utilization frequency, and a "**library search index**" defined as the total number of times the user looks for the patient's historical images while current images are being reviewed from the WS. This index can be computed by dividing the total number of "Library Search" functions requested by the total number of WS usage. This index can also be used as a measure of "facilitation" of the neuroradiology operation.

The parameter T is also used to compute the costs required to prepare images obtained from MZH for interpretation by neuroradiologists at UCSF as a means to answer the second question. Note that we are not attempting to compute the cost effectiveness which is a very difficult parameter to measure (8–10). Instead we try to estimate whether preparing for the workstation reading actually costs less than the film reading, assuming both systems have already been in place. In doing so, we focus on the weekend and evening examinations since these periods are most problematic in the radiology operation due to the shortage of personnel.

Neuroradiology service at MZH

At MZH, there is an active neuroradiology service performing from 15–20 CT/MR cases per day and 1–4 CT scans per night from the emergency room. A neuroradiology fellow and attending provide coverage during the day until approximately 6:00 pm. During this time, all examinations are also transmitted to UCSF over read by other experts within the neuroradiology section. The neuroradiology faculty from UCSF rotate to MZH on a daily basis either by shuttle or by personal automobile.

Emergency call at MZH is provided on a first line base by the UCSF resident on call who is physically at UCSF. Before the workstations were installed, films were made after the scan and were delivered to UCSF by the technologist (courier service) for the on-call resident to read. After the installation of the WSs, the resident reviews emergency cases done with the two WSs, a verbal and written report are then transmitted to the referring physician at MZH.

Image acquisition

Neuroradiology CT and MR images are collected by the PACS acquisition computers automatically during the examination where these images are converted to the ACR/NEMA^ image format (4) and forwarded to a PACS controller (1). The PACS controller organizes these images with other related data from HIS and RIS and creates a new patient folder or inserts them into an existing folder. The folder is transmitted to both workstations (WS) in the in-patient and the out-patient reading area. On average, the folder is available at the WSs within half an hour after the examination is completed.

^ or DICOM

^ 35

Display workstations

The 2K WS is based on a SUN SPARCserver 470 computer (Mountain View, CA) two 2500 line monitors (UHR-4820P MegaScan display system, AVP, Littleton, MA) for images, and a text monitor for patient and study directories. Each station has a local parallel transfer disk with 5.2 gigabyte storage ok

and

which can display a page (20 512 line CT or MR) of images in 1.5 s (Storage Concepts, Irvine, CA). All software programs, developed in-house, were written in C programming language, Unix operating system, and X-window user interface (1,6). All current in-patient and out-patient folders are available in the local disk. Each patient folder contains all current images, some historical images, and the directory of all diagnostic reports. The complete patient directory in the local storage is displayed on the text monitor. The user first scrolls the cursor and finds the desired patient by clicking the mouse to activate the "Patient Select" function. If the patient has more than two image sets, clicking the "Image Select1" and "Image Select2" will display the two proper sets on monitors 1 and 2, respectively. It takes approximately 1.5–2.0 s after the selection to display a full page of 16 images on each monitor. There are two functions in the WS allowing a user to retrieve additional images which are not in the local storage from the PACS's 2.6 terabyte optical disk library (ODL), The "Library Search" to look for images from past examinations of the current patient being reviewed, The "Find Patient" for retrieving images of any patient. It takes an average of 30–45 s to retrieve the first image set from the ODL. By clicking the "Report Select" icon, diagnostic reports can be retrieved instantaneously through an interface with the RIS.

The WS also is equipped with easy-to-use real-time simple image processing functions such as cine mode, tile mode, window/level, preset look-up-table, zoom/scroll, and region of interest measurement. Neuroradiologists can use either WS in the in-patient or the out-patient reading area or both at the same time to review or discuss cases.

Operational environment

During the time that data were taken for this study, the operational environment in the Neuroradiology Section can be summarized as follows:

1. All neuro-images from 10 CT and MR scanners from UCSF and Mt Zion Hospital (MZH) were transmitted to the PACS. The PACS distributed all neuro-images regardless of in-patient or out-patient to both WSs. Both WSs had similar equipment, same database, and identical images. There was no such distinction as which WS is the source or the destination.
2. We placed these two WSs, one in the neuro in-patient reading room, and the other in the out-patient reading room, both at UCSF. The reason we put these WSs at two different rooms was not to separate in-patient and out-patient images but was due to the fact that neuroradiologists rotated to these two different areas to perform their duties. WSs at both sites would allow them to review both in- and out-patient images at either site. The out-patient room only opened from 8 am to 6 pm, whereas the in-patient reading room was open 24 h. Therefore, the WS in the in-patient room was used more often than the one in the out-patient area not because of the number difference in in-patient and out-patient examinations, but because of the availability of access time.
3. Neuroradiologists could read both in-patient and out-patient images from either WSs or films, and they had no preference where to read them.
4. MZH had no WS. All images obtained there, either from in-patient or out-patient examinations, were transmitted to the two WSs at UCSF. All MZH neuro-images could be read at both WSs. An attending staff from UCSF was always stationed at MZH during regular working hours where films were used as the primary means for reading. The attending consulted with a sub-specialist at UCSF who could use either WS in the in-patient or out-patient area. All off hour cases were read from UCSF with the two WSs.
5. There was no modality difference in the two WSs. In the database, there was a patient folder for each patient containing all modality images either CT or MR, in- or out-patient exam, performed at MZH or at UCSF, or both of the patient.

Data collection

We collected two types of data as a means to analyze the WS utilization and the operational cost for preparing the film and workstation readings. First, all CT/MR monthly procedures performed at UCSF and MZH from September 1994 to March 1996 were extracted through the RIS. The data were tabulated as monthly neuro CT/MR examinations shown in Fig. 1. These data were used as a baseline for computing the WS utilization index. We implemented a user log program in each WS to automatically record the WS utilization by functions, and user's habit. Data were collected from September 1994 to March 1996 for the in-patient WS, and from May 1995 to March 1996 for the out-patient WS. These data were used for computing the WS utilization index.

Even though we selected a passive approach, we still would like to track if the WS was used for a particular case, how often were the films used in conjunction with the WS? And, for what reason did the users choose not to use the WS. These data were very difficult to obtain on-line and could only be

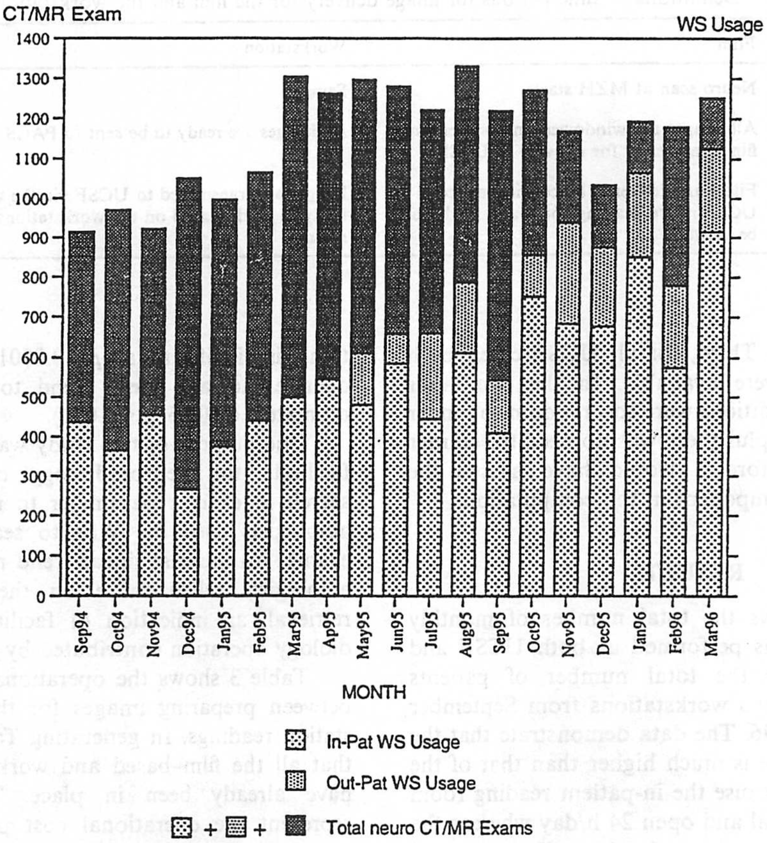

Fig. 1. Total neuro CT/MR examinations and in-patient and out-patient workstation (WS) utilization. The WS utilization index given in Fig. 2 is obtained by (in-patient WS + out-patient WS)/(total neuro CT/MR exams).

collected retrospectively through a survey. A survey form was distributed in July 1996 as a means to answer these questions. Results demonstrate that 85% of the cases performed at MZH during evenings and weekends the radiologists did not read the films again. Other examinations were about 50%. The mode of the choice depended on which one was available first. Most MR studies performed at UCSF which required more than 100 images, films were first used then followed by the WS with the cine mode.

The second type of data is for cost analysis. Since we wanted to compare the cost for preparing for the film reading versus that for the workstation reading, we had to record relevant data pertinent to a period of time when both methods were in use. For this reason, we recorded all neuro CT procedures performed at MZH from 1 February to 31 October 1994 and computed the T for both preparation times. After October 1994, the film reading was used sparsely. Only neuro CT examinations were collected because almost all evening and weekend emergency cases at MZH were CT examinations. Table 1 shows how T was computed for preparing the film and the workstation reading, and Table 2 tabulates the time required for each time period within T. For each time period within T, we can associate a value based on the cost estimate. The result is the operational costs of preparing images for the film and the workstation reading.

There are several reasons why we selected after hours and weekend cases at MZH for the cost analysis. First, this time duration was most suitable for comparing the difference in costs between film reading and softcopy readings because both readings were done at UCSF but the images generated were outside UCSF. Before the installation of the WSs all readings were from film, whereas after the installation all readings were from WSs. This environment is very similar to two controlled periods which enforced the method of reading for each period. Second, daytime cases at MZH were read by an attending staff at MZH using film and consulted by staff at

Table 1. Definitions of time periods for image delivery for the film and the workstation reading

T = from T_0 to T_2	Film	Workstation
T_0	Neuro scan at MZH starts	Same
T_1	All images are windowed and printed onto films and ready for delivery to UCSF	All images are ready to be sent to PACS
T_2	Films are delivered by courier service to UCSF neuro reading room and ready to be viewed	Images are transmitted to UCSF via the wide area network and ready to be displayed on the workstations at the neuro reading rooms

UCSF using WSs. Third, for all UCSF cases, both films and WSs were available. In the two latter situations, the conditions were too random to render significant results, plus there was no need for courier service and therefore it would have missed the communication component in the computation.

RESULTS

Figure 1 shows the total number of monthly neuro examinations performed at both UCSF and MZH as well as the total number of patients reviewed via the two workstations from September 1994 to March 1996. The data demonstrate that the inpatient WS usage is much higher than that of the out-patient WS because the in-patient reading room is inside the hospital and open 24 h/day whereas the outpatient area has an operation hours from 8 am to 6 pm. Figure 2 shows the "Library Search" usage from the two workstations while a patient's images are being reviewed. Figure 3 depicts the WS utilization index and the library search index. The WS utilization index shows that the usage of the WSs moves up steadily from 40% to over 80% (slope estimate 2.7±0.53, $p<0.001$). That is, almost 80% of the neuro cases are reviewed from the two workstations. The Chi-square test for linear trend is significant at $p<0.0001$, demonstrating a definite increase of WS utilization (11). We interpret this upward trend as a facilitation of the neuroradiology operation. The library search index shows that about 50% of the time the neuroradiologist also looks for images from older examinations while current images are being reviewed. The Chi-square test for linear trend is significant at $p<0.0001$, demonstrating a definite increase linear trend to over 50% (slope estimate 1.6±0.56, $p<0.001$).

Table 2. Time required before images become available for reading after the examination Unit: minutes

	T_0-T_1	T_1-T_2	T
Film	6–8	23	29–31
Workstation	10–15	13–19	23–34

One purpose of this study was to see if the WSs facilitate the neuroradiology operation. Library search index is a parameter to measure if neuroradiologists used the WSs to search for historical exams. An increase linear trend means that neuroradiologists relied more on the WSs for image retrieval, an indication of facilitation of neuroradiology operation contributed by the WSs.

Table 3 shows the operational cost comparison between preparing images for the film and workstation readings. In generating Table 3 we assumed that all the film–based and workstation equipment have already been in place. Thus, the figures represent the operational cost per case. We only estimated the costs for examination done during weekends and evenings since a neuroradiologist/fellow is always on site at MZH and no courier service is required during normal operation hours. The courier service is normally done by the technologist who performed the examination. The technologist delivers the films to UCSF from MZH after the examination and charges for the extra time. Although the cost for the T1 line lease is for the entire month, we made the assumption that it was installed as if it was only for the weekend and evening use, which inflates the rate for the workstation preparation cost. For the storage cost estimation, we only computed the cost for producing the films and the cost for storing the images on the optical disk as a long term archive. Other possible costs were ignored. Results from Table 3 demonstrate that the cost for preparing images for weekend and evening workstation reading is substantially less than that for the film reading.

Other results derived from this study include the WS utilization hours, WS functions used, and the time duration of each WS session. For the in-patient WS, it was used almost hourly with two peaks at 8–10 am and 4–5 pm. For the out-patient WS, it was

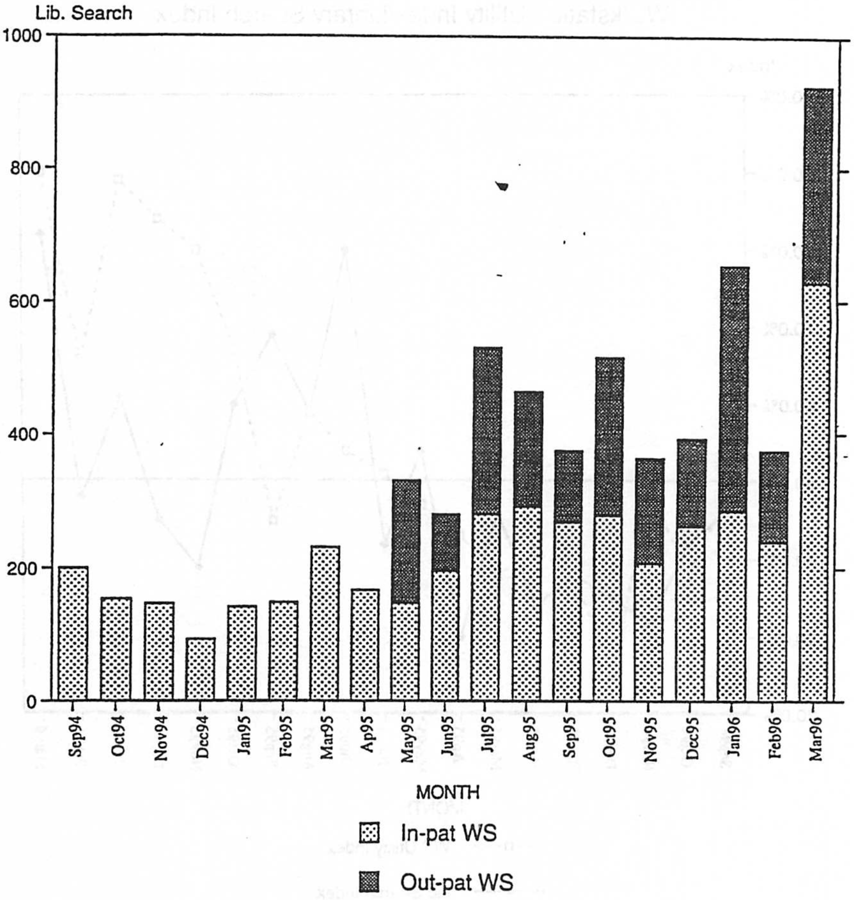

Fig. 2. Total number of Library Search for historical images of the current patient being reviewed.

mostly used from 8 am to 6 pm with two peaks at 10 am and 12 pm. Of the 29 available functions in the WSs, the following seven: "Patient Select", "Image Select", "Zoom and Scroll", "Cine Mode", "Window/Level", "Library Search", and "Sort Patient" were used most often. Statistics collected in August 1995 indicates that for the in-patient and the out-patient WS, these seven functions were used 4196/4410 = 95%, and 867/953 = 91%, respectively. The denominator represents the total number of functions used whereas the numerator is that of the seven functions. To our surprise, "Select Report" was very seldom used even though the WSs can retrieve previous diagnostic reports corresponding to the patient examination being reviewed from the RIS instantaneously. As for the duration of each WS session, both the in- and out-patient WSs exhibit a 0 to 4 min review time.

DISCUSSION

We have installed two workstations, one in the in-patient and the second in the out-patient reading area for neuroradiology applications since September 1994. In this paper we attempt to answer two questions: whether these WSs facilitate neuroradiology operation and if they reduce the reading preparation cost. We derived a workstation utilization index and traced this index for a period of 19 months. This index increases from 40% in September 1994 to over 80% in March 1996 demonstrating that 80% of the examinations were reviewed from these workstations, a true indication of the workstation utilization. A second index called the library search index which shows that about 50% of the time the neuroradiologist uses the WSs to look for images from historical examinations while current images are being reviewed. Based on these two indices, we

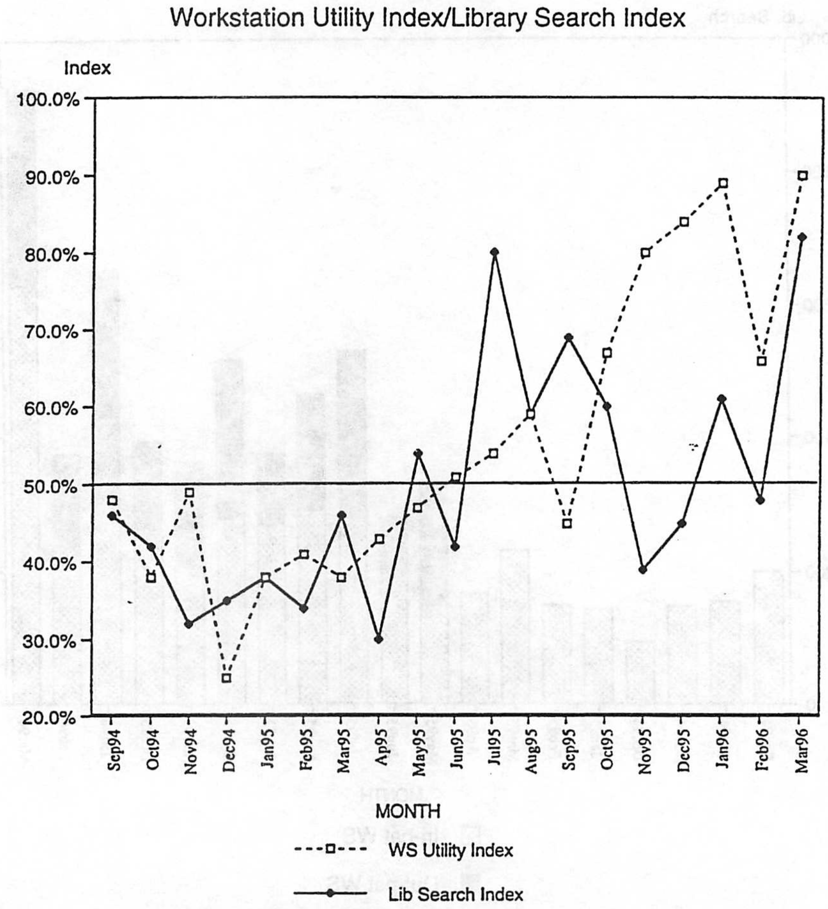

Fig. 3. WS Utilization Index derived from Fig. 1: —□— Library Search Index derived from Figs. 1 and 2, (total Lib Search)/(total WS utilization): —◆—.

conclude that these WSs do facilitate the neuroradiology operation.

In computing the WS utilization index we made the assumption that each time a patient's examination was requested, it would count as one entry. However, we did not consider the fact that the same case might have been reviewed before with the WSs. Thus, the results may only represent the WS utilization with respect to the total number of examinations and not truly represent that 80% of the cases were reviewed by using the WSs. We realized this drawback and have modified the autolog program to trace the number of times a case is reviewed via the WSs. The result of which will be given in a subsequent report.

Table 3 shows the image preparation costs for weekends and evenings. Results demonstrates that the cost to prepare for workstation reading is substantially less than that for the film reading. In making this estimation we had made several assumptions. First, we did not consider the time saved by clinical personnel as a result of the workstation reading. Second, we only took into consideration the weekend and evening operation, other contributing factors during regular hours operation were not considered. We had also ignored many cost factors related to the film-based and digital-based operations as well as the initial investment of the PACS assuming that it has already been in place. This latter assumption may seem unrealistic since the PACS investment is quite substantial (12). However, for most recently opened hospitals (for example, Hammersmith Hospital in England; Baltimore VA Medical Center; Madigan Army Medical Center, Washington; and Vienna Social and Medical Center East (SMZO) (13–16)) and all future health care centers, out-patient facilities, and clinics being planned or under construction now (for example,

Table 3. Image preparation costs for the film and workstation readings (unit: $/case)

	Film	Workstation
Image delivery	12.50(1)	13.50(3)
Storage	10.00(2)	1.00(4)
Total	22.50	14.50

2/h

(1) Courier weekend and evening rate and over time: $22/h ×1.5 Delivery time (Table 2 T1–T2): 23/60 h $22×1.5×23/60 h = $12.50…

(2) Film cost Average 30 images/case on 2 to 4 sheets: $10/case.

(3) Image transmission T1 line lease from phone company $540/month, 40 cases in evenings and weekends/month, $540/40 cases = $13.50/case.

(4) Digital storage optical disk (2600 Mbytes)/$100 = 26 Mbytes/$1. One CT study averages 20 Mbytes or less than $1.

New York Hospital, NY; Saint John's Medical Center at Santa Monica, CA; and Brooks Army Medical Center, TX), hospital administrators have allocated capital budget required for a digital-based operation in the planning process. Thus, it is important for us to derive some actual data from clinical experience to verify that digital-based operations actually save daily operation costs. The weekend and evening operation has been a very difficult problem for the radiology department to handle due to insufficient personnel. Our results demonstrate that workstation reading actually saves operation cost even though the saving of other personnel time due to digital operation had not been included in the estimate. However, we would like to point out that we did not address the cost of how to integrate existing facilities, a relatively common problem in today's health care environment. Such a study requires long term data collection and is being rigorously pursued by the group at University of Pennsylvania (10) and others (8).

During the past 2 years, the WSs in the neuroradiology in- and out-patient reading areas have been in daily clinical use with the utilization index steadily increasing from 40% to 80%. In the past several months, it passes 1000 times per month. Based on this study, we firmly believe that workstation reading does facilitate inter-hospital neuroradiology operation and reduce its cost.

SUMMARY

Picture archiving and communication systems are being installed nationally and internationally. However, it is relatively difficult to measure its impact to health care delivery. This paper attempts to focus on its utility in neuro-imaging. In particular, we try to answer two questions: First, does softcopy reading facilitate the operation in neuro-imaging? Second, what is the difference in cost between preparing softcopy reading versus traditional film reading? Nineteen months of clinical data were collected and analyzed. The results demonstrate that softcopy reading utilization index goes up from 40% in September 1994 when the workstation was first introduced to over 80% in March 1996. Results also exhibit that it costs much less to prepare image for softcopy reading than for film reading.

Acknowledgement—This work has been partially supported by the IBM Almaden Research Center, PHS grant PO1-CA-51198, NLM contract NO1-LM-4-3508, and CalREN grant ATMN-007, Pacific Bell. We would also like to thank Dr James Sayre for the statistical analysis.

1 2

REFERENCES

; Lou, S.L.; Wong, A.W.K.; Arenson, R.L.;

1. Huang, H. K.; Andriole, K.; Bazzill, T. ~~et al.~~ Design and implementation of a PACS: The second time. J. Dig. Imag. 92:1–14; 1996.
2. Huang, H. K.; Wong, A. W. K.; Lou, S. L. ~~et al.~~ Clinical experience with a second-generation hospital-integrated PACS. J. Dig. Imag. 94:1–17; 1996.

; Bazzil. T.; Andr A.; Zhan J.; Wm Lee, J.K.

3. Huang, H. K.; Arenson, R. L.; Dillon, W. P. B. ~~et al.~~ Asynchronous transfer mode (ATM) technology for radiologic communication. AJR 164:1533–1536; 1995.

; Lou, S.L Bazzill, Wong, A.W

4. ACR/NEMA digital imaging and communication standard committee. Digital Imaging and Communications ACR-NEMA 300-1988, Washington, DC: National Electrical Manufacturers Association; 1989.
5. Digital Imaging and Communications in Medicine (DICOM), Part 5 Addendum—Data structures and encoding extensions, 36–43, Committee Draft Version 0.5—December 1994.
6. Lou, S. L.; Huang, H. K.; Arenson, R. L. Workstation design-image manipulation, image set handling, and display issues. Radiologic Clinics North Amer. 34:525–544; 1996.
7. Lou, S. L.; Huang, H. K. Assessment of a neuroradiology PACS in the clinical environment. AJR 159:1321–1327; 1992.
8. Langer, S.; Wang, J. A goal based cost-benefit analysis for film versus filmless radiology departments. J. Dig. Imag. 9:104–112; 1996.
9. Langlotz, C. P.; Even-Shoshan, O.; Seshadri, S. ~~B.~~ S. ~~et al.~~ A methodology for the economic assessment of PACS. SPIE Med. Imag. 2165:584–592; 1994.

Brikman Kishore, S Kundel, H Schwartz, J.S.

10. ~~Kundel, H.L.; Seshadri, S. B.; Langlotz, C. P. *et al.* A prospective study of a PACS: information flow and clinical action in a medical intensive care unit. Radiology XX:XX–yy; 1997.~~
11. Agresti, A. An introduction to categorical data analysis. New York: John Wiley;1996: 34-35.
12. Huang, H. K. PACS for biomedical imaging. New York: VCH–John Wiley;1996: 424–431.
13. Strickland, N. H. Hammersmith PACS: some lessons learned in implementing a filmless hospital. Proceedings 14th Intern. EuroPACS Meeting, Crete, Hellas, 3–5 October 1996; 12–17.
14. Protopapas, Z.; Siegel, E. L.; Reiner, B. I. ~~et al.~~ PACS training for physicians: lessons learned at the Baltimore VA Medical Center. J. Dig. Imag. 9:131–136; 1996.

; Pomeranz S.M.; Pich E.R.; Wiser M.; Hoppe F.J.

15. Smith, D. V.; Smith, S.; Bender, G. N. ~~et al.~~ Evaluation of the medical diagnostic imaging support system based on 2 years of clinical experience. J. Dig. Imag. 8:75–87; 1995.

Carter, J.R.; Kim, ~~Y.~~; Cawthon, M.A.; Leckie, R. Weiser, J.C.; Romlein, J.; Goeringer, F.

16. Mosser, H. M.; Partan, G.; Hruby, W. Clinical routine operation of a filmless radiology department: three year experience. SPIE Med. Imaging 2435:321–327; 1995.

1: Langlotz, C.P.; Kundel, H.L.; Brikman H.M; Redfern, R.R.; Horii, S.C.; Schwartz, J.
The Effect of PACS/CR on Cost of care and length of stay in a medical intensive care unit

About the Author—H.K. HUANG, DSc, FRCR (Hon.), Professor and Vice Chairman, Director of Radiological Informatics Laboratory, Department of Radiology, UCSF with a joint appointment in the UCSF/UC Berkeley Bioengineering Graduate Program. Dr Huang has been working on PACS research and development since 1982. He implemented a PACS at UCLA in 1991, and a second generation PACS at UCSF in 1994. His current research interests are in medical multimedia, high speed medical image transmission, and medical imaging informatics infrastructure design. Dr Huang has published over 180 research papers and co-authored six books, and trained over 50 PhD students and post-doctoral fellows in medical imaging related research during the past 20 years.

About the author—S.L. LOU received a BS degree in Biomedical Engineering from Chung-Yuan Christian University at Taiwan, R.O.C. in 1982 and the PhD degree in Biomedical Physics from University of California at Los Angeles (UCLA) in 1991. He was a visiting assistant professor in the Division of Medical Imaging, Department of Radiological Sciences at UCLA from 1991 to 1992. He is currently an assistant professor in the Laboratory for Radiological Informatics, Department of Radiology, University of California at San Francisco (UCSF). He also holds a joint faculty appointment in the UCSF/UC Berkeley Bio-Engineering Graduate Program. His major research activities in past 10 years have been in design and implementation of Picture Archiving and Communication Systems (PACS), digital communication methodology applied in PACS, image data compression, image mapping techniques, and digital mammogram display enhancement.

About the Author—WILLIAM P. DILLON, MD, completed his residency in diagnostic radiology at the University of Utah in 1982 and a fellowship in Neuroradiology at the University of California San Francisco in 1983 where he has since been a full time faculty member. He is a senior member of the American Society of Neuroradiology (ASNR) is presently Chief of the Section of Neuroradiology and Professor of Radiology, Neurology, and Neurosurgery at UCSF. Dr Dillon has a strong interest in adult neuroradiology as well as head and neck radiology.

Dr Dillon is active in research as well as clinical neuroradiology. He has authored or co-authored more than 100 papers in the medical literature as well as numerous chapters. He has co-edited one textbook on CT of head and neck.

Dr Dillon is a past president of the American Society of Head and Neck Radiology and is presently Treasurer of the ASNR. He has also served the ASNR as a member of the Strategic Planning Committee, the Scientific Program Committee, the Education committee, the Task Force on Manpower and Training, the Training and Standards Committee, and functioned as the liaison of the ASHNR on the Executive Committee of the ASNR. He is a deputy editor of the American Journal of Neuroradiology and serves on the editorial review boards of four other journals.

© 1997 Elsevier Science B.V. All rights reserved.

Technical Issues in Full-Field Direct Digital Telemammography

H.K. Huang[1], S.L. Lou[1], Edward Sickles[2], David Hoogstrate[1],
Mohammad Jahangiri[1], Fei Cao[1], Jun Wang[3]

1. Laboratory for Radiological Informatics, 2. Breast Imaging Section,
3. Now with Philips Research Lab, Palo Alto, CA

Department of Radiology, University of California San Francisco,
530 Parnassus Avenue, Rm. CL-158, San Francisco, CA 94143-0628, USA

1. Introduction

Current attempts at controlling breast cancer concentrate on early detection by means of mass screening, periodic mammography and physical examinations. Ample evidence is now available to indicate that such screening indeed can be effective in lowering the death rate [1]. However, state-of-the-art mammography utilizes film-screen recording systems, which have several technical limitations that reduce its effectiveness: the film gradient must be balanced against the need for wide latitude and detection of microcalcifications. In addition, portrayal of the clarity of the margins of breast masses are reduced due to the presence of film noise in the displayed image, film processing artifacts can degrade the mammographic image, and the day-to-day variability inherent in automated film processors can produce suboptimal image quality. Full-field direct digital mammography promises to overcome most of these problems, at the same time providing additional features not available with standard mammographic imaging[2-5]. Real-time Telemammography adds to these advantages by utilizing expert mammographers (rather than general radiologists) as interpreters of the mammography examinations.

We are in the process of setting up a telemammography system between two campuses at UCSF: the Breast Imaging Section at Mt. Zion Hospital (MZH), the Laboratory for Radiological Informatics (LRI), and the Ambulatory Care Center, Parnassus campus, two miles apart. This paper discusses some technical issues in developing telemammography including full-field direct digital mammography (FFDDM), image compression, high resolution workstations, communication networks, and telemammography protocols.

2. Direct Digital Mammography

2.1. Digital Mammography systems

Currently, there are four manufacturers designing digital mammography systems: Bennett, Lorad, General Electric, and Fischer. Table 1 summaries the current pros and cons of these four systems.

Table 1. Pros and Cons of the four prototype direct digital mammography systems

(1) Bennett (TREX Medical Group, Danbury, CT)

Pros
- Field upgradable to existing film/screen mammo units
- Short exposure times

Cons
- Expensive (for CCDs & Fiber Optic Tapers)
- Dead spaces between modules
- Requires grid for scattered radiation which increases dose to patient
- Bulky package because of CCDs, fiber optics, and electronics

(2) Lorad (TREX Medical Group, Danbury, CT)

Pros
- Inexpensive
- Decreased development time because design of camera is fundamentally the same as their biopsy camera

Cons
- Bulky package because of lens-based design
- Patient motion and discomfort due to long image acquisition time required to step and translate the detector over the entire field of view
- Requires precise mechanical translation of detector and collimator for subsequent image stitching and processing
- Image processing and stitching is a difficult task due to parallax issues

(3) General Electric (Milwaukee, WI)

Pros
- Field upgradable to existing mammo units
- Potentially small package when 50 micron pixel size is achieved (elimination of mechanical translation)

Cons
- Requires precise mechanical translation of detector to achieve an accurate effective 50 micron pixel size and for subsequent image processing
- Expensive technology at this time
- Requires grid for scattered radiation, which increases dose to patient.

(4) Fischer Imaging (Denver, CO)

Pros
- Detector technology is less expensive than Bennett and GE approaches
- Scatter rejection of slot scanner provides improved image quality per unit dose
- Decreased dose for 5cm and greater due to spectral optimization of system

Cons
- Requires precise alignment and mechanical scanning
- Package is bulky, due to CCDs, fiber, and electronics
- Mechanical/aesthetic design of camera cover is difficult due to pendulum scanning approach and necessity for small package
- Dead zone at edges of field of view due to camera width and camera ramp-up time/distance
- X-ray tube heat loading may shorten life of tube
- Increased development time due to ground-up engineering of entire system
- 4.5 s scan time may cause discomfort (motion will not be an issue because slot time is only 200 ms).

2.2 Full-Field Direct Digital Mammography

After carefully evaluating the pros and the cons of these four approaches, we selected the Fischer full-field direct digital mammography system (FFDDM) for our telemammography system for the following reasons[6,7]: the probability and the timing of implementation of a direct digital system in the clinical setting, the track record of the manufacturers in conducting a mammography research and development program, and our past working relationship with the manufacturer. Table 2 summarizes the specifications of the Fischer FFDDM system. Figure 1 shows the prototype unit with the Fischer engineers. As of March, 1997, the first system has been installed in our Breast Imaging Section at MZH connecting to the LRI for clinical evaluation.

Table 2 Specifications of the Fischer FFDDM System

Image Area	221 mm x 270 mm
Detector	Charge-coupled devices (CCD)
Image Scan Time	slot scan, 6.0 secs (nominal)
kV Range	25-45 kVP
Tube Current	200 mA at 45 kVP
Target	Tungsten
Focal Spot Size	0.30 mm (nominal), 0.15 mm (High Res.)
Pixel Size	54 x 54 microns (nominal), 27 x 27 microns (High res.)
Image Matrix	4K x 5K pixels (nominal), 12 bits/pixel
Spatial Resolution	9 lp/mm (nominal), 18 lp/mm (High Res.)
Detective Quantum Eff.	greater than or equal to 50% at f(0)
Scatter-to-Primary	less than or equal to 0.15

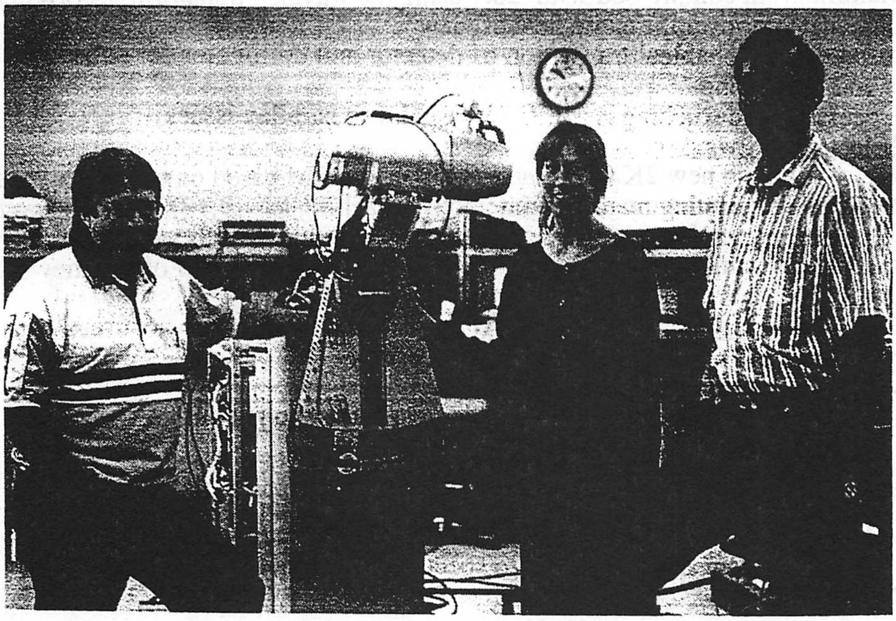

Figure 1. A prototype full-field direct digital mammography unit with Fischer's engineers (left to right: G. Jeffery, M. Piccaro, S. Maydew)

2.3. Image Compression

FFDDM generates a 4K x 5K x 2 = 40 Mbyte image. Obviously, some data compression is needed to reduce its size to facilitate storage and communication. We have developed an on-line structure lossless and a wavelet lossy compression algorithm for this purpose. The on-line lossless method is based on segmentation of the breast from the background and then applying the prediction coding on the breast. The algorithm can be used while data is being acquired from the FFDDM with an average compression ratio of 3 to 4:1[8]. The wavelet lossy method can achieve very high compression ratios without losing diagnostic quality. Figure 2 shows an example with the original image, the 20:1 decompressed image using the wavelet transform and a simple uniform quantization, and an image showing the difference between the two.

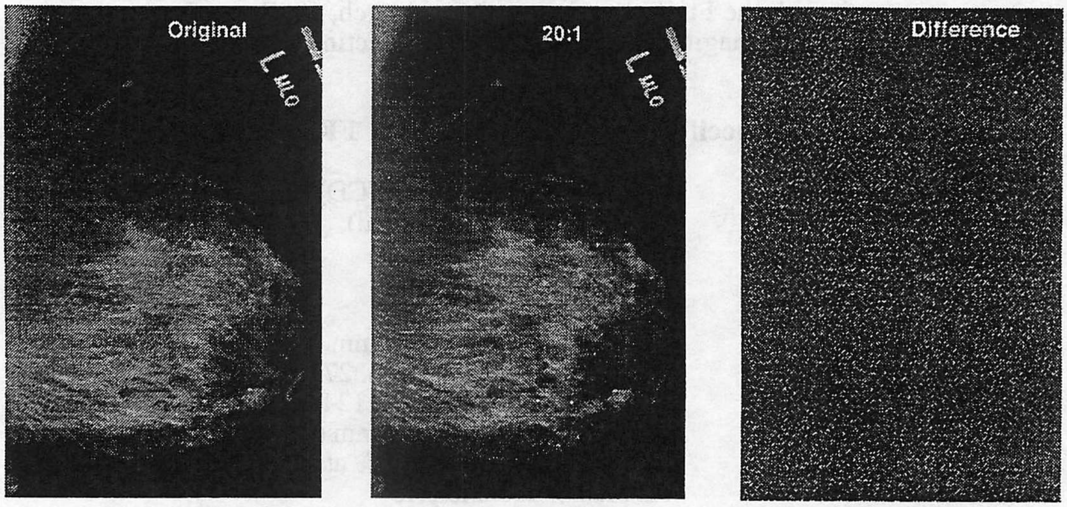

Figure 2. A Mammogram compressed with 20:1 using the wavelet transform. L: original, M: reconstructed, and R: difference image.

2.4. Display Workstation

Workstation Architecture

We are developing a new 2K workstation for the FFDDM based on our experience with an existing 2K system for a mammography interactive teaching file [9,10]. The new system is based on an Ultra Sparc 2 platform (Sun Microsystems, Mountain View, CA) with two DOME MD5/SBX boards (Waltham, Mass). Figure 3 shows the block diagram of this new display system.

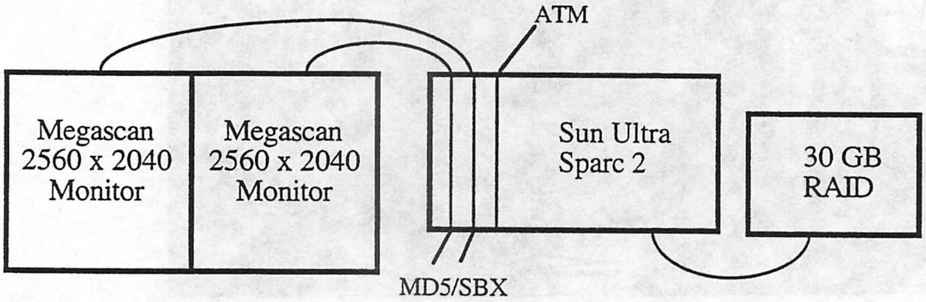

Figure 3. Schematic of the 2K mammography display workstation.

Display format

A standard mammographic examination consists of a craniocaudal and mediolateral oblique view of each breast, a total of four images per examination. For comparison purposes, four images from a prior examination of similar views are also used. Therefore, an optimal display mode should show eight images in proper orientation with one key stroke [11]. We have developed three display formats: one-on-one, two-on-one, and four-on-one monitor, all with scroll and zoom, shown in Figure 4.

3. Telemammography

3.1. Image Communication between MZH and ACC

We use the asynchronous transfer mode (ATM) OC-3 (155 Mbits/sec) technology for both WAN and LAN [12]. Currently we can transmit a 40 Mbyte mammogram in 5.3 seconds (memory-to-memory) with the ATM. With this ATM communication speed, real-time telemammography can be utilized.

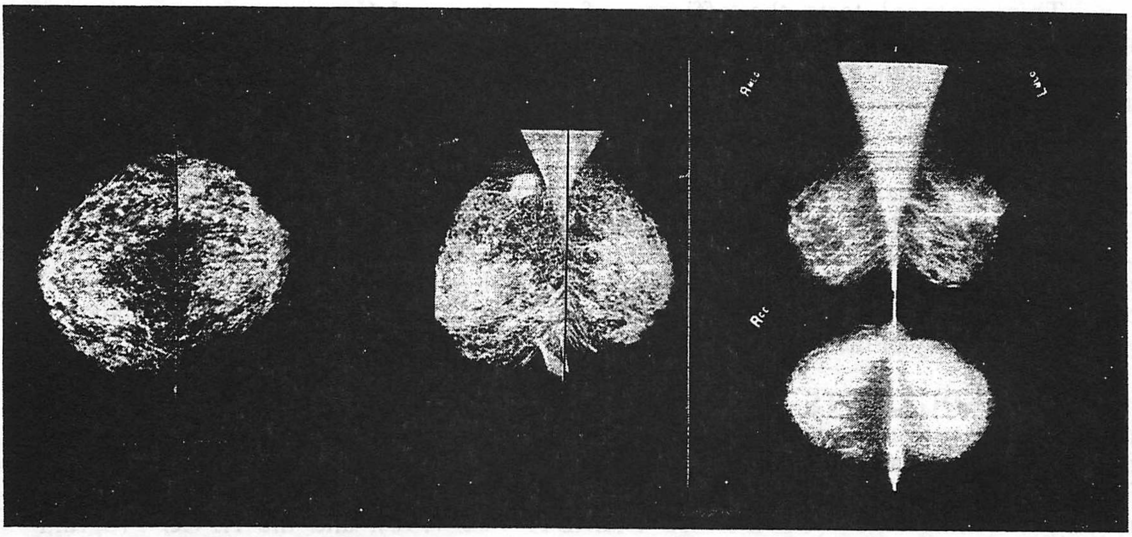

Figure 4. Three types of display format: one-on-one (see Fig. 2 left), two-on-one (left and middle), and four-on-one (left and middle) monitor.

3.2 Concept of an Expert Center

Telemammography is built on the concept of an expert center. Radiologists who work in several different offices or hospitals will be able to monitor and interpret examinations that are carried out in a nearby or even at a distant location or locations. This will permit those radiologists with the greatest interpretive expertise to manage and read in real time **all** mammography examinations, an operational procedure far superior to the alternative of choosing between deferred interpretation by expert readers or real-time interpretation by general radiologists [13,14]. Real time is defined in this context as a very rapid turnaround time between examination and interpretation. In addition, mammography screening in mobile units will be made more efficient, not only by overcoming the need to transport films from the site of examination to the site of interpretation, but also by permitting image interpretation while patients are still available for repeat or additional exposures. Furthermore, telemammography can be used to facilitate second-opinion interpretation, in effect making world-class mammography expertise immediately accessible to community-practice radiologists.

3.3 Telemammography Protocols

We are setting up three protocols: telediagnosis, teleconsultation and telemanagement for evaluating the effectiveness of telemammography.

Telediagnosis

This protocol tests the clinical effectiveness of telemammography from image transmission of full-field direct digital mammograms versus on-site interpretation of conventional film-screen mammograms.

Teleconsultation

This protocol tests the efficacy of remote consultation on **problem cases**. The aim here is to evaluate the ability of telemammography to facilitate real-time consultation between on-site general diagnostic radiologists and remotely-located expert mammographers. Currently, such consultations are tedious, time-consuming, and logistically complex, to the point where they usually are reserved for only the most confusing cases. If successful, teleconsultation should enhance the consultative process such that it becomes much more widely utilized, thereby bringing mammographic interpretive expertise to bear at the community practice level.

Telemanagement

This protocol tests the efficacy of **remote real-time management and interpretation** of mammography examinations. The goal of telemanagement to completely replace the on-site general radiologist with remotely-located expert mammographers is more ambitious than that of teleconsultation.

4. Future Directions

We are in the first phase of a three year comprehensive program in developing the application of telemammography. The current phase is to resolve the technical issues of a telemammography system at MZH discussed in this paper. The second phase is to set up a second FFDDM in the Ambulatory Care Center at UCSF in order to compare the difference in operating environments between the two sites. The last phase is to collect patient data to evaluate the efficacy of the three clinical protocols.

ACKNOWLEDGMENTS

This research is partially supported by the California Breast Cancer Research Program: "Real-Time Telemammography" (IRB-0148), the US Army Medical Research Materiel Command: "Full-field Direct Digital Telemammography" (DAMD-96-C-6111) and "A Digital Breast Imaging Teaching File" (USAMRMC DAMD17-94-J-4196), and the HPCC Program, National Library of Medicine: "A High-Performance Testbed Network for Collaborative Health Care" (N01-LM-4-3508). The authors would like to thank M. Tesic, M. Piccaro, S. Maydew, G. Jeffery and P. Campbell of Fischer Imaging Corporation for their contributions, and James Sayre of UCLA for the experimental design.

REFERENCES

[1] Boring CC, Squires TS, Tong T. 1992. *Cancer Statistics.* CA; 42:19-38.

[2] Sickles EA. 1993. Current Status of Digital Mammography. *In* Proceedings of the 7th International Congress on Senology. Amsterdam, Elsevier.

[3] Nelson MT. 1995. A Clinician's View of Digital Mammography. Proc. 4th Intern. Conf. Imag. Management and Comm. (IMAC 95).

[4] Huang H.K. 1996. Teleradiology Technologies and Some Service Models. *Comp. Med. Imaging & Graphics* 20:59-68.

[5] Fajardo LL, Yoshino MT, Seeley GW, et al. 1990. Detection of Breast Abnormalities on Teleradiology Transmitted Mammograms. *Invest Radiol.* 25: 1111-1115.

[6] Toker E. and M. Piccaro. 1993. Design and Development of a Fiber Optic TDI CCD-Based Slot-Scan Digital Mammography System. *SPIE Proc.*, Med. Imag., 2009.

[7] Tesic M. and Piccaro M.F. 1996. Digital Mammography Scanner: Performance Characteristics and Preliminary Clinical Results. The Institute of Electrical Engineers, *IEEE*, Savoy Place, London WC2R OBL, UK, pp. 3/1-3/7.

[8] Wang J. 1996. "Three-Dimensional Medical Image Compression Using Wavelet Transform and Parallel Computing" , Ph.D. Dissertation. UCLA.

[9] Lou S.L., Huang HK, Breant CM. 1992. A 2K Radiological Image Display Station. *Radiology* 185(P), 146.

[10] Moskowitz M, Wang J., Huang H.K., Sickles E., et al.. 1995. High Resolution Display System for Mammograms. *Proc. SPIE Medical Imaging* 2431-44.

[11] Lou S.L., Sickles E., Wang J., Huang H.K. 1994. A High Resolution Display System for Mammograms. *Radiology,* 193(P), 474.

[12] Huang H.K., Wong W.K., Lou S.L. et al. 1996. Clinical Experience with a Second-Generation Hospital-Integrated PACS. *JDI* 9:151-166.

[13] Sickles E.A., Ominsky S.H., Sollitto R.A., Galvin H.B., Monticciolo D.L. 1990. Medical Audit of a Rapid-throughput Mammography Screening Practice: Methodology and Results of 27,114 Examinations. *Radiology.* 175-323-327.

[14] Sickles E.A. 1992. Quality Assurance: How to Audit your Own Mammography Practice. *Radiol Clin North Am.* 30:265-275.

from RSNA '97

Course No. 725

Update Course on Technical Aspects of Breast Imaging

Arthur G. Haus, Co-director, *Rochester, NY*
Martin J. Yaffe, PhD, Co-director, *Toronto, ON*

B. Telemammography: Technical Aspects

H. K. Huang, DSc, *San Francisco, CA*

Telemammography consists of 4 components: a full-field direct digital mammography (FFDDM) unit, image storage devices, a multiple-monitor high-resolution display workstation, and a high-speed communication network connecting these components.

FFDDM can produce a full-field direct digital 5K × 4K mammogram with 4,096 gray levels in 5 seconds with a dosage equivalent to that of a conventional screen-film image. After the image capture, digital mammograms can be stored in a fast redundant array of inexpensive disks (RAID) for immediate review, or a 2.6-terabyte optical disk library for 50,000 images. Multiple FFDDM images can be displayed on a 2-monitor workstation, with 2.5K × 2K resolution. Display software can display a subsampled 2.5K × 2K image or roam a 5K × 4K image in real time. In networking, an image can be sent from the FFDDM or RAID to the workstation by using the asynchronous transfer mode (ATM OC-3) technology for both local or remote viewing in 5 seconds. The telemammography prototype system at the Breast Imaging Center, UCSF, will be used as an example to illustrate some of these components.

Learning objectives: (1) To learn the basic terminology used in telemammography. (2) To review current available technology. (3) To understand how a telemammography system works. (The telemammography research at UCSF is funded by the U.S. Army Medical Research and Materiel Command, with Fischer Imaging Corp, Denver, Colo, as a collaborative partner.)

C. Computer-aided Diagnosis and Telemammography: Clinical Perspective

Edward A. Sickles, MD, *San Francisco, CA*

To be clinically useful, computer-aided diagnosis (CAD) must outperform double reading by a human observer. Appropriate goals are (1) to reduce the false-negative, false-positive, or both types of false mammographic interpretations by flagging incorrectly interpreted areas on mammograms for rereview and (2) to do this in a user-friendly, rapid-throughput manner that does not require image interpreters to undertake repeated interpretation of the great majority of already-interpreted examinations. The most probable clinical role for CAD is to provide 2nd interpretations to supplement those already provided by radiologists. In the United States, it is highly unlikely that CAD will be used to prescreen mammograms (so that radiologists need only examine films containing computer-detected abnormalities), because neither CAD-software providers nor practicing radiologists will be willing to accept medicolegal responsibility for CAD false-negative cases.

To be clinically useful, telemammography must permit real-time, user-friendly, rapid-throughput soft-copy interpretation of digitally acquired whole-breast mammograms. Potential clinical roles include (1) allowing groups of radiologists who work in different offices/hospitals to monitor and interpret examinations off site, so that those radiologists with greatest interpretive expertise will read all or mostly all examinations and (2) facilitating 2nd-opinion interpretation, by making remote but world-class mammography expertise accessible in real time to community-practice radiologists.

Learning objectives: To learn the clinical requirements for successful computer-aided diagnosis and telemammography, and the potential roles for these techniques in clinical practice. (E.A.S. is the principal investigator of telemammography research funded by the U.S. Army Medical Research and Materiel Command, with Fischer Imaging Corp, Denver, Colo, as a collaborative partner.)

Tuesday Morning • Room S404AB

■ Physics (Image Processing: PACS, Workstations)

In joint sponsorship with the American Association of Physicists in Medicine

PRESIDING: **Douglas M. Tucker, PhD,** Houston, TX

Computer Code: H11 • 1½ hours

706 • 11:33 AM

Full-Field Direct Digital Mammogram (FFDDM) Display Workstation (DWS)

M.I. Jahangiri, MD, MPH, San Francisco, CA • S.L. Lou, PhD • D.R. Hoogstrate, BS • H.K. Huang, DSc

PURPOSE: To efficiently display and manipulate a 4K x 5K x 12bits FFDDM image on a DWS is a challenging task. This study is to identify criteria and methodology that must be taken into account in designing a FFDDM DWS.

METHODS AND MATERIALS: The criteria that should be accomplished in a FFDDM DWS include (1) comparison display, (2) less than 1.5 second per mammogram display performance, (3) real-time on-screen manipulation. Our workstation is configured with a Sun Ultra-2 computer with 512 Mbyte memory, two 2K x 2.5K MegaScan image display monitors, two DOME MD/5SBX display boards, fast/wide SCSI disks and a disk array unit. Our graphic user interface and image display implementation are based on X-Motif windowing system and DOME DIMPL image display and manipulation software library. The workstation features include: (1)configurable display layout-and-format such as 1-on-1, 2-on-1, and 4-on-1, (2)manual window and level, (3) zoom-and-scroll, (4) magnifier glass window, (5)orthogonal angle rotation/mirroring, (6) on-screen image exchange

RESULTS: The workstation is capable of automatically displaying FFDDM images in a designated layout-format which mammographers favor for comparison studies. The workstation takes about 5 seconds and 2.5 seconds to display a 40-Mbyte mammogram from the fast/wide SCSI and from disk array unit respectively. The performance of all the image manipulation features provided is almost real-time.

CONCLUSIONS: With the workstation configuration stated, the criteria (1) and (3) can be accomplished. However, the data input/output throughput of neither the SCSI disk nor the disk array unit is fast enough to meet the requirement to display a 40-Mbytes mammogram in less than 1.5 seconds. We are working to improve this requirement.

Learning Objectives:

1. FFDDM workstation
2. Graphical User Interface for multiple large images.
3. System Logic Design for digital mammography display. [See also *info*RAD exhibit 9440.]

708 • 11:51 AM

Portable DICOM-Compliant PC/NT-based Diagnostic Workstation with Asynchronous Transfer Mode Technology

H. Zhang, MS, San Francisco, CA • G. Lei, MS • A.W. Wong, BS

PURPOSE: To develop a portable DICOM-compliant low-cost PC/NT-based diagnostic workstation (WS) with Asynchronous Transfer Mode (ATM) and Ethernet connectivity to PACS.

MATERIALS AND METHODS: We have developed a WS which is PC-based with a DOME Md2/PCI board, two 1,600 x 1,280 resolution monitors, and an asynchronous transfer mode (ATM) OC-3 communication board. Implemented software includes: (a) a DICOM server, which automatically receives images from the DICOM-compliant PACS Controller; (b) a patient folder manager, which incorporates the local database to group multiple studies from the individual patients; (c) a sophisticated display program with automatic image pre-processing functions, such as window and level pre-set; and (d) a DICOM retriever which allows radiologists to query and retrieve previous studies from the PACS archive.

RESULTS: (1) PC/NT-based WS is lower cost than the UNIX based WS. (2) Integration of DICOM and ATM network into the diagnostic workstation facilitates and speeds up image communication. (3) Image pre-processing functions minimize requirement for image manipulation thereby improving radiologists' efficiency in a time-critical clinical environment.

CONCLUSION: Our PC/NT-based full-functioned WS demonstrates that it can be implemented cost-effectively for PACS applications.

Learning Objectives:

(1) To provide a PC/NT-based architecture of the diagnostic workstation. (2) To report the use of ATM technology in the workstation. (3) To describe the use of DICOM communication protocols in the workstation, and to illustrate the automatic image pre-processing. (4) To show the performance of the workstation. [See also scientific exhibit 0417PH.]

Wednesday Afternoon • Room S404AB

■ Physics (Image Processing: Computed Radiology)

In joint sponsorship with the American Association of Physicists in Medicine

PRESIDING: **Nicholas J. Hangiandreou, PhD,** Rochester, MN
Computer Code: P11 • 1 hour

1254 • 3:15 PM

Automatic Lookup Table (LUT) Adjustment of Computed Radiographic (CR) Images in Picture Archiving and Communication System (PACS) Environment

J. Zhang, PhD, San Francisco, CA • H.K. Huang, DSc

PURPOSE: The lookup table (LUT) of raw CR images need to be adjusted before they are displayed on PACS workstations for diagnosis. Some serious factors affect the determination of an optimal LUT: (1) most CR images have background due to X-ray collimation; (2) some CR images need gradation processing to enhance specific anatomical features; and (3) CRT-based monitors have nonlinear Gamma curves which are different between monitors. This presentation gives an automatic method to adjust the CR image LUT in a PACS environment.

MATERIALS AND METHODS: Our department operates two CR systems (Fuji 9000 and AC-2) generating about 1.2 gigabytes of image data daily. The method involves three steps: (1) use a background recognition and removal algorithm to remove CR image background, then calculate the histogram of the background removed images to determine proper display parameters; (2) extract anatomical information from the image header to carry out gradation processing based on manufacturer provided curves; and (3) use a calibrator to perform a Gamma correction and obtain the linear relationship between the pixel value input and the luminance output of a display workstation.

RESULTS: With his method implemented, we collected data from five consecutive days with 330 CR images from PACS, the LUTs in 91% of the images were properly adjusted with improved visual quality.

CONCLUSIONS: The automatic LUT adjustment improves CR image visual quality and decreases user intervention and quality assurance time.

Learning Objectives:

(1) To illustrate a method to automatically adjust the LUT of a CR image which can improve its visual quality on the monitor. (2) To describe CR image post-processing procedure in a picture archiving and communication system. (3) To report the performance and results of automatic LUT adjustment of CR images in PACS environment.

Friday Morning • Room S405AB

■ Neuroradiology (Epilepsy)

PRESIDING: **Stephen Chan, MD,** New York, NY
Computer Code: U14 • 1½ hours

1661 • 11:42 AM

Relative Accuracy of MR Imaging-hippocampal Volumetry, T2 Relaxometry, 1H-MRSI, and FDG-PET in Lateralizing Temporal Lobe Epilepsy

K. Soo Hoo, Jr, BSc, San Francisco, CA • R.C. Knowlton, MD • S.T. Wong, PhD • K.D. Laxer, MD • R.A. Hawkins, MD, PhD

PURPOSE: To compare the lateralization of MRI hippocampal volumetry (HV), T2 relaxometry, ^{1}H-MRSI, and FDG-PET in patients with unilateral temporal lobe epilepsy (TLE) using computer image registration, interactive segmentation, and quantitation tools. Concordance of lateralization is necessary for surgical resection of epileptogenic focus.

MATERIAL AND METHODS: An electronic image database system has been developed on Unix workstation platforms to support image retrieval, image registration, image processing, and database management capabilities. Patient images are retrieved from PACS and other imaging sources. FDG-PET is automatically registered to the MRI image dataset. Hippocampal volumes of interest are interactively segmented by expert clinicians, and then quantitative measurements of glucose metabolism, hippocampal volume, T2 relaxometry, and ^{1}H-MRSI are calculated and correlated. Twenty-five unilateral temporal lobe epilepsy patients were prospectively studied. T2 relaxometry exams were performed in 13 of the 25 patients. Lateralization of FDG-PET, HV, and ^{1}H-MRSI was compared in 23 patients. All data are analyzed under an interactive 3-D visualization environment.

RESULTS: HV lateralized 65% of 25 patients, NAA/(Cho+Cr) 61%, [NAA] 57%, and FDG-PET 87% . Combining the HV and NAA/(Cho+Cr) results together lateralized 87% of the patients. Of eight patients without hippocampal atrophy, four with NAA/(Cho+Cr), three with [NAA], and six were lateralized with FDG-PET. T2 relaxometry lateralized no patients without hippocampal atrophy. Only hippocampal atrophy correlated with seizure free outcome.

CONCLUSION: The combination of HV and ^{1}H-MRSI lateralized as accurately as PET. Bilaterally abnormal MRI and ^{1}H-MRSI measures do not preclude good surgical outcome.

SCIENTIFIC EXHIBITS

SPACE 0395PH

Integrated DICOM-based Image Archive System for PACS

A.W. Wong, BS, San Francisco, CA • H.K. Huang, DSc

A distributed image archive system based on the DICOM communications standard and file format has been implemented. The system uses a high-speed redundant array of inexpensive disks (RAID) for data caching and an optical disk library for permanent storage of images. Mallinckrodt's Central Test Node (CTN) software was modified to incorporate the 155 Mbps asynchronous transfer mode (ATM) network for communication of images. Implemented mechanisms include (a) a storage class provider (SCP), which accepts images from PACS acquisition nodes and archives images in DICOM Part 10 file format; (b) a storage class user (SCU) for distributing images to display workstations; and (c) a query/retrieve SCP, which allows images to be retrieved from display workstations. The system provides a simple yet efficient method for archiving and retrieving digital images. It archives DICOM-standard CT, MR, CR, and digital mammographic images directly. Non-DICOM images are first encoded to DICOM and archived. This exhibit describes the system configuration and our implemented strategies in image stacking, archiving, migration, pre-fetching, and routing, study grouping, and platter management.

SPACE 0403PH

Knowledge-based Lung Nodule Detection from Helical CT

S.G. Erberich, Dipl Inf, San Francisco, CA • K. Song, MD • H. Arakawa, MD • H.K. Huang, DSc • W. Richard, MD • K.S. Hoo, Jr, BS • et al

Helical CT with 7mm and 1mm slice thicknesses is mainly used to diagnose solitary and metastatic lung nodules. The exhibit shows a method for the automatic detection of lung nodules with a diameter of 3mm and larger from Helical CT, the 3D lung nodule database, and JAVA technology in clinical client/server applications. The presented algorithm is based on 3D segmentation and 2D/3D Hough transform. A knowledge-based rule tree classifies suspicious lesions as true or false nodules. The resulting nodule voxels and their geometrical, textual and fractal characteristics, and patient clinical information are organized and stored in a database. The radiologist uses a JAVA viewer to access the database to view CT images superimposed with the marked nodules and related information, to refine the results by modifying the nodule voxels, and to update the database. We have collected 40 patients from UCSF PACS, 15 solitary pulmonary nodule cases and 25 multiple nodules cases. Results show that the detection of lesions which appear in more than one slice (3D lesion) is less likely to result in false positive nodules (blood vessels and bronchial trees) than 2D detection. True positive and false positive nodules will be illustrated graphically.

Learning Objectives:

(1) Description of an automatic nodule detection method. (2) Report about the lung nodule 3D database design and PACS link. (3) Introduction of JAVA technology for clinical applications.

SPACE 0417PH

Portable DICOM-compliant PC/NT-based Diagnostic Workstation with Asynchronous Transfer Mode Technology

G. Lei, MS, San Francisco, CA • H. Zhang, MS • A.W. Wong, BS

We have developed a portable diagnostic workstation (WS) which is PC-based with a DOME Md2/PCI board, two 1,600 x 1,280 resolution monitors, and an asynchronous transfer mode (ATM) OC-3 communication board plus an Ethernet board. Implemented software includes: (a) a DICOM server, which automatically receives images from the DICOM-compliant PACS Controller; (b) a patient folder manager, which incorporates the local database to group multiple studies from the individual patients; (c) a sophisticated display program with automatic image pre-processing functions, such as window and level pre-set; and (d) a DICOM retriever which allows radiologists to query and retrieve previous studies from the PACS DICOM-compliant archive. Our PC/NT-based full-functioned WS demonstrates that (1) PC/NT-based WS is lower cost than the UNIX based WS and can be implemented cost-effectively for PACS applications. (2) Integration of DICOM and ATM network into the diagnostic workstation facilitates and speed up image communication. (3) Image pre-processing functions minimize requirement for image manipulation thereby improving radiologists efficiency in a time-critical clinical environment.

Learning Objectives:

1. To provide a PC/NT-based architecture of the diagnostic workstation. 2. To report the use of ATM technology in the workstation. 3. To describe the use of DICOM communication protocols in the workstation, and to illustrate the automatic image pre-processing facilities. 4. To show the performance of the workstation. **[See also scientific paper 708.]**

SPACE 0647BR

Full-Field Direct Digital Telemammography: Technical Components

S.A. Lou, PhD • H.K. Huang, DSc, San Francisco, CA • E.A. Sickles. MD • D.R. Hoogstrate, BS • M.I. Jahangiri, MD, MPH • F. Cao, PhD • et al

We have established a full-field direct digital telemammography (FFDD) system between two campuses at UCSF: the Breast Imaging Section at Mt. Zion Hospital and the Lab for Radiological Informatics, Parnassus campus, two miles apart. This exhibit presents four technical components in the system including the FFDDM, image compression, high resolution workstation, and communication network. For the FFDDM, we use the SENOSCAN with a novel CCD detector from Fischer Imaging. The image size is 3,870 x 3,100. In image compression we have developed an on-line structure lossless compression with an average compression ratio of 3 to 4:1. The display workstation is based on a SUN Ultra Sparc 2 with two DOME MD5/SBX boards and two 2.5K x 2 K Megascan monitors. Digtial mammograms can be displayed in two modes: a portion of 5K x 4K or subsampled 2.5K x 2K. We use the asynchronous transfer mode (ATM) OC-3 (155 Mbits/sec) for both WAN and LAN in communication. Currently we can transmit a 40 Mbyte mammogram in 5.3 seconds. We are in the technical phase of a three-year program developing telemammography applications. The next two phases are telemammography protocols and system evaluation.

Learning Objectives:

1. Technical components in a telemammography system 2. Technical aspect of a full-field direct digital mammography system 3. On-line lossless mammography compression 4. Asynchronous transfer mode communication technology 5. 2.5K x 2K display system for digital mammogram

*info*RAD EXHIBITS

SPACE 9111CAI

An Interactive Digital Breast Imaging Teaching File

F. Cao, PhD, San Francisco, CA • E.A. Sickles, MD • H.K. Huang, DSc

A digital breast imaging teaching file developed during the last two years in our laboratory has been used successfully at UCSF as a routine teaching tool for training radiology residents and fellows in mammography. Building on this success, we have ported the teaching file from the old Pixar imaging/Sun SPARC 470 display system to our newly designed telemammography display workstation (Ultra SPARC 2 platform with two DOME' s Md5/SBX display boards). The new workstation is compatible with a full-field direct digital mammography image format and is also more cost-effective than the old system. We will demonstrate in this exhibit the newly ported digital teaching file and its sophisticated computer-aided instruction (CAI) model, which simulates the management sequences used in imaging interpretation and work-up. Each user can be prompted to respond by making his/her own observations, assessments, and work-up decisions as well as the marking of image abnormalities. This effectively replaces the traditional 'show-and-tell' teaching file experience with an interactive, response-driven type of instruction.

Learning Objectives:

-Assess new high-resolution display technologies for digital mammograms
-Test the interactive teaching file as an effective training tool
-Understand the CAI model and the method of its implementation
[Supported by the RSNA Research and Education Fund.]

SPACE 9307NT

Optimizing Paper Printouts of CT and MR Examinations using a Windows-Based Software Solution

J. Stahl, MD, Hamburg/Saar, Germany • B. Kramann, MD, PhD

Paper printouts can be helpful in reducing film costs, provided that proper constraints are obeyed. In most cases, the limited spatial resolution of common laser printers restricts the use of paper prints to secondary copies for the referring physician. However, paper printouts have several advantages: They are easy to read even when no lightbox is available, they can be attached to the patients file, and they can be produced at minimum costs. We have developed a software that can access images from various scanners and print them to a laser printer connected to a desktop PC. This software optimizes the result in several ways: First, it allows the selection of rectangular ROI's within the image. These ROI's are automatically arranged on the printable area and scaled so that most of the printer's resolution can be used. Second, an automatic segmentation algorithm removes black image background to save toner. Third, all parameters are set up automatically to minimize operator intervention. The software has proven to be both effective and useful in clinical routine.

Learning Objectives:

Become familiar with the specific advantages and drawbacks of paper printouts compared to laser film images.
Learn how to adjust scaling, contrast and brightness to optimize quality of paper printouts.
Understand the concept of automatic background removal and its limitations. **[Supported by the RSNA Research and Education Fund.]**

SPACE 9440WKS

Tele-Consultation for Thoracic Imaging

J. Zhang, PhD, San Francisco, CA • K. Song, MD • H.K. Huang, DSc • A.W. Wong, BS • J. Stahl, MD

Real-time consultation between physician and expert radiologist is critical for timely and adequate management of problem cases. In thoracic imaging, consultation requires the interpretation of CR, CT, and MR images. This exhibit simulates the tele-consultation for thoracic imaging procedure. Both the general physician and the expert have a workstation (WS) designed specifically for tele-consultation purpose. The connection between two sites is an asynchronous transfer mode (ATM) network. Users at both sites can interactively study the same thoracic image sets including CR, CT, and MR images on its own WS simultaneously through a real-time cursor. Both users can annotate, draw regions of interest, change the look-up-table, and use cine mode. In this exhibit, two NT-based tele-consultation WSs will be demonstrated, each with an Intel PC, a DOME Md2/PCI board driving a 1,200 x 1,600 monitor, and an ATM connection. Two video phones are used for voice communication. Either a general physician or an expert can initiate a consultation procedure by first retrieving a case from the simulated database with thoracic images in DICOM format and start the tele-consultation procedure.

Learning Objectives:

1. Understand the technology involved in tele-consultation
2. Learn to use a consultation workstation
3. Participate in a consultation session

[Supported by the RSNA Research and Education Fund.]

SPACE 9450WKS

Full-Field Direct Digital Mammogram (FFDDM) Display Workstation (DWS)

M.I. Jahangiri, MD, MPH, San Francisco, CA • S.L. Lou, PhD • D.R. Hoogstrate, BS • H.K. Huang, DSc

PURPOSE: To demonstrate a DWS for the display and manipulation a 4K x 5K x 12bits FFDDM image.
METHODS AND MATERIALS: Our workstation consists of a Sun Ultra-2 computer with 512 Mbyte memory, two 2K x 2.5K MegaScan image display monitors, two DOME MD/5SBX display boards, fast/wide SCSI disks and a disk array unit. Our graphic user interface and image display implementation are based on X-Motif windowing system and DOME DIMPL image display and manipulation software library. The workstation features include: (1) configurable display layout-and-format such as 1-on-1, 2-on-1, and 4-on-1, (2)manual window and level, (3) zoom-and-scroll, (4) magnifier glass window, (5)orthogonal angle rotation/mirroring, (6) on-screen image exchange.
RESULTS: The workstation is capable of displaying FFDDM images in a designated layout-format which mammographers favor for comparison studies. The performance of all the image manipulation features provided is almost real-time.
CONCLUSIONS: We have achieved a design goal with a focus on a flexible and portable core which could be used independently of (1) number of display monitors (2) number of images per display monitor (3) third party vendors supported hardware/software libraries.

Learning Objectives:

1. FFDDM workstation
2. Graphical User Interface for multiple large images. **[Supported by the RSNA Research and Education Fund.]**

*info*RAD THEATER SCHEDULE

November 30, 1997

Theater 1

4:00 PM An Interactive Digital Breast Imaging Teaching File
Fei Cao, PhD

Theater 2

12:00 PM Experience With PACS Implementation
H. K. Huang, DSc

December 2, 1997

Theater 1

12:00 PM Optimizing Paper Printouts of CT and MR Examinations Using a Windows-Based Software
Johannes Stahl, MD

Theater 2

2:30 PM Digital Mammogram Display Workstation
S.L. Lou, PhD

December 3, 1997

Theater 2

12:30 PM Tele-Consultation for Thoracic Imaging
Koun Sik Song, MD

December 4, 1997

Theater 2

11:00 AM Full-Field Direct Digital Mammogram (FFDDM) Display Workstation
Mohammad I. Jahangiri, MD, MPH